THE UNIVERSITY
of EDINBURGH

Insights into the function and protein network of TALPID3

Amy Margaret Fraser

Doctor of Philosophy

College of Medicine and Veterinary Medicine

University of Edinburgh

2018

Declaration

I declare that this thesis is an original report of my research, was written by me and has not previously been submitted for any other degree. The experimental work and analysis of the results was entirely my own and any collaborative contributions have been clearly indicated in the text. References are provided for the literature and resources included in the text.

Amy Margaret Fraser

September 2018

Abstract

More than 1500 proteins have been identified as centrosome or cilia proteins, however it is still unknown how these proteins form networks to control functions such as centrosome orientation, maturation and ciliogenesis. TALPID3 is a centrosomal protein that plays a role in centrosome orientation and migration, ciliogenesis and Hedgehog pathway signal transduction. Although several proteins that interact with TALPID3 have been identified, the TALPID3 protein interacting network has not been established. Loss of TALPID3 leads to a loss of ciliogenesis, as seen in the embryonic lethal *talpid*^{3} chicken. Unlike the *talpid*^{3} chicken however, human ciliopathy patients with mutations in *KIAA0586* (human *TALPID3* orthologue) have a range of defects that often do not result in lethality.

Human *KIAA0586* was modelled in the chicken, in order to understand the functional domains that are affected by mutations that are predicted to be hypomorphic. A construct containing human *KIAA0586* was able to rescue Hedgehog-dependent expression patterns, when electroporated into the developing neural tube of *talpid*^{3} chicken embryos. An attempt to introduce a fluorescent tag at the endogenous *TALPID3* locus to look at specific subcellular localisation, proved unsuccessful; however a super resolution imaging approach confirmed localisation of TALPID3 to the centrosome. Structured Illumination Microscopy showed that TALPID3 localises to the distal end of centrioles with more TALPID3 on one centriole than the other centriole, but no specific regions of localisation elsewhere in the cell.

A proteomic approach on isolated centrosomes was undertaken to investigate the TALPID3 protein network. Proteomic studies in the centrosome have previously been carried out in KE37 cells, however in order to establish alternative cell lines, specifically chicken Primordial Germ Cells (PGCs), as models for studying the centrosome and cilia, this study was completed in human Jurkat cells and chicken PGCs. PGCs can be derived from the *talpid*^{3} flock, therefore by including chicken PGCs the aim was to construct the centrosomal proteome of *talpid*^{3} vs wildtype centrosomes from *talpid*^{3} PGCs. Through this study, I have shown that Jurkat cells have a low frequency of ciliogenesis with modifications of the centrioles that correlate with their low ciliogenesis frequency; however PGCS are capable of forming cilia and have modifications of the centrioles that correlate with their ability to form cilia, highlighting PGCs as a suitable cell model for carrying out centrosome and cilia studies. A mass spectrometry screen on centrosomes isolated from Jurkat cells and PGCs failed to identify TALPID3; however, the screen identified CCDC77 and CCDC127 as novel centrosome proteins, which was confirmed by immunofluorescence. CRISPR/Cas9 editing, demonstrated that mutations in CCDC127 resulted in a significant reduction of ciliogenesis and altered centrosome protein localisation patterns in RPE1 cells.

Isolation of centrosomes from PGCs did not prove effective for constructing the proteome of *talpid*^{3}, therefore an alternative approach was taken using protein extracted from whole cell lysate of *talpid*^{3} and wildtype PGCs. A quantitative proteomic study was undertaken in *talpid*^{3} PGCs with the aim

of understanding how protein networks are altered in *talpid*^{3}. Following a Tandem Mass Tag (TMT) mass spectrometry approach, pathway analysis in Ingenuity Pathway Analysis software (IPA) identified down-regulation of protein pathways linked to regulation of the actin cytoskeleton and showed an overall change to protein pathways associated with cholesterol biosynthesis. Immunofluorescence in *talpid*^{3} embryo sections was used to examine changes to proteins involved in actin regulation, including F-actin, Profilin, Cofilin, Twinfilin and RhoC.

The main findings of this thesis include evidence that *talpid*^{3} embryos can be used to model human ciliopathy mutations, demonstrate that PGCs are a primary cell model that can be used to study the centrosome and identify CCDC127 as a novel centrosome protein that is necessary for ciliogenesis in human RPE1 cells. Additionally, the findings show that protein pathways associated with the regulation of the actin cytoskeleton are downregulated in *talpid*^{3}. Together the results produced in this thesis provide insight into the centrosome from the perspective of chicken PGCs as well as a better understanding of protein pathways altered in *talpid*^{3}.

Lay Summary

The drive to better understand human health and what causes disease is a major focus of research today. Diseases arise due to mutations in genes, often causing abnormalities during development of the embryo, prior to birth. Genes that are switched on are able to make protein, however mutations often switch the gene off resulting in a loss of protein. One such example of a group of diseases that occur during development is 'ciliopathies.' Ciliopathies encompass a range of diseases that present with varying symptoms including but not limited to breathing abnormalities, liver disease, kidney disease, extra fingers, abnormal eye movement and intellectual disability. Ciliopathies are caused by mutations in genes that are necessary for forming cilia. Cilia are hair-like extensions that protrude from cells and use a group of proteins found in the centrosome, as an anchor, to project out of the cell. They are found on all cells in the body and are required for communication between cells during development and throughout adult life. *TALPID3* is an example of a gene that when mutated fails to form the correct protein, thus disrupting the cilia and resulting in a ciliopathy.

In order to study diseases, research is usually carried out on cell or animal models that mimic the disease or condition of interest. Where animal models are available, it is possible to generate cell lines from the animal to produce an accessible system in which to study the disease more easily. The *TALPID3* gene was first discovered in a chicken flock when chicks failed to

hatch because of a mutation in *TALPID3*. Chickens are one of the animal models regularly used in research and because the *talpid*^{3} chicken is readily available, it is possible to generate cell lines from this chicken to provide *talpid*^{3} cell models. The objectives of this project were to identify and study proteins that are linked to ciliopathies, to better understand *TALPID3* by studying the TALPID3 protein and to identify ways of modelling human diseases caused by mutations in *TALPID3*.

In this study, I demonstrated that the *talpid*^{3} chicken is a tool that can be used to model the mutations in *TALPID3* in human ciliopathy patients, providing a means to understand the disease and symptoms of the patients. By studying a group of proteins that are involved in the process of making cilia in cells, I identified a previously unknown protein, CCDC127 that when mutated leads to a loss of cilia in cells. In addition, I identified chicken Primordial Germ Cells (PGCs) as a cell line that have protein patterns that correlate with its ability to form cilia thus identifying a new cell model for studying ciliopathies. I generated PGCs from the *talpid*^{3} chicken flock to study the TALPID3 protein. This allowed me to identify groups of proteins that communicate with each other in the cell and cause some of the symptoms seen in the *talpid*^{3} chicken flock and patients with *TALPID3* ciliopathies. In summary, this study has demonstrated models for studying proteins that are necessary for cilia, with a focus on the TALPID3 protein and how to model human *TALPID3* mutations in the chicken.

Acknowledgements

First and foremost I would like to thank my supervisor, Megan Davey for your endless support and encouragement over the past four years, without which none of this would have been possible. You have provided guidance and advice, while allowing me the freedom to direct my own project. Your passion for science and vast knowledge has inspired me throughout.

Thank you to all the past and present members of the Davey lab – Lynn McTeir, Josie Bodle, Dillan Saunders, Louise Stephen and Edward Johnson – for your advice and encouragement both in and out of the lab. In particular, a huge thank you to Lynn – I could not have done it without you. You taught me everything I needed to know in the lab and regardless of what time in the morning I was starting a complicated experiment, you were always there to help and support me. Thank you for encouraging me and believing in me every step of the way.

Thank you to Mike McGrew for your advice and the many discussions regarding PGCs and editing. Thank you to Lorna Taylor for all your help and support in the lab, as well as endless giggles in the office. Thank you to Joni MacDonald for your words of encouragement and providing me with an endless supply of coffee while writing up. Thank you to James Glover for your help and advice throughout my PhD. Thank you to Joe Rainger for your help and guidance in the lab. Thank you to Holly Hardy for your help with formatting and advice regarding actin. Thank you to Anirudh Patir for your endless patience while helping me with statistics and your willingness to help with the graph making in R. Thank you to Scott Dillon for your patience while teaching me how to use IMARIS. Thank you to Tom Wishart, Sam Eaton and Laura Graham for all your help with the proteomic aspects of my project. Your knowledge and advice regarding mass spectrometry and words of encouragement throughout the past four years, in particular while writing my thesis, have been invaluable. Thank you to Bob Fleming and Graeme Robertson for your expert advice regarding imaging and microscopy. Thank

you to Ann Wheeler and Matt Pearson for all your help with the SIM imaging. Thank you to Dougie Lamont, Amy Tavendale and the rest of the team at FingerPrints Proteomics for your time and expert knowledge regarding mass spectrometry. Thank you to BBSRC EASTBIO Doctoral Training Programme for funding my research and affording me the opportunity to obtain my PhD.

Thank you to all my friends who have supported me over the past four years, in particular Emma Bonthrone, Eilidh McGowan, Claire Stenhouse, Emma Moore and Corey Hastings who have offered words of advice and encouragement as well as distractions when needed. I cannot thank you all enough for always believing in me and never questioning my lack of communication while I was writing up.

I would like to say a huge thank you to my girlfriend, Lucy. You have provided a constant source of love, support and laughter. You never once questioned my ability to finish writing this thesis, instead providing me with words of wisdom, putting up with my grumpy bad writing days and providing a shoulder to cry on when I needed it.

Finally I want to say thank you to my family. Anne and Maura, you have constantly supported me and encouraged me to pursue my dreams, for which I will always be grateful. Hannah and Tom, thank you for endless giggles, statistics advice and for believing in me. Last but not least, thank you Mum and Dad. You have been there for me every step of the way and I could not have done it without you. You have celebrated all of the small victories with me along the way, encouraged me to keep going when it got tough, listened, without complaint, to all the rants and tears while I wrote up and believed in me, even when I did not. I dedicate this thesis to you.

Table of Contents

List of Figures

List of Tables

Chapter 1. General Introduction

1.1 Formation and function of the centrosome

The centrosome is the main microtubule organising centre in the cell (Gould & Borisy, 1977; Joshi et al., 1992), consisting of two centrioles, the mother centriole and the daughter centriole, which are surrounded by the satellites within the pericentriolar material. The mother and daughter centriole are held together by filamentous interconnecting fibres between the proximal ends of each centriole (Bornens et al., 1987). As the centrosome orientates and migrates towards the cell surface, ciliary vesicles derived from the Golgi apparatus dock with the distal end of the mother centriole at the distal appendages, marking the conversion to the basal body (Keeling et al., 2016; Schmidt et al., 2012; Sorokin, 1962). The basal body then docks at the plasma membrane, forming the transition zone at the base of the cilium (Figure 1.1) (Aubusson-Fleury et al., 2012; Schmidt et al., 2012).

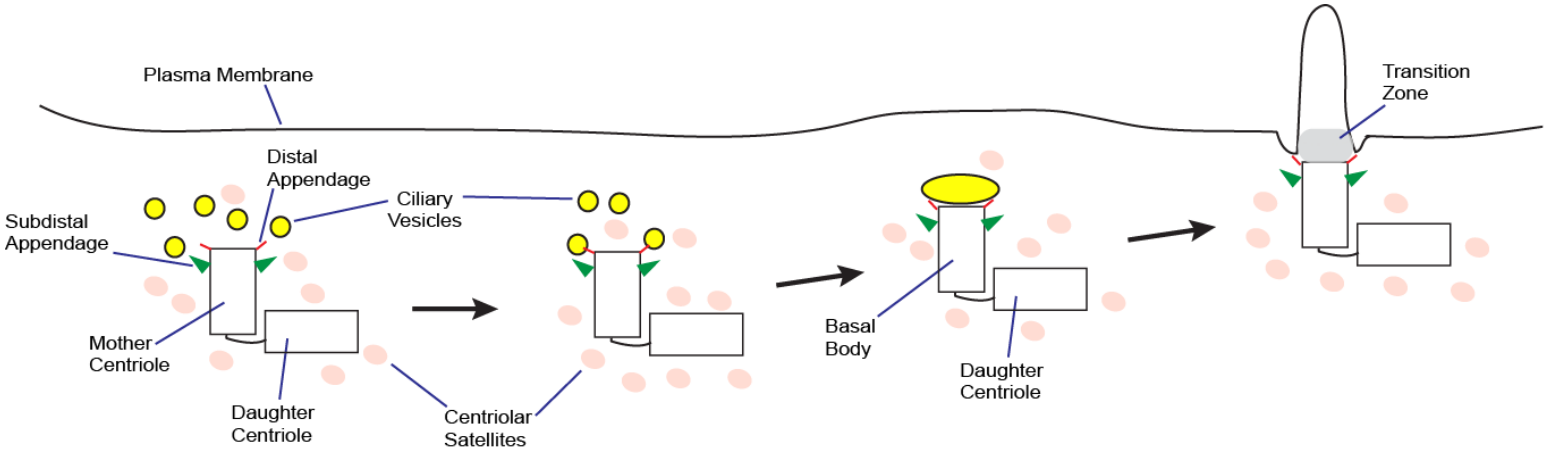

Figure 1.1 Schematic of the steps involved in basal body docking and ciliogenesis. The mother and daughter centriole are held together by filamentous interconnecting fibres between the proximal ends of each centriole and are surrounded by centriolar satellites in the pericentriolar material. Distal and subdistal appendages mark the distal end of the mother centriole. Ciliary vesicles derived from the Golgi apparatus accumulate at the distal end of the mother centriole and dock with the distal appendages. This marks the conversion of the mother centriole to the basal body as it migrates towards and docks with the plasma membrane, forming the transition zone and initiating ciliogenesis.

The assembly of procentrioles is initiated at the G1-to-S transition of the cell cycle by PLK4 and Cep152 (Habedanck et al., 2005). Centrioles have a distinct barrel-shaped structure, composed of microtubules arranged in ninefold rotational symmetry. The ninefold arrangement of the microtubules is organised by the cartwheel, first observed using electron microscopy in 1960 (Gibbons & Grimstone, 1960). This well-conserved mechanism appears at the early stages of centriole assembly (Hirono, 2014), and as the name suggests takes the form of a hub and spokes, the main component of which is the protein SAS-6 (Guichard et al., 2013; Winey & O'Toole, 2014). PLK4 and Cep152 are involved in recruitment of SAS-6 and STIL to the region of the mother centriole to organise the cartwheel formation (Tang et al., 2011). STIL interacts directly with CPAP (Kitagawa et al., 2011; Tang et al., 2011), a cell cycle regulated protein with similar protein levels as SAS-6 during the cell cycle (Tang et al., 2009).

A single cartwheel is composed of a central ring (the hub), from which nine filaments arise (the spokes) that attach to the A-tubule of the triplet microtubule. The filaments connect to the A-tubule via a structure called the pinhead (Hirono, 2014). The triplet microtubules consist of the A tubule, B tubule and C tubule, of which the main component is tubulin (Li et al., 2012; Winey & O'Toole, 2014). There are also linkers found between consecutive A and C tubules in many organisms (Figure 1.2) (Winey & O'Toole, 2014). Typically multiple cartwheels are stacked on top of each other in the lumen of the centriole and occupy approximately 100 nm of the proximal end of the lumen (Hirono, 2014). This arrangement is well conserved but there are

variations; in humans the microtubules are arranged in triplets whereas *Drosophila* and *C. elegans* have doublet and singlet microtubules respectively (Winey & O'Toole, 2014). There are also differences in length of centrioles; typically centrioles are 400-450 nm in length and contain several layers of cartwheel stacks, however *Trychonympha* for example have a long centriole measuring about 4 μm and contains cartwheels filling 90% of the lumen (Gibbons & Grimstone, 1960; Hirono, 2014). Centriolar elongation requires a complex of proteins including CPAP, SPICE1 and Cep120 (Comartin et al., 2013b); Centrobin has also been implicated in centriolar elongation (Gudi et al., 2011). Additionally CP110 plays a role in regulation of centriole length by capping the distal end, with evidence to suggest that CPAP and CP110 play antagonistic roles in the extent of tubulin added during centriole elongation to control the length of centrioles (Schmidt et al., 2009).

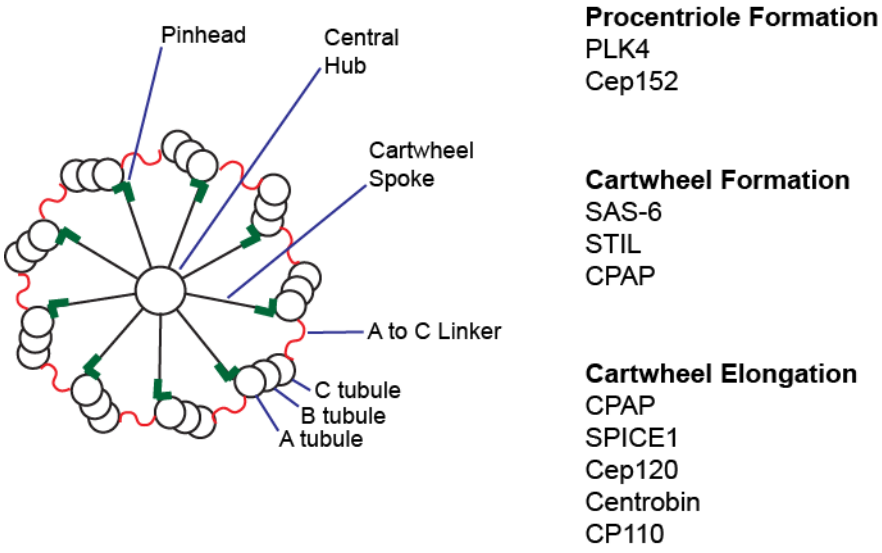

Figure 1.2 Cartwheel structure of the centriole seen in a cross section. Many layers of these structures are stacked on top of one another inside the lumen of the centriole. Different proteins are responsible for controlling different aspects of centriole formation.

The centrosome and the cell cycle are closely linked; the duplication of centrosomes is coordinated with the cell cycle progression. At the G1-S phase transition during the cell cycle, the procentriole duplication cycle begins with the formation of a cartwheel at the proximal end of each centriole. These procentrioles then elongate until the end of G2 phase, when they have reached approximately the size of a mature centriole. During this time the centrioles remained linked together, however by the end of G2, the centrioles separated and the older centriole in each pair matures and develops distal and subdistal appendages. Prior to mitosis (M phase), the mother centriole in each pair is able to nucleate increased microtubules for spindle assembly, allowing the centrosomes to move to opposite sides of the cell as spindle poles. Following mitosis, the paired centrioles in each cell disengage, allowing the mother centriole to become a basal body and dock at the plasma membrane to form a primary cilium in G0 phase (Figure 1.3) (Fu et al., 2015; Kobayashi & Dynlacht, 2011; Wang et al., 2014).

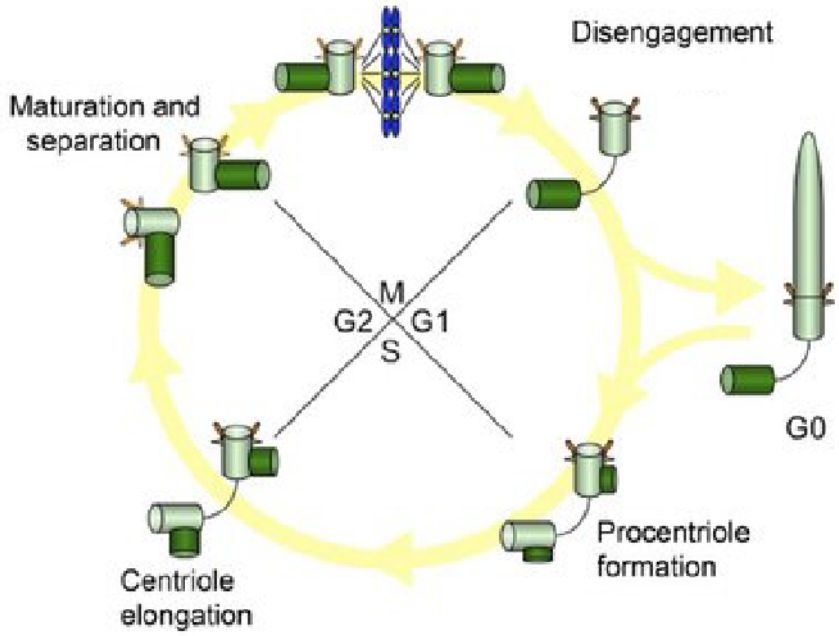

Figure 1.3 Centrosome duplication and the cell cycle. Procentrioles form at the G1-S phase transition of the cell cycle. The procentrioles elongate through to the end of G2, when they mature and separate. During mitosis, centrioles form spindle poles at the opposite sides of the cell. Following mitosis, the paired centrioles disengage to allow formation of a primary cilium from the basal body at G0 phase. Adapted from Kobayashi & Dynlacht, 2011.

Through the centrosomes role as the microtubule organising centre of the cell, it nucleates microtubules and controls their length and number; in doing so, the centrosome helps to regulate transport of complexes, position of cellular organelles, cell motility, cell shape, polarity and segregation of the chromosomes during cell division (Abal et al., 2002; Pitaval et al., 2017; Schatten, 2008). In addition, the centrosome orchestrates ciliogenesis when the cell enters the G0 phase of the cell cycle; the mother centriole matures to form the basal body which can orientate towards and dock with the cell membrane to form a cilium (Park et al., 2008; Sorokin, 1968). Maturation is marked in the mother centriole by distal and subdistal appendages that dock cytoplasmic microtubules and anchor the mother centriole to the cell membrane when it becomes a basal body during ciliogenesis (Figure 1.4) (Ishikawa et al., 2005; Tanos et al., 2013); this requires a series of proteins such as Cep164, ODF2, MACF1, Cep89, SCLT1, FBF1 and Cep128, which localise to the distal and subdistal appendages (Graser et al., 2007; May-Simera et al., 2016; Mönnich et al., 2018; Tanos et al., 2013; Tateishi et al., 2013).

The role of CP110 is not only limited to controlling centriolar length but also plays a role in ciliogenesis, with evidence to suggest it can act as both a suppressor and promoter of ciliogenesis (Spektor et al., 2007; Tsang et al., 2008; Yadav et al., 2016). Studies show that Cep97 recruits CP110 to the centrosome where it interacts with Cep290 to suppress ciliogenesis in cells (Spektor et al., 2007; Tsang et al., 2008). Cep290 also plays a key role at the transition zone, where it is required for microtubule and membrane linkers

and helps to regulate entry of proteins into the ciliary compartment (Anand & Khanna, 2012; Craige et al., 2010). The transition zone is located distal to the basal body at the base of the cilium and mediates linkage to the ciliary membrane, establishes a barrier to membrane diffusion and acts as a gate to maintain ciliary protein homeostasis (Czarnecki & Shah, 2012). This region at the base of the cilium is surrounded by the ciliary pocket, an invagination of the membrane, that acts as the site of exocytosis and endocytosis for vesicles transporting lipids and proteins from the trans-Golgi complex to the ciliary membrane (Figure 1.4) (Pedersen et al., 2016).

Satellite proteins can also play a role in ciliogenesis, with PCM1, a key protein component of satellites, promoting ciliogenesis through interactions with specific groups of satellite associated proteins including Mib1, OFD1, Cep131, Cep72 and Cep290 (Wang et al., 2016). Satellites were first described as electron dense masses around the centrosome; they are now known to contain numerous proteins involved in centrosome maintenance and ciliogenesis and act as vehicles for protein trafficking towards the centrosome (Hori & Toda, 2017; Tollenaere et al., 2015). Proteins such as TALPID3 have a more complex role, interacting with a range of different proteins including CP110, MACF1, PCM1 and Cep120 (Kobayashi et al., 2014; May-Simera et al., 2016; Wu et al., 2014). These TALPID3-interacting proteins localise to different regions within the centrosome and are involved in regulation of different processes, leading to the question of how TALPID3, which has been shown to localise to the distal ends of centrioles and control orientation of the centriole prior to docking (Kobayashi et al., 2014; Stephen

et al., 2015), can interact with these proteins despite localising to different regions and being involved in different functions.

Additionally there are groups of proteins required for the maintenance and assembly of cilia such as the Intraflagellar transport (IFT) proteins and the BBSome proteins that localise to the centriolar satellites and the membrane of the cilium (Nachury et al., 2007; Nakayama & Katoh, 2018; Pedersen et al., 2008). The IFT proteins mediate bidirectional trafficking of ciliary proteins along ciliary microtubules; this transport role is required for cilia assembly as well as cilia maintenance (Lechtreck, 2015; Nakayama & Katoh, 2018). The BBSome is a complex of Bardet-Biedl Syndrome proteins that are thought to mediate membrane trafficking to the primary cilium through a link with Rab8, which targets vesicles to the cilium to promote ciliary elongation (Jin et al., 2010; Nachury et al., 2007). The BBSome moves in association with IFT trains and is involved in the assembly and stabilisation of IFT particles (Wei et al., 2012; Williams et al., 2014). Other ciliary components are more involved in the function of the cilium instead of the formation or maintenance of the cilia. For example the GTPase ADP ribosylation factor-like 13b (Arl13B) helps to regulate Hedgehog pathway signalling through regulation of Smoothened entry into the cilium and the distribution of Smoothened once in the cilium (Larkins et al., 2011). Although this only covers a small portion of proteins that make up the centrosome and cilia proteomes, it provides some insight into the nature of the dynamic interactions within the centrosome (Figure 1.4).

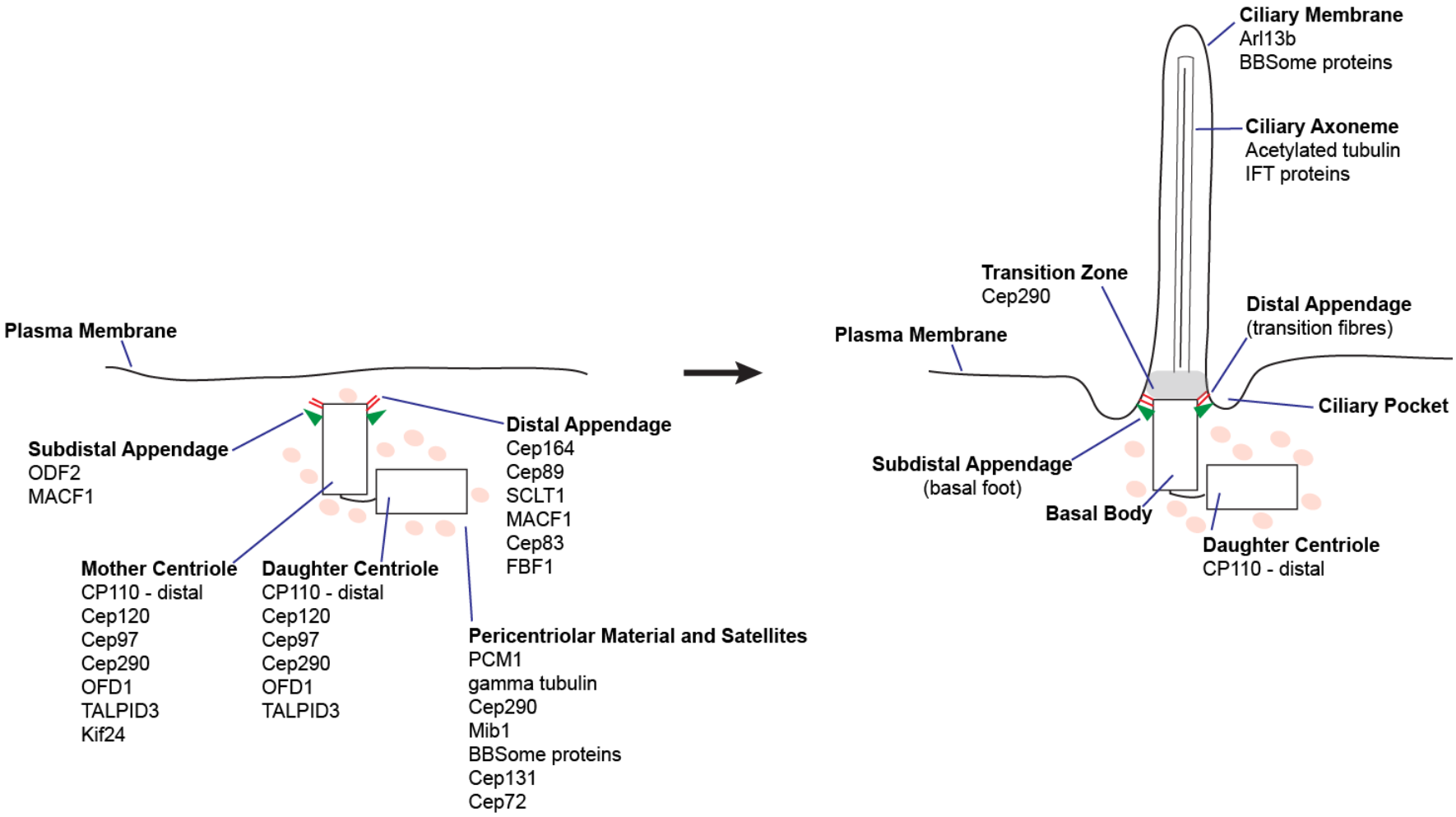
Plasma Membrane
Subdistal Appendage
ODF2
MACF1
Distal Appendage
Cep164
Cep89
SCLT1
MACF1
Cep83
FBF1
Mother Centriole
CP110 - distal
Cep120
Cep97
Cep290
OFD1
TALPID3
Kif24
Daughter Centriole
CP110 - distal
Cep120
Cep97
Cep290
OFD1
TALPID3
Pericentriolar Material and Satellites
PCM1
gamma tubulin
Cep290
Mib1
BBSome proteins
Cep131
Cep72
Ciliary Membrane
Arl13b
BBSome proteins
Ciliary Axoneme
Acetylated tubulin
IFT proteins
Transition Zone
Cep290
Distal Appendage
(transition fibres)
Plasma Membrane
Ciliary Pocket
Subdistal Appendage
(basal foot)
Basal Body
Daughter Centriole
CP110 - distal

Figure 1.4 Centrosome and cilia structure and protein localisation. Prior to ciliogenesis the centrosome is composed of a mother and daughter centriole that migrate towards and orientate at the plasma membrane. The mature mother centriole can be distinguished from the daughter centriole by the presence of distal and subdistal appendages. The distal appendages act as the site for vesicle docking. The mother centriole becomes the basal body as it docks to the plasma membrane via the distal and subdistal appendages. The region distal to the basal body at the base of the cilium is known as the transition zone. This region at the base of the cilium is surrounded by the ciliary pocket, which acts as the site for delivery and retrieval of vesicles. The centrioles are surrounded by the pericentriolar material, which contains the satellites. A complex network of proteins is required for correct formation and orientation of the mother and daughter centrioles prior to ciliogenesis. Some of the proteins localise to multiple sub-structures within the centrosome and change localisation during ciliogenesis.

There are over 1500 proteins known to be associated with the centrosome-cilium interface (Gupta et al., 2015). This benchmark dataset of proteins was collated from CentrosomeDB (Alves-Cruzeiro et al., 2013; Nogales-Cadenas et al., 2009) and Syscilia (Dam et al., 2013) and named the centrosome and cilium database (CCDB) (Gupta et al., 2015). Despite having identified the main groups of proteins that are required for the formation of centrosomes and how they interact, it is still not fully understood how the remaining proteins interact to form networks. A review in 2012 applied Gene Ontology (GO) cellular component cluster analysis to 599 human centrosome proteins, which grouped the proteins into 9 main clusters, which were then further subdivided into 43 categories; by showing the many different subgroups that centrosome proteins can be divided into based on where they localise and what processes they control, the review demonstrates the complexity of the protein networks in the centrosome (Habermann & Lange, 2012).

Following docking of the basal body at the cell membrane, the formation of a cilium (ciliogenesis) occurs. The cilia that form can be grouped into two categories: primary cilia and motile cilia. Primary cilia are non-motile organelles that can be found on the surface of almost all cells and act as a major site of signal transduction within the cell for key pathways including Hedgehog pathway signal transduction, Wnt signalling, Notch signalling, Hippo signalling, PDGFR signalling, mTOR signalling and GPCR signalling (Goetz et al., 2009; Huangfu et al., 2003; May-Simera & Kelley, 2012; Oh & Katsanis, 2013; Wheway et al., 2018). Motile cilia are usually found on

tissues that have the ability to produce multiple cilia, such as endothelial linings, enabling the cilia to beat in a synchronised manner to aid movement of particles over the surface of the tissue (Brooks & Wallingford, 2014; Ishikawa & Marshall, 2011; Sorokin, 1968). Motile cilia can also function independently as a single structure for example in sperm and the tail of Trypanosomes (Inaba & Mizuno, 2016; Ralston et al., 2009). The structure of primary and motile cilia differs based on their function; primary cilia are composed of nine doublet microtubules (Figure 1.5 A) that stem from the triplet microtubules within the basal body and continue the length of the cilium, whereas motile cilia contain nine peripheral doublet microtubules as well as an additional pair of central, singlet microtubules (9 + 2), radial spokes and outer and inner dynein arms (Figure 1.5 B) that allows them to bend and beat (Ishikawa & Marshall, 2011; Satir et al., 2014).

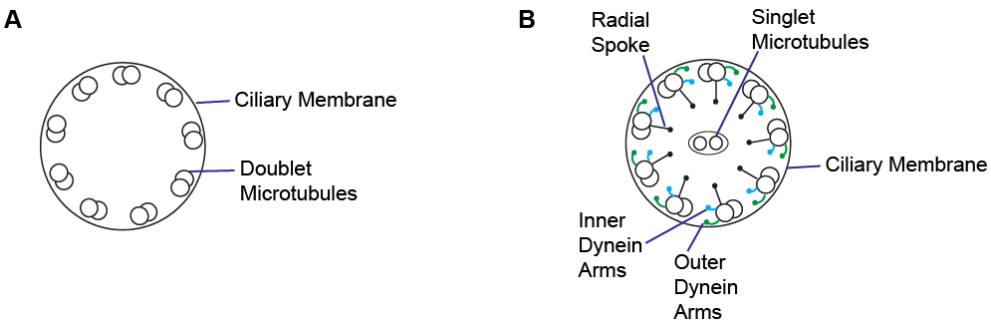

Figure 1.5 Cross section of primary and motile cilia. (**A**) Cross section of a primary non-motile cilia with a 9 + 0 arrangement of microtubules. (**B**) Cross section of a motile cilia with a 9 + 2 arrangement of microtubules that enables the cilia to bend and beat.

1.2 Signalling at the cilium and ciliopathies

The first evidence of the importance of cilia in the Hedgehog signalling transduction pathway came in a mouse mutagenesis screen that identified mice with phenotypes characteristic of Sonic hedgehog signalling defects, as having mutations that disrupt IFT proteins (Huangfu et al., 2003). The mechanism was not fully understood, however it was known that both the Hedgehog signalling pathway and ciliary function were important in a range of human diseases (Bale, 2002; Huangfu et al., 2003; Sloboda, 2002). The G-protein coupled receptor Smoothened (SMO), which is essential for Hedgehog signalling was subsequently discovered to localise to the cilium in the presence of Sonic hedgehog ligand (Corbit et al., 2005), providing the link between cilia and Hedgehog signalling. These studies demonstrated that Sonic hedgehog (SHH) acting through the transmembrane receptor Patched1 (PTCH1) (Goodrich et al., 1996; Marigo et al., 1996) regulates SMO activity and translocation to the cilium. In the presence of ligand, SHH binds PTCH1 to remove it from the ciliary membrane. SMO is no longer inhibited by PTCH1 and can translocate to the cilium where full length Gli proteins can be processed to their activator forms (GliA). Where cells are not exposed to SHH ligand, PTCH1 remains localised to the ciliary membrane where it inhibits SMO, resulting in the processing and cleavage of Gli proteins to their repressor forms (GliR) (Figure 1.6). Exploration of the mechanism by which SMO, IFT and Hedgehog signalling are linked, demonstrated that IFT in the mouse is required for both Gli activator and repressor function and for the proteolytic processing of Gli3 (Liu et al., 2005; May et al., 2005). The Gli

proteins accumulate at the ciliary tip prior to modification and translocation (Haycraft et al., 2005), however whether IFT proteins control this through direct transport of the Gli proteins or whether they indirectly influence Gli proteins through their requirement during cilia assembly was not known. More recent studies have demonstrated that some IFT proteins, such as IFT25 and IFT27 are not required for the formation of the cilium, instead they are involved in Hedgehog signalling through their role in promoting Gli localisation to the ciliary tip (Eguether et al., 2014; Eguether et al., 2018).

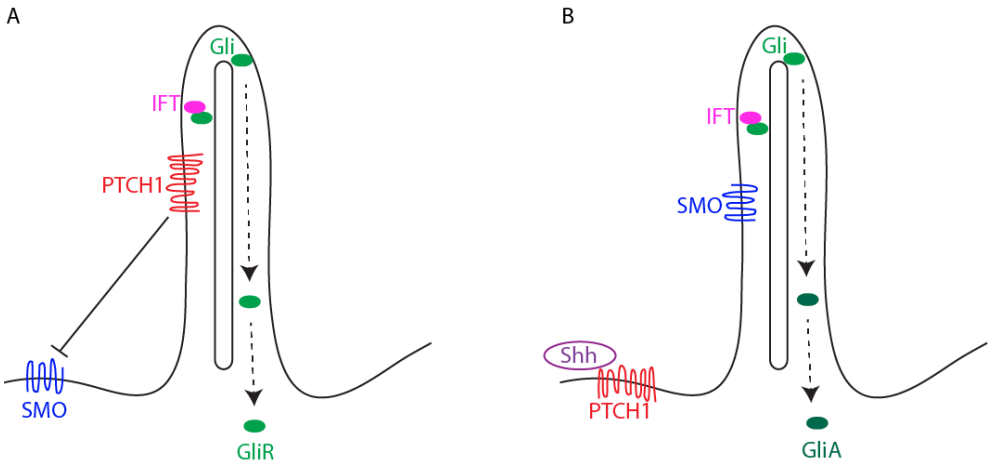

Figure 1.6 Schematic of Hedgehog signalling in the primary cilium. (**A**) In cells lacking Hedgehog ligand, PTCH1 localises to the ciliary membrane and inhibits SMO. Following transport of Gli proteins to the tip of the cilium, this results in full length Gli proteins being processed and cleaved to form the Gli repressor proteins (GliR). (**B**) In the presence of Hedgehog ligand, Shh binds to PTCH1 removing it from the ciliary membrane and allowing translocation of SMO to the ciliary membrane. Following transport of full length Gli proteins to the tip of the cilium by IFT transport, Gli is processed to its activator form (GliA).

Hedgehog signalling is necessary for normal development of all organ systems in mammals and Hedgehog signalling requires cilia, thus demonstrating the importance of cilia in development (Bangs & Anderson, 2017; Goetz et al., 2009). Genetic mutations that result in defective protein formation leading to abnormal cilia formation and function lead to a group of disorders known as ciliopathies (Reiter & Leroux, 2017). Many of the phenotypes associated with ciliopathies are characteristic of defective Hedgehog signal transduction, including a range of abnormalities predominantly affecting the kidney, eye, liver, brain and skeletal organisation (Hildebrandt et al., 2011; Waters & Beales, 2011). Additionally, cilia malformations have been linked to diabetes, obesity, skeletal dysplasias and microcephaly to name a few (Chavali et al., 2014; Waters & Beales, 2011).

There is also evidence to suggest that large scale genomic changes and environmental factors can affect proteins involved in the centrosome and cilia during development to produce ciliopathy phenotypes. For example Trisomy 21, which is the most prevalent human chromosomal disorder, and Zika virus have both been linked to defects in centrosomes and cilia (Gabriel et al., 2017; Galati et al., 2018). Pericentrin, which localises to the centrosome and supports trafficking to and from the centrosome, is located on chromosome 21 (Doxsey et al., 1994; Galati et al., 2018; Jurczyk et al., 2004). Individuals with Trisomy 21 have a triplication of chromosome 21, leading to an increased level of pericentrin. This increased level of pericentrin results in fewer and shorter cilia with decreased levels of Sonic

hedgehog signalling, demonstrating how genomic changes can alter gene dosage balance in the centrosome, causing ciliopathy phenotypes (Galati et al., 2018). Zika virus, which is associated with microcephaly in newborns, has recently been shown to cause premature differentiation of neural progenitors as a result of centrosome defects (Gabriel et al., 2017). Neural progenitors infected with Zika virus fail to recruit Microcephaly-linked proteins such as Cep153, PCNT and CPAP to the centrosome (Alcantara & O'Driscoll, 2014; Gabriel et al., 2016, 2017; Guernsey et al., 2010; Lancaster et al., 2013; Rauch et al., 2008). In addition, Zika virus infected cells have been shown to have decreased levels of the distal appendage protein Cep164 as well as mother centrioles that lack appendages (Gabriel et al., 2017). These changes to centrosomes result in neural progenitor cells differentiating too early thus causing microcephaly (Alcantara & O'Driscoll, 2014) and demonstrating how environmental cues can alter centrosome and cilia function.

Microcephaly is not only caused by Zika virus but also caused by mutations in centrosome and cilia genes as well as centrosome amplification (Chavali et al., 2014; Malvezzi et al., 2018; Marthiens et al., 2013; Waters et al., 2015). Microcephaly is thought to arise from abnormal neurogenesis, resulting in a change to the number of neural progenitors, abnormal cell fate decisions and abnormal neuronal migration patterns (Chavali et al., 2014; Thornton & Woods, 2009). Mutations in Microcephaly-linked centrosome genes have been shown to impair centriole production, cause centriole amplification and impair centriole length. For example, cells with abnormal centrosome

numbers take longer to form a bipolar spindle, leading to mitotic delay; mitotic delay is the major phenotype seen following depletion of WDR62, ASPM and STIL. This mitotic delay can eliminate the proliferative potential of progenitors thus leading to microcephaly (Novorol et al., 2013).

Non-motile or sensory ciliary disorders are caused by defects in primary cilia and are characterised by a wide variety of phenotypes. The role of primary cilia in signalling pathways controls and maintains cell and tissue polarity, transduction of sensory stimuli and stem cell proliferation and maintenance; therefore, the phenotypes associated with defective primary cilia cover a wide range, including but not limited to cystic kidneys, neuronal developmental abnormalities, retina defects, liver fibrosis, pancreatic defects and skeletal abnormalities (Mitchison & Valente, 2017).

There has been mixed evidence regarding a potential role for cilia in Wnt Signalling (May-Simera & Kelley, 2012). The Wnt signalling pathway regulates key aspects of cell fate determination, cell migration, cell polarity neural patterning and organogenesis during development. Wnt proteins bind the receptor Frizzled, stimulating signal transduction cascades including the canonical or Wnt/β -catenin dependent pathway and the non-canonical or β-catenin-independent pathway. The non-canonical pathway can be further divided into the Planar Cell Polarity pathway and the Wnt/Ca^{2+} pathway (Komiya & Habas, 2008). One of the first pathways to be associated with cilia dysfunction was the non-canonical Wnt planar cell polarity (PCP) pathway (Ross et al., 2005). The PCP pathway coordinates polarisation of cells within the plane of the epithelial cell layer and is also required during

organ morphogenesis for convergent extension (Komiya & Habas, 2008; Lapébie et al., 2011).

Two Planar Cell Polarity components, Inversin and Dishevelled, were identified at the basal body (Otto et al., 2003; Park et al., 2008), and mutations in Inversin cause the ciliopathy Nephronophthisis (Otto et al., 2003; Simons et al., 2005). In addition, three genes, *DUBORAYA, OFD1* and *SEAHORSE* have been linked to ciliogenesis and the Planar Cell Polarity pathway in zebrafish; mutations in each of these genes results in a classical curved body and curly tail phenotype as well as other ciliopathy-like characteristics (Dale et al., 2009). A study found that IFT88, the gene mutated in cystic kidney disease in mice, is required for establishing epithelial planar cell polarity (Jones et al., 2008), linking ciliary genes to the PCP pathway. Additional findings showed that correct positioning of the basal bodies and formation of polarised cellular structures are disrupted when ciliary proteins are disrupted (Gerdes et al., 2007; Oishi et al., 2006; Park et al., 2008). Mice mutants for the core PCP component *Fuz* have neural tube defects, skeletal dysmorphologies and Hedgehog signalling defects that are caused by disrupted ciliogenesis (Gray et al., 2009; Tabler et al., 2013). These characteristics are similar to the phenotypes observed in many ciliopathy patients, demonstrating how defects in primary cilia can lead to ciliopathy phenotypes caused by disrupted PCP (Waters & Beales, 2011).

In addition to a role for cilia in the non-canonical Wnt PCP pathway, evidence suggests a role for cilia in the canonical Wnt/β -catenin dependent pathway; knockdown of several BBS genes and several other ciliary-associated genes

resulted in hyperactive canonical Wnt responses (Gerdes et al., 2007). In the canonical Wnt cascade, Wnt ligand binds the Frizzled receptors thereby stabilising β-catenin; in the absence of Wnt ligand, β-catenin is degraded by the APC degradation complex (Komiya & Habas, 2008; May-Simera & Kelley, 2012). APC also plays a role in organisation of the cytoskeletal network (May-Simera & Kelley, 2012) and APC has been shown to localise asymmetrically to the mother centriole supporting a role for APC in cilia formation and function (Jakobsen et al., 2011). A factor linking both canonical and non-canonical Wnt signalling to the cilium is the Rho family GTPase, Cdc42. It is a key component in Wnt-dependent cytoskeletal rearrangements and a key component in cell polarity; additionally a complex consisting of Cdc42/Par6/aPKC localises to the cilium and is required for ciliogenesis in mammalian cells (Fan et al., 2004).

In conclusion, greater than 20 studies have reported a relationship between the primary cilium and Wnt signalling, however not all studies are in agreement. For example, *IFT88* zebrafish mutants that lack all cilia were shown to have normal canonical and non-canonical Wnt signalling (P. Huang & Schier, 2009). Additionally *IFT88, IFT72* and *KIF3A* mutant mouse embryos all lack primary cilia and demonstrate normal activation of a transgenic canonical Wnt reporter (Ocbina et al., 2009). The result of conflicting evidence has led to the proposal of two theories; the first theory suggests that Wnt signalling is regulated by the basal body and not directly linked to ciliogenesis and the second theory suggests that only certain ciliary and

basal body proteins have roles in Wnt signalling and that those roles are independent of their function in the cilia (Oh & Katsanis, 2013).

Defects in motile cilia can also result in ciliopathies, characterised by dysfunction of tissues and organs that rely on specialised ciliary and flagella machinery to generate fluid flow or movement within fluids, for example in the airways and the Fallopian tubes (Mitchison & Valente, 2017). Disruptions to ciliary motility almost exclusively results in primary ciliary dyskinesia (PCD), which results in respiratory distress, chronic sinopulmonary disease, infertility and can be accompanied by organ laterality defects (Praveen et al., 2015; Reiter & Leroux, 2017). Mutations in more than 30 genes have been shown to cause primary ciliary dyskinesia, however this only accounts for 65% of patients demonstrating the need for identifying further causes of the disease (Knowles et al., 2013; Praveen et al., 2015).

There are now more than twenty disorders included in the ciliopathy spectrum; combined, ciliopathies affect nearly all major organs, including kidney, brain, limb, retina, liver, and bone (McIntyre et al., 2013; Novarino et al., 2011). Even within one disorder, the phenotypic range is huge and can be vastly different even among members of the same family meaning that clinical diagnosis can be difficult (Novarino et al., 2011). Joubert Syndrome is one such ciliopathy that results from defects in the primary cilium. It is classified by brain and spinal malformations and can be diagnosed by the Molar Tooth Sign (MTS) seen on an axial MRI brain scan. Abnormalities in the caudal midbrain, superior cerebellar peduncles and hypoplasia of the midline cerebellar vermis are responsible for the molar tooth sign (Maria et

al., 1999; Parisi, 2009). Intellectual impairment or developmental delay, hypotonia in infancy, abnormal eye movements and irregular breathing (M. A. Parisi, 2009) are all characteristics of Joubert Syndrome. The neural defects seen in Joubert Syndrome are likely to be caused by disruptions to signalling pathways that require cilia. The Sonic hedgehog pathway plays a role in cerebellar development, driving progenitor proliferation; in addition, Shh signalling plays a role in human stem cells and formation of adult neural stem cells (Spassky et al., 2008). Disruptions in cilia can lead to a decrease in canonical Wnt signalling and cell proliferation in the developing cerebellum, which causes cerebellar vermis hypoplasia and deep interpeduncular fossa that closely resembles the MTS seen in Joubert patients (Abdelhamed et al., 2013). A subset of patients with Joubert Syndrome present with retinal defects, renal abnormalities and liver abnormalities (Romani et al., 2013). It is thought that cilia in the kidney are responsible for mechanosensory and chemosensory functions that transmit extracellular signals, such as urine flow into the cell, and maintain renal epithelial planar cell polarity and oriented cell division, resulting in healthy renal function. However, abnormalities in cilia disrupt these processes, leading to abnormal renal function and cystic kidneys (Huang & Lipschutz, 2014; Papakrivopoulou et al., 2014). In conclusion, multiple roles for cilia in signalling pathways as well as chemosensory and mechanosensory functions can lead to the phenotypes seen in ciliopathy patients such as those with Joubert Syndrome.

The number of diseases that fall under the broader category of ciliopathies and the wide range of phenotypes associated with ciliopathies demonstrates the importance of centrosome and cilia function during development and throughout adult life. In particular, it highlights the need to identify the protein networks within the centrosome and determine how they function together to control centrosome formation, polarity, ciliogenesis and the signalling pathways associated with cilia. To date, there is no cure for ciliopathies, only treatment of the symptoms. Attempts have been made to treat ciliopathies using gene therapy (Chhin et al., 2009; Mcintyre et al., 2012; Simons et al., 2011); however, for gene therapy to be effective in the future, a better understanding of exactly how the mutations are affecting multiple tissues, the degree of penetrance in different tissues and the severity of the phenotypes associated with it will be required (McIntyre et al., 2013).

1.3 ***TALPID3/KIAA0586***

The *talpid*^{3} chicken arose through a spontaneous recessive mutation discovered due to reduced hatchability (embryonic lethality) observed by Hunton in 1960. The *talpid*^{3} chicken mutant was first described by Ede and Kelly as having extensive abnormalities in the head, trunk and limbs (Ede & Kelly, 1964; Ede & Kelly, 1964). The *talpid*^{3} chicken produces an abnormal shortened TALPID3 protein (Davey et al., 2006) caused by an insertion mutation of a single Thymidine residue in the *TALPID3* gene. The mutation

causes a stop codon nine residues after the thymidine insertion, stopping translation and resulting in the production of a protein that is only 366 amino acids in length (Davey et al., 2006). It is now known that TALPID3 is a centrosomal protein (Andersen et al., 2003; Yin et al., 2009) that plays a role in centrosome orientation and migration, ciliogenesis and Hedgehog pathway signal transduction (Stephen et al., 2013). Since the discovery of *TALPID3*, two knockout mouse models have been made and a knockout zebrafish model (Bangs et al., 2011; Ben et al., 2011; Wu et al., 2014). Additionally, a group of human ciliopathy patients have been identified as having mutations in *KIAA0586* (human *TALPID3* orthologue) (Figure 1.7) (Akawi et al., 2015; Alby et al., 2015; Bachmann-Gagescu et al., 2015; Fleming et al., 2017; Malicdan et al., 2015; Roosing et al., 2015; Stephen et al., 2015).

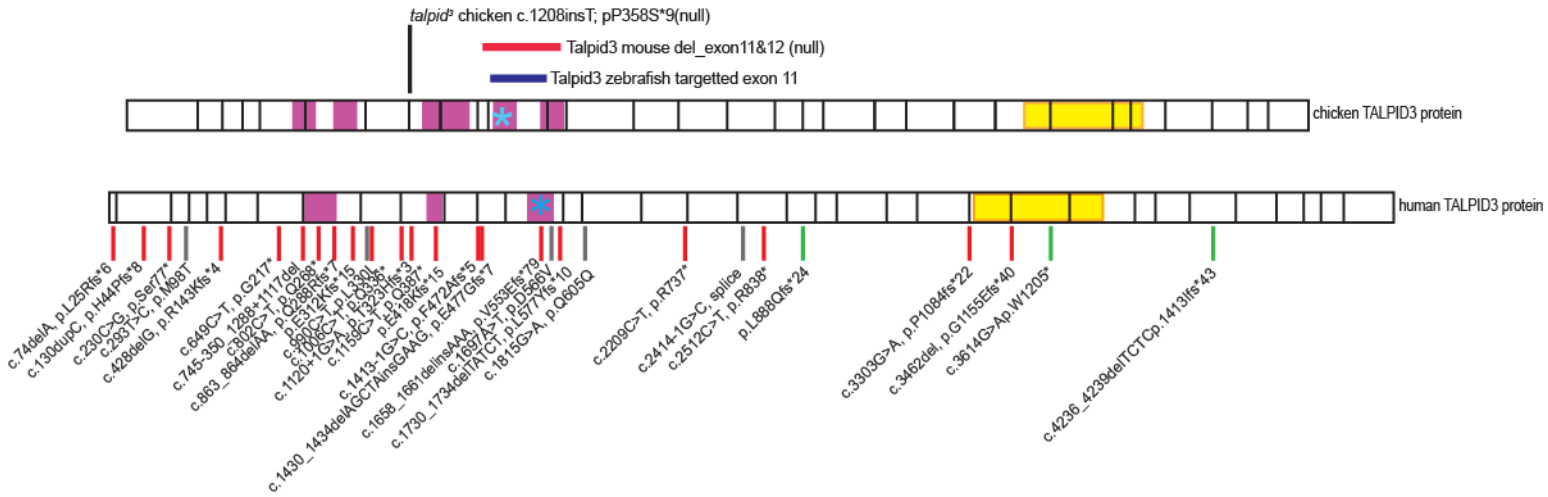

Figure 1.7 Schematic of chicken TALPID3 protein and human KIAA0586 protein demonstrating where the chicken, mouse, zebrafish and human mutations occur. The coiled-coil domains are marked in purple, with the conserved coiled-coil domain essential for function marked by a blue asterisk. The yellow region marks the predicted intrinsically disordered domain. The black line above the chicken protein schematic marks where the protein is truncated in the *talpid*^{3} chicken mutant. The red line above the chicken protein schematic marks the region deleted in the talpid3$^{-/-}$ mouse model. The blue line above the chicken protein schematic marks the region mutated in the *TALPID3* knockdown zebrafish model. The lines below the human KIAA0586 protein mark all the known human patient mutations, demonstrating the wide range of mutations that are not limited to the conserved essential coiled-coil domain. Red lines indicate mutations that result in a premature stop codon, grey lines indicate a splice variant mutation and green lines indicate single deleterious mutations.

The chicken, zebrafish and mouse models all share a similar facial phenotype that results in hypoteleorism in the chicken, fused medial and lateral nasal processes in the mouse and mild cyclopia in the zebrafish. Additionally all three models have polydactyly, which presents in the zebrafish as symmetrical pectoral fins, as well as vasculature defects and skeletal defects (Bangs et al., 2011; Ben et al., 2011; Ede & Kelly, 1964; Davey et al., 2007; Davey et al., 2006; Mohammed, 1986). Other characteristics include abnormalities in the chicken liver and lungs, abnormal heart looping in the mouse not seen in the chicken and a cystic kidney phenotype in the zebrafish and chick (Bangs et al., 2011; Ben et al., 2011; Davey et al., 2014; Yin et al., 2009).

TALPID3 mutations in all the animal models (*talpid*^{3} chicken, talpid3$^{-/-}$ mouse and the *TALPID3* knockout zebrafish) are lethal and causes a loss of both primary and motile cilia (Figure 1.8) (Bangs et al., 2011; Ben et al., 2011; Stephen et al., 2013; Yin et al., 2009). In *talpid*^{3} mutants, the basal bodies fail to orientate and migrate to the apical surface of the cell, resulting in a failure of the basal body to dock (Stephen et al., 2013, 2015; Yin et al., 2009), thus resulting in a loss of ciliogenesis. This loss of basal body migration and docking was also seen in the mouse mutant and the zebrafish mutant (Bangs et al., 2011; Naharros et al., 2018), confirming the shared role for TALPID3 in all three models. The loss of ciliogenesis is responsible for Hedgehog signalling pathway defects, which leads to abnormal levels of Gli proteins causing many of the abnormalities associated with defective Hedgehog

signalling in the mutant *TALPID3* models (Bangs et al., 2011; Ben et al., 2011; Davey et al., 2006).

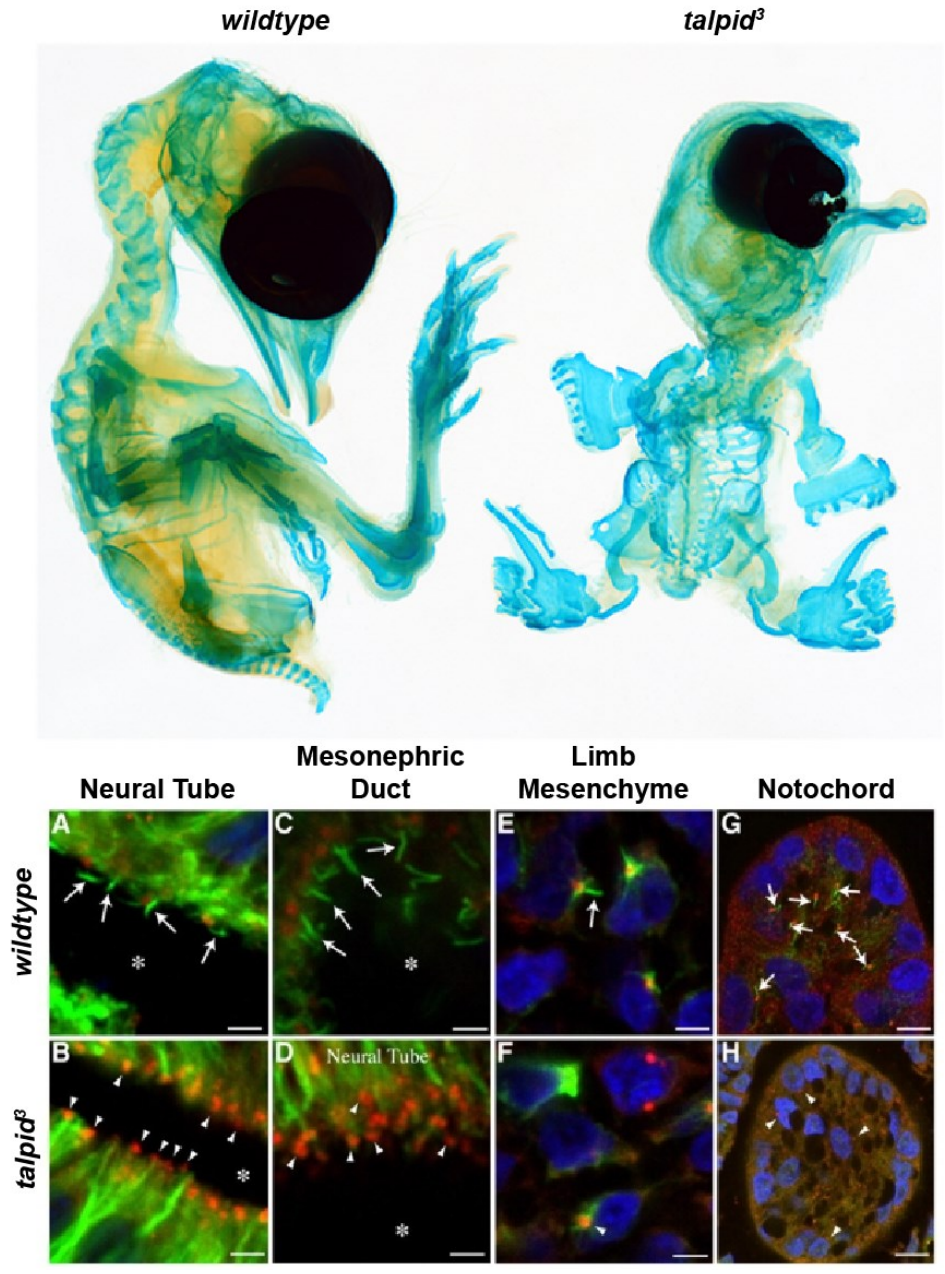

Figure 1.8 Talpid^3 chicken mutant. Cartilage skeletons of E14 *talpid^3* mutant and wildtype sibling, showing skeletal defects including polysyndactyly in wings and legs of mutant. Image taken from Davey et al., 2018. (**A-H**) Anti-gamma tubulin (red) to mark centrosomes and anti-acetylated tubulin (green) to mark cilia. Wildtype tissue sections contain cilia indicated by white

arrows. *Talpid*^{3} mutant tissue sections are lacking cilia as marked by white arrowheads. Taken from Yin et al., 2009.

In the developing limb bud of wildtype chick embryos, both Gli3 activator (Gli3A) and Gli3 repressor (Gli3R) proteins are expressed; Gli3R is present in a gradient along the anterior-posterior axis with higher levels of Gli3R in the anterior region of the limb bud. However, *talpid*^{3} mutant limb buds have a much higher level of Gli3A and fail to form the Gli3R gradient. Characterisation of dorsoventral patterning of the neural tube in *talpid*^{3} demonstrated that there is a loss or reduction of ventral genes (loss of function phenotype) accompanied by a ventral expansion of the genes expressed in the dorsal neural tube (gain of function phenotype), which shows a loss of Hedgehog function and failure of Gli3A function. Despite the increased levels of Gli3A compared to Gli3R in the mutant, evidence in the neural tube shows that the Gli3A protein produced fails to function correctly in *talpid*^{3} (Davey et al., 2006). Rescue of the abnormal dorsoventral patterning of the neural tube can be achieved by electroporation of an activated Gli construct that is able constitutively translocate to the nucleus or by electroporation of a full length TALPID3 construct, demonstrating that this abnormal patterning in the talpid3 neural tube is caused by failure of correct Hedgehog signal transduction pathway (Davey et al., 2006; Yin et al., 2009). Dorsoventral patterning of somites is also disrupted in *talpid*^{3}, with an expansion and shift of cell types into more dorsal domains, which resembles a gain of function phenotype. This results in displacement of cells that mark boundaries between the myotome and dermomyotome during development (Davey et al., 2006).

Hedgehog signalling plays a key role in liver development by acting to control the balance between hepatoblast proliferation and differentiation into hepatocytes; additionally Sonic hedgehog plays a role in liver regeneration and repair, highlighting a need for cilia on liver cells (Hirose et al., 2009; Ochoa et al., 2010). However, cilia are not just required for hedgehog signalling in the liver, cilia on cholangiocytes, the epithelial cells lining the bile duct, are much longer and are required for mechanosensory, osmosensory and chemosensory functions (Masyuk et al., 2006). Loss of the long cilia on cholangiocytes leads to cystic and fibrotic liver disease (Strazzabosco & Somlo, 2011). In *talpid*^{3}, the loss of short cilia in the liver suggests that hepatic abnormalities are due to aberrant Hedgehog signalling, however loss of long cilia on cholangiocytes could also contribute to liver fibrosis seen in *talpid*^{3} (Davey et al., 2014).

Talpid^{3} mutants have severe abnormalities in lung development, which can be mimicked in the wildtype by introducing the Sonic Hedgehog inhibitor cyclopamine. This evidence, combined with the loss of primary cilia in the three main tissue types of the lung suggest that the disruption of lung morphogenesis and consequent defects in the epithelium and mesenchyme in *talpid*^{3} is a result of the loss of Hedgehog signalling (Davey et al., 2014). Defects, including haemorrhaging and oedema, are also present in *talpid*^{3} (Ede & Kelly, 1964; Davey et al., 2007; Mohammed, 1986). These defects have also been attributed to the aberrant Hedgehog signalling due to a loss of cilia. Similar to the loss of polarised gene expression in *talpid*^{3} limb buds

that leads to polydactyly, the antero-posterior vascular pattern is also lost in the *talpid*^{3} limb as a result of loss of Gli3R function (Davey et al., 2007).

The inability of centrosomes to orientate in *talpid*^{3} highlights a role for TALPID3 in polarity, independent of Hedgehog signalling (Stephen et al., 2015). This role for TALPID3 is supported by the polycystic kidney phenotype that is frequently due to a loss of orientated cell division (Happé et al., 2011; Yin et al., 2009), cell migration defects that could be due to a loss of cell polarity (Bangs et al., 2011), as well as more recent work in the *TALPID3* mutant zebrafish model (Naharros et al., 2018). The skin and inner ear, two highly polarised tissues independent of Hedgehog signalling, are disrupted in *talpid*^{3}. *Talpid*^{3} skin lacks characteristic rostral-caudal polarisation that is found in wildtype. Additionally, the hair cells of the inner ear in wildtype have a highly polarised structure that is determined by the non-canonical Wnt-PCP signalling pathway. Wildtype inner ear hair cells form an orientated actin-based stereocilia bundle, which forms a kinocilium and orientates in a specific direction; in contrast, inner ear hair cells in *talpid*^{3} lack a kinocilium and form stereocilia bundles that lack specific orientation demonstrating the disrupted polarity in *talpid*^{3} mutants (L. A. Stephen et al., 2015). An additional actin phenotype was reported in the *talpid*^{3} mutant, which showed a discontinuous band of F-actin at the apical edge of the developing neural tube as well as fewer stress fibres (and fewer focal adhesions) in *talpid*^{3} mutant limb cells compared to wildtype (Wang et al., 2018; Yin et al., 2009).

The human *KIAA0586* ciliopathy patients present with a range of characteristics that are similar to the chicken, mouse and zebrafish models, such as skeletal defects, brain defects and in a small number of cases polydactyly (Akawi et al., 2015; Alby et al., 2015; Bachmann-Gagescu et al., 2015; Malicdan et al., 2015; Roosing et al., 2015; Stephen et al., 2015), supporting the conserved role for *KIAA0586/TALPID3* during development. However, unlike the chicken, mouse and zebrafish models, only a small number of human patients with mutations in *KIAA0586* have been reported to be lethal (Alby et al., 2015) instead presenting with a much less severe phenotype. The majority of the patients were diagnosed with Joubert Syndrome, which can be identified by the presence of the Molar Tooth Sign on an axial MRI brain scan (Maria et al., 1999; Parisi, 2009); the molar tooth sign is typically accompanied by intellectual impairment or developmental delay, hypotonia in infancy, abnormal eye movements and irregular breathing (Parisi, 2009). Ciliogenesis in *KIAA0586* ciliopathy patients has not been explored widely, however in the three patients where ciliogenesis was examined, a significant reduction in ciliogenesis was observed but not a complete loss (Alby et al., 2015; Malicdan et al., 2015).

In conclusion, the abnormalities seen in the *talpid*^{3} chicken, the talpid3$^{-/-}$ mouse and the *TALPID3* knockdown zebrafish demonstrate the severe phenotype caused by a loss of TALPID3 protein during development. The similarities in the phenotype observed in all three mutant models demonstrates the conserved function of TALPID3 and its requirement during embryonic development. The human patients share many of the phenotypes

and demonstrate a reduction in ciliogenesis, thus supporting a conserved function of KIAA0586 in humans. However, the less severe phenotype associated with human *KIAA0586* ciliopathy patients and the lack of complete loss of ciliogenesis in humans suggests a potential difference in the way the human mutations affect protein production.

1.3.1 TALPID3 protein interacting network

TALPID3 was first identified as a hypothetical centrosome protein in a proteomic study aimed at characterising the proteins in the centrosome (Andersen et al., 2003). A further proteomic study aimed at mapping the centrosome identified KIAA0586 with other known and novel centrosome proteins, all of which were grouped based on their localisation to substructures within the centrosome. This study placed TALPID3 in the centrosome (Jakobsen et al., 2011), confirming previous studies (Andersen et al., 2003; Yin et al., 2009), however it did not specify localisation to any substructures within the centrosome or its potential localisation elsewhere in the cell. Following a proteomic screen for members of the CP110-containing complexes, immunoprecipitation showed that KIAA0586 binds to CP110 and more weakly interacts with Cep97, Cep290 and Kif24. Immunohistochemistry to confirm the proteomic results showed that KIAA0586 forms a ring-like structure around CP110 at the distal end of the centriole in human RPE1 cells (Kobayashi et al., 2014). Despite the interaction between TALPID3 and CP110, MEFs taken from $CP110^{-/-}$ mice showed no change to TALPID3 localisation, demonstrating that CP110 is not needed for recruitment of TALPID3 to the basal body (Yadav et al., 2016). The cell studies in RPE1 cells suggest that TALPID3 might interact with CP110 to prevent CP110 from suppressing cilia formation, however the $CP110^{-/-}$ mouse demonstrates that CP110 also acts as a positive regulator of ciliogenesis (Yadav et al., 2016) suggesting a more complex role for the protein and a different role for the interaction of TALPID3.

Examination of KIAA0586 and Cep290 showed that ablation of either protein resulted in an accumulation of centriolar satellites in cells able to produce cilia. Additionally, the study found that KIAA0586 and Cep290 are needed to recruit Rab8a to the centrosome during the early stages of ciliogenesis, suggesting an interaction between KIAA0586 and Rab8A (Kobayashi et al., 2014). Immunostaining for Cep290, in human fibroblasts lacking KIAA0586, showed that loss of KIAA0586 corresponded to an abnormal extended pattern of Cep290 (Alby et al., 2015), suggesting that Cep290 acts downstream of KIAA0586. Loss of KIAA0586 or Cep290 results in an accumulation of PCM1 granules around the centrosome leading to an accumulation of centriolar satellites that corresponds to defects in cilia formation (Kobayashi et al., 2014). This accumulation of satellites is consistent with accumulation of PCM1 seen in *talpid*^{3} cells (Stephen et al., 2015). PCM1 is required for restricting the E3 ligase, Mindbomb1 (Mib1), to the satellites. Loss of PCM1 results in translocation of Mindbomb1 to the centriole, where it interacts with and destabilises TALPID3 resulting in a loss of ciliogenesis (Wang et al., 2016). This suggests a regulatory pathway involving PCM1, Mib1 and TALPID3.

Co-staining of embryonic fibroblasts, taken from a patient homozygous for c.1815G>A splice variant mutation in *KIAA0586*, showed that loss of KIAA0586 does not affect the localisation of the distal appendage protein Cep164 or the subdistal/distal appendage protein ODF2 (Alby et al., 2015). *Talpid*^{3} mutants do not show a change in Cep164 localisation despite a loss of centriole orientation, however the CEP164 puncta are smaller than in

wildtype (Stephen et al., 2015). Loss of KIAA0586 does not lead to a loss of distal or subdistal appendages. Therefore, despite Cep164 being shown to localise in a ring around KIAA0586 at the distal end of the mother centriole (Kobayashi et al., 2014), these results demonstrate that Cep164 does not interact with KIAA0586.

KIAA0586 has also been shown to interact with Cep120, a centrosome protein that is required for centriole duplication and elongation (Comartin et al., 2013a; Mahjoub et al., 2010; Wu et al., 2014). KIAA0586 regulates asymmetric localisation of Cep120 to the daughter centriole; specifically the region between amino acids 470-638 of KIAA0586 is essential for Cep120 to bind to KIAA0586 (Wu et al., 2014). Overexpression of Cep120 causes abnormal centriole elongation resulting in the production of extra-long centrioles (Comartin et al., 2013b; Lin et al., 2013). This, taken with the data showing KIAA0586 is needed for Cep120 to asymmetrically localise to the daughter centriole, suggests that KIAA0586 inhibits Cep120 through its interaction. Additionally TALPID3 has been shown to interact with Microtubule-Actin Cross Linking Factor 1 (MACF1), a ciliogenesis protein that is required in the early stages of ciliogenesis and required for maintenance of basal body positioning in differentiated tissue (May-Simera et al., 2016). Taken together, the protein interactions described above between KIAA0586/TALPID3 and other centrosome proteins suggest a complicated network in which KIAA0586 is essential for distinct roles and protein networks involved in different processes controlling centriole function (Figure 1.9).

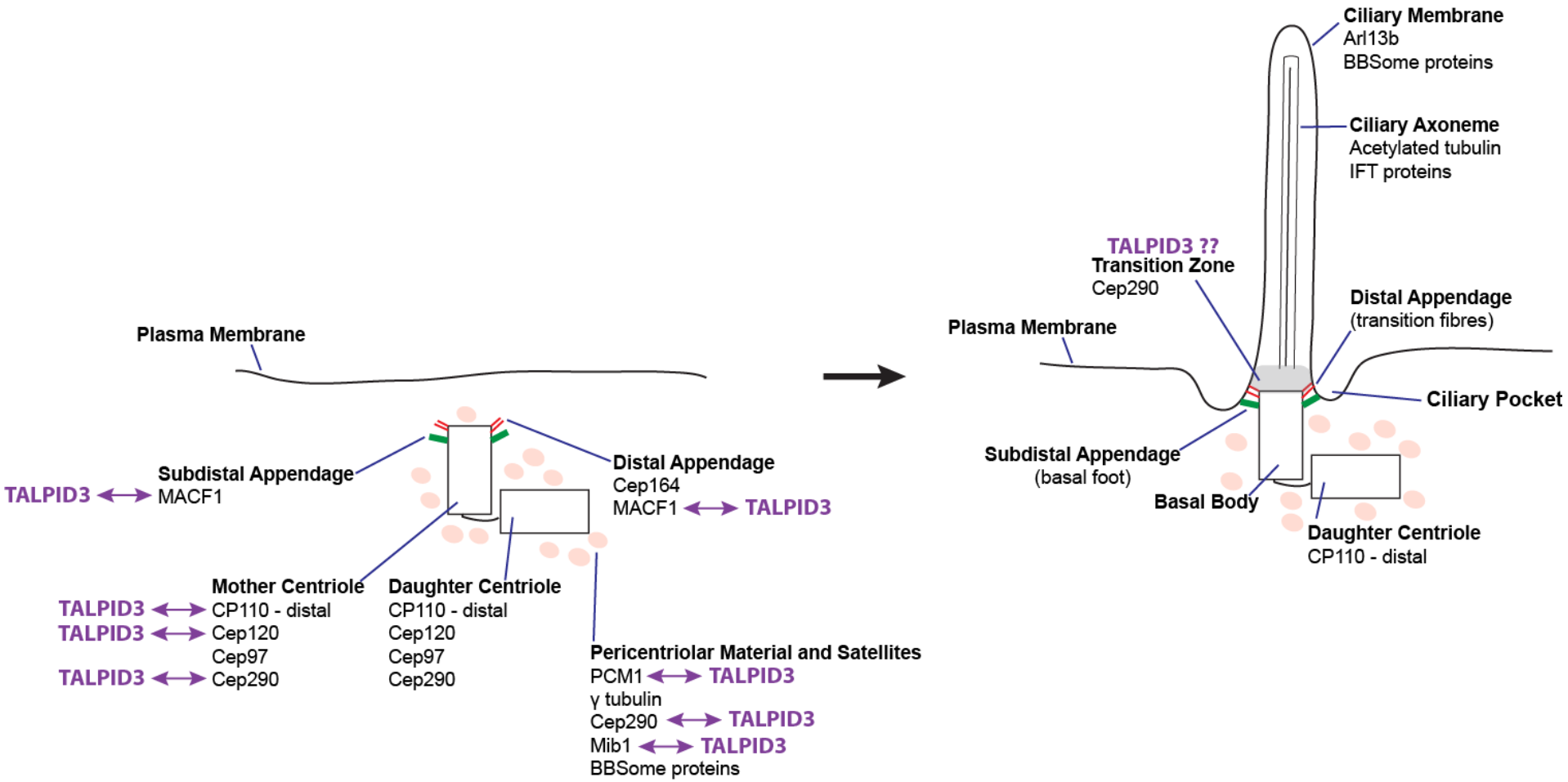
Plasma Membrane
Subdistal Appendage
MACF1
TALPID3
Distal Appendage
Cep164
MACF1 TALPID3
Mother Centriole
CP110 - distal
Cep120
Cep97
Cep290
TALPID3
TALPID3
TALPID3
Daughter Centriole
CP110 - distal
Cep120
Cep97
Cep290
Pericentriolar Material and Satellites
PCM1 TALPID3
γ tubulin
Cep290 TALPID3
Mib1 TALPID3
BBSome proteins
Ciliary Membrane
Arl13b
BBSome proteins
Ciliary Axoneme
Acetylated tubulin
IFT proteins
TALPID3 ??
Transition Zone
Cep290
Distal Appendage
(transition fibres)
Plasma Membrane
Ciliary Pocket
Subdistal Appendage
(basal foot)
Basal Body
Daughter Centriole
CP110 - distal

Figure 1.9 TALPID3 protein interactions at the centrosome. TALPID3 interacts with proteins in the centrosome that are involved in different processes and are known to localise to distinct regions. TALPID3 interacts with proteins found in the mother and daughter centrioles, proteins in the pericentriolar material and also MACF1, which is found at the appendages on the mother centriole. Each of these proteins is involved in slightly different functions within the centrosome and with the exception of CP110 and Cep290, are not known to interact with one another. There is no further evidence to confirm whether TALPID3 has a role in ciliogenesis after orientation and docking of the basal body at the cell membrane, however it is possible that TALPID3 localises to the transition zone during ciliogenesis.

1.3.2 What gaps still remain in our knowledge of TALPID3/KIAA0586?

There are still questions surrounding the functional domains of TALPID3/KIAA0586, due to the inability to predict the protein structure of the predicted intrinsically disordered domain (Davey et al., 2006; Yin et al., 2009). Evidence from complementation assays and localisation studies suggest that the TALPID3/KIAA0586 protein has additional functional domains at the C-terminal that rely on the essential coiled-coil domain for localisation to the centrosome (Davey lab, unpublished; Kobayashi et al., 2014; Yin et al., 2009). The phenotypes associated with the lethal animal models compared to the varying non-lethal phenotypes associated with the human *KIAA0586* ciliopathy patients suggest that the human patients may have an unidentified compensatory mechanism to provide some protein function (Akawi et al., 2015; Bachmann-Gagescu et al., 2015; Bangs et al., 2011; Ben et al., 2011; Davey et al., 2006; Malicdan et al., 2015; Roosing et al., 2015; Stephen et al., 2015). The remaining unanswered questions highlight the need for an approach to model the human mutations using an assay that can provide insight into the functional domains within the protein.

TALPID3/KIAA0586 has been confirmed as a protein that localises to the centrosome and that is required for correct centriole orientation prior to basal body docking at the cell membrane during ciliogenesis (Bangs et al., 2011; Ben et al., 2011; Kobayashi et al., 2014; Stephen et al., 2015; Yin et al., 2009). However, it is still unclear what centrosome proteins TALPID3 interacts with or when and where in the centrosome it interacts with those

proteins, to control centriole orientation. A number of proteins including CP110, PCM1, Cep290, MACF1, Cep120 and Mib1 have been shown to interact with TALPID3 (Kobayashi et al., 2014; May-Simera et al., 2016; L. Wang et al., 2016; Wu et al., 2014), however these proteins are involved in different functions during centriole formation and ciliogenesis, highlighting the complexity of the role of TALPID3 in the centrosome. TALPID3 has also been shown to localise to the distal end of the centrioles (Kobayashi et al., 2014; Wu et al., 2014), which leads to the question of how it interacts with proteins that localise elsewhere in the centrosome, such as PCM1, which localises to the pericentriolar material and how it can produce a satellite phenotype (Kobayashi et al., 2014; Stephen et al., 2015) from its position at the mother centriole. In addition to a complicated network of protein interactions in the centrosome, evidence from the actin phenotype seen in *talpid*^{3} mutant suggests that TALPID3 could play a role in the regulation of the actin cytoskeleton (Yin et al., 2009). This potential involvement in the regulation of actin suggests that TALPID3 may also have a functional role outside the centrosome. Therefore, it is likely that TALPID3 has a role in several different protein networks that control different functions, instead of multiple different proteins being involved in a novel 'TALPID3 protein network,' highlighting the need for further proteomic studies into the *talpid*^{3} proteome. In addition, the dynamic localisation of TALPID3 during the cell cycle has remained unexplored; a tool to examine the endogenous localisation of TALPID3 during the cell cycle could provide some insight into

when and where in the centrosome TALPID3 has the opportunity to interact with other centrosome proteins.

1.4 General thesis aims

To date, the predicted intrinsically disordered domain in TALPID3 has led to failed attempts to determine the structure of the protein as well as hampering attempts to identify additional functional domains. Furthermore, the complicated nature of TALPID3 protein interactions in the centrosome has also prevented identification of the complete TALPID3 protein network.

My thesis had three main aims. The first aim was to identify a method to model human KIAA0586 ciliopathy mutations that would allow identification of hypomorphic mutations and could provide insight into additional functional domains. The second aim was to identify a proteomic approach that was viable for studying the TALPID3 proteome in chicken Primordial Germ Cells, providing a proteomic method to study the *talpid*^{3} mutant proteome in a ciliated cell line for the first time. The third aim was to use the identified proteomic approach to uncover novel insights into the *talpid*^{3} proteome regarding altered protein pathways in *talpid*^{3} compared to wildtype.

Chapter 2. Materials and Methods

2.1 Nomenclature of *KIAA0586/TALPID3*

In accordance with the Chicken Gene Nomenclature Committee (CGNC) *TALPID3* and TALPID3 were used for designation of the chicken gene and protein, respectively. In accordance with the Human Gene Nomenclature Committee (HGNC), *KIAA0586* and KIAA0586 were used for designation of the human gene and protein, respectively. Although the current gene symbol for the mouse gene is 2700049A03Rik and mouse protein is 2700049A03RIK, I have used *KIAA0586* and KIAA0586 as the gene and protein names respectively. Where I make a generic conclusion on the function of the orthologues of *KIAA0586* I have used *KIAA0586*. As published, I have referred to the chicken model as *talpid*^{3} and the mouse model as talpid3$^{-/-}$ through-out this thesis. The nomenclature of human *KIAA0586* mutations described in this thesis refers to reference sequence NM_001244189.1 (corresponding protein: NP_001231118.1).

2.2 Cell Culture

Cell culture was completed in a sterile hood. All live cell experiments were completed under sterile conditions, with all equipment and materials

cleaned and sterilised with 70% ethanol prior to use. An Olympus CK2 Inverted microscope was used for analysing all cells.

2.2.1 Culturing cells

Human RPE1 (retinal pigmented epithelial) cells were cultured in DMEM/F12 media (Lonza BE04-687F/U1), supplemented with 10% fetal bovine serum (FBS) (PAA A15-151), 1% L-glutamine and 1% streptomycin/penicillin at 37°C, 5% CO_2 (carbon dioxide). Cells were passaged every 2-3 days. To passage cells, media was removed, cells were washed twice with 2-3 ml of pre-warmed DPBS (Life Technologies 14190094) to remove residual media. Cells were treated with 1 ml of TrypLE (Life Technologies 12604013) at 37°C for 2-5 minutes until dissociated. Following dissociation, 2-3 ml of DMEM/F12 media was added to stop the dissociation reaction. Cells were then pelleted in a falcon tube at 180 x g for three minutes in a Sigma 3-16 centrifuge, supernatant was discarded and cells were resuspended in fresh media, pre-warmed to 37°C.

Human Jurkat cells were cultured in suspension in RPMI 1640 (Life Technologies 21875034), supplemented with 10% FBS at 37°C, 5% CO_2. Cells were passaged every 2-3 days. To passage cells, media containing cells in suspension was transferred to a Falcon tube and pelleted at 180 x g for three minutes in a Sigma 3-16 centrifuge. The supernatant was discarded and the pellet was resuspended in fresh media, pre-warmed to 37°C.

Chicken Primordial Germ Cells (PGCs) were cultured in FAOT media in suspension at 37°C, 5% CO_2. PGC media: Diluted DMEM was made up with 76% DMEM (Life Technologies 21068-028), 22% tissue culture grade water, supplemented with 1% Sodium pyruvate and 1% MEM Vitamin Solution. The diluted DMEM was supplemented with B27 (50x), Glutamax (100x), NEAA (100x), Nucleosides (100x), Pyruvate (100x), B-mercaptoethanol, $CaCl_2$, Ovalbumin (20%) and Na Heparin (50 mg/ml) to make B27 diluted DMEM. This was stored at 4°C and protected from the light. From the B27 diluted DMEM, FAOT media was made with h-Activin (25 µg/ml), h-FGF2 (25 µg/ml) and Ovotransferin (10 mg/ml). FAOT was also stored at 4°C and protected from the light. The PGCs were fed or passaged every 2-3 days. To feed cells, half of the media that cells were suspend in was removed and discarded and replaced with fresh media pre-warmed to room temperature. To passage, media containing cells in suspension was transferred to Eppendorf tubes and cells were pelleted at 1.7 rpm for four minutes in a miniSpin plus Eppendorf centrifuge, supernatant was discarded and cell pellet was resuspended in fresh media pre-warmed to room temperature.

2.2.2 Freezing cells

RPE1 cells at approximately 80% confluency were pelleted at 180 x g for three minutes in a Sigma 3-16 centrifuge. Supernatant was discarded and cells were resuspended in 2 ml culture media supplemented with an additional 60% FBS and 10% DMSO (Sigma D2650) and divided between two

cryogenic tubes. Cells were initially snap frozen at -80°C where they remained for 24 hours, following which they were transferred on dry ice to -150°C for long-term storage.

Jurkat cells at approximately 80% confluency were pelleted at 180 x g for three minutes in a Sigma 3-16 centrifuge. Supernatant was discarded and cells were resuspended in 2 ml culture media supplemented with 5% DMSO and divided between two cryogenic tubes. Cells were initially snap frozen at -80°C where they remained for 24 hours, following which they were transferred on dry ice to -150°C for long-term storage.

PGCs at approximately 80% confluency were pelleted at 1600 rpm for 4 minutes in a miniSpin plus Eppendorf centrifuge. Cells were resuspended in 250 µl of B27 stock solution media. 250 µl of freezing media (B27 stock solution media with 8% DMSO, 10% Biosera CS and 37.5 µl 20mM $CaCl_2$) was added and mixed by gently pipetting up and down. The cells were divided between two cryovial tubes, labelled and frozen at -80°C. 24 hours later, the cells were transferred on dry ice to -150°C for long-term storage.

2.2.3 Thawing cryopreserved cells

Cells were removed from -150°C storage and transferred on dry ice to cell culture lab. RPE1 cells and Jurkat cells were thawed at 37°C in a water bath and PGCs were thawed gradually at room temperature. 1 ml of pre-warmed cell-appropriate media was added, cells were pelleted and supernatant

removed. Cells were then resuspended and seeded at an appropriate density.

2.2.4 Deriving *talpid*^{3} flock primordial germ cell lines

Eggs from the *talpid*^{3} flock were incubated for 50-60 hours, until the embryos were Hamburger Hamilton stage 15-16. Eggs were windowed and the membrane was removed. A needle was inserted into the dorsal aorta and approximately 1 µl of blood was removed by mouth pipetting, typically containing approximately 50 cells. Needles were pulled on a Moving-Coil Microelectrode Puller Model 753 (Campden Instruments Limited) using the following settings: pre-pull heating time 57, initial pull force 159, main pull force 286, main pull delay 49, heater control 139. Blood was transferred to a single well in a sterile 48-well plate containing 300 µl of FAOT media. 90 µl of FAOT media was removed and replaced with 100 µl of fresh FAOT media every 2-3 days for 10-14 days. After 10-14 days, cultures were pelleted, resuspended in 500 µl FAOT and transferred to a single well in a 24-well plate. The cell lines were cultured and expanded as described previously (section 2.2.1).

2.2.5 Cell transfections

For RPE1 cell transfections: 1.5 µg DNA was mixed with 100 µl Opti-MEM I reduced serum media (Gibco, cat no. 31985-0620) and incubated at room temperature for 5 minutes. 2 µl of Lipofectamine2000 (Invitrogen cat no. 11668027) was added to 100 µl of Opti-MEM I per transfection and

incubated at room temperature for 5 minutes. DNA and Lipofectamine2000 mixes were added together and incubated at room temperature for 20 minutes. RPE1 cells were grown in a 6-well plate, to 70% confluence. Media on cells was replaced with 3 ml Opti-MEM I and the DNA/Lipofectamine mix was added to the cells. Cells were incubated in transfection mix for 24 hours at 37°C, 5% CO_2. After incubation, Opti-MEM I was removed and replaced with DMEM/F12 media for several hours to allow recovery of cells. After 2-3 hours, puromycin was added at a concentration of 5 µg/µl to select for positively transfected cells. After 48 hours, the media containing puromycin was removed and replaced with fresh DMEM/F12 media.

For chicken PGC transfections: 200,000 cells were used per transfection. 2 µg of DNA was added to 150 µl of Opti-MEM I serum media (Gibco, cat no. 31985-0620) in a screw top 1.5 ml Eppendorf tube. 2 µl of Lipofectamine2000 (Invitrogen cat no. 11668027) was added to 148 µl of Opti-MEM I in a separate screw top 1.5 ml Eppendorf tube. Both tubes were incubated at room temperature for approximately 20 minutes. Tubes were combined (transfection mix) and flicked 5 times to mix, then incubated at room temperature for 25 minutes to allow complexes to form. Cells were pelleted at 1600 rpm for 4 minutes and media removed. Cells were resuspended in 750 µl of Opti-MEM, to wash and then re-pelleted at 1600 rpm for 4 minutes. All media was removed and cells were resuspended in 50 µl of Opti-MEM per transfection. 50 µl of cells in suspension was added to 300 µl of transfection mix by gently pipetting up and down 5 times. Cells were incubated upright at 37°C, 5% CO_2 for approximately 6 hours, with cap

loosened to allow CO_2 and oxygen to enter the Eppendorf tube. Following approximately 6 hours of incubation, cells were pelleted at 2200 rpm for 10 minutes, transfection solution was discarded and cells were resuspended in FAOT media and transferred to a fresh well in a 24-well plate. 24 hours later, 2.0 µl of 0.1 mg/ml of Puromycin was added to transfected cells and incubated for 48 hours to select for positively transfected cells. After 48 hours, cells were pelleted at 1600 rpm for 4 minutes, washed with B27 stock media and re-pelleted at 1600 rpm for 4 minutes. Cells were then resuspend in fresh FAOT media.

2.3 Protein

2.3.1 Protein extraction from cells

RPE1 cells, Jurkat cells or chicken PGCs were expanded in culture. Cells were pelleted at 180 x g in a Sigma 3-16 centrifuge. Cells were resuspended in 1 ml of ice cold DPBS to wash, then re-pelleted at 4000 rpm, 4°C for 3 minutes. DPBS was removed and pellet resuspended in 50-150 µl of SDT label free lysis buffer: 100mM Tris-HCl (pH7.6), 4% (w/v) sodium dodecyl sulfate and 1% HALT protease inhibitors (100X). A mini homogeniser was used to resuspend pellet, following which sample was incubated on ice for 30 minutes. Sample was then centrifuged at 20,000 x g, 4°C for 20 minutes. Supernatant, containing protein, was removed, transferred to a fresh, labelled tube and then stored at -80°C to prevent degradation.

2.3.2 Centrosome Isolation

Cells in suspension were grown up to a density of approximately 2 x 10^6 cells/ml in T-160 flasks. Total number of cells for carrying out centrosome isolation was approximately 1 x 10^9. Cells were treated with 60 ng/ml nocodazol (stock solution: 5 mg in 10 ml DMSO, stored at -20°C) and 1 µg/ml cytochalasin D (stock solution: 2 mg in 1 ml DMSO stored at -20°C) for 1 hour at 37°C, to prevent association of microtubules with the centrosome during isolation. Cells were transferred to 50 ml falcon tubes and pelleted at 2500 rpm, 10 minute, 4°C. Cell pellet was washed with half the initial suspension volume of 1 X TBS (Tris-buffered saline: 10 mM Tris.HCl, pH 7.4 / 150 mM NaCl, stored at 4°C) (25 ml per 50 ml tube), then washed again with half the previous volume of TBS 0.1-8% sucrose buffer (100 ml TBS + 80 g sucrose made up to 1 Litre with distilled water, made fresh) (12.5 ml per 50 ml tube). Cells were re-pelleted between each wash at 2500 rpm, 5 minutes, 4°C. Cells were resuspended in 20 ml TBS 0.1-8% sucrose buffer per tube. Lysis buffer (1 mM Hepes pH 7.2, 0.5% NP-40, 0.5 mM $MgCl_2$, 0.1% β-mercaptoethanol, 1 mM PMSF + 1 µg/ml leupeptidin, peptstatin A and aprotinin, made fresh) was added and then incubated on ice for 5 minutes. Nuclei/chromatin was pelleted at 4000 rpm for 10 minutes at 4°C. Lysate was filtered through one layer of medical gauze to remove chromatin and nuclei. 10 mM Hepes was added to lysate to digest the remaining chromatin and 10 µg/ml DNAse I was added to lysate and incubated for 30 minutes at 4°C. Lysate was transferred to centrifuge tubes and 5 ml 50% sucrose solution was gently pipetted to the

bottom of the tube. Centrosomes were deposited onto the 50% sucrose cushion, by spinning at 11000 rpm for 20 minutes at 4°C in a TH13 rotor. 50% sucrose cushions and centrosomes were removed, pooled and mixed. Centrosomes in sucrose solution were gently pipetted into a new centrifuge tube on top of a discontinuous sucrose gradient: 5 ml 70% sucrose, 3 ml 50% sucrose, 3 ml 40% sucrose. All sucrose solutions were made weight/weight sucrose to gradient buffer (10 mM K.Pipes pH 7.2, 0.1% Triton X-100, 0.1% β-mercaptoethanol). The sucrose gradient was centrifuged at 25000 rpm for 75 minutes at 4°C in a SW28 rotor, in a Beckman Coulter Optima L-100K UltraCentrifuge, to collect the centrosomes at the bottom of the centrifuge tube. Elution was performed at room temperature by making a hole in the bottom of the centrifuge tube using a 20G needle. Twenty 0.5 ml fractions were collected and snap frozen in liquid nitrogen, labelled and stored at -80°C.

2.3.3 Protein extraction from centrosomes

Centrosomes from fractions 6-10, determined based on previous protocol (Andersen et al., 2003), were spun out of sucrose solution at 100,000 x g in a SW28 rotor on a Beckman Coulter Optima L-100K Ultracentrifuge. Supernatant was poured off; the remaining sucrose solution was removed by pipette taking care not to disturb the protein pellet. Pellet was transferred to a 1.5 ml Eppendorf and any protein pellet left behind was scraped off and transferred to 1.5 ml Eppendorf to ensure no loss of protein.

Protein was pelleted at 20,000 x g, 4°C for 20 minutes. Excess supernatant was removed. Pellet was resuspended in 50 µl of SDT label free lysis buffer: 100 mM Tris-HCl (pH7.6), 4% (W/V) sodium dodecyl sulfate and 1% HALT protease inhibitor cocktail (100X). To resuspend completely, sample was pipetted up and down. A mini homogeniser was used when the pellet was big or difficult to resuspend by pipetting. Protein sample was incubated on ice for 20 minutes, then centrifuged at 20,000 x g, 4°C for 20 minutes. Supernatant, containing centrosome proteins, was transferred to a new 1.5 ml Eppendorf tube. Pellet was kept as a negative control and both were stored at -80°C.

2.3.4 BCA Assay

Concentration of protein samples was calculated using a Thermo Scientific Pierce microBCA Protein Assay kit (23235), following user manual instructions in the kit. Working solution was made up using 50% reagent A, 48% reagent B and 2% reagent C. BSA protein contained in kit was vortexed and used for making protein standards as follows: blank, 2 µg/µl, 4 µg/µl, 6 µg/µl, 8 µg/µl, 10 µg/µl and 20 µg/µl. All protein samples to be quantified were vortexed and diluted in working solution, adding 1 µl of each protein sample to 1 ml of working solution. All protein standards and protein samples were done in duplicate. Protein standards and samples were mixed by hand, incubated at 60°C for 60 minutes and decanted into cuvettes (Fisher Scientific, Cuvette semi-micro disposable 10 mm light path

11547692). Samples were read on a spectrophotometer at 562 nm to determine optical density. The standards were used to calculate a standard curve and concentration of the protein sample was calculated based on the standard curve.

2.3.5 Western Blot

5 -20 µg of protein, in a volume of 10 µl, was loaded onto a gel. 5 µl of sample buffer (loading dye) was added to each sample and vortexed. Samples were incubated at 98°C for two minutes to linearise protein. 20 X MES or 20 X MOPS running buffer was diluted to a working concentration of 1 X. Packaging, including white strip and comb of a 12-well or 15-well NuPAGE Novex 4-12% Bis-Tris Protein Gel, 1.0 mm was removed. Where large molecular weight proteins were being analysed, a NuPAGE 3-8% Tris-Acetate Protein Gel, 1.0 mm, 15-well gel was used and run in 1 X NuPAGE Tris-Acetate SDS Running Buffer. The wells in the gel were washed with 1 X running buffer by pipetting buffer into wells. Gel was loaded into tank, along with a buffer dam if only one gel was being run in the tank. The middle section of the gel tank was filled with 1 X running buffer; following confirmation that the running buffer did not leak into the sides of the gel tank, sides of tank were filled with running buffer. 2 µl of MagicMark protein ladder (LC5602) was loaded followed by 10 µl of each sample to appropriate wells. Gel was run at 80 V for 5 minutes to check running evenly, following which gel was run at 180 V for 55 minutes. Protein was transferred from gel

to a PVDF membrane using an iBlot1. Anode Stack (bottom) was placed in the iBlot device and a small volume of running buffer was placed on bottom stack to prevent drying out. The gel was removed from the encasement and placed on the PVDF membrane of the anode stack. Filter paper, soaked in deionised water, was placed on top of the gel, followed by the Cathode Stack (top) with copper electrode side facing up. Air bubbles were removed using Blotting Roller and the sponge was placed on the inner side of the lid, with the metal contact at the top right. The iBlot was run on the P3 programme for 7 minutes. PVDF membrane was removed for staining and other components of the stack were discarded.

PVDF membrane was carefully rolled with no overlap and placed in a 50 ml falcon tube. A brief wash with PBS was carried out. PBS was replaced with 5 ml of Odyssey Blocking buffer (PBS), and incubated on a roller at room temperature for 30 minutes. Blocking buffer was discarded and replaced with 5 ml of appropriate primary antibody diluted in Odyssey Blocking buffer (see Table 2.1 for dilutions) with 0.1% tween20, which was left rolling at 4°C overnight. Primary antibody was washed off with 6 x 5 minute washes in PBS, rolling at room temperature. Secondary antibody diluted (1:5000) in 5 ml of Odyssey Blocking buffer, 0.1% tween20, was added and incubated on a roller at room temperature for 90 minutes. The tube was covered in foil to protect from the light. Secondary antibody was washed off with 6 x 5 minute washes in PBS, rolling at room temperature. Membrane was stored in PBS, at 4°C, protected from the light until imaging. Image of membrane was obtained on the LI-COR Odyssey Imaging System.

Where two antibodies were used on the same membrane simultaneously, measures were taken to ensure the antibodies had different host species or antibodies produced a single specific band that was distinct in size with no non-specific bands, to prevent ambiguous results.

2.3.6 Immunofluorescence on cells

Adherent cells were seeded on coverslips. Where ciliogenesis was being examined, cells were cultured in serum-free media for 24 hours, following seeding on coverslips, to induce ciliogenesis.

Suspension cells were grown to appropriate confluence, pelleted, resuspended in 200 µl of cell-appropriate media and spread across poly-L-lysine slides; the slides were incubated at 4°C for 10 minutes to ensure cells adhered to slide. Where ciliogenesis was being examined, cells were serum-starved for 24 hours to induce ciliogenesis, prior to being pelleted and adhered to poly-L-lysine slides.

All cells on coverslips and slides were washed gently with PBS to remove media. Cells were fixed in ice cold methanol for 10 minutes at 4°C, washed 3 times with ice cold PBS and incubated with 100 µl blocking buffer (5% goat serum, 0.1% triton X-100 in PBS) at room temperature for 90 minutes. Non-adherent cells on slides were covered with Parafilm to prevent drying out. Following blocking, primary antibodies were diluted appropriately (Table 2.1) in blocking buffer, pipetted onto cells and incubated overnight at 4°C. Non-adherent cells on slides were covered with Parafilm to prevent drying

out. Primary antibody was removed and cells washed for 1 hour in PBS, rocking at room temperature. Secondary antibodies were diluted appropriately (Table 2.1) in blocking buffer, pipetted on cells and incubated at room temperature for 1 hour in the dark to protect from light. Non-adherent cells on slides were covered with Parafilm to prevent drying out. Secondary antibody was removed and cells washed with PBS for 2 hours, rocking at room temperature. Dapi was diluted 1:35 in PBS, pipetted on the cells and incubated at room temperature for 10 minutes in the dark. Cells were washed in PBS for 10-20 minutes, rocking at room temperature. Excess PBS was removed and slides were mounted on glass cover slips with 2-3 drops of ProLong Gold Antifade Reagent (P10144). Excess PBS was removed from cover slips containing adherent cells and placed on glass slides with 1 drop of ProLong Gold Antifade Reagent (P10144). All mounted slides were retained in the dark at room temperature to cure, prior to imaging.

2.3.7 Cryosectioning and Immunofluorescence on tissue sections

Following fixation, tissue was washed twice in PBS before being washed in gelatine (7% 300 Bloom Gelatine/10% Sucrose) at 37°C. The tissue was then embedded in a block of gelatine with the correct orientation for sectioning. A drop of OCT was added to a square piece of corkboard and the block of gelatine containing the fixed tissue placed in the OCT. The sample was snap frozen in isopentane pre-chilled to -80°C, wrapped in foil, labelled and stored

at -80°C until sectioning. For sectioning, the blocks were transferred to a Cryostat on dry ice, sectioned at 10 µM and sections were spread evenly across poly-L-lysine slides for immunofluorescence staining. Slides containing tissue sections were allowed to dry at room temperature for approximately 30 minutes, washed in PBS at 37°C to remove gelatine and then blocked (5% goat serum, 0.1% triton X-100 in PBS) for approximately 2-3 hours at room temperature, while covered in Parafilm to prevent drying out of tissue. Primary antibodies were diluted appropriately (Table 2.1) in blocking buffer, pipetted onto tissue sections, covered in Parafilm and incubated overnight at 4°C. Primary antibody was removed and cells washed for approximately 90 minutes in PBS while rocking at room temperature. Secondary antibodies were diluted appropriately (Table 2.1) in blocking buffer, pipetted on cells, covered in Parafilm and incubated at 37°C for 1 hour in the dark to protect from light. Where F-actin was also analysed, Phalloidin (A12381) was diluted 5 µl in 200 µl of blocking buffer and incubated on tissue sections for 30 minutes at room temperature in the dark. Phalloidin was washed off with PBS for approximately 1 hour, rocking at room temperature. Dapi was diluted 1:5000 in PBS and incubated on tissue sections at room temperature for 10 minutes in the dark. Dapi was washed off in PBS for approximately 30 minutes, rocking at room temperature. Excess PBS was removed and slides were mounted on glass cover slips with 2-3 drops of ProLong Gold Antifade Reagent (P10144).

Table 2.1 Antibodies used in this thesis. IF indicates application in immunofluorescence and WB indicates application in Western Blot.

Antibody	**Source**	**Species**	**Dilution (Application)**
Gamma Tubulin	Sigma (T5326)	Mouse	1:1000 (IF) 1:2500 (WB)
Gamma Tubulin	Sigma (T5192)	Rabbit	1:1000 (IF) 1:2500 (WB)
Acetylated Tubulin	Sigma (T7451)	Mouse	1:1000 (IF)
Acetylated Tubulin	Sigma (T3526)	Rabbit	1:1000 (IF)
KIAA0586	Sigma (HPA050249)	Rabbit	1:100 (IF)
ARMC3	Sigma (HPA037824)	Rabbit	1:100 (IF)
MYCBPAP	Sigma (HPA023257)	Rabbit	1:100 (IF)
RIBC2	Sigma (HPA003210)	Rabbit	1:100 (IF)
VWA3A	Sigma (HPA041696)	Rabbit	1:100 (IF)
MACF1	Santa Cruz (sc-377534)	Rabbit	1:500 (IF) 1:200 (WB)
CCDC77	Sigma (HPA038854)	Rabbit	1:100 (IF) 1:625 (WB)
CCDC127	Sigma (HPA045052)	Rabbit	1:100 (IF) 1:1250 (WB)
CP110	Abcam (ab99337)	Rabbit	1:500 (IF) 1:2000 (WB)
CP110	ProteinTech (12780-1-AP)	Rabbit	1:500 (IF) 1:500 (WB)
PCM1	Abcam (ab72443)	Rabbit	1:500 (IF)
Pericentrin	Abcam (ab4448)	Rabbit	1:500 (IF)

Antibody	Source	Species	Dilution (Application)
Arl13b	Abcam (ab83879)	Rabbit	1:500 (IF)
Cep164	ProteinTech (22227-1)	Rabbit	1:500 (IF) 1:200 (WB)
GAPDH1	Millipore (CS207795)	Mouse	1:2500 (WB)
Pax6	DSHB	Mouse	1:5 (IF)
Pax7	DSHB	Mouse	1:5 (IF)
Islet1	DSHB	Mouse	1:2 (IF)
Nkx2.2	DSHB	Mouse	1:2 (IF)
Nkx6.1	DSHB	Mouse	1:100 (IF)
Testin	Sigma (HPA015269)	Rabbit	1:300 (WB)
E-Cadherin	BD Biosciences (610181)	Mouse	1:2500 (WB)
Gamma Actin	MCA5776GA	Mouse	1:500 (WB)
RHOC	Abcam (ab180785)	Rabbit	1:500 (WB) 1:100 (IF)
RHOC	Santa Cruz (sc-393090)	Mouse	1:100 (WB)
Twinfilin	Sigma (HPA018116)	Rabbit	1:350 (IF) 1:250 (WB)
Cofilin	Santa Cruz (sc-33779)	Rabbit	1:100 (IF) 1:200 (WB)
Profilin	Abcam (ab180830)	Rabbit	1:100 (IF) 1:1000 (WB)
LaminA	Abcam (ab26300)	Rabbit	1:1000 (WB)
LaminB1	Abcam (ab16048)	Rabbit	1:1000 (WB)
SMCHD1	Sigma (HPA039441)	Rabbit	1:250 (WB)

Antibody	Source	Species	Dilution (Application)
Fibronectin	BD Biosciences (610078)	Mouse	1:200 (WB)
MYL3	Santa Cruz (sc-100550)	Mouse	1:200 (WB)
NDUFB7	Santa Cruz (sc-365552)	Mouse	1:100 (WB)
IDI1	Santa Cruz (sc-100550)	Mouse	1:200 (WB)
Neuropilin	Santa Cruz (sc-5307)	Mouse	1:200 (WB)
WDR1	Santa Cruz (sc-393154)	Mouse	1:100 (WB)
NHERF-1	Santa Cruz (sc-271552)	Mouse	1:100 (WB)
Homer	Santa Cruz (sc-17842)	Mouse	1:500 (WB)
Anti-Rabbit IgG Alexa Fluor 594	Invitrogen (A21207)	Donkey	1:500 (IF)
Anti-Mouse IgG Alexa Fluor 594	Invitrogen (A21203)	Donkey	1:500 (IF)
Anti-Mouse IgG Alexa Fluor 488	Invitrogen (A11017)	Goat	1:500 (IF)
Anti-Rabbit IRDye 689RD	Odyssey (926-68071)	Goat	1:5000 (WB)
Anti-Mouse IRDye 800CW	Odyssey (926-32212)	Donkey	1:5000 (WB)

2.4 Mass Spectrometry based proteomics

2.4.1 Label free proteomics applied to protein extracted from isolated centrosomes

Protein samples were extracted in SDT lysis buffer containing 100 mM Tris-HCl (pH7.6), 4% (W/V) sodium dodecyl sulfate (VWR) and 1% HALT protease inhibitor cocktail (100X) (see section 2.3.3). Protein concentration was determined using a micro BCA assay (see section 2.3.4).

The following mass spectrometry experiments were performed by FingerPrints proteomic facility at the University of Dundee.

Aliquots of protein preparations were processed through FASP (filter-aided sample preparation) involving buffer exchange to 8 M urea and alkylation with 50 mM iodoacetamide prior to a double digestion with trypsin (Roche, sequencing grade); lysates were exchanged by urea on a standard filtration unit, to allow detergent removal, buffer exchange, chemical modification and protein digestion. The filter membrane used retains high-molecular-weight substances (protein and DNA), to allow low-molecular-weight substances (impurities and digested peptides) to be excluded. Protein preparations underwent a double digestion with trypsin (Roche, sequencing grade), initially for four hours at 30°C and then overnight at 30°C.

Resulting peptides were desalted then separated using an Ultimate 3000 RSLCnano system (Thermo Scientific, running dual column setup) coupled to a LTQ OrbiTrap Velos Pro (Thermo Scientific). Peptides were initially trapped

on an Acclaim PepMap 100 C18 trap column (100 µM inner diameter x 2 cm length) with 0.1% formic acid (Buffer C). After 3 minutes of trap enrichment peptides were eluted onto an Acclaim PepMap RSLC C18 column (75 µM x 50 cm) with a linear gradient of 2-4% Solvent B (80% acetonitrile in 0.08% formic acid) over 150 minutes with a constant flow of 0.3 µl/min. The HPLC system was coupled to a linear ion trap Orbitrap hybrid mass spectrometer (LTQ-OrbiTrap Velos Pro, Thermo Scientific) via a transfer line (20 µM x 50 cm) attached to an Easy Spray emitter (7 µM ID) (Thermo Scientific) to the mass spectrometer via an Easy-Spray source with temperature set at 50°C and a source voltage of 1.9 kV. Full-scan mass spectrometry survey spectra (*m/z* 335-1800) in profile mode were acquired in the Orbitrap with a resolution of 60 000 after accumulation of 1 000 000 ions. The 15 most intense peptide ions from the preview scan in the Orbitrap were fragmented by collision-induced dissociation (normalised collision energy, 35%; activation Q, 0.250; activation time, 10.000 ms) in the LTQ after the accumulation of 5000 ions. Dynamic exclusion parameters were set as follows: repeat count, 1; repeat duration, 30 seconds; exclusion list, 500; exclusion duration, 45 seconds; exclusion mass width, ± 10 ppm (relative to reference mass). Maximal filling times were 500 mseconds for the full scans and 100 mseconds for the MS/MS scans. Parameters for the MS/MS scan included: minimum signal required, 50005; isolation width, 2.00; default charge state, 2. OrbiTrap Velos .RAW data files were extracted and converted to mascot generic files (.mgf) using the Spectrum Selector and Spectrum Exporter nodes within Proteome Discoverer (Thermo Scientific,

v1.4.1.14). Extracted data was then searched against the Chicken UniProt database using the Mascot Search Engine (Mascot Daemon Version 2.3.2). The parameters used to search in the Mascot Search Engine included: type of search, MS/MS ion search; enzyme, Trypsin/P; fixed modifications, Carbamidomethyl (C); variable modifications, acetyl (N-term), Dioxidation (M), Gln->pyro-Glu (N-term Q) and Oxidation (M), Deamidated (MQ); mass values, monoisotopic; protein mass, unrestricted; peptide mass tolerance plus/minus 10 ppm (# ^{13}C = 2); fragment mass tolerace, plus/minus 0.6 Da; maximum missed cleavages, 2; instrument type, ESI-TRAP.

2.4.2 Analysis of Jurkat centrosome protein datasets following mass spectrometry

The first sample (Jurkat sample 1) consisted of protein from two independent centrosome isolation samples pooled. The second Jurkat sample (Jurkat sample 2) consisted of protein from three independent centrosome isolation samples pooled. Mass spectrometry on the first sample identified 1226 proteins, of which 612 were associated with two or more unique peptides and were included in further analysis. Mass spectrometry on the second sample identified 1304 proteins of which 575 were associated with two or more unique peptides and were included in further analysis. I combined proteins with two or more unique peptides from Jurkat sample 1 and Jurkat sample 2 and removed duplicates so they were only represented once, resulting in 1131 individual proteins identified by

accession number. Further comparisons and analysis were completed using the gene name associated with each protein, consequently the combined total of Jurkat proteins for further analysis was 816 proteins, as 315 accession numbers had no gene name associated with them.

2.4.3 Analysis of primordial germ cell centrosome protein dataset following mass spectrometry

Mass spectrometry identified 796 proteins, of which 791 proteins were associated with two or more unique peptides and also had gene names or identifiers associated with them. These 791 proteins were included in further analysis.

2.4.4 Tandem Mass Tag Proteomics applied to protein from *talpid*^{3} and wildtype PGCs

Protein samples were extracted in SDT lysis buffer containing 100 mM Tris-HCl (pH7.6), 4% (W/V) sodium dodecyl sulfate (VWR) and 1% HALT protease inhibitor cocktail (100X) (see section 2.3.1). Protein concentration was determined using a micro BCA assay (see section 2.3.4).

The following mass spectrometry experiments were performed by FingerPrints proteomic facility at the University of Dundee.

Samples underwent FASP (filter-aided sample preparation) processing. Each sample was reduced with 100 mM DTT and samples were then processed

using the FASP protocol (Wisniewski et al., 2009) with some modifications. Following removal of SDS with 8 M urea, filters were washed 3 times with 100 mM Tris-HCL pH 8 and then washed another 3 times with 100 mM triethyl ammonium bicarbonate (TEAB). Proteins on the filters were then digested twice at 30°C with trypsin (2 x 6.25 µg), first overnight and then for another 6 hours in a final volume of 200 µl.

Samples then underwent TMT (tandem mass tag) labelling and fractionation. Desalted tryptic peptides (100 µg per sample) were dissolved in 100 µl of 100 mM TEAB. The 10 different TMT labels were dissolved in 41 µL of anhydrous acetonitrile, and each label was added to a different sample. The mixture was incubated for 1 hour at room temperature and the labelling reaction was stopped by adding 8 µL of 5% hydroxylamine.

Following labelling with TMT, samples were mixed, desalted and then dried in a speed-Vac at 30°C. Samples were dissolved in 200 µL ammonium formate (10 mM, pH 10) and peptides were fractionated using RP-High pH HPLC. A C18 Column from Waters (XBridge peptide BEH, 130Å, 3.5 µm 2.1 X 150 mm, Ireland) with a guard column (XBridge, C18, 3.5 µm, 2.1X10mm, Waters) were used on an Ultimate 3000 HPLC (Thermo-Scientific). Buffers A and B used for fractionation consist of 10 mM ammonium formate in milliQ water and 10 mM ammonium formate with 90% acetonitrile respectively; both buffers were adjusted to pH 10 with ammonia. Fractions were collected using a WPS-3000FC auto-sampler (Thermo-Scientific) at 1 minute intervals. Column and guard column were equilibrated with 2% buffer B for 20 minutes at a constant flow rate of 0.2 ml/min. Samples (175 µl) were loaded onto the

column at 0.2 ml/min, and the separation gradient started 1 minute after the sample was loaded onto the column. Peptides were eluted from the column with a gradient of 2% buffer B to 5% buffer B in 6 minutes then from 5% buffer B to 60% buffer B in 50 minutes. The column was washed for 16 minutes at 100% buffer B and equilibrated at 2% buffer B for 20 minutes as mentioned above. The fraction collection started 1 minute after injection and stopped after 80 minutes (total of 80 fractions, 200 µl each). The total number of fractions concatenated was set to 20 and the content of the fractions was dried and suspended in 50 µl 1% formic acid prior to analysis with LC-MS.

Following fractionation, samples were analysed by LC-MS analysis. Analysis of peptides was performed on a Q-exactive-HF (Thermo Scientific) mass spectrometer coupled with a Dionex Ultimate 3000 RS (Thermo Scientific). LC buffers were the following: buffer A (2% acetonitrile and 0.1% formic acid in Milli-Q water (v/v)) and buffer B (80% acetonitrile and 0.08% formic acid in Milli-Q water (v/v)). Aliquots of 15 µL of each sample were loaded at 5 µL/min onto a trap column (100 µm × 2 cm, PepMap nanoViper C18 column, 5 µm, 100 Å, Thermo Scientific) equilibrated in 98% buffer A. The trap column was washed for 6 minutes at the same flow rate and then the trap column was switched in-line with a Thermo Scientific, resolving C18 column (75 µm × 50 cm, PepMap RSLC C18 column, 2 µm, 100 Å). The peptides were eluted from the column at a constant flow rate of 300 nl/min with a linear gradient from 95% buffer A to 40% buffer B in 122 minutes, and then to 98% buffer B by 132 minutes. The column was then washed with 95% buffer B for

15 minutes and re-equilibrated in 98% buffer A for 32 minutes. Q-Exactive HF was used in data dependent mode. A scan cycle comprised MS1 scan (m/z range from 335-1800, with a maximum ion injection time of 50 ms, a resolution of 120000 and automatic gain control (AGC) value of $3x10^6$) followed by 15 sequential dependant MS2 scans (with an isolation window set to 0.7 Da), resolution at 60000, maximum ion injection time at 200 ms and AGC $1x10^5$. To ensure mass accuracy, the mass spectrometer was calibrated on the first day that the runs were performed.

2.4.5 MaxQuant Analysis of TMT LC-MS Data

Following LC-MS analysis, data was processed in MaxQuant (Version 1.5.2.8). The parameters used to search in the MaxQuant search engine included: fixed modifications, Carbamidomethyl (C); decoy mode, revert; Special AAs, KR; Include contaminants, true; MS/MS tol. (FTMS), 10 ppm; Top MS/MS peaks per 100 Da. (FTMS), 12; MS/MS deisotoping (FTMS), true; MS/MS tol. (ITMS), 0.06 Da; Top MS/MS peaks per 100 Da. (ITMS), 8; MS/MS deisotoping (ITMS), false; MS/MS tol. (TOF), 40 ppm; Top MS/MS peaks per 100 Da. (TOF), 10; MS/MS deisotoping (TOF), true; MS/MS tol. (Unknown), 0.5 Da; Top MS/MS peaks per 100 Da. (Unknown), 8; MS/MS deisotoping (Unknown), false; PSM FDR, 0.01; Protein FDR, 0.01; Site FDR, 0.01; Use normalised ratios for occupancy, true; Minimum peptide length, 7; Minimum score for unmodified peptides, 0; minimum score for modified peptides, 40; minimum delta score for unmodified peptides, 0; minimum

delta score for modified peptides, 6; minimum unique peptides, 0; minimum razor peptides, 1; minimum peptides, 1; use only unmodified peptides, true; modifications include in protein quantification, Acetyl (Protein N-term), Oxidation (M); peptides used for protein quantification, razor; discard unmodified counterpart peptides, true; minimum ratio count, 2; re-quantify, false; use delta score, false; iBAQ, false; iBAQ log fit, false; match between runs, true; matching time window (minute), 0.7; alignment time window (minute), 20; find dependent peptides, false; labelled amino acid filtering, true; RT shift, false; advanced ratios, true; AIF correlation, 0.47; first pass AIF correlation, 0.8; AIF topx, 20; AIF min mass, 0; AIF SIL weight, 4; AIF ISO weight, 2; AIF iterative, true; AIF threshold FDR, 0.01.

2.4.6 Analysis of TMT protein dataset following MaxQuant analysis

Proteins were identified based on peptide identification in Uniprot and relative quantification was analysed in MaxQuant. Mass spectrometry identified 7052 proteins across the ten protein samples. Of the 7052 proteins identified, 403 did not have quantitative values associated with them and were excluded from any further quantitative analysis. 44 proteins had zero unique peptides associated with them and were also excluded from any further analysis. One of the proteins with no quantitative values associated also had zero unique peptides. This left 6606 proteins with

quantitative values and one or more unique peptides associated with the protein that were taken forward for further analysis.

2.4.7 Validation of TMT mass spectrometry dataset

Many commercially available antibodies are not specific for chicken and do not recognise the chicken protein; therefore, all the antibodies were tested in controlled conditions on a western blot using chicken and human protein extracted from cells prior to use in validating the TMT mass spectrometry dataset. Twenty-four test western blots (Appendix 7) were completed prior to validating the chicken PGC mass spectrometry. Gamma (γ) tubulin, E-cadherin, Testin and gamma (γ) actin were identified as proteins in all ten PGC protein samples following mass spectrometry that worked well in western blot and recognised the chicken protein. The gamma tubulin antibody was raised against amino acids 38-53 of human gamma tubulin protein. This region is not found in other members of the tubulin family and when aligned, human and chicken gamma tubulin protein have 99% sequence similarity, confirming specificity for gamma tubulin with this antibody. The E-cadherin antibody recognises the cytoplasmic domain regardless of phosphorylation and recognises amino acids 735-883 of the human E-cadherin protein. When aligned with the equivalent region of the chicken E-cadherin protein, human and chicken share 89% sequence similarity. E-cadherin has a predicted molecular weight of 120 kDa, although bands have been reported from 80-120 kDa for E-cadherin previously. The

testin antibody recognises a domain in the middle of the human Testin protein. When aligned, human and chicken Testin proteins share 89% sequence similarity. The gamma actin antibody recognises human gamma actin protein. When compared to chicken gamma actin, the human and chicken proteins share 99% sequence similarity.

2.5 Molecular Biology

2.5.1 Transformation of chemically competent cells

XL-Gold competent cells were removed from -80°C and thawed on ice. 1 µl β-mercaptoethanol was added per 25 µl of XL-Gold competent cells being transformed and incubated on ice for 10 minutes. 2 µl of appropriate DNA was added to cells, mixed and incubated on ice for 30 minutes. Cells were heat shocked at 42°C for 30 seconds on a thermocycler and then incubated on ice immediately afterwards for 2 minutes to recover. 600 µl of pre-warmed SOB media was added and incubated at 37°C, shaking for 1 hour. LB agar plates containing 100 µg/ml Ampicillin were incubated at 37°C to dry out for 1 hour. Following incubation, cells were centrifuged at 5 rpm for 1 minute. 400 µl of SOB media was removed and remaining media was used to resuspend the pellet. Resuspended cells were spread across the pre-warmed LB agar ampicillin plates. Plates were labelled and incubated inverted at 37°C overnight.

2.5.2 Growth of colonies

For Minipreps, single colonies were picked and grown overnight in 5 ml LB broth containing 100 µg/ml ampicillin at 37°C, shaking. For Maxipreps, single colonies were picked and grown during the day as a starter culture in 5 ml of LB broth containing 100 µg/ml ampicillin at 37°C, shaking. After 4-8 hours of incubation, the starter culture was poured into a conical flask containing 200 ml of LB broth with 100 µg/ml ampicillin and grown overnight at 37°C shaking.

2.5.3 MiniPrep

Overnight 5 ml cultures were pelleted and used for Minipreps; The Qiagen QIAprep Spin Miniprep kit (27104) was used and the user manual was followed. Briefly, bacterial cultures were pelleted, resuspended, lysed under alkaline conditions, neutralised and then adjusted to high salt binding conditions to allow DNA binding to a silica membrane. Endonucleases and salts were removed through wash buffers and the DNA eluted in 30-50 µl water. DNA was nanodropped to determine concentration and then stored short term at 4°C and long term at -20°C.

2.5.4 MaxiPrep

Overnight 200 ml cultures were pelleted and used for Maxipreps; The Invitrogen PureLink HiPure Plasmid Filter MaxiPrep Kit (K210016) was used

and the user manual was followed. Briefly, overnight cultures were pelleted, resuspended in buffer, loaded onto a column, washed and eluted in 50-100 µl of water. DNA was nanodropped and then stored at -20°C.

2.5.5 Guides into px462 Vector

Oligos (Table 2.2) were resuspended to a final concentration of 100 µM. Reaction was set up to phosphorylate and anneal oligos: 1 µl of sgRNA top (100 µM), 1 µl of sgRNA bottom (100 µM), 1 µl T4 ligation buffer 10X, 1 µl T4 PNK, 6 µl ddH_20 to make a final volume of 10 µl. Reaction was run on a thermocycler: 37°C for 30 minutes; 95°C for 5 minute; ramp down to 25°C at 5°C $minute^{-1}$. The phosphorylated and annealed oligos were diluted 1:200. sgRNA was cloned into a pSpCas9 vector by setting up a ligation reaction: 1 µl (100 ng) px459 vector, 2 µl of diluted oligos, 2 µl Tango buffer 10X, 1 µl DTT (10 mM), 1 µl ATP (10 mM), 1 µl FastDigest *BbsI*, 0.5 µl T7 ligase, 11.5 µl ddH_20 to make reaction up to 20 µl total. The reaction was incubated on a thermocycler for 1 hour. 6 cycles were completed: 37°C for 5 minutes, 21°C for 5 minutes. The ligation reaction was treated with Plasmid Safe to remove any residual linearised DNA: 11 µl ligation reaction, 1.5 µl PlasmidSafe buffer 10X, 1.5 µl ATP (10 mM), 1 µl PlasmidSafe exonuclease to make a total volume of 15 µl. The reaction was incubated on a thermocycler: 37°C for 30 minutes, 70°C for 30 minutes. Product was stored at -20°C until transformation.

Table 2.2 CRISPR guides used in this thesis

Guide Name	Gene	Oligo Sequence
CCDC77 guide1 top	CCDC77	caccgAGAGGCACATTGACCCAATT
CCDC77 guide1 bottom	CCDC77	aaacAATTGGGTCAATGTGCCTCTc
CCDC77 guide2 top	*CCDC77*	caccgGCAGACAGGGGTGTGTGTTG
CCDC77 guide2 bottom	*CCDC77*	aaacCAACACACACCCCTGTCTGCc
CCDC127 guide1 top	*CCDC127*	caccgGTGGCGTTAAGGGAACGCTG
CCDC127 guide1 bottom	*CCDC127*	aaacCAGCGTTCCCTTAACGCCACc
CCDC127 guide2 top	*CCDC127*	caccgAGGCCGGATATTCCAATTTG
CCDC127 guide2 bottom	*CCDC127*	aaacCAAATTGGAATATCCGGCCTc
Talpid 5’ guide3 top	*TALPID3*	caccgCTATGAAGCCTTCATGGAAG
Talpid 5’ guide3 bottom	*TALPID3*	aaacCTTCCATGAAGGCTTCATAGc
Talpid 5’ guide5 top	*TALPID3*	caccgGCACCAGCCAGGACTCGCTG
Talpid 5’ guide5 bottom	*TALPID3*	aaacCAGCGAGTCCTGGCTGGTGCc
Talpid 3’ guide2 top	*TALPID3*	caccGCCCGAGTTGTTCATGTGAGA
Talpid 3’ guide2 bottom	*TALPID3*	aaacTCTCACATGAACAACTCGGGc
Talpid 3’ guide3 top	*TALPID3*	caccGCCTTCTCACATGAACAACTC
Talpid 3’ guide3 bottom	*TALPID3*	aaacGAGTTGTTCATGTGAGAAGGc

Guide Name	Gene	Oligo Sequence
Talpid 3’ guide4 top	*TALPID3*	caccGGCACAACTCGTGCATCTCCT
Talpid 3’ guide4 bottom	*TALPID3*	aaacAGGAGATGCACGAGTTGTGCc

2.5.6 PCR

Primers (Table 2.3) were designed in Primer3 or in the NEBuilder Assembly Tool for design of primers used in Gibson Assembly. PCR reactions were set up using Phusion or FastTaq DNA polymerase. The NEB Tm Calculator was used to determine annealing temperature for primers. A 3-step PCR reaction was used where the annealing temperatures were below 72°C and a 2-step reaction was used where annealing temperatures were 72°C or above. For every 1000 bp of intended amplicon, the extension time was increased by 1 minute. 100 ng of DNA per reaction was used. Reactions with Phusion typically contained 4 µl of HF buffer, 0.4 µl of dNTP, 0.2 µl of 10 pMol primers and 0.2 µl of Phusion made up to a total volume of 20 µl. Reactions with FastTaq typically contained 1.5 µl Mg+ buffer, 0.3 µl dNTP, 0.3 µl 50 pMol primers and 0.1 µl FastTaq made up to a total volume of 15 µl. A typical PCR reaction would be carried out in the following format:

	Denaturation	98°C	30 seconds
30-35 x	Denaturation	98°C	10 seconds
	Annealing	54-72°C	30 seconds
	Extension	72°C	1-2 minutes
	Extension	72°C	5 minutes

Table 2.3. Primers used in this thesis

Primer Name	Primer Sequence	Polymerase	Annealing T°	Extension Time	Number of Cycles
CCDC77 Fwd1 Seq	ACCCATAATCCTTCCATGCCA	Phusion	60°C	1 minute	35
CCDC77 Rev1 Seq	AGAGTCCCCGTACCTACAGT	Phusion	60°C	1 minute	35
CCDC77 Fwd2_3 Seq	GAGAATCGCTTGAACCCAGA	Phusion	64°C	1 minute	35
CCDC77 Rev2_3 Seq	ACCTTTCCAGTTCCTATGCTTAG	Phusion	64°C	1 minute	35
CCDC127 Fwd1_2	CCCGACATGTCTGCTGTTG	FastTaq	56°C	1 minute	35
CCDC127 Rev1_2	CTCCGACCCCATTCCCTG	FastTaq	56°C	1 minute	35
CCDC127 Fwd2_2	CCCGGCTCTGGTCTAGTTTT	FastTaq	54°C	1 minute	32
CCDC127 Rev2_2	CTGCTTCCATCACCACCATC	FastTaq	54°C	1 minute	32
5’ Talpid3 Right Arm Fwd	CGAGCTGTACAAGGGAGGTGGAGGAGGTGGAGCGGCTCCAGCACCA GCCAG	Phusion	72°C	2 minutes	30
5’ Talpid3 Right Arm Rev	TATGGTCGACCTGCAGGCGGCCGCGAGAGAATGGATGCCCCACAGGC	Phusion	72°C	2 minutes	30

Primer Name	Primer Sequence	Polymerase	Annealing T°	Extension Time	Number of Cycles
5’ Talpid3 Left Arm Fwd	TCCCGGCCGCCATGGCGGCCGCGGGTCTGAAGCACCACTCCCTCTG	Phusion	72°C	2 minutes	30
5’ Talpid3 Left Arm Rev	CCTTGCTCACCATAGCGGAGAGGTTAGCAGCGG	Phusion	72°C	2 minutes	30
GFP Fwd	TAACCTCTCCGCTATGGTGAGCAAGGGCGAGGA	Phusion	72°C	2 minutes	30
GFP Rev	ACCTCCTCCACCTCCCTTGTACAGCTCGTCCATGCC	Phusion	72°C	2 minutes	30
3’ Talpid3 Right Arm Fwd	TCCCGGCCGCCATGGCGGCCGCGGGTTTTTATTAACTTCAGCTCACC	Phusion	65.5°C	1 minute	32
3’ Talpid3 Right Arm Rev	ACCTCCTCCACCTCCTCTTCTCACATGAACAACTC	Phusion	65.5°C	1 minute	32
3’ Talpid3 Left Arm Fwd	GCTGTACAAGTAAAAGTCTGAAGAGATGCAAGAAG	Phusion	65.5°C	1 minute	32
3’ Talpid3 Left Arm Rev	TATGGTCGACCTGCAGGCGGCCGCGCAACAATTCTGAATTTCTGAG	Phusion	65.5°C	1 minute	32
Venus Fwd	TCATGTGAGAAGAGGAGGTGGAGGAGGTGGAATGGTGAGCAAGGG CGAG	Phusion	65.5°C	1 minute	32
Venus Rev	TCTCTTCAGACTTTTACTTGTACAGCTCGTCCATG	Phusion	65.5°C	1 minute	32

2.5.7 DNA Extraction for Sequencing

Following PCR, amplicons were run on a 1% agarose gel, bands were viewed on a Kodak Gel Logic 200 Imaging System and isolated from the gel for purification using a scalpel. The DNA contained within the agarose slice was then purified using the PureLink Quick Gel Extraction Kit (K210012), following user manual instructions. Gel slices were weighed to determine volume of reagents to use and the extraction was carried out following the instructions in the user manual using a centrifuge. 5 µl of clean DNA combined with 1 µl of 6.4 pMol primer was added to a PCR tube and sent to Edinburgh Genomics for Sanger Sequencing using BigDye v3.1 Terminator Cycle Sequencing Kit (Thermofisher P/N AB0384/240; BS034042).

2.5.8 DNA Extraction for Gibson Cloning

Following PCR, amplicons were run on a 1% agarose gel, bands were viewed on a Kodak Gel Logic 200 Imaging System and isolated from the gel for purification using a scalpel. The amplicon contained within the agarose slice was then purified using a GeneJet PCR Purification Kit from Thermo Scientific (cat no. K0701), following the user manual. Briefly, binding buffer was added to the PCR reaction and transferred to a purification column. Column was washed and waste eluted by centrifugation. 20-50 µl of elution buffer was added to the column and purified DNA was eluted by centrifugation into a clean Eppendorf tube, concentration checked by nanodrop and stored at -20°C.

2.5.9 DPN1 Treatment

Following PCR amplification of GFP and Venus, the amplicon was treated with DPN1 to digest any remaining plasmid. The reaction was set up with 20 µl of Venus DNA, 5 µl of 10 X buffer, 1 µl of DPN1 and made up to a total reaction volume of 50 µl with water and incubated for 1 hour at 37°C. To inactivate DPN1, the reaction was purified using a purification column from the GeneJet PCR Purification kit from Thermo Scientific (cat no. K0701) following the user manual instructions.

2.5.10 Preparation of pGEM-T Easy Vector for Gibson Cloning

A pGEM-T Easy vector was used as the backbone for Gibson cloning. A digestion reaction was set up with 1 µl of pGEM-T Easy vector, 1 of µl EcoR1, 2 µl of 10 X CutSmart buffer and made up to a total volume of 20 µl with water. The reaction was incubated at 37°C for 1 hour. Linearised pGEM-T easy vector was run on a 1% agarose gel and the resulting band was extracted using a scalpel. The band containing the linearised vector was purified using a PureLink Quick Gel Extraction Kit (K210012), following the user manual instructions.

2.5.11 Gibson Cloning

Gibson cloning was used to make the plasmid template that was used for homology directed repair during CRISPR/Cas9 gene editing experiments. The

Gibson Cloning used a 1-step reaction to incorporate multiple fragments together into a plasmid, by using overlapping ends to join the fragments together. Following amplification of fragments, PCR purification and preparation of the pGEM-T Easy vector, the cloning reaction was set up following the user manual instructions. A 1:1 ratio of fragments to vector was added to 10 µl of Gibson cloning master mix and made up to a total volume of 20 µl with water. The reaction was incubated on a thermocycler at 50°C for 1 hour. Briefly, during the Gibson Assembly reaction, exonuclease chews back the 5' ends, the resulting single-stranded regions at the ends of adjacent fragments anneal, DNA polymerase incorporates nucleotides to fill the gaps and DNA ligase joins the adjacent DNA sections, thus removing any nicks in the DNA. The reaction was stored at 4°C until it was transformed (see section 2.5.1), colonies grown (see section 2.5.2) and a miniprep was completed (see section 2.5.3). To confirm correct assembly of fragments, a restriction digest was completed using EcoR1 for the plasmid designed to target the 5' end of *TALPID3* and BAMH1 combined with NOT1 for the plasmid designed to target the 3' end of *TALPID3.* The restriction digests were run on a 1% agarose gel and examined for specific size of bands to confirm that all the fragments had annealed correctly.

2.5.12 RNA probes for *in situ* hybridisation

Chicken ESTs (Table 2.4) were ordered for genes of interest and DNA extracted. DNA was linearised by restriction digest using NotI enzyme at

37°C for two hours. Inactivation of enzyme was achieved by incubation at 65°C for twenty minutes. Sodium acetate precipitation was used to concentrate linearised DNA. RNA probe was then synthesised in a 18.5 µl reaction of RNAse free water, 5x transcription buffer, 0.1 M DTT, DIG-RNA labelling mix 10X (cat no. 1277073910), RNAse inhibitor, RNA polymerase T3 and the linearised plasmid. Reaction was incubated at 37°C for a minimum of 2 hours. Probe was purified using the Illustra ProbeQuant Kit (G50 Column, 27-5335-01, GE Healthcare UK Lt.), following the user manual. The probe was then stored in Hybridisation buffer (50% formamide, 5X SSC, 2% Blocking Powder (Boehringer), 0.1% Trition X, 0.1% CHAPS, 20 µg/ml tRNA (Boehringer 109495), 5 mM EDTA, 50 µg/ml Heparin (Sigma H2144)) and stored at -20°C.

Table 2.4 Chicken ESTs used to make RNA probes in this thesis

Gene targeted	**Chicken EST**
CCDC127	ChEST805b15
CCDC77	ChEST294b19
TALPID3	ChEST757p14

2.6 Chicken Embryo Work

2.6.1 Chicken models

For all experiments involving *talpid*^{3} flock embryos, eggs were obtained from the *talpid*^{3} flock, which are maintained as described previously (Stephen et al., 2015). Embryos for RNA *in situ* hybridisation were obtaine↕d from Isa Brown hens, maintained at The Roslin Institute. Chicken embryos were sacrificed by a schedule one method that is not a regulated procedure under UK Home Office rules.

2.6.2 Incubation and dissection of chicken embryos

For embryo experiments, all eggs were incubated at 37°C until they had reached the desired stage based on Hamburger and Hamilton staging. Where manipulations were carried out, the egg was windowed, DMEM + antibiotics was introduced and the membrane was removed. Following the manipulation, eggs were re-sealed with sellotape and re-incubated until the stage required for analysis. To dissect embryos, membranes were disrupted and the embryo was transferred to ice cold PBS, where the embryonic membranes were removed before further dissection or fixation in 4% PFA (4 g Para formaldehyde per 100 ml of DEPC PBS). All manipulations and dissections were carried out using a Leica MZ6 Microscope, using a Schott KL1500 LCD light source.

2.6.3 Dehydration of Embryos prior to RNA *in situ* hybridisation

Following dissection and fixation in 4% PFA, embryos were washed twice with cold DEPC PBS (1 ml DEPC in 1 litre of PBS solution, autoclaved) for 10 minutes, while shaking. Embryos were dehydrated through 25%, 50% and 75% methanol/DEPC PBST (DEPC PBS + 1 ml Tween20) for ten minutes each, while shaking. Embryos were transferred to 100% methanol and then stored at -20°C until RNA *in situ* hybridisation.

2.6.4 RNA *in situ* hybridisation

Embryos, stored in 100% methanol at -20°C, were rehydrated through a methanol gradient until they were in 100% PBT. Embryos were treated with 1:1000 (20 µg/ml) proteinase K (K-03115836001, Roche) diluted in PBS, on ice. Embryos were incubated for 1 minute per stage of their development. Embryos were washed in PBT and refixed in 4% PFA for 20 minutes on ice. Embryos were re-washed with PBT and then incubated overnight in pre-warmed hybridisation buffer (50% formamide, 5 X SSC, 2% Blocking Powder (Boehringer), 0.1% Triton X-100, 0.1% CHAPS, 20 µg/ml tRNA (Boehringer 109495), 5 mM EDTA, 50 µg/ml Heparin (Sigma H2144)) at 67.5°C with gentle agitation. Hybridisation buffer was replaced with the RNA probe (see 2.5.12) and incubated at 67.5°C for 2-3 days. Following incubation with probe, embryos were washed in a series of buffers at 70°C: 2 x 10 minutes buffer A (2 x saline sodium citrate buffer), 3 x 20 minutes buffer B (2 x saline sodium citrate, 0.1% CHAPS), 3 x 20 minutes buffer C (0.2 x saline sodium citrate,

0.1% CHAPS). Embryos were then washed twice in KTBT (50 mM Tris-HCL pH7.5, 150 mM NaCl, 10 mM KCl, 1% Triton X-100) for 10 minutes at room temperature, following which embryos were blocked in blocking buffer (20% heat inactivated fetal calf serum/KTBT) for 2-3 hours at room temperature. Blocking buffer was replaced with 1:1000 mouse Anti-DIG-AP Fab fragment (Anti-Digoxigenin-AP, Fab fragment cat no. 1093274) in blocking buffer, overnight at 4°C. The following day, embryos were washed 5 x for 1 hour in KTBT (50 mM Tris-HCL pH7.5, 150 mM NaCl, 10 mM KCl, 1% Triton X-100) at room temperature and left in KTBT overnight at 4°C. Embryos were transferred to Bijou vials and washed 2 x 5 minutes at room temperature with freshly made NTMT buffer (100 mM Tris-HCl pH9.5, 50 mM $MgCl_2$, 100 mM NaCl, 0.1% triton X-100). For the detection solution, 35 µl NBT (N-6876 Sigma, stock solution 100 mg/ml 70% DMF (dimethylformamide), use 3.5 µl/ml) and 35 µl BCIP (B-8503 Sigma, stock solution 50 mg/ml DMF, use 3.5 µl/ml) was added to 10 ml NTMT (100 mM Tris-HCl pH9.5, 50 mM MgCl, 100 mM NaCl, 0.1% Triton X-100). Detection solution was added to embryos and refreshed as necessary. Embryos were checked every 10-15 minutes for expression. Once expression patterns could be clearly seen, the detection reaction was stopped by replacing the detection solution with 4% formal saline (10% formalin neutral buffered, in PBS). To deepen staining for imaging, embryos were incubated in NTET (1 ml of 5 M NaCl, 1 ml of 0.5 EDTA pH8, 5 ml of 1 M Tris-HCl pH8, 0.5 ml of Tween20, 42.5 ml of dH_20). Once embryo stain was appropriate level for imaging, NTET was removed and embryos were placed back into 4% formal saline.

Once images had been obtained of embryos following whole mount *in situ* hybridisation, embryos were embedded in gelatine (7% 300 Bloom Gelatine/10% Sucrose) and snap frozen in isopentane pre-chilled to -80°C prior to sectioning. Embryos were sectioned at 30 µm on the cryostat for analysis of tissue specific expression.

2.6.5 Electroporation

For transfection of constructs of interest in the chick, injection followed by electroporation in the neural tube of developing chick embryos was carried out. Following 48 hours of incubation to reach Hamburger-Hamilton stage 10-12, eggs were windowed and the membrane was removed. The neural tube was injected with 1 µg/µl DNA + 0.02% FastGreen dye. DNA constructs included: empty-pCAGGS, pCAGGS-eGFP, pCAGGS-hsKIAA0586 (full length human KIAA0586), pCAGGS-hsKIAA0586c.1697A>T,p.D566V (human ciliopathy mutation in KIAA0586). All injected DNA was comprised of the construct of interest combined with pCAGGS-eGFP to allow visualisation of successful electroporations. Injections were carried out by mouth pipette, needles were pulled on a Moving-Coil Microelectrode Puller Model 753 (Campden Instruments Limited) using the following settings: pre-pull heating time 57, initial pull force 159, main pull force 286, main pull delay 49, heater control 139. Electrodes were placed either side of the neural tube at the site of the injection and embryos were immediately electroporated at 20-25 V five times with 100 ms intervals. 2-3 drops of DMEM + 1%

penicillin/streptomycin was added to the embryo and then covered with sellotape to prevent embryos from drying out. Embryos were re-incubated until Hamburger-Hamilton stage 20-24. Embryos were examined for green fluorescence in the neural tube on a Zeiss Axio Zoom.V16 microscope, to identify embryos that were successfully integrated the DNA following electroporation. If fluorescence was present, embryos were dissected in ice cold PBS and the section of neural tube containing fluorescence was dissected out and fixed in 4% PFA at room temperature for 1-2 hours prior to embedding in gelatine for sectioning on the cryostat.

2.7 Microscopy

2.7.1 Confocal Microscopy

All confocal images were taken on an Inverted Zeiss LSM 710 Confocal microscope. Cells were imaged using a x63 oil lens. Tissue sections were imaged using a x10 lens, x20 lens, x40 oil lens or x63 oil lens. Image processing was completed in ZEN (black edition) software, Zen (blue edition) software or ImageJ software.

2.7.2 Structured Illumination Microscopy (SIM)

Super-resolution microscopy allows for the observation of fluorescent samples at resolutions beyond the diffraction of light limit. All super-resolution images were acquired using structured illumination microscopy.

Briefly, Structured Illumination Microscopy (SIM) uses patterned illumination, usually stripes, to excite samples. Emitted fluorescence is recorded in a range of positions and orientations; the interaction between the excitation pattern and the sample produces Moiré patterns and allows capture of high frequency information at low spatial frequencies. In 3-D SIM, the illumination is modulated in three dimensions and reconstruction of the final super-resolved image requires a greater number of raw images collected at different orientations of the structured illumination. Samples were prepared on high precision cover-glass (Zeiss, Germany). 3D SIM images were acquired on a Nikon-Structured Illumination Microscope (Nikon Instruments, UK) using a 100x 1.49NA lens and refractive index matched immersion oil (Nikon Instruments). Samples were imaged using a Nikon Plan Apo TIRF objective (NA 1.49, oil immersion) and an Andor DU-897X-5254 camera using 405, 488 and 561 nm laser lines. Z-step size for Z stacks was set to 0.120 um as required by manufacturer's software. For each focal plane, 15 images (5 phases, 3 angles) were captured with the NIS-Elements software. SIM image processing, reconstruction and analysis were carried out using the N-SIM module of the NIS-Element Advanced Research software. Images were checked for artefacts using the SIMcheck software (http://www.micron.ox.ac.uk/software/SIMCheck.php). Images were reconstructed using NiS Elements software v4.6 (Nikon Instruments, Japan) from a z-stack comprising of no less than 1 µm of optical sections. In all SIM image reconstructions the Wiener and Apodization filter parameters were kept constant. Reconstructed images were exported as .nd2 files, converted

to LIM files using IMARIS file converter software and imported into IMARIS for segmentation, further processing and analysis.

2.7.3 Single cell sorting for clonal cell lines

Single cells were deposited into individual wells of 96 plates using an Automatic Cell Deposition Unit (ACDU) on a Becton Dickinson FACS Aria III high speed Fluorescence Activated Cell Sorter. The Single Cell digital purity filter was used to avoid introducing contaminating cells. Each cell was contained within a droplet of approximately 5 nl of sterile phosphate buffered saline (PBS) as it was sorted.

2.8 Statistical, Software and Bioinformatics Analysis

The value of significance is accepted as $p < 0.05$ throughout all statistical tests. Data was collected in Excel and all statistical tests were carried out in Minitab. The test used for statistical analysis is specified in the captions of figures or main text of this thesis. Graphs were generated in R (R Core Team, 2013).

2.8.1 FANTOM5 Zenbu Analysis

Zenbu in FANTOM5 was used to predict transcriptional expression of KIAA0586 transcripts. KIAA0586 was searched in the FANTOM5 human promoterome view, transcripts were identified in the UCSC_RefSeq_hg19_20120101 tab and transcripts of interest were examined for evidence of promoter activity in different tissue and cell types in the FANTOM5 CAGE Phase1 CTSS human tracks pooled filtered with 3 or more tags per library.

2.8.2 Alignment Analysis

Sequence alignments were completed using Clustal Omega from EMBL-EBI (Clustalo, V1.2.4). Protein sequences for alignments were taken from NCBI, based on the following accession numbers: *Nematostella vectensis*, ACJ61010; *Saccoglossus kowalevskii*, XP_002735892.1; *Danio rerio*, NP_001245157; *Gallus gallus*, AAZ22766; *Homo sapiens*, NP_001231118; *Mus musculus*, NP_001156850. Sequence alignments were imported into Jalview (Version 2), where protein domains were annotated (Waterhouse et al., 2009).

2.8.3 DAVID Analysis

The Database for Annotation, Visualisation and Integrated Discovery (DAVID) provides a set of functional annotation tools aimed at

understanding the biological meaning behind a large dataset or list of genes. Lists of genes, extracted from proteomic datasets, were uploaded into DAVID and submitted for analysis using the official gene symbol. The species was selected to limit annotations of gene lists to the species of the proteomic dataset being analysed. For human Jurkat cells, *homo sapiens* was selected; for chicken PGCs, *gallus gallus* was selected. Functional annotation clustering was used to determine Gene Ontology (GO) terms associated with the datasets, clusters of genes and the enrichment scores of those clusters.

2.8.4 Ingenuity Pathway Analysis

To understand potential cellular pathways that may be modified as a result of protein changes in different conditions, the Ingenuity Pathway Analysis (IPA) application (Ingenuity Systems, Silicon Valley, CA) was used as previously described (Mcgorum et al., 2015). Pathway analysis has been demonstrated to highlight downstream molecular consequences relating to a specific underpinning difference in a system. The interaction data was limited as follows: direct and indirect interactions; experimentally observed data only; maximum 35 molecules per network. P-values were calculated in IPA using a right-tailed Fishers exact test, allowing the programme to determine how relevant the network is to the current analysis. Z-scores were generated in IPA and represent a statistical measure of the match between an expected relationship direction and the observed protein expression. Positive z-scores indicate activation (orange) and negative z-scores indicate

inhibition (blue). Where no activity pattern was observed, z-scores were unavailable (grey).

2.8.5 Image Studio Lite Western Blot Band Analysis

All fluorescent Western blot images were obtained on the LICOR imaging system using Image StudioLite Software. Size of bands was calculated through Image Studio Lite by marking the protein standard band sizes. Relative quantification of bands was also carried out in Image StudioLite giving a read-out of signal for each band, which allowed calculation of relative fold change between bands.

2.8.6 ImageJ Cell Counter

Images of cells stained for gamma tubulin and acetylated tubulin were obtained using the 40x oil lens on the Zeiss LSM 710 Confocal microscope. Images were converted to .jpeg files and imported into ImageJ. Images were converted to an RGB (Red Green Blue) stack to separate the channels into separate images, ensuring an unbiased count. The cell counter plugin was used, which allowed cilia to be counted in one channel and nuclei (to represent each cell stained) to be counted separately in another channel. Each count was recorded on the image and images saved. The results were recorded in a table and exported as an excel file. Following collection of numbers of ciliated cells, the data was normally distributed; therefore, an

unpaired two-tailed student t-test was carried out to determine statistical significance between individual mutated cell lines and unedited cell lines.

2.8.7 Extraction of list of centrosome proteins from the Andersen (2003) dataset

The list for the KE37 cells comprised of 552 proteins identified from centrosome preparations (Andersen et al., 2003); the proteins were identified using the International Protein Index (IPI), which has since closed. To allow a comparison of the KE37 cell proteins with the Jurkat protein identifications, the UniProtKB ID/AC was extracted, where it was included in the KE37 raw dataset. Where accession numbers that are no longer used were included, the UniProt Retrieve ID/Mapping feature was used to convert the IDs to UniProtKB ID/AC. Of the 552 proteins identified in the KE37 raw dataset, a list of 505 proteins was extracted that could be matched with known accession numbers. Of those 505, there were thirteen proteins in duplicate following the ID conversion. The final list of proteins taken from the KE37 cell dataset comprised of 492 proteins, identified by accession number.

Chapter 3. Investigating the functional domains and localisation of KIAA0586

3.1 Introduction

The *talpid*^{3} chicken flock contains a mutation that results in a severe embryonic lethal phenotype (Davey et al., 2006), however human ciliopathy patients with mutations in *KIAA0586* (human *TALPID3* orthologue) result in a much wider range of ciliopathy phenotypes from relatively mild to more severe, with only some cases of early lethality (Akawi et al., 2015; Alby et al., 2015; Bachmann-Gagescu et al., 2015; Malicdan et al., 2015; Roosing et al., 2015; Stephen et al., 2015). The following chapter explores ways of modelling the human mutations in *talpid*^{3} embryos in order to understand the functional domains that are affected by mutations that are predicted to be hypomorphic. In addition, this chapter explores tools to study the subcellular localisation of TALPID3.

3.1.1 Functional domains of TALPID3/KIAA0586

Analysis of the TALPID3 protein in chicken, mouse and zebrafish has identified a conserved coiled-coil domain (Figure 3.1) that is essential for function (Figure 3.2) (Bangs et al., 2011; Ben et al., 2011; Yin et al., 2009). This region was deleted in mouse and zebrafish to produce the talpid3$^{-/-}$ mouse model and the TALPID3 knockout zebrafish model, confirming this

region as being essential for function (Bangs et al., 2011; Ben et al., 2011). The conserved coiled-coil domain is also found in the human KIAA0586 protein, as well as the broader category of chordates. Conservation is determined based on the presence of a coiled-coil domain in a region of the protein sequence that aligns with and has greater than 60% similarity to that of the chicken, mouse, zebrafish and human KIAA0586 proteins. A study in human RPE1 cells demonstrated that amino acid residues 466-602 of human KIAA0586, which contains the conserved coiled-coil domain was able to localise to centrosomes in human RPE1 cells (Kobayashi et al., 2014), thus supporting the conserved function of this domain in human KIAA0586. There is additional evidence in RPE1 cells to suggest that a region at the N-terminal of human KIAA0586 also weakly localises to the centrosome (Kobayashi et al., 2014), suggesting that human KIAA0586 might require two distinct regions of KIAA0586 to localise to the centrosome (Figure 3.2) (Kobayashi et al., 2014).

A second region towards the C-terminal of TALPID3 contains a predicted intrinsically disordered domain (Figure 3.2) (Davey et al., 2006; Yin et al., 2009). Disordered domains can enable the protein to have multiple interactions with multiple different proteins, due to the increased levels of flexibility and lack of stable secondary and tertiary structure (Dunker et al., 2002; Sormanni et al., 2015), thus supporting the suggestion that the disordered domain in TALPID3 most likely contains unidentified functional domains. This domain is not highly conserved at the amino acid level, however chicken, mouse, zebrafish and human KIAA0586 proteins have all

been shown to contain predicted intrinsically disordered domains at a similar C-terminal region of the protein (Figure 3.1). The presence of the predicted intrinsically disordered domain has prevented successful structural modelling of the TALPID3 protein. Evidence in human RPE1 cells suggests that there are no additional C-terminal domains in human KIAA0586 protein that are required for targeting the protein to the centrosome (Kobayashi et al., 2014), suggesting that the functional C-terminal domains rely on the essential coiled-coil domain for targeting to the centrosome and that any function assigned to the C-terminal is secondary to centrosome localisation.

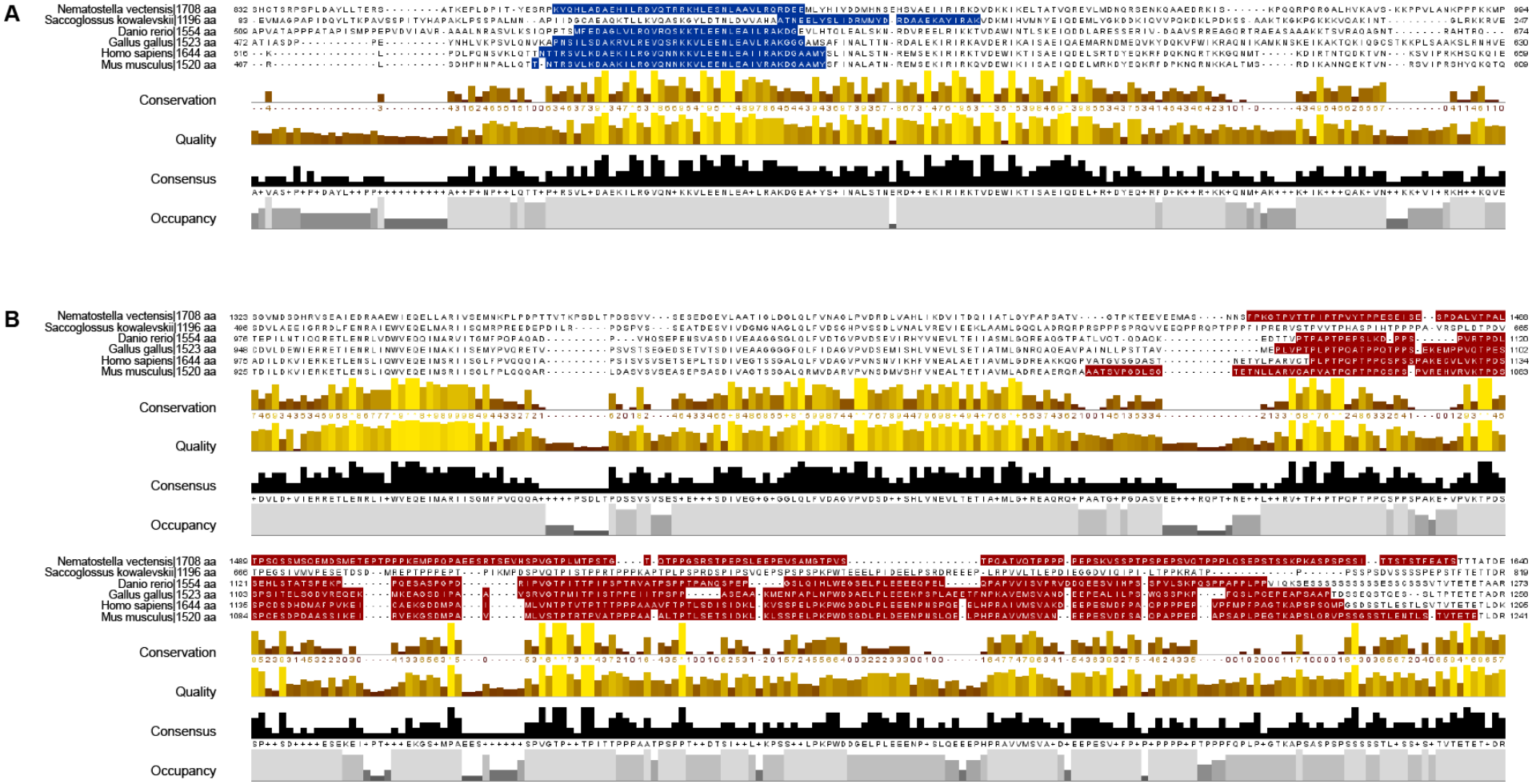
A
Nematostella vectensis|1708 aa
Saccoglossus kowalevskii|1196 aa
Danio rerio|1554 aa
Gallus gallus|1523 aa
Homo sapiens|1644 aa
Mus musculus|1520 aa
Conservation
Quality
Consensus
Occupancy
B
Nematostella vectensis|1708 aa
Saccoglossus kowalevskii|1196 aa
Danio rerio|1554 aa
Gallus gallus|1523 aa
Homo sapiens|1644 aa
Mus musculus|1520 aa
Conservation
Quality
Consensus
Occupancy

Figure 3.1 Alignment of the conserved sequence of TALPID3/KIAA0586 essential coiled-coil domain and the predicted intrinsically disordered domain. (**A**) The conserved coiled-coil domain that is essential for function is marked in blue. (**B**) The predicted intrinsically disordered domain that is predicted to contain functional domains highlighted in red. The first sequence, *Nematostella vectensis* (Starlet sea anemone), is conserved, containing both the coiled-coil domain and an intrinsically disordered domain. The second sequence, *Saccoglossus kowalevskii* (Acorn worm), is not conserved. It contains a coiled-coil domain in a similar region, but does not appear to share sequence similarity and does not contain an intrinsically disordered domain. The bottom four sequences are *Danio rerio* (zebrafish), *Gallus gallus* (chicken), *Homo sapiens* (human) and *Mus musculus* (mouse) respectively and all contain the conserved coiled-coil domain and the intrinsically disordered domain. (See Appendix 1 for full alignment).

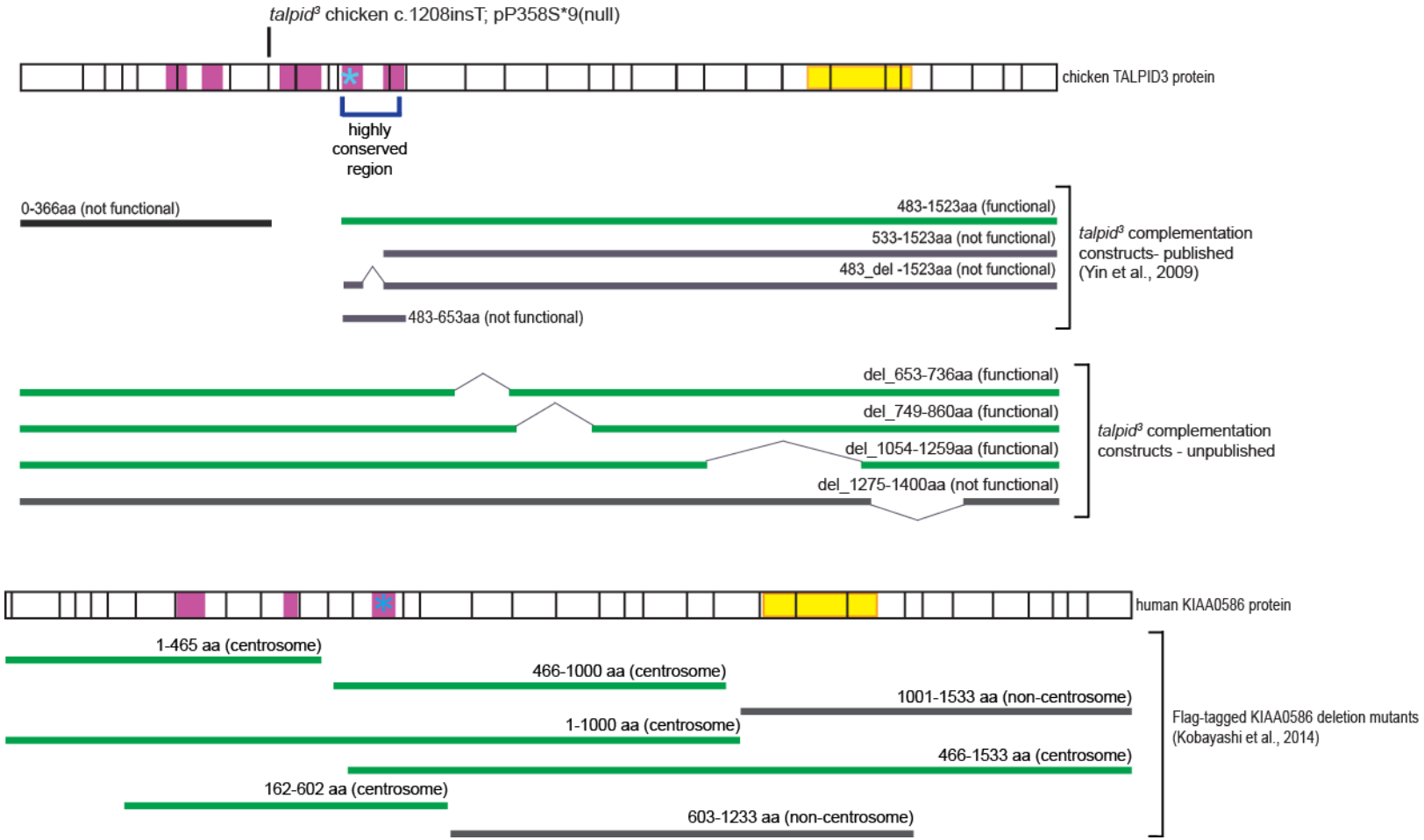
talpid3 chicken c.1208insT; pP358S*9(null)
chicken TALPID3 protein
highly conserved region
0-366aa (not functional)
483-1523aa (functional)
533-1523aa (not functional)
483_del -1523aa (not functional)
483-653aa (not functional)
talpid3 complementation constructs- published (Yin et al., 2009)
del_653-736aa (functional)
del_749-860aa (functional)
del_1054-1259aa (functional)
del_1275-1400aa (not functional)
talpid3 complementation constructs - unpublished
human KIAA0586 protein
1-465 aa (centrosome)
466-1000 aa (centrosome)
1001-1533 aa (non-centrosome)
1-1000 aa (centrosome)
466-1533 aa (centrosome)
162-602 aa (centrosome)
603-1233 aa (non-centrosome)
Flag-tagged KIAA0586 deletion mutants (Kobayashi et al., 2014)

Figure 3.2 TALPID3/KIAA0586 functional domain studies. Schematic of TALPID3 chicken protein and human KIAA0586 protein, with the *talpid*^{3} chicken mutation annotated. Black vertical lines along proteins indicate exon boundaries. Purple boxes mark coiled-coil domains and the yellow box marks the predicted intrinsically disordered domain. A blue asterisk marks the coiled-coil domain in the conserved region that is essential for function. Green lines represent functional regions of protein or regions that localise to the centrosome. Grey lines represent non-functional regions of protein or regions that do not localise to the centrosome. The complementation assay (Yin et al., 2009) demonstrating that the conserved coiled-coil domain is essential but not sufficient for function is directly below the chicken protein. The second complementation assay (Davey lab, unpublished) tested regions of the C-terminal by deleting sections of the protein including regions that overlap with the predicted intrinsically disordered domain, demonstrating a region of function between amino acid residues 1275-1400. The Flag-tagged KIAA0586 deletion mutants tested in human RPE1 cells are presented under the human protein schematic (Kobayashi et al., 2014) and show a region at the N-terminal of KIAA0586 that localises to the centrosome as well as a region containing the conserved essential coiled-coil domain that localises to the centrosome.

3.1.2 Ciliopathies associated with *KIAA0586*

Mutations in *KIAA0586* have been shown to cause ciliopathies including Joubert syndrome, Short-Rib Polydactyly syndrome (SRPS) and Jeune syndrome (Akawi et al., 2015; Alby et al., 2015; Bachmann-Gagescu et al., 2015; Fleming et al., 2017; Malicdan et al., 2015; Pauli et al., 2018; Roosing et al., 2015; Stephen et al., 2015; Vilboux et al., 2017). Joubert syndrome is classified by brain and spinal malformations and can be diagnosed by the Molar Tooth Sign. The Molar Tooth Sign is caused by a deep interpeduncular fossa, elongated, thick and mal-oriented superior cerebellar peduncles and absent or hypoplastic cerebellar vermis that give the appearance of a "molar tooth" at the junction of the midbrain and hindbrain on an axial MRI (Gleeson et al., 2004; Maria et al., 1999; Parisi, 2009). Common clinical characteristics also include hypotonia, abnormal eye movements and abnormal breathing patterns (Maria et al., 1999; Parisi, 2009; Parisi et al., 2007). Short Rib Polydactyly syndrome and Jeune syndrome fall under the same group of skeletal dysplasias characterised by a constricted thoracic cage, short ribs and shortened tubular bones (Ho et al., 2000; Huber & Cormier-Daire, 2012). Additional features can include polydactyly, renal, liver and retinal involvement (Baujat et al., 2013; Huber & Cormier-Daire, 2012). Transduction of the Hedgehog signalling pathway is important in skeletal development for patterning of the limb, intramembranous ossification in craniofacial bones and endochondral ossification in other parts of the skeleton, joint formation and maintenance and repair of bones

throughout life (Alman, 2015; Ehlen et al., 2006; Yang et al., 2015), hence the range of skeletal abnormalities associated with ciliopathies.

The ciliopathy patients contain a range of mutations that affect different regions of the KIAA0586 protein and cause a wide range of phenotypes, which mostly follow a pattern of more severe phenotypes associated with mutations at the N-terminal region of the KIAA0586 protein, prior to the essential coiled-coil domain (Figure 3.3) (Akawi et al., 2015; Alby et al., 2015; Bachmann-Gagescu et al., 2015; Malicdan et al., 2015; Roosing et al., 2015; Stephen et al., 2015). Of the mutations identified, one particular mutation appears to arise more frequently. This mutation, c.428delG p.Arg143Lysfs*4 (seen on Figure 3.3) is predicted to result in a premature stop codon, resulting in production of only 143 amino acids, and therefore, predicted to be incompatible with life; however, the evidence from patients suggests that the mutation is hypomorphic and that there is still some functional KIAA0586 protein being produced (Pauli et al., 2018). This common variant mutation is found at a Minor Allele Frequency of 0.003916 (378 out of 96,534 alleles) in the ExAC database, which shows it is found in healthy individuals in the general population. With a Minor Allele Frequency of <0.05 this is considered a rare common variant mutation. Most of the patients identified with *KIAA0586* mutations contain compound heterozygous mutations, and the majority of published compound heterozygous cases (34/49) contain the common variant mutation, c.428delG (p.Arg143Lysfs*4), as one of the mutations, thus supporting the common variant mutation as having some functional protein (Akawi et al., 2015; Bachmann-Gagescu et

al., 2015; Malicdan et al., 2015; Roosing et al., 2015; Stephen et al., 2015). There are two reported cases where a patient is homozygous for the common variant mutation and presents with a Joubert syndrome phenotype (Bachmann-Gagescu et al., 2015; Roosing et al., 2015) and one healthy individual homozygous for this mutation (Pauli et al., 2018). In one homozygous case the patient presents with a Molar Tooth Sign, abnormal eye movements and brainstem heterotopia; however, this patient also has a rare deleterious variant in another known Joubert syndrome gene, which could be contributing to the phenotype (Bachmann-Gagescu et al., 2015). In the second homozygous case, the patient presents with a Molar Tooth Sign and no additional phenotypic details available; there are no additional known Joubert syndrome gene mutations identified in the patient suggesting that the common variant mutation could be responsible for the Molar Tooth Sign (Roosing et al., 2015). Taken together, the relatively mild ciliopathy phenotypes of patients with the common variant mutation and the viability of patients who are homozygous for the common variant mutation suggests that some functional KIAA0586 protein is being produced despite this mutation.

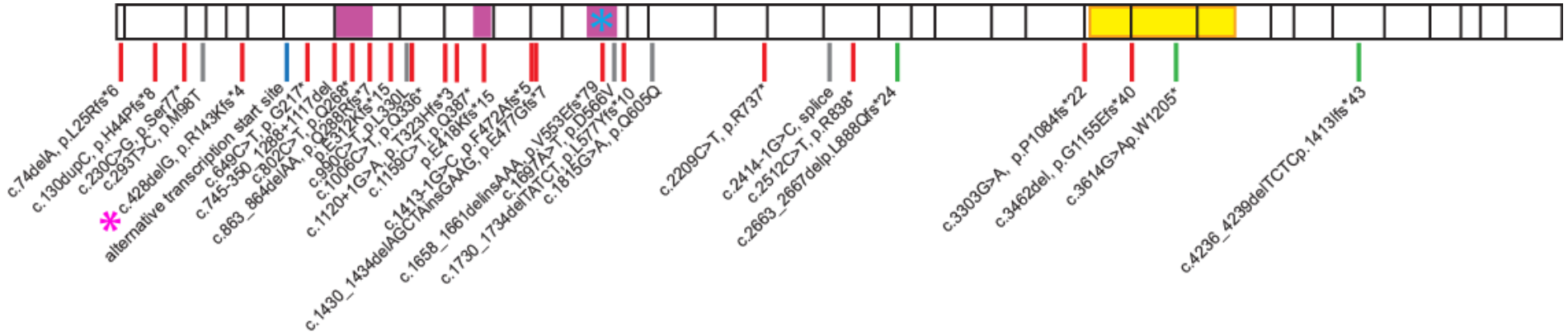

Figure 3.3 Human ciliopathy patient mutations mapped on a schematic of the human KIAA0586 protein. Black vertical lines along the protein indicate exon boundaries. Purple boxes mark coiled-coil domains in the protein, the blue asterisk indicates the conserved coiled-coil domain that is essential for function and the yellow box indicates the predicted intrinsically disordered domain. Red horizontal lines indicate mutations that cause premature stop codons. Grey horizontal lines indicate splice variant mutations and green horizontal lines indicate single heterozygous deleterious mutations. The pink asterisk indicates the common variant mutation. The blue horizontal line indicates a predicted potential alternative start codon that could be used for protein expression in human.

The severity of the phenotype seen in patients is largely associated with the region of the protein that is affected in the patient. Where mutations occur prior to the essential coiled-coil domain and the patient does not contain the common variant mutation, patients tend to present with a more severe phenotype consisting of additional abnormalities such as polydactyly and shortening of the long bones (Bachmann-Gagescu et al., 2015; Malicdan et al., 2015) and in the most severe cases, embryonic lethality (Alby et al., 2015). Unlike the severe embryonic lethal phenotype seen in animal models lacking TALPID3, only two homozygous *KIAA0586* mutations have been identified as producing a lethal phenotype (Figure 3.4) (Alby et al., 2015). Both the homozygous c.230C>G, p.Ser77* variant and the homozygous c.1815G>A (splice) variant resulted in embryonic lethality (Alby et al., 2015). In both cases, the phenotypes were severe, with skeletal abnormalities including polydactyly, short ribs and micromelia. Additionally the foetuses presented with cleft palate and cerebral phenotypes. Testing confirmed nonsense-mediated decay of *KIAA0586* in the foetus homozygous for the c.230C>G, p.Ser77* variant, confirming that no functional KIAA0586 protein was produced. There were three live births of individuals homozygous for the c.1815G>A (splice) variant, however all died soon after birth (Alby et al., 2015), which suggests that no functional protein was produced and provides further evidence that the C-terminal of the protein is required for function.

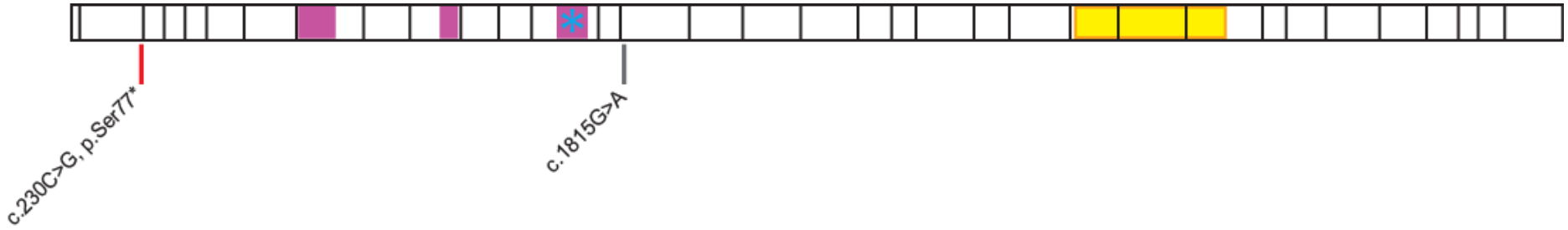

Figure 3.4 Schematic of lethal mutations in *KIAA0586* in human ciliopathy patients. The mutation c.230C>G, p.Ser77* is found in a homozygous state and results in lethality. The mutation c.1815G>A is found in a homozygous state and results in lethality. The red line at c.230C>G, p.Ser77* indicates that the mutation is predicted to result in a premature stop codon. The grey line at c.1815G>A indicates that the mutation is predicted to result in a splice variant mutation.

Despite only a few cases of embryonic lethality being associated with mutations in human *KIAA0586*, the evidence from the *talpid*^{3} chicken mutant, the talpid3$^{-/-}$ mouse and the *TALPID3* knockdown zebrafish suggests that all of the patients would present with severe phenotypes linked to Hedgehog signalling pathway defects such as polydactyly, skeletal defects, brain and neural abnormalities (Bangs et al., 2011; Ben et al., 2011; Davey et al., 2006). However, this is not observed, instead only a small number of cases fall into the category of severe non-lethal ciliopathy phenotypes (Figure 3.5) including polydactyly and skeletal defects (Bachmann-Gagescu et al., 2015; Malicdan et al., 2015). There are three patients with mutations in both *KIAA0586* alleles that present with a more severe phenotype, including severe eye abnormalities, polydactyly and skeletal defects (Bachmann-Gagescu et al., 2015; Malicdan et al., 2015). Of the three patients, one is compound heterozygous for c.745-350_1288+1117del and c.130dupC, p.H44Pfs*8, the second patient is compound heterozygous for c.745-350_1288+1117del and c.990C>T, p.L330L and the third patient is homozygous for c.1697A>T, p.D566V. The two compound heterozygous patient mutations occur prior to the essential coiled-coil domain suggesting that the protein loses the essential region for function, which could explain the more severe phenotype. The third patient, although occurring after the essential coiled-coil domain still disrupts the conserved region which most likely explains the more severe phenotype. Additionally there are three single rare deleterious variants that are associated with more severe phenotypes, including severe eye abnormalities, polydactyly and skeletal

defects (Bachmann-Gagescu et al., 2015). The single rare deleterious mutations are found after the conserved essential coiled-coil domain, more towards the C-terminal and the predicted intrinsically disordered domain of the KIAA0586 protein. These mutations towards the C-terminal in patients with a more severe ciliopathy phenotype, support the studies suggesting that an important functional domain is found at the C-terminal of KIAA0586. These patients however also contain additional mutations in other ciliopathy genes including *TCTN3*, *C2CD3* and *AHI1* (Bachmann-Gagescu et al., 2015). Mutations in all three genes can caused Joubert Syndrome and mutations in *TCTN3* and *C3CD3* can also cause orofaciodigital syndrome (Bachmann-Gagescu et al., 2015; Cortés et al., 2016; Parisi et al., 2006; Thomas et al., 2012), suggesting that there could also be other factors that contribute to the severe ciliopathy phenotype observed in the patients with single rare deleterious mutations in *KIAA0586*.

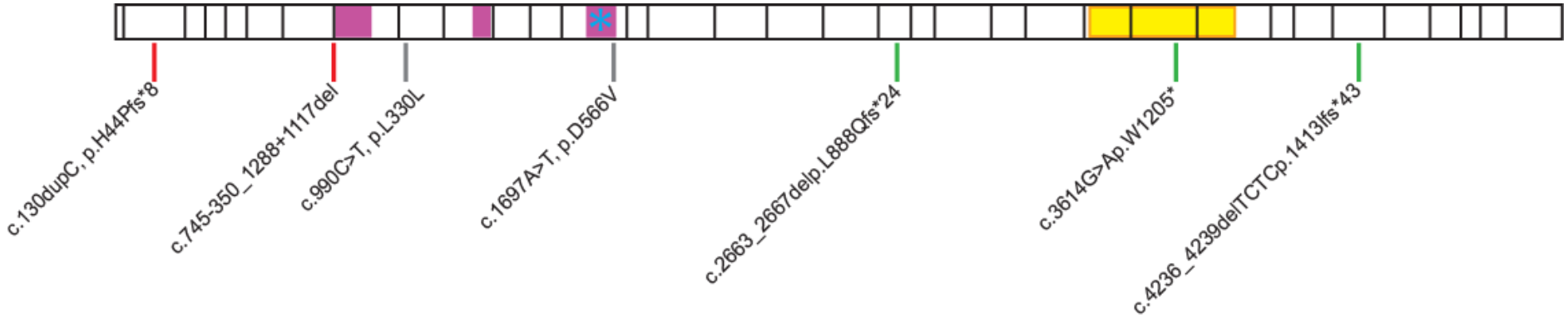

Figure 3.5 Schematic of mutations in KIAA0586 that are linked to a severe non-lethal patient phenotype. The annotated mutations, identify those that are associated with a more severe patient phenotype. As well as typical characteristics of Joubert syndrome such as a Molar Tooth sign, developmental delay, hypotonia and abnormal eye movements at birth, these patients have a range of skeletal defects, polydactyly, more severe neural defects and more severe eye abnormalities. The mutation c.745-350_1288+1117del is found in a compound heterozygous state in one patient combined with c.130dupC and in a compound heterozygous state with another patient with c.990C>T. The mutation c.1697A>T was found in a homozygous state. Red lines indicate mutations that result in a premature stop codon. Grey lines indicate a splice variant mutation. The green lines represent mutations that present as single rare deleterious variants in patients with severe phenotypes.

Ciliopathy patients containing the remaining mutations in *KIAA0586* present with relatively mild phenotypes, the majority of which are caused by compound heterozygous mutations consisting of the common variant mutation and a second mutation (Akawi et al., 2015; Bachmann-Gagescu et al., 2015; Malicdan et al., 2015; Roosing et al., 2015; Stephen et al., 2015). There is no apparent pattern between where the second mutations occur in relation to the essential coiled-coil domain and what the phenotype of the patient is, however the presence of the common variant mutation is predicted to account for the mild phenotype of most these patients by producing some functional protein (Pauli et al., 2018). Of the patients with mild phenotypes, there are three exceptions to the pattern that do not contain the common variant mutation but still present with a mild phenotype (Figure 3.6). Of these three patients, one is homozygous for c.2414-1G>C (splice) (Roosing et al., 2015), which occurs after the essential coiled-coil domain and may still produce some of the functional region of protein, thus explaining the relatively mild phenotype. The mutation c.74delA, p.L25Rfs*6 is homozygous (Roosing et al., 2015) and given the early point in the protein at which it occurs, it is possible that an alternative start codon is also able to produce protein in order to produce some functional protein in this patient to explain the mild phenotype. The c.1430_1434delAGCTAinsGAAG, p.E477Gfs*7 mutation occurs in combination with c.3303G>A, p.P1084fs*22 (Bachmann-Gagescu et al., 2015); both of these mutations are predicted to result in a premature stop codon, suggesting loss of function of the protein. However, the mild

phenotype associated with this compound heterozygous mutation suggests that there may be functional protein; the second mutation occurs after the essential coiled coil domain, which could explain the presence of functional protein and therefore the mild phenotype. Although these mutations present as the exceptions to the trend of lack of severity in patient phenotypes, it is possible that this mutation is not consistent in all tissue types; different expression levels and transcription start codons in different tissue types could explain the patient's lack of phenotypic severity, and is not uncommon in ciliopathy patients with overlapping ciliopathy phenotypes and syndromes (Ware et al., 2011).

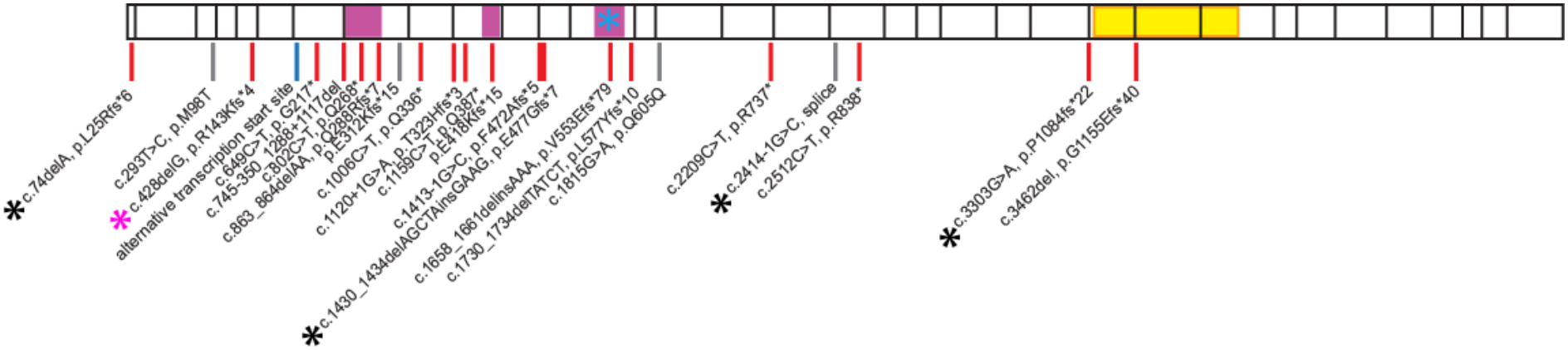

Figure 3.6 Schematic of mutations in KIAA0586 that are found in patients with a mild phenotype. Patients classified as having a mild phenotype have been diagnosed with Joubert syndrome; most of these patients present with the Molar Tooth Sign, developmental delay, hypotonia, ataxia and often abnormal eye movements early on in life. With the exception of the mutations indicated by a black asterisk, all of these mutations are found in patients with compound heterozygous mutations combined with the common variant mutation, which is marked by the pink asterisk. Of the mutations that do not occur in combination with the common variant mutation, c.74delA, p.L25Rfs*6 is homozygous, c.2414-1G>C, splice is homozygous and c.1430_1434delAGCTAinsGAAG, p.E477Gfs*7 occurs in combination with c.3303G>A, p.P1084fs*22. Red horizontal lines indicate mutations that cause premature stop codons. Grey horizontal lines indicate splice variant mutations. The blue line indicates a potential alternative start codon.

One explanation for the possible production of functional protein, for example in patients with the common variant mutation, is a potential downstream alternative start codon that exists in human *KIAA0586*. The alternative start codon, identified in Zenbu in FANTOM5, produces a shorter protein of 1463 amino acids (NM_001244193/NP_001231122) (Figure 3.7 A) that still contains the essential coiled-coil domain required for function and localisation to the centrosome (Lizio et al., 2015). CAGE data in FANTOM5 demonstrates that this transcript is expressed in a range of human tissue and cell types, supporting this prediction (Figure 3.7 B). Although unconfirmed in patients, mutations that produce premature stop codons prior to this alternative start codon, such as the common variant mutation, might still produce functional protein from this alternative start codon. It is also possible that expression only occurs from this alternative start codon in some tissue types, which would explain why only some tissues and organs are affected in patients with mutations in *KIAA0586*. This is one possible explanation for some of the less severe phenotypes seen in ciliopathy patients with mutations in *KIAA0586* and may explain why some of the human mutations appear to be hypomorphic.

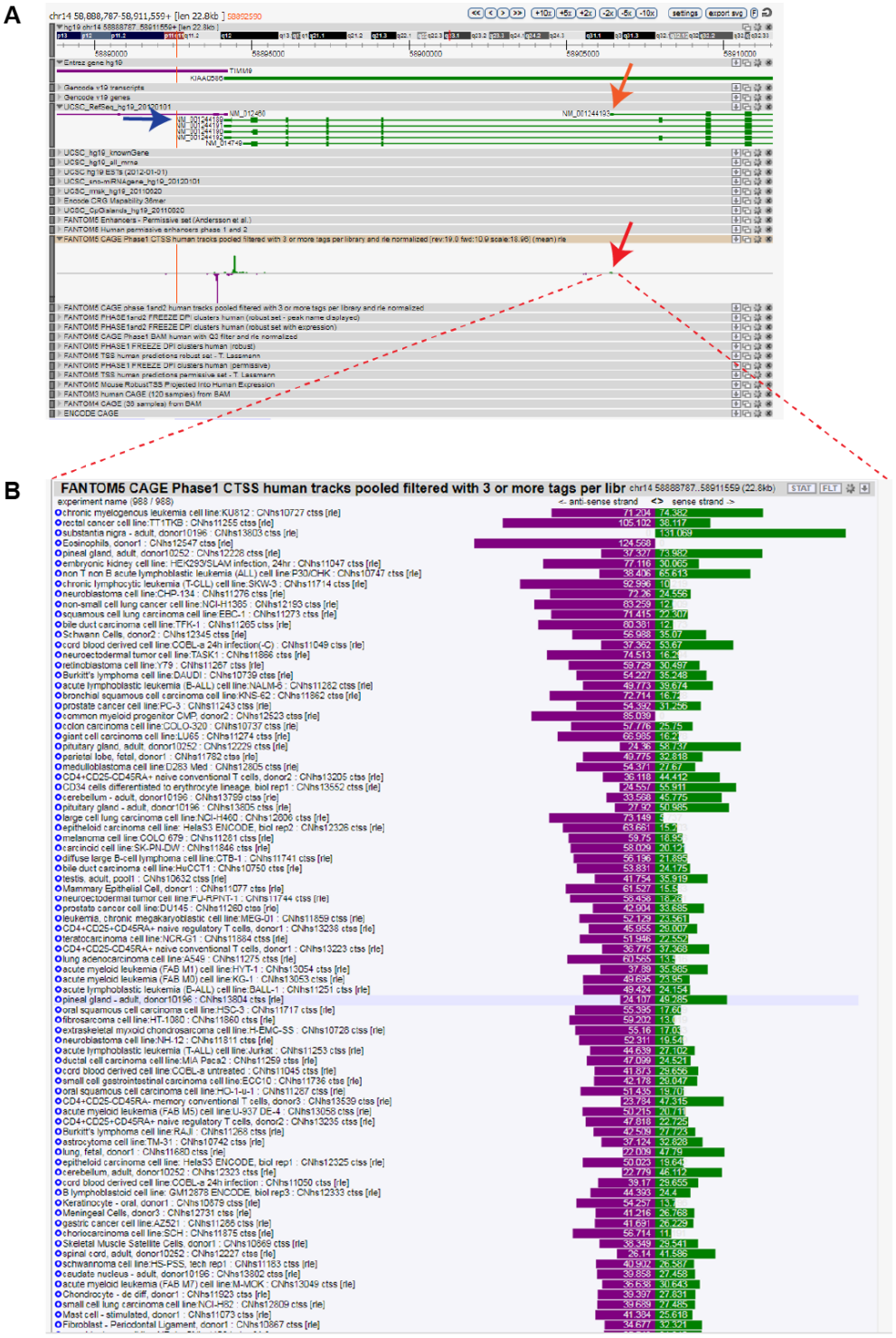

Figure 3.7 The presence of predicted alternative start codon for human KIAA0586 was identified on Zenbu in Fantom5. (**A**) A blue arrow indicates the transcript that represents human KIAA0586 that produces a protein of 1644 amino acids (NM_001244189). The orange arrow indicates an alternative downstream transcript that would produce a KIAA0586 protein of 1463 amino acids (NM_001244193). The red arrow marks the transcription start site associated with NM_00244193. (**B**) The dotted lines from the red arrow indicate FANTOM5 CAGE data that shows the expression of the transcript associated with NM_00244193 in a range of different

human cell lines and tissue types. This range of expression demonstrates that the alternative start codon is expressed and could be a valid explanation for the ability to produce functional KIAA0586 protein in human ciliopathy patients with a less severe phenotype.

3.1.3 TALPID3/KIAA0586 localisation studies

As well as questions surrounding how mutations in *KIAA0586* can provide such a wide range of phenotypes in human patients, there are still questions that remain unanswered relating to the dynamic localisation and protein interacting network of TALPID3. Multiple antibodies against KIAA0586 exist that were raised against a range of different regions of the KIAA0586 protein. Of these antibodies, one was raised against the C-terminal of chicken TALPID3 (Yin et al., 2009) and one was raised against the N-terminal of mouse KIAA0586 (Wu et al., 2014), while the remaining antibodies were raised against various regions of human KIAA0586 (Kobayashi et al., 2014; Stephen et al., 2015; Yadav et al., 2016). Despite all of these antibodies showing localisation of KIAA0586 to the centrosome, there has been some conflicting evidence with two studies showing localisation of KIAA0586 to both the mother and daughter centrioles (Kobayashi et al., 2014; Yin et al., 2009), and one study showing that KIAA0586 localises more to the mother centriole than the daughter centriole (Wu et al., 2014). Protein tagging has also been used as a way to study the localisation of KIAA0586 and to identify proteins that interact with KIAA0586 (Davey et al., 2006; Kobayashi et al., 2014). A C-terminal TALPID3-myc tag and an N-terminal TALPID3-HA tag in cultured chicken cells showed cytoplasmic localisation (Davey et al., 2006), suggesting that the overexpression of TALPID3 prevents correct localisation. A Flag-KIAA0586 tag in human cells proved more effective, demonstrating localisation to the centrosome (Kobayashi et al., 2014), however a tagged protein is not expressed from the endogenous locus and this study was

completed in wildtype RPE1 cells that already express KIAA0586 showing that the levels observed were higher than would be expected in normal healthy conditions (Kobayashi et al., 2014). Although overexpression studies can provide a wealth of information, they may not accurately reflect the expression pattern from the endogenous locus and can produce artefacts in other cellular processes, affect protein folding and disturb downstream regulation (Fetter et al., 2015; Gibson et al., 2013), therefore demonstrating the need for an alternative tool to monitor endogenous levels of TALPID3.

Despite antibodies against KIAA0586 and KIAA0586-protein tags showing localisation to the centrosome, these methods both have limitations that prevent analysis of endogenous KIAA0586 protein levels in a dynamic state. The pattern of localisation of KIAA0586 to the centrosome, does not explain how mutations in *KIAA0586* can lead to a satellite phenotype in *talpid*^{3} mutant cells or in human RPE1 cells depleted of KIAA0586 (Kobayashi et al., 2014; Stephen et al., 2015); in addition it does not explain the actin phenotype seen in *talpid*^{3} (Yin et al., 2009), which leads to the question of where in the cell is KIAA0586 interacting with proteins such as PCM1 to influence satellite dispersal as well as how and where does KIAA0586 control actin regulation and organisation. These unanswered questions highlight the need for a new approach to study the dynamic localisation of KIAA0586 at endogenous levels, to understand the dynamic localisation of KIAA0586 and to identify the KIAA0586 interacting proteins.

3.1.4 Aims

To date, it has not been possible to uncover the actual structure (Acharya Lab, personal communication) or predicted structure of TALPID3, or to identify all of the functional domains, which may help to understand both TALPID3 function and structure, in part due to the predicted intrinsically disordered domain found at the C-terminal of TALPID3 and the lack of tools to study TALPID3 at an endogenous level. The recent discovery of ciliopathy patients with mutations in *KIAA0586* has presented a variety of phenotypes ranging from mild to severe, which if modelled could help to identify hypomorphic mutations leading to an insight into additional regions in the protein that are necessary for function. The aim of this study was to determine if *KIAA0586* ciliopathy mutations can be modelled in *talpid*^{3} embryos, in an attempt to understand the phenotypes associated with each mutation and where the important functional domains are in the protein. In addition, the study aimed to overcome previous complications of studying the subcellular localisation of TALPID3, by introducing a fluorescent tag at the endogenous locus of *TALPID3* in primary chicken cells, which would also provide a tool for future studies into the protein network of TALPID3.

3.2 Results

3.2.1 Electroporation of human *KIAA0586* can rescue Hedgehog-dependent expression patterns in the *talpid*^{3} neural tube

The patterning of neural progenitors along the dorsoventral axis of the developing neural tube requires highly regulated signalling events, one of which is Sonic Hedgehog (Briscoe & Ericson, 1999). The initial source of Sonic Hedgehog signal for neural patterning comes from the notochord, which lies below the ventral midline of the neural plate. The specification of cell types within the ventral neural tube depends on levels of Sonic Hedgehog, with a gradient running high to low from ventral to dorsal (Goetz et al., 2009). Cells in the dorsal half of the neural tube generate neurons that relay sensory information, whereas cells in the ventral half of the neural tube generate motor neurons and ventral interneurons. The distinct groups of motor neurons and ventral interneurons arise at distinct positions in the ventral neural tube (Briscoe & Ericson, 1999). For example Nkx2.2, Islet1 and Nkx6.1 are expressed in specific progenitor cells in the ventral neural tube whereas Pax7 expression is limited to dorsal progenitors (Figure 3.8 A). Due to abnormal Hedgehog signalling, the Hedgehog-dependent expression patterns in the *talpid*^{3} neural tube are lost during early development in the chick. *Talpid*^{3} mutants have a gain of function phenotype in the dorsal neural tubes that presents as a ventral expansion of the expression domains, such as Pax7 (Figure 3.8 B); a loss of function phenotype is seen in the ventral

neural tube of *talpid*^{3} mutants, which presents as a loss of expression domains such as Nkx2.2, Nkx6.1 and Islet1 (Figure 3.8 B). This loss of function phenotype results from the loss of the Hedgehog gradient due to loss of cilia.

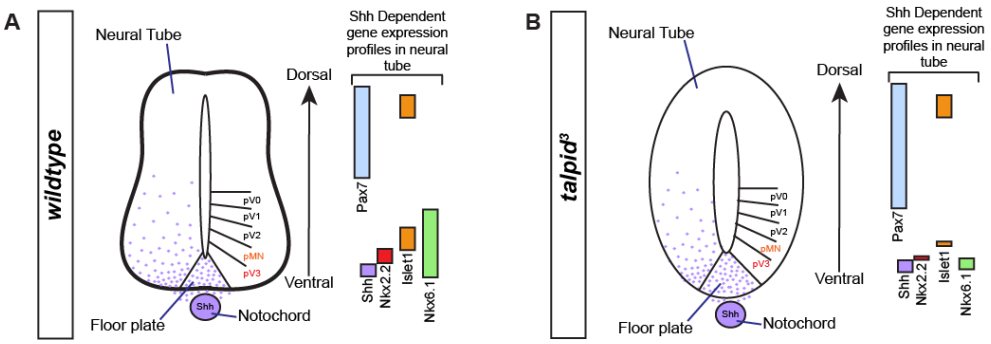

Figure 3.8 Schematic showing expression domains in the wildtype neural tube compared to abnormal expression domains in the *talpid*^{3} neural tube. (**A**) Schematic of wildtype neural tube with normal Pax7, Nkx2.2, Islet1 and Nkx6.1 expression domains annotated. (**B**) Schematic of *talpid*^{3} neural tube with abnormal Pax7, Nkx2.2, Islet1 and Nkx6.1 expression domains of caused by the mutation in *TALPID3*.

In order to determine if full length human *KIAA0586* could rescue Hedgehog-dependent neural tube patterning in *talpid*^{3}, electroporation with a full length human *KIAA0586* cDNA construct (pCAGGS-hsKIAA0586) was carried out in the neural tube of *talpid*^{3} and wildtype embryos and Hedgehog-dependent expression patterns and cell types were examined. The construct being tested, was injected at approximately the base of the neural tube of Hamburger Hamilton stage 10-12 *talpid*^{3} flock embryos. The embryo was electroporated, immediately following successful injection of the DNA construct into the neural tube, by placing electrodes either side of the neural tube at the level of injection. Embryos were then allowed to develop for a further 48-60 hours to Hamburger Hamilton stage 22-24. The embryos were examined for signs of successful electroporation by the presence of eGFP expression in the neural tube. A section of the neural tube between the forelimb and hindlimb containing eGFP was harvested and sectioned, to analyse for rescue of expression.

Control electroporations of pCAGGS-eGFP showed no change in expression patterns of Pax7, Islet1, Nkx2.2 or Nkx6.1 in wildtype embryos (Figure 3.9 A, C, E, G) or Pax7, Islet1 and Nkx2.2 in *talpid*^{3} embryos compared to the non-electroporated side (Figure 3.9 B, D, F). These results demonstrate that the injection technique, the introduction of eGFP and the electroporation technique do not change the Hedgehog-dependent expression patterns in the neural tube.

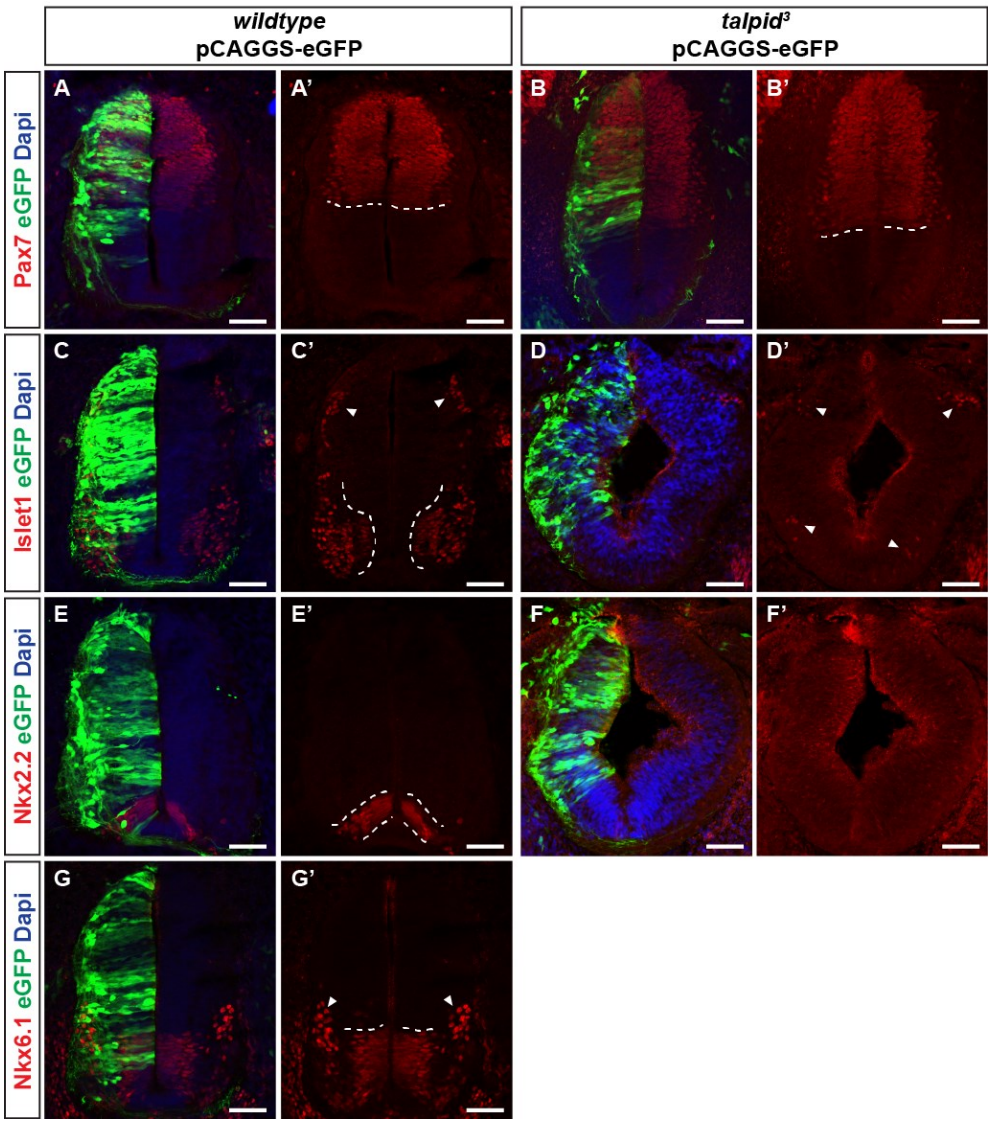

Figure 3.9 Control electroporation of pCAGGS-eGFP into the developing neural tube does not change Hedgehog-dependent expression patterns. Following electroporation with pCAGGS-eGFP, cells that took up the DNA are marked by eGFP, Dapi marks the nuclei in blue and the protein expression being examined is in red. (**A**) The expression pattern of Pax7 remains unchanged in the dorsal region of the electroporated side of the wildtype neural tube, when compared to the non-electroporated side. Domains are marked by white dashed lines. (**B**) The ventrally extended expression pattern of Pax7 remains unchanged in the electroporated side of the *talpid*^{3} neural tube when compared to the non-electroporated side. Domains are marked by a white dashed lines. (**C**) The expression pattern of Islet1 remains unchanged in wildtype at the lateral edge of the ventral neural tube in differentiating motor neurons of the electroporated side, when compared to the non-electroporated side. Domains are marked by white dashed lines. The dorsal domain of Islet1 is marked by white arrowheads. (**D**) The loss of expression of Islet1 remains unchanged in *talpid*^{3} at the lateral edge of the ventral neural tube in the electroporated side, when compared to the non-electroporated side. A few cells expressing Islet1 are indicated by white

arrowheads. The dorsal domain of Islet1 is marked by white arrowheads. (**E**) The expression pattern of Nkx2.2 remains unchanged in the ventral neural tube of the electroporated side in wildtype when compared to the non-electroporated side. Domains are marked by white dashed lines. (**F**) The loss of expression of Nkx2.2 remains unchanged in the ventral neural tube of the electroporated side in *talpid*^{3} when compared to the non-electroporated side. (**G**) The expression pattern of Nkx6.1 remains unchanged in the ventral neural tube of wildtype in the electroporated side, when compared to the non-electroporated side. Domains are marked by white dashed lines. Arrowheads mark the regions of expression at the lateral edges of the neural tube. All scale bars, 50 μm.

On electroporation of pCAGGS-ggKIAA0586 (chicken *TALPID3* construct), a rescue of expression patterns of Pax7 and Islet1 was seen in *talpid*^{3} embryos. The abnormal ventral expansion of Pax7 expression was reduced to a smaller domain that remained in the dorsal half of the neural tube on the electroporated side in *talpid*^{3}, more closely resembling the expression pattern in Pax7 in the wildtype (Figure 3.10 A, B). Islet1 expression was rescued at the site of electroporation in the *talpid*^{3} neural tube, showing a similar expression domain to that of the wildtype; the non-electroporated side of the neural tube did not express Islet1 (Figure 3.10 C, D). Electroporation failed to rescue expression of Nkx2.2 in the *talpid*^{3} neural tube (Figure 3.10 E, F). In conclusion, these results show that expression of chicken *TALPID* in *talpid*^{3} can rescue Hedgehog dependent neural tube patterning of Pax7 and Islet1, but under the conditions of this experiment was unable to rescue expression of Nkx2.2. These results demonstrate that chicken *TALPID3* can rescue both gain of function and loss of function phenotypes seen in the *talpid*^{3} neural tube. Additionally, these results demonstrate that following electroporation of a functional construct in the neural tube, the conditions of this experiment are appropriate for rescuing both gain of function and loss of function phenotypes in *talpid*^{3}.

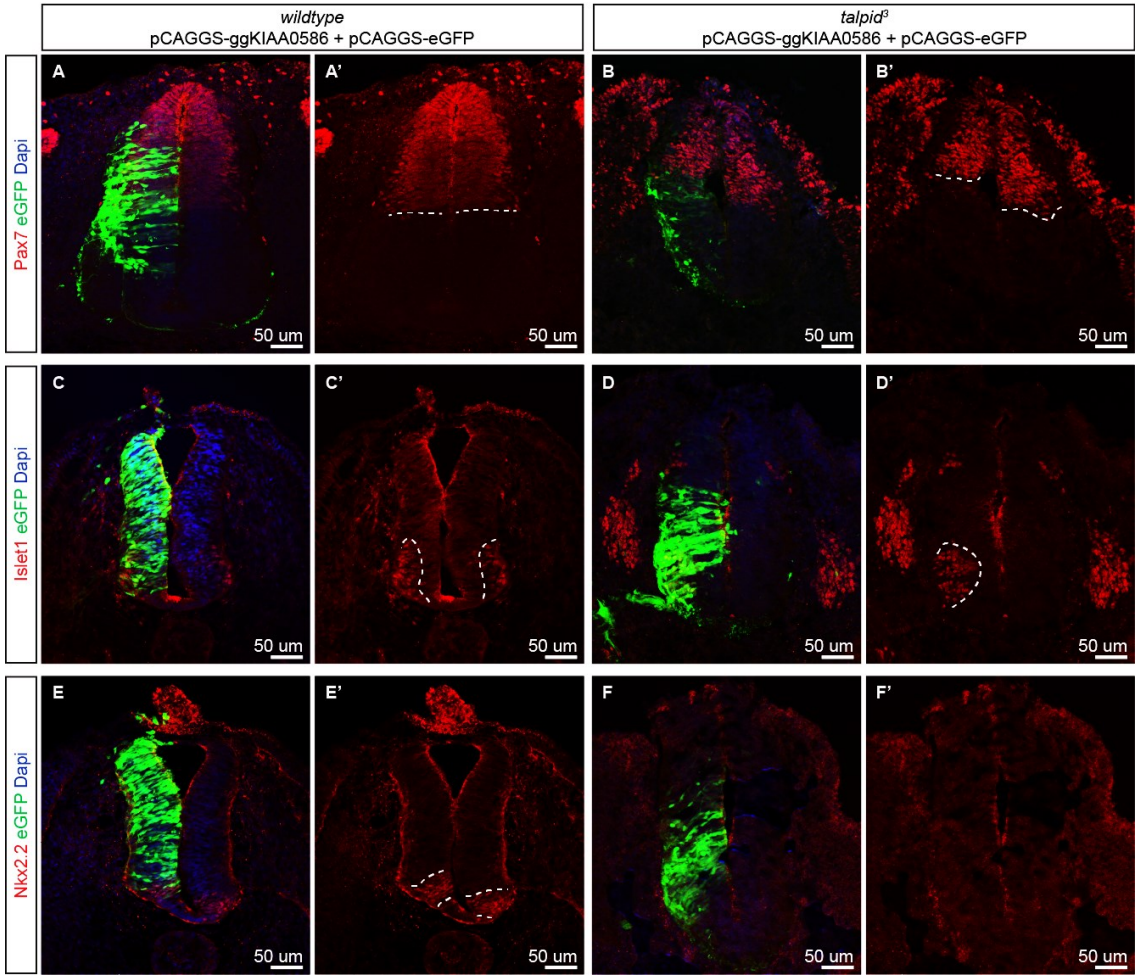
wildtype
pCAGGS-ggKIAA0586 + pCAGGS-eGFP
talpid3
pCAGGS-ggKIAA0586 + pCAGGS-eGFP
Pax7 eGFP Dapi
Islet1 eGFP Dapi
Nkx2.2 eGFP Dapi
A
A'
B
B'
C
C'
D
D'
E
E'
F
F'
50 um

Figure 3.10 Electroporation of full length chicken TALPID3 rescues expression in the *talpid*^{3} neural tube. Following electroporation with pCAGGS-ggKIAA0586 and pCAGGs-eGFP, cells that took up the DNA are marked by eGFP, Dapi marks the nuclei in blue and the protein expression being examined is in red. (**A**) Expression of Pax7 is found in the dorsal region of the neural tube in wildtype and remains unchanged on the electroporated side. (**B**) Expression of Pax7 is extended ventrally in *talpid*^{3}, but is reduced to a more dorsal region following rescue on the electroporated side of the neural tube. Expression domains of Pax7 are marked by a white dashed line on both sides of the neural tube. (**C**) Expression of Islet1 is found at the lateral side of the ventral neural tube in wildtype and remains unchanged on the electroporated side. (**D**) Islet1 expression is lost in *talpid*^{3}, but is rescued on the electroporated side of the neural tube, marked by a white dashed line. (**E**) Expression of Nkx2.2 is found in a small region of the ventral neural tube in wildtype and remains unchanged on the electroporated side. (**F**) Nkx2.2 expression is lost in *talpid*^{3}. No rescue of Nkx2.2 was observed following electroporation. All scale bars, 50 µm.

On electroporation of pCAGGS-hsKIAA0586, a rescue of the gain of function expression pattern of Pax7 was seen; additionally a partial rescue of the loss of function expression pattern of Iselt1, Nkx2.2 and Nkx6.1 was seen. The partial rescue of Islet1 and Nkx2.2 both showed a non-cell autonomous effect (Figure 3.11). The abnormal ventral expansion of Pax7 expression was reduced to a smaller domain that remained in the dorsal half of the neural tube on the electroporated side in *talpid*^{3} (n=4), more closely resembling the expression pattern in wildtype (Figure 3.11 A, B). The electroporated side of the *talpid*^{3} neural tube contained additional Islet1-expressing cells towards the lateral edge of the neural tube (n=2)(Figure 3.11 C, D); these cells were not all marked by eGFP expression, suggesting a non-cell autonomous effect. There was a small clump of Nkx2.2-positive cells in the ventral region of the neural tube on the electroporated side in *talpid*^{3} (n=2) (Figure 3.11 E, F); similar to Islet1, the cells were not all marked by eGFP expression, suggesting a non-cell autonomous effect. There were also Nkx6.1-positive cells that spanned a larger domain in the ventral region on the electroporated side in the *talpid*^{3} neural tube (n=4) when compared to the non-electroporated side (Figure 3.11 G, H).

In conclusion, these results show that expression of human *KIAA0586* in *talpid*^{3} can rescue neural tube patterning of Pax7. Additionally, expression of human *KIAA0586* in *talpid*^{3} can partially rescue expression of Nkx6.1 and can produce a non-cell autonomous effect in Islet1 and Nkx2.2. These results suggest that human *KIAA0586* can function in the *talpid*^{3} chick to rescue the gain of function phenotype seen in the dorsal region of the neural tube, thus

supporting the use of the *talpid*^{3} chick for modelling human *KIAA0586* ciliopathy patient mutations in order to identify functional protein domains. The inability of human *KIAA0586* to fully rescue the loss of function phenotype seen in the ventral neural tube of *talpid*^{3} suggests that KIAA0586 may play a role in the cilia environment needed for responsiveness to Hedgehog signalling and that the protein domain responsible for this role differs between chicken and human.

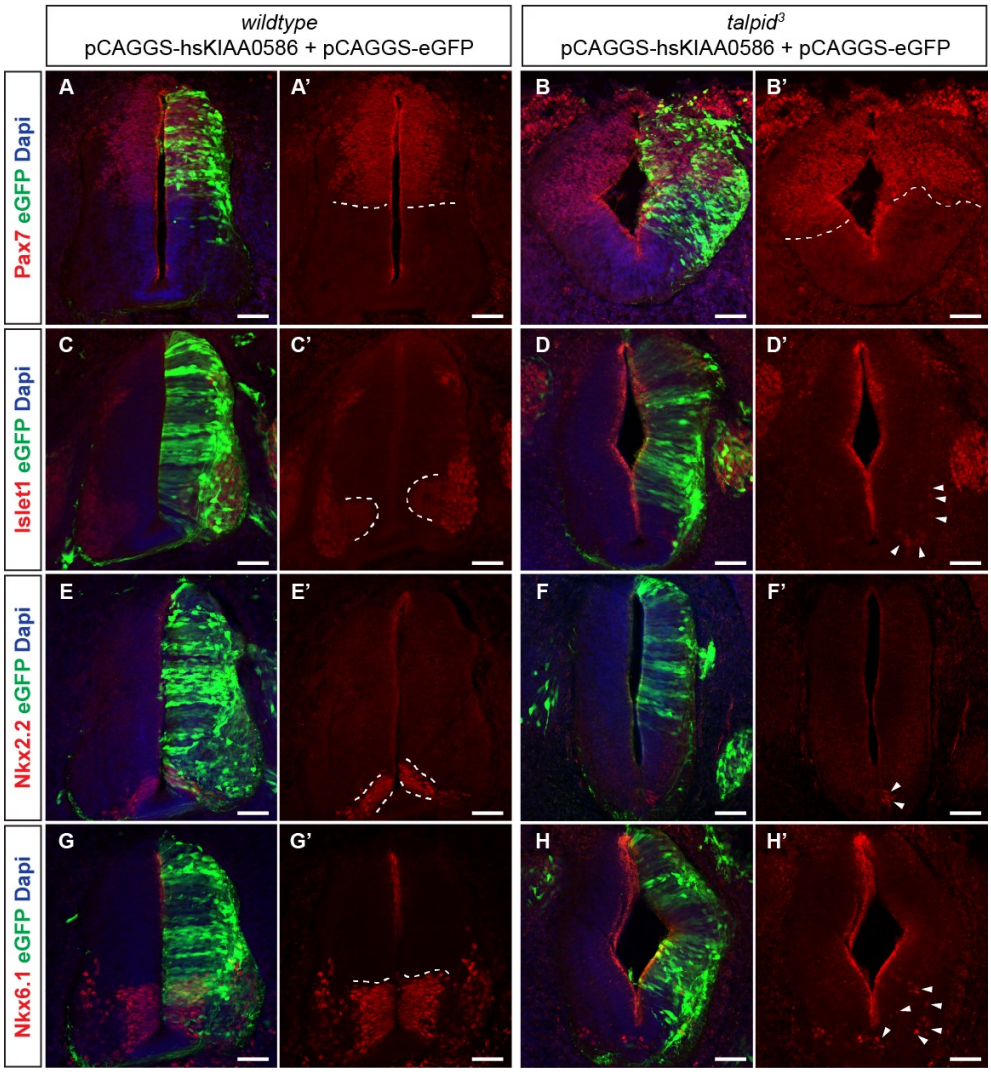

Figure 3.11 Electroporation of full length human KIAA0586 rescues expression in the talpid3 neural tube. Following electroporation with

pCAGGS-hsKIAA0586 and pCAGGs-eGFP, cells that took up the DNA are marked by eGFP, Dapi marks the nuclei in blue and the protein expression being examined is in red. (**A**) Expression of Pax7 is found in the dorsal region of the neural tube in wildtype and remains unchanged on the electroporated side. (**B**) Expression of Pax7 is extended ventrally in *talpid*^{3}, but is reduced to a more dorsal region following rescue on the electroporated side of the neural tube. Expression domains of Pax7 are marked by a white dashed line on both sides of the neural tube. (**C**) Expression of Islet1 is found at the lateral side of the ventral neural tube in wildtype and remains unchanged on the electroporated side. (**D**) Islet1 expression is lost in *talpid*^{3}. There are more cells expressing Islet1, marked by white arrowheads, on the electroporated side of the neural tube, suggesting rescue. (**E**) Expression of Nkx2.2 is found in a small region of the ventral neural tube in wildtype and remains unchanged on the electroporated side. (**F**) Nkx2.2 expression is lost in *talpid*^{3}. A small group of Nkx2.2 positive cells, marked by white arrowheads are seen on the electroporated side of the neural tube suggesting non-cell autonomous rescue. (**G**) Expression of Nkx6.1 is found in the ventral region of the neural tube in wildtype and remains unchanged on the electroporated side. (**H**) Nkx6.1 expression is lost in *talpid*^{3}. There are some cells expressing Nkx6.1, marked by white arrowheads, on the electroporated side of the neural tube suggesting rescue. All scale bars, 50 µm.

Having shown that human *KIAA0586* can rescue the gain of function phenotype in the dorsal neural tube of *talpid*^{3}, a ciliopathy patient mutation was modelled in *talpid*^{3} flock embryos to determine if hypomorphic mutations could be identified and whether from this modelling, additional functional domains could be identified in KIAA0586. In order to identify a mutation to model, *KIAA0586* ciliopathy mutations were examined for evidence of having some function based on remaining domains in the protein and patient phenotype associated with the mutation. A known patient mutation, c.1697A>T, p.D566V, (Figure 3.12) was chosen to model in the neural tube of developing *talpid*^{3} flock embryos. The mutation is a homozygous mutation found in a patient presenting with a Molar Tooth Sign, polydactyly and neurological defects (Bachmann-Gagescu et al., 2015). Unlike many of the patients presenting with mild forms of Joubert syndrome, the polydactyly associated with this patient suggested that the single amino acid change caused a severe change to the protein. Additionally, this mutation arises after the potential alternative start codon and results in a single amino acid change instead of a premature stop codon which suggests that nonsense-mediated decay does not occur. The mutation is recessive and the parents of the affected individual have a normal phenotype, therefore no change would be expected when modelling in wildtype embryos. Additionally, because the patient is homozygous for this mutation, any functional conclusions drawn from modelling the mutation can be directly linked to the phenotype associated with the patient instead of determining which mutation is responsible for functional abnormalities,

which would be the case in patients with compound heterozygous mutations; therefore modelling of c.1697A>T, p.D566V was attempted in *talpid*^{3} flock embryos.

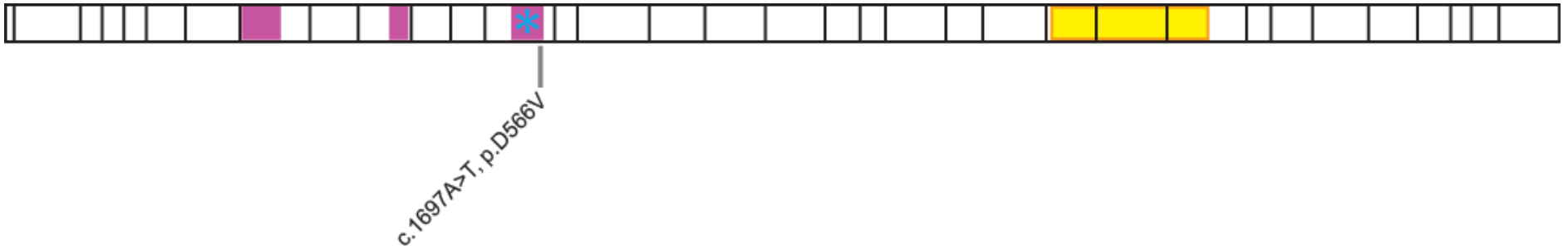

Figure 3.12 Schematic of human KIAA0586 protein with mutation c.1697A>T, p.D566V that was chosen to model in talpid3 flock embryos. Black vertical lines along the protein indicate exon boundaries. Purple boxes mark coiled-coil domains in the protein, the blue asterisk marking the conserved coiled-coil domain that is essential for function and the yellow box indicates the predicted intrinsically disordered domain.

On electroporation of pCAGGS-c.1697A>T,p.D566V into the neural tube of *talpid*^{3} flock embryos Pax7, Islet1, Nkx2.2 and Nkx6.1 remained unchanged in the wildtype neural tube (Figure 3.13 A-D) (n=3). No *talpid*^{3} embryos survived so analysis was not undertaken to determine if pCAGGS-c.1697A>T,p.D566V could functionally replace ggKIAA0586 (chicken TALPID3).

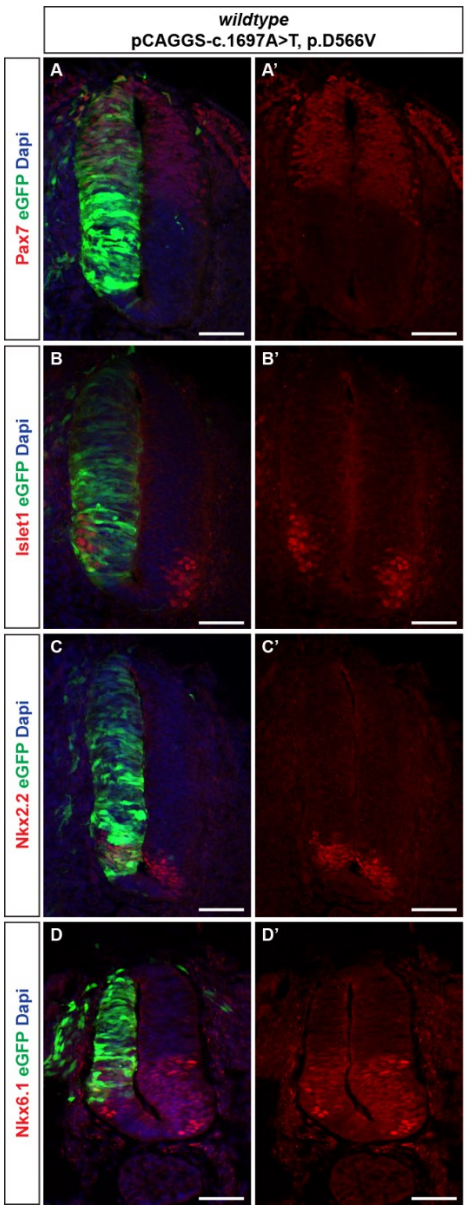

Figure 3.13 Electroporation of human ciliopathy mutation c.1697A>T, p.D566V does not alter expression in the neural tube of wildtype chicken embryos. Following electroporation with pCAGGS-c.1697A>T,p.D565V + pCAGGS-eGFP, cells that took up the DNA are marked by eGFP, Dapi marks the nuclei in blue and the protein expression being examined is in red. (**A**) Expression of Pax7 is found in the dorsal region of the neural tube and remains unchanged on the side electroporated with the mutant construct. (**B**) Expression of Islet1 is found in the lateral regions of the ventral neural tube and remains unchanged on the side electroporated with the mutant construct. (**C**) Expression of Nkx2.2 is found in the ventral neural tube and remains unchanged on the side electroporated with the mutant construct. (**D**) Expression of Nkx6.1 is found in the ventral third of the neural tube and remains unchanged on the side electroporated with the mutant construct. All scale bars, 50 µm.

3.2.2 Targeting the endogenous locus of *TALPID3* with a fluorescent tag

In order to overcome challenges presented by analysing the subcellular localisation with antibodies against TALPID3, CRISPR/Cas9 editing was designed and carried out with the aim of incorporating a fluorescent tag, through homology directed repair, at the endogenous locus of *TALPID3* in chicken Primordial Germ Cells (PGCs). By making a chicken cell line that stably expressed fluorescently labelled TALPID3, I intended to provide a tool to examine the dynamic subcellular localisation of TALPID3 at endogenous levels throughout the cell cycle while also providing a tool that could be used in future targeted proteomic studies. In addition this tool could be used to model the human *KIAA0586* ciliopathy mutations to determine if the KIAA0586 protein localisation is altered in response to the mutations, for example movement to the satellites, which could help to explain the previously described satellite phenotype associated with reduced levels or loss of KIAA0586 protein (Kobayashi et al., 2014; Stephen et al., 2015). TALPID3 is a centrosome protein therefore, due to the centrosome playing a key role in regulating the cell cycle (Doxsey et al., 2005), it is likely that the levels and localisation patterns of TALPID3 change during the cell cycle.

CRISPR/Cas9 editing was designed to incorporate an eGFP protein tag (Lippincott-Schwartz & Patterson, 2003) at the N-terminal of TALPID3 (Figure 3.14 A, B); the N-terminal of TALPID3 was chosen for targeting because rescue studies have shown that it is not needed for function (Yin et al., 2009). By targeting a region that was not necessary for function the aim

was to reduce the potential for disrupting the functional domains of TALPID3 when a fluorescent protein tag was added. The homology repair template was designed with homology arms of 1.5 kilobase pairs in length that targeted the region surrounding the ATG start codon of TALPID3. A flexible linker was incorporated between the fluorescent eGFP protein tag and TALPID3 to prevent disruption to the normal folding of TALPID3 (Argos, 1990; Chen et al., 2013). The glycine-rich flexible linker consisted of six amino acids, with serine dispersed between the glycine; glycine is small and serine is polar, providing a flexible and soluble linker that should allow appropriate movement, interaction and space between the eGFP tag and the TALPID3 protein (X. Chen et al., 2013). However, studies have shown that fluorescent protein tags at the N-terminal are more likely to disrupt normal localisation of the protein (Palmer & Freeman, 2004), therefore additional CRISPRs were designed to incorporate a fluorescent tag at the C-terminal of TALPID3 (Figure 3.14 C, D). The homology repair template for the C-terminal of TALPID3 was designed to include a Venus fluorescent protein tag, homology arms that were 500 base pairs in length and a flexible linker region that contained two extra glycine residues. Venus is a variant of yellow fluorescent protein (YFP) that is stable and has brighter fluorescence than eGFP (Nagai et al., 2001). Localisation studies of centrosome proteins can be challenging due to the low expression levels and size of the organelle being imaged, therefore Venus was chosen as the fluorescent protein tag for the C-terminal because it is brighter than eGFP and could be more easily imaged in the centrosome. The DNA templates for both the 5’ and 3’ end of *TALPID3*

were generated by Gibson Cloning, to allow joining of multiple fragments in a single reaction using overlapping ends. Pairs of guides were designed for both the N-terminal and the C-terminal targeting as this has been shown to produce fewer off-target effects (Ran et al., 2013). Following transfection of the CRISPRs and homology repair templates into chicken PGCs, the cells were examined for incorporation of the fluorescent tag at the endogenous locus of TALPID3. Despite several attempts, there was no successful incorporation of eGFP or Venus at the N-terminal or the C-terminal of TALPID3, respectively. PGCs are amenable to gene editing (Taylor et al., 2017), therefore the lack of success was most likely due to the design of an inefficient homology directed repair template or the fluorescent protein tag being incompatible with TALPID3 protein function in the design that was used. In conclusion, attempts to fluorescently tag TALPID3 at the N-terminal and C-terminal proved unsuccessful, meaning that a different approach to study the dynamic localisation of TALPID3 is required; additionally, an alternative approach or tool will be required to analyse the protein interacting network of TALPID3.

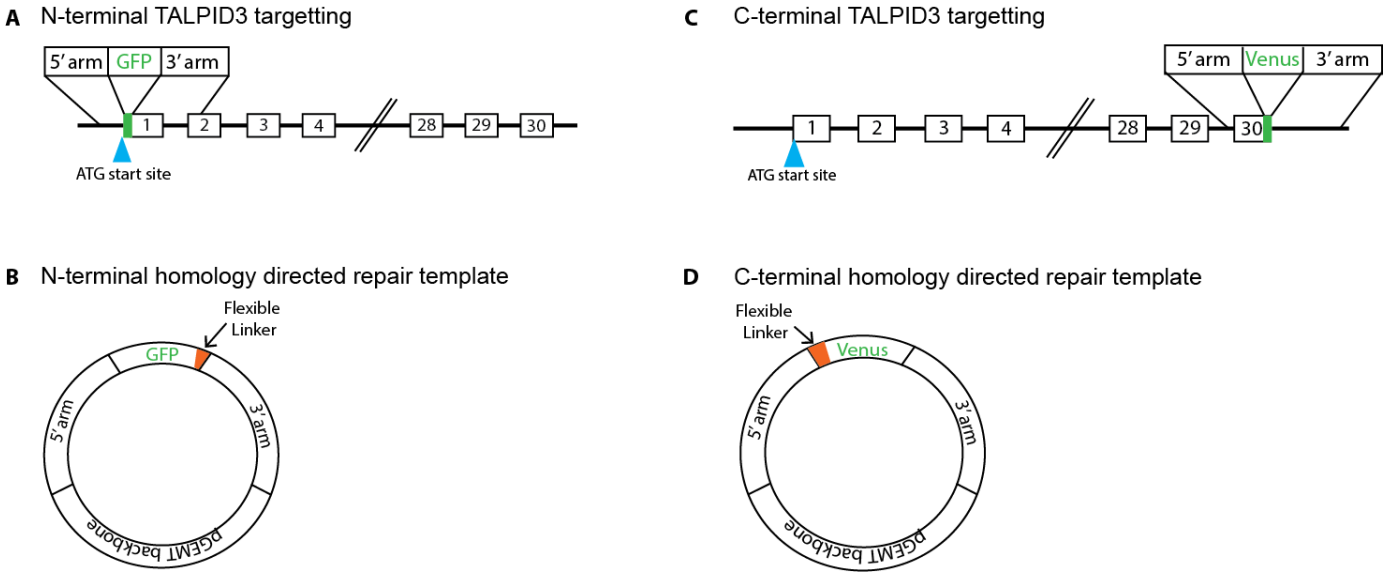

Figure 3.14 Schematic of chicken TALPID3 targeting design with CRISPR/Cas9. (**A**) Schematic of the design to target the N-terminal region of chicken TALPID3, using CRISPRS to introduce a GFP tag. The 5' arm and 3' arm each represent regions of homology that are approximately 1.5 kilobase pairs in length. The blue arrowhead indicates the ATG start codon. (**B**) The schematic represents the DNA repair template used for homologous recombination at the N-terminal of TALPID3 during CRISPR targeting. The flexible linker, marked in orange, is a region of 6 amino acids that is rich in glycine with serine dispersed between the glycine. (**C**) Schematic of the design to target the C-terminal region of chicken TALPID3 using CRISPRs to introduce a Venus tag. The 5' arm and 3' arm each represent regions of homology that are approximately 500 base pairs in length. The blue arrowhead indicates the ATG start codon. (**D**) The schematic represents the DNA repair template used for homologous recombination at the C-terminal of TALPID3 during CRISPR targeting. The flexible linker, marked in orange, represents a region of eight amino acids that is rich in glycine with serine dispersed between the glycine.

3.2.3 Super resolution imaging of KIAA0586 and candidate centrosome proteins shows distinct localisation patterns at the centrosome

I subsequently undertook super resolution using a newly produced (unpublished) antibody against KIAA0586. The antibody was raised against human KIAA0586 and recognised 146 amino acids (1313-1458 amino acids) in a region after the predicted intrinsically disordered domain at the C-terminal of the protein. In human RPE1 cells, low resolution imaging with the antibody showed localisation to the centrosome (Figure 3.15 A). Negative controls, omitting primary antibodies, showed no localisation patterns in the cells confirming that there was no nonspecific binding of the secondary antibody. Structured Illumination Microscopy (SIM) imaging showed that KIAA0586 localised to one end of both the mother and the daughter centrioles (Figure 3.15 B). Additionally the results showed that the region of KIAA0586 on each centriole co-localised with gamma tubulin and that there was more KIAA0586 localising to one centriole than the other (Figure 3.15 C). A previous report suggested that KIAA0586 localises more to the mother centriole than the daughter centriole (Wu et al., 2014), however without an additional marker to distinguish between the centrioles, these results do not confirm which centriole has more KIAA0586. 3D models, that provide a more reliable visual representation of where the proteins localise in relation to one another, can be produced in Imaris Software from the reconstructed images acquired on the SIM. 3D modelling of the centrosome showed a distinct region of KIAA0586 at one end of each centriole with a

region of co-localisation with gamma tubulin on each centriole (Figure 3.15 D). In support of the primary antibody being specific, all imaging of centrosome proteins (TALPID3, ARMC3, MYCBPAP, RIBC2, VWA3A) in cells following immunofluorescence, was completed at the same time, under the same condititions; following super resolution imaging, each centrosomal protein showed a different pattern of localisation in the centrosome in relation to gamma tubulin.

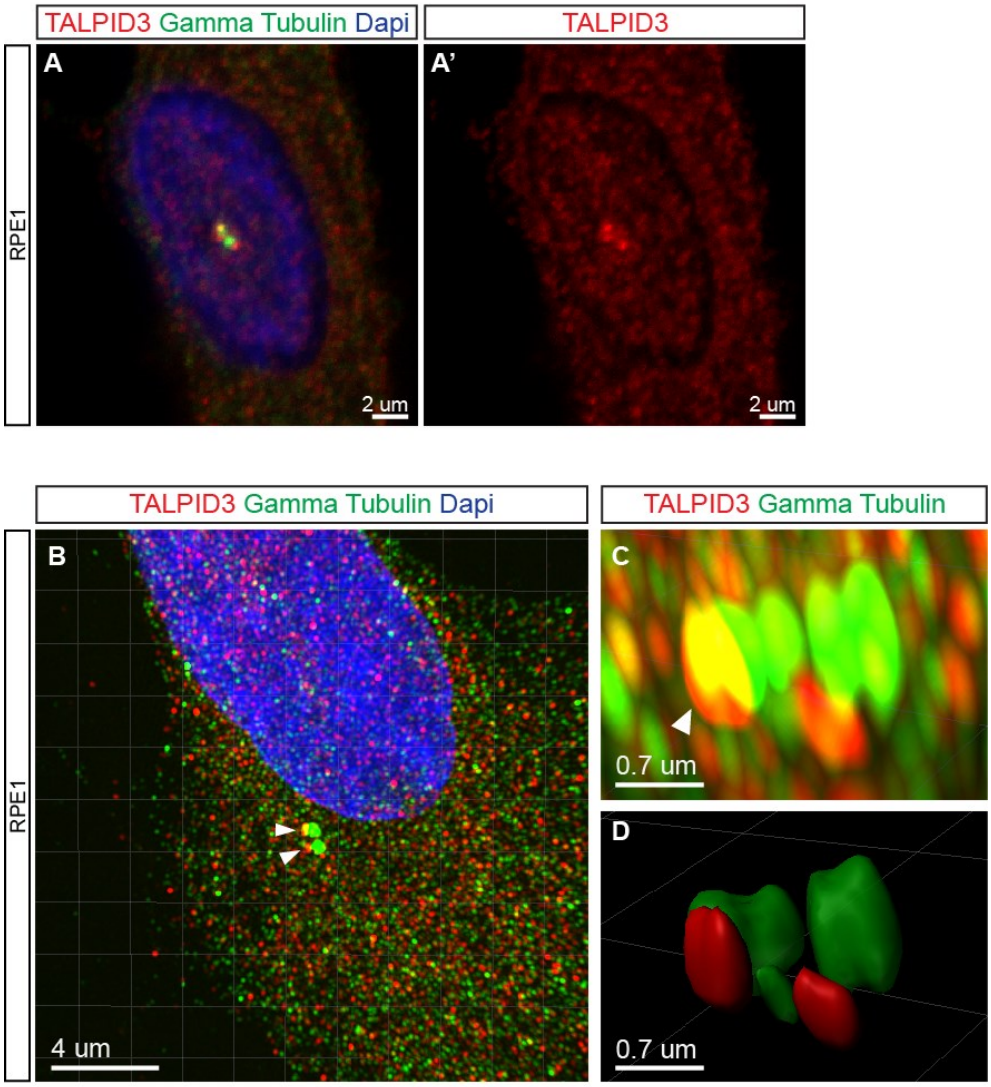

Figure 3.15 KIAA0586 localises to the distal end of centrioles in the centrosome. (**A**) Immunofluorescence for KIAA0586 (red) using a newly produce antibody against KIAA0586, gamma tubulin (green) and Dapi (blue) in human RPE1 cells. (**B**) Super resolution imaging for KIAA0586 (red), gamma tubulin (green) and Dapi (blue) in human RPE1 cells shows KIAA0586 co-localising with gamma tubulin at the centrioles. A white arrowhead marks each of the centrioles. (**C**) Single plane reconstruction at a higher magnification shows KIAA0586 at the ends of both centrioles, partially co-localising with gamma tubulin, with more KIAA0586 on one centriole than the other. The centriole with more KIAA0586 is marked by a white arrowhead. (**D**) 3D modelling in Imaris shows the structural localisation of KIAA0586 at the centrioles. All scale bars as specified in figure.

Bioinformatic analysis was used to identify novel cilia and centrosome proteins with a motile cilia signature, from RNA-Sequencing data taken from a pool of 52 human tissues (The Genotype-Tissue Expression (GTEx) Project). The tissues were analysed for high expression of FOXJ1, a gene required for specification of motile cilia (Yu et al., 2008). Co-expression analysis was used to identify genes that had a similar pattern of expression to FOXJ1 and were expressed in tissues also expressing FOXJ1. The candidate genes were then tested, identifying ARMC3, MYCBPAP, RIBC2 and VWA3A as candidate centrosome proteins (Patir et al., 2019, in preparation). ARMC3 (Armadillo Repeat Containing 3) belongs to a family of proteins that function in signal transduction, development, cell adhesion, mobility and tumor initiation and metastasis (Li et al., 2006); mutations in ARMC3 have been shown to cause sperm motility defects (Pausch et al., 2016). MYCBPAP (AMAP-1, Cod106) is expressed during development in neuronal and sensory cells in the inner ear and brain as well as the testis (Reisinger et al., 2005; Yukitake et al., 2002). RIBC2 (RIB43A domain with coiled-coils 2) has been identified as a gene that is silenced in some cases of ulcerative colitis inflammatory bowel disease (Kang et al., 2016). Additionally, RIBC2 has been shown to be highly expressed in testis, localises to the ciliary axoneme and is involved in ciliary motility (Chung et al., 2014). VWA3A (Von Willebrand Factor A Domain Containing 3A) is a protein coding gene that when mutated can lead to Ovarian cancer; VWA3A has a high association with survival in patients with Ovarian cancer (Madden et al., 2014).

Super resolution imaging of the four candidate centrosome proteins showed distinct patterns of localisation to the centrioles that were different to KIAA0586. Imaging showed that ARMC3 had a small region of co-localisation with gamma tubulin at the centrioles, as well as localisation around the centrioles (Figure 3.16 A-D). MYCBPAP co-localised with gamma tubulin on both centrioles as well as localising to the end of both centrioles (Figure 3.16 E-H). RIBC2 co-localised with gamma tubulin on both centrioles (Figure 3.16 I-L). VWA3A did not co-localise with gamma tubulin, instead localising to a region adjacent to the centrioles (Figure 3.16 M-P). Low resolution imaging suggested that only MYCBPAP and RIBC2 localised to the centrioles, however super resolution imaging showed that ARMC3 also localised to the centrioles, demonstrating the value of super resolution imaging to determine if a protein localises to the centrosome. 3D modelling proved particularly useful when imaging VWA3A, by demonstrating that the regions that looked like co-localisation of VWA3A and gamma tubulin were in different planes and therefore not co-localising. Super resolution for ARMC3, MYCBPAP, RIBC2, VWA3A and KIAA0586 all showed slightly different localisation patterns at the centrioles, with different patterns of co-localisation with gamma tubulin; these results support specificity of the antibodies, including the KIAA0586 antibody and highlight the power of super resolution imaging for identifying protein localisation at the centrosome.

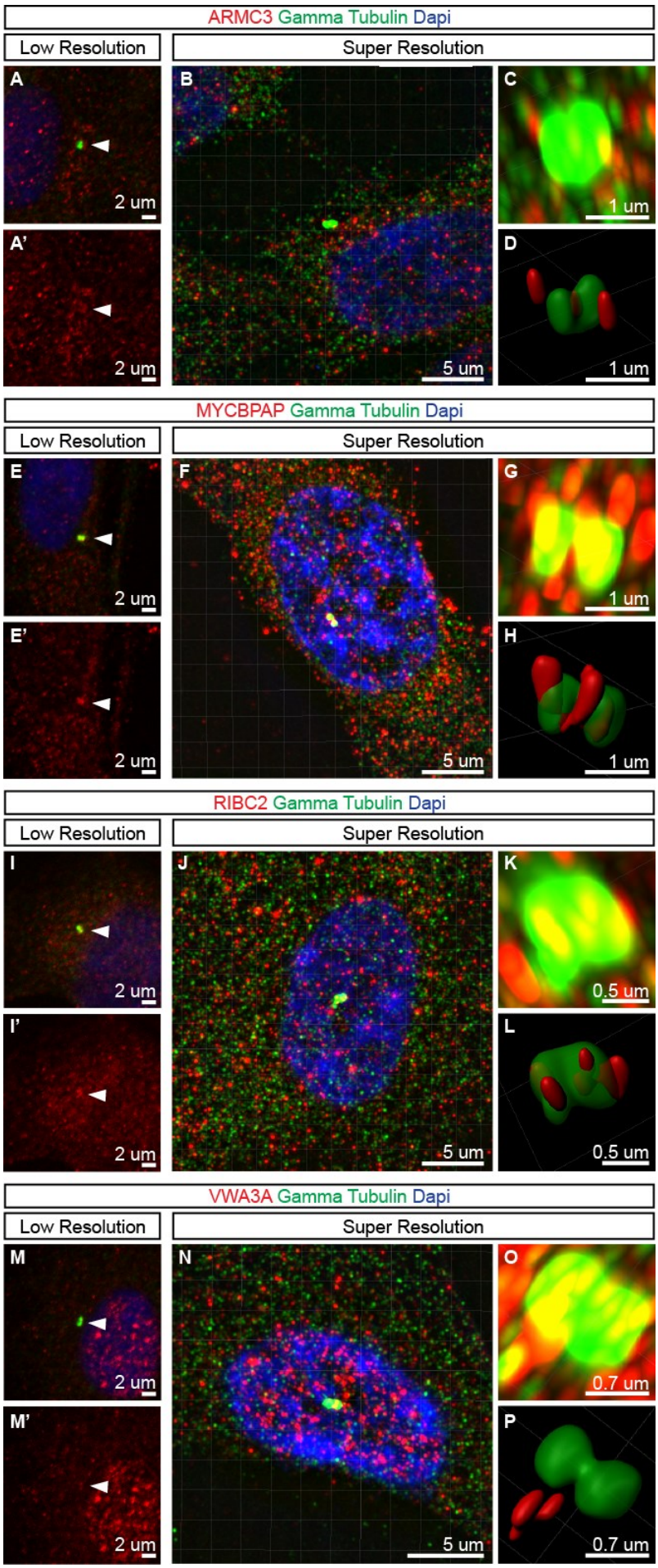
ARMC3 Gamma Tubulin Dapi
Low Resolution
Super Resolution
A
2 um
A'
2 um
B
5 um
C
1 um
D
1 um
MYCBPAP Gamma Tubulin Dapi
Low Resolution
Super Resolution
E
2 um
E'
2 um
F
5 um
G
1 um
H
1 um
RIBC2 Gamma Tubulin Dapi
Low Resolution
Super Resolution
I
2 um
I'
2 um
J
5 um
K
0.5 um
L
0.5 um
VWA3A Gamma Tubulin Dapi
Low Resolution
Super Resolution
M
2 um
M'
2 um
N
5 um
O
0.7 um
P
0.7 um

Figure 3.16 Super resolution imaging of centrosome protein candidates identified in a bioinformatics cilia screen. Centrosome protein candidates, ARMC3, MYCBPAP, RIBC2 and VWA3A are in red, gamma tubulin is in green and Dapi is in blue. (**A, E, I, M**) Low resolution imaging of candidate proteins suggests that only MYCBPAP and RIBC2 co-localise with gamma tubulin at the centrosome. Centrosomes indicated by white arrowheads. (**B, F, J, N**) Super resolution imaging at a low magnification suggests that MYCBPAP, RIBC2 and VWA3A co-localise with gamma tubulin at the centrosome. (**C, G, K, O**) Single plane reconstruction at a higher magnification suggests that all four candidate centrosome proteins co-localise with gamma tubulin, based on regions of overlapping red and green. (**D, H, L, P**) 3D modelling in Imaris demonstrates that ARMC3, has a small region of co-localisation with gamma tubulin at the centrioles, MYCBPAP and RIBC2 both show a much broader region of co-localisation with gamma tubulin at the centrioles and VWA3A does not co-localise with gamma tubulin at the centriole. Instead, VWA3A localises adjacent to the centrioles. All scale bars as annotated on figure.

The region of KIAA0586 recognised by the antibody had 51% sequence conservation between human and chicken KIAA0586 proteins. Using *talpid*^{3} PGCs as negative controls the antibody showed distribution similar in wildtype and *talpid*^{3} PGCs, demonstrating that it was not specific in chicken cells (Figure 3.17 A and B). This result was not unexpected given the low sequence conservation between human and chicken KIAA0586 protein sequence at the recognition site of the antibody.

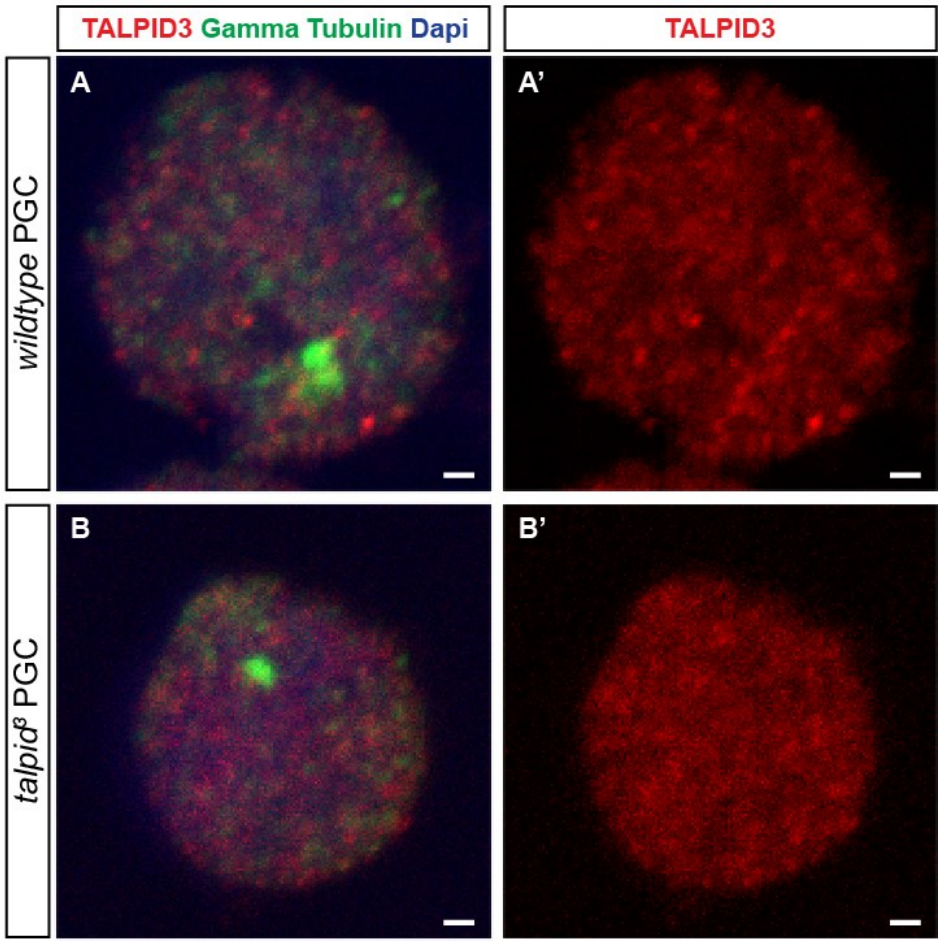

Figure 3.17 Anti-KIAA0586 antibody is non-specific for TALPID3 in chicken PGCs. (**A**) Immunofluorescence for TALPID3 (red), gamma tubulin (green) and Dapi (blue) shows lack of localisation of TALPID3 to the centrosome in wildtype chicken PGCs. (**B**) Immunofluorescence for TALPID (red), gamma tubulin (green) and Dapi (blue) shows lack of localisation of TALPID3 to the centrosome in *talpid*^{3} chicken PGCs. Although localisation of TALPID3 in the

centrosome would not be expected for *talpid*^{3} PGCs as there is no TALPID3 protein, the lack of localisation in the wildtype and similar non-specific red staining in both wildtype and *talpid*^{3} PGCs suggests that the antibody does not recognise the chicken TALPID3 protein. All scale bars, 1 μm.

3.3 Discussion

This study has demonstrated for the first time that human *KIAA0586* can rescue the gain of function Hedgehog-dependent expression patterns in the dorsal neural tube of *talpid*^{3} embryos, enabling the identification of hypomorphic mutations and increasing the understanding of functional domains in KIAA0586. Despite lack of success tagging the endogenous locus of chicken TALPID3 with a fluorescent protein tag, this study has used super resolution imaging to show that KIAA0586 localises to the distal ends of both centrioles with more KIAA0586 localising to one centriole than the other in human RPE1 cells. Super resolution imaging was also used to show localisation patterns of novel centrosome proteins, identified through a screen to identify the human motile cilia associated transcriptional signature; combined with the super resolution imaging of TALPID3, this data highlights the power of using super resolution imaging to observe different centrosome protein localisation patterns.

Unlike the chicken TALPID3 construct, which was able to rescue both gain of function and loss of function phenotypes in the *talpid*^{3} neural tube, the human KIAA0586 construct was only able to fully rescue gain of function phenotypes. Rescue of the Hedgehog-dependent expression pattern in *talpid*^{3} occurs when a cell takes up the TALPID3/KIAA0586 construct, returning the cells ability to form a cilium and thus respond to the Sonic Hedgehog gradient extending from the notochord and floorplate. Due to the ventral to dorsal gradient of Hedgehog ligand extending from the floorplate and notochord, the cells in the dorsal neural tube are acting in the absence

of Hedgehog ligand. Therefore following rescue in the dorsal neural tube of *talpid*^{3}, Patched1 (PTCH1) is localised to the cilium, inhibiting the presence of Smoothened (SMO) at the cilium and causing processing and truncation of Gli proteins to their shortened repressor forms. This leads to the rescue of the Pax7 gain of function phenotype, following electroporation with the chicken TALPID3 construct and the human KIAA0586 construct. Following rescue in the ventral neural tube with chicken TALPID3, Hedgehog ligand binds the transmembrane protein PTCH1, allowing translocation of SMO to the ciliary membrane, which in turn leads to the translocation of full length Gli protein (activator form) to the nucleus. This leads to a rescue of the Islet1 loss of function phenotype in *talpid*^{3}. However, electroporation of human KIAA0586 is unable to fully rescue this loss of function phenotype, instead only showing a small number of cells that express the correct ventral domain markers, which suggests a partial rescue. This result suggests that human KIAA0586 functions differently during the translocation of SMO to the ciliary membrane, which implies that there might be a difference in functionality of the domains between chicken and human KIAA0586.

PTCH1 and SMO do not directly interact, instead there is evidence to suggest that PTCH1 controls a SMO-binding compound (Arensdorf et al., 2016; Chen & Struhl, 1998). Therefore it is possible that TALPID3/KIAA0586 plays a role in activation of SMO, either by acting on PTCH1 or by acting on a PTCH1-controlled SMO-binding compound. The region of KIAA0586 responsible for this could differ between the chicken and human proteins, which could

explain the inability of human KIAA0586 to rescue the loss of function phenotype in the ventral neural tube of *talpid*^{3}.

Smoothened knockouts (*Smo*$^{-/-}$) show a similar phenotype to *talpid*^{3} in the neural tube. Cells fail to express markers of ventral neuroprogenitor populations such as Nkx2.2, Nkx6.1 and Olig2, demonstrating that specification of these populations have an absolute requirement for Hedgehog signalling (Wijgerde et al., 2002). Based on the knowledge that specification of these ventral neuroprogenitor populations requires Hedgehog signalling, the small number of cells expressing Islet1, Nkx2.2 and Nkx6.1 following electroporation with human KIAA0586 suggests that these cells are the result of a partial rescue. A more recent study has shown that endogenous levels of PTCH1 are able to inhibit SMO activity by a non-cell autonomous mechanism in nearby cells (Roberts et al., 2016). This could explain the unexpected non-cell autonomous result seen in Islet1 and Nkx2.2 expression following electroporation with the human KIAA0586 construct. Additionally this supports a partial rescue of the ventral expression domains following electroporation with human KIAA0586.

Super resolution imaging was used to examine centrosome localisation of four candidate proteins with a motile cilia signature as well as localisation of TALPID3. Imaging of centrosome proteins following immunofluorescence can be a challenging way of looking at localisation due to the size of the centrosome. Super resolution imaging provides a more reliable tool to look at localisation of proteins in such a small structure when compared to confocal imaging. Using confocal microscopy, ARMC3, MYCBPAP, RIBC2,

VWA3A and TALPID3 look very similar with a region of co-localisation with gamma tubulin at the centrosome. However, super resolution imaging combined with 3D reconstruction of the images provided a more accurate visual representation of each of these proteins, demonstrating that each protein had a slightly different localisation pattern.

The establishment of several consortium and databases has been used to identify an expanding list of cilia-associated genes/proteins and their function (Arnaiz et al., 2009; Nogales-Cadenas et al., 2009; Roepman et al., 2012). Additionally, studies have also focused their investigations into the proteins and genes associated with motile cilia (Blackburn et al., 2017; Campbell et al., 2016; Choksi et al., 2014; El Zein et al., 2009; Ostrowski, 2002); however, the majority of these studies have been conducted in model organisms, looking at a specific tissue. These experimental approaches capture ciliary components that may be shared with other structures and functions out with the cilium. The study used to identify ARMC3, MYCBPAP, RIBC2 and VWA3A used a transcriptomic approach from 52 different tissue types to identify the motile cilia signature. The primary analysis used in this study demonstrates that previous cilia databases do contain genes associated with biological functions, non-specific to cilia, thus highlighting the importance of this study to capture motile cilia genes conserved across tissues (Patir et al., 2019, in preparation). Hence study provides a resource that validates and describes putative human motile cilia genes conserved across motile ciliated tissues, the roles of which can be further examined

through functional studies, thereby picking apart the motile cilia machinery (Figure 3.18).

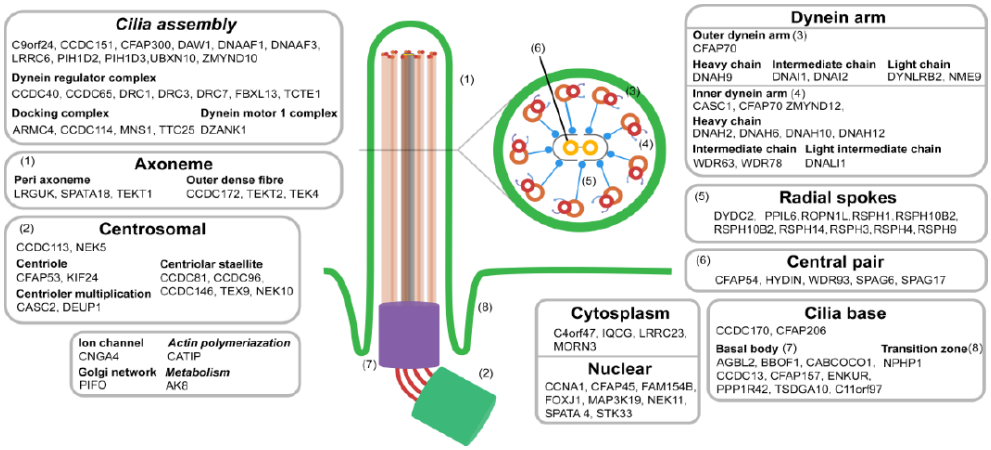

Figure 3.18 Annotation of the derived signature genes. Annotation of signature motile cilia genes based on their function (italics) or spatial localization in the context of cilia. Signature genes with no cilia/centrosomal evidence or with no specific function or localization identified in the cilia/centrosome have been excluded (Patir et al., 2019, in preparation).

3.3.1 Conclusions and future studies

Having shown that human KIAA0586 can only partially rescue the loss of function mutation in the ventral neural tube of *talpid*^{3}, a future study could look at the ability of the human KIAA0586 construct to rescue ciliogenesis in cells in the neural tube. This would provide information as to whether human KIAA0586 is able to rescue ciliogenesis but is unable to rescue loss of function mutations for example through the activity of SMO. Alternatively a western blot on tissue taken from the ventral neural tube could be used to look at the ratio of full length Gli activator proteins compared to the truncated Gli repressor proteins. A higher level of Gli repressor protein in the ventral neural tube would support the hypothesis that human KIAA0586 plays a role not just in ciliogenesis but is also in the PTCH1-mediated control of SMO.

Having demonstrated that *talpid*^{3} can be used to model human KIAA0586 ciliopathy patient mutations, a future study could set up an allelic series of mutations to be electroporated into the neural tube and embryos examined for Hedgehog-dependent expression changes in both wildtype and *talpid*^{3}. A series of mutations, consisting of those that arise after the potential alternative start codon, do not result in premature stop codons to eliminate mutations resulting in nonsense-mediated decay and have more severe or different phenotypes associated with the patients could be modelled in *talpid*^{3} to gain a better understanding of what functional domains are lost or compromised in these patients to cause their symptoms (Figure 3.19). By analysing rescue of Hedgehog-dependent expression patterns in the neural

tube of *talpid*^{3} embryos, hypomorphic mutations could be identified, which could help provide a unique insight into the potential functional domains at the C-terminal. Additionally the single heterozygous deleterious mutations that are found towards the C-terminal of KIAA0586 (Bachmann-Gagescu et al., 2015) could be modelled as part of the allelic series; as single heterozygous mutations, these mutations in particular c.3614G>A, p.W1205* which is found in the predicted intrinsically disordered domain, could provide an understanding of the domains required for function at the C-terminal of the KIAA0586 protein.

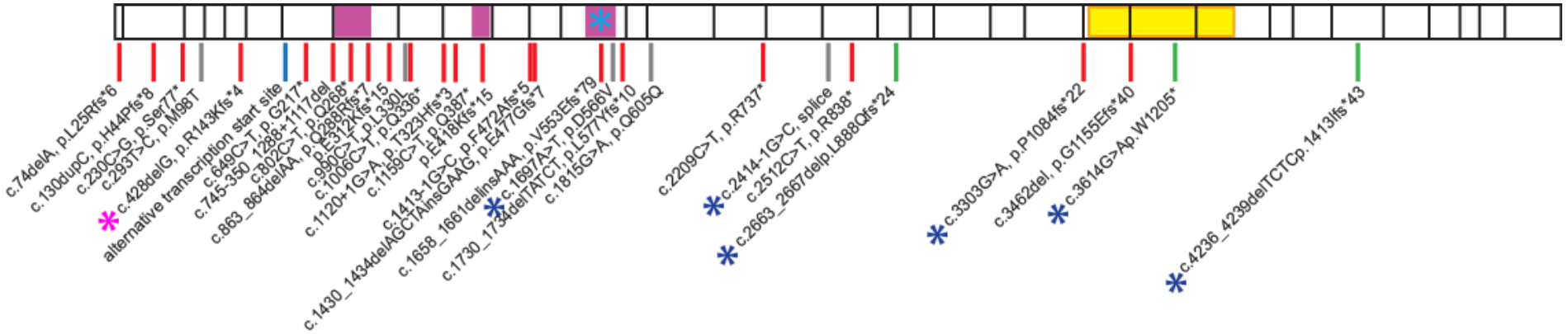

Figure 3.19 Human KIAA0586 ciliopathy patient mutations, marked by dark blue asterisk, that could be included in a future study aimed at modelling an allelic series in *talpid*^{3}. The schematic represents the human KIAA0586 protein. The dark blue asterisks identify mutations that could be included in an allelic series to be modelled in the *talpid*^{3} flock. Black vertical lines along the protein indicate exon boundaries. Purple boxes mark coiled-coil domains in the protein, the light blue asterisk indicates the conserved coiled-coil domain that is essential for function and the yellow box indicates the predicted intrinsically disordered domain. Red horizontal lines indicate mutations that cause premature stop codons. Grey horizontal lines indicate splice variant mutations and green horizontal lines indicate single heterozygous deleterious mutations. The pink asterisk indicates the common variant mutation. The blue horizontal line indicates a potential alternative start codon that be used for protein expression in human.

Chapter 4. Identifying centrosome proteins through proteomic approaches in human Jurkat cells and chicken Primordial Germ Cells

4.1 Introduction

Previous centrosome proteomic studies have used non-ciliated human KE37 cells to uncover novel proteins. The following chapter explores ways to apply centrosome proteome studies to alternative cell lines not usually used in the field of centrosome and cilia studies, thus identifying cell models for future centrosome studies and uncovering novel centrosome proteins.

4.1.1 Isolation of Centrosomes

A protocol for isolating centrosomes was first described in 1984 to study microtubule nucleation and stabilisation. Sucrose gradient sedimentation was used to isolate centrosomes from N115 Neuroblastoma cells and Chinese Hamster Ovary (CHO) cells (Mitchison & Kirschner, 1984). N115 cells, a loosely adherent cell line, gave a good yield of centrosomes but were heterogeneous in size with one to ten centrioles per cell. For this reason, CHO cells, an adherent cell line, were used due to their homogenous centrosomes and well-characterised centriole cycle (Mitchison & Kirschner,

1984). The following adaptations were made to correct for the difference in adherence: washes were carried out on the plate, instead of via centrifugation; an extra lysis buffer wash was added; the plates were incubated on a shaker to loosen the cells; 50x PE buffer was added to the lysate containing centrosomes and a low spread spin was carried out to remove chromatin instead of the filtration step.

This sucrose gradient sedimentation protocol was then adapted for the isolation of centrosomes from human KE37 cells to look in more detail at the components of the centrosome and the structural features that allow centrioles to associate within the centrosome (Bornens et al., 1987). The main modifications to the protocol involved the lysis steps and the centrosome purification procedure (Bornens et al., 1987). Mitchison and Kirschner treated the cells with the microtubule and microfilament dissociation drugs, Nocodazol and Cytochalasin, prior to lysis to prevent association of microtubules with the centrosome during isolation (Mitchison & Kirschner, 1984); Bornens et al. used these dissociation drugs at lower concentrations to avoid splitting of centrosomes and disruption of the pericentriolar material. Antiproteases, including Aprotinin, Leupeptin, Pepstatin and PMSF were included in the lysis buffer to inhibit proteolysis of pericentriolar material. A low Mg^{2+} concentration prevented excessive swelling of nuclei and DNAse treatment was added to prevent contamination with residual chromatin (Bornens et al., 1987). The original protocol used a Ficoll cushion to concentrate the centrosomes prior to sucrose gradient centrifugation, but this step was excluded due to loss of

centrosomes. Exclusion of the Ficoll cushion and instead using direct sedimentation onto a sucrose gradient took the yield of centrosomes to 60% in comparison to 15-20% when the Ficoll cushion was used (Bornens et al., 1987). In conclusion, the adaptations described were carried out to ensure a higher yield of intact centrosomes from cells in suspension, suggesting that this protocol could be used to produce a high yield of isolated centrosomes from a wide range of different cell types in suspension.

Following the adaptations described above, the protocol to isolate centrosomes from KE37 cells has been successfully used to identify and study proteins in the human centrosome (Andersen et al., 2003; Bauer et al., 2016; Jakobsen et al., 2011). KE37 cells, an immortalised T lymphoblast cell line, were chosen for centrosome isolation because they grow in suspension and they have a low cytoplasmic to nuclear ratio (Bornens et al., 1987). They are an immortalised T cell line taken from acute lymphoblastic leukaemia cells, suggesting that they do not provide a representative model of what normally happens in healthy human cells (Burger et al., 1999). Immortalised cell lines may not be the most relevant models for studying disease (Horvath et al., 2016; Masters & Stacey, 2007) demonstrating the need for more physiologically relevant cell lines. In addition, T-cells are non-ciliated cells that form an immune synapse instead of a cilia (Finetti et al., 2009). The key role of the centrosome in ciliogenesis, highlights a need for centrosome proteomic studies to be carried out in a ciliated cell line. Although adapted for KE37 cells, this protocol could be used to isolate centrosomes from alternative non-adherent cells lines, providing a more versatile approach to

identifying centrosome proteins from different types of cells as well as different model organisms.

4.1.2 Centrosome Proteome Studies in KE37 Cells

The established centrosome isolation protocol in KE37 cells, was first used in combination with Mass Spectrometry based proteomics to determine the complex protein composition within the centrosome (Andersen et al., 2003). At the time of this study, there were approximately 60 proteins known to be associated with the centrosome; by using mass spectrometry on isolated centrosomes, Andersen et al. identified 47 of the 60 known centrosome proteins as well as a further 90 uncharacterised proteins. 32 of the 90 uncharacterised proteins were cloned and 19 of the 32 were confirmed as centrosomal by immunofluorescence (Andersen et al., 2003). In a second attempt to identify centrosome proteins from their mass spectrometry dataset, the group tracked relative abundance of peptides through five sucrose gradient fractions. This method of quantitation was based on relative amounts of the same peptide as opposed to absolute quantitation (Andersen et al., 2003).

Despite a large coverage, several known proteins were not detected; this was attributed to low abundance of the proteins, loss during purification or because the components did not associate with the centrosome to a significant degree under the conditions of the experiment (Andersen et al., 2003). This study also demonstrated that a high proportion of centrosome

proteins (75%) contained coiled-coil domains, an observation that has remained consistent in subsequent studies (Andersen et al., 2003; Bauer et al., 2016; Jakobsen et al., 2011). An additional study using centrosomes isolated from KE37 cells aimed to examine the dynamic composition and localisation of the centrosome proteome through a 'Mass Spectrometry-screen' combined with an 'HPA-screen' (Jakobsen et al., 2011). This method allowed identification of centrosome proteins in centrosome isolates, followed by validation through localisation studies using antibodies from the Human Protein Atlas (HPA) (Barbe et al., 2008). Jakobsen et al. also incorporated SILAC (stable isotope labelling with amino acids in cell culture) into their mass spectrometry screen, providing an accurate way of quantifying the abundance of proteins in the centrosome isolates (Jakobsen et al., 2011). Previously, abundance of peptides across five fractions (Andersen et al., 2003) had allowed for the relative amount of the same peptide to be determined, providing a means of distinguishing between centrosomal proteins and nonspecific proteins based on the difference in peptide elution profiles between the two categories. The new approach using SILAC labelling (Jakobsen et al., 2011) increased the accuracy of protein quantitation in comparison to the relative abundance method. A further quantitative proteomics approach using selected reaction monitoring (SRM) and EGFP-tagging of endogenous proteins allowed high specificity detection of defined proteins in a complex mixture and quantification at a specific subcellular location through fluorescent signal quantification (Bauer et al., 2016). The study highlighted the challenges of

studying proteomes where the proteins are expressed at low levels, such as in the centrosome. The selected reaction monitoring approach combined with EGFP-tagging, was designed to overcome the complication that comes with trying to quantify proteins that are expressed at low levels, thus better understanding centriole regulation and duplication under physiological conditions (Bauer et al., 2016). This approach was more successful for absolute quantitation of specific low-abundance proteins within the centrosome when compared to previous quantitative studies (Andersen et al., 2003; Jakobsen et al., 2011), however, there were limitations. The main limitations included the inability to monitor proteins through the cell cycle because of technical mass spectrometry constraints and complications during fluorescence quantification due to photo bleaching and the possibility that the fluorescent tag might interfere with protein function. Importantly this quantitative proteomics approach could not be used to identify novel centrosome proteins due to the need to target specific, previously identified proteins in the centrosome (Bauer et al., 2016).

In summary, isolation of centrosomes combined with mass spectrometry has accelerated our understanding of the centrosome network, providing a tool for identifying novel centrosome proteins, studying protein interactions within the centrosome and quantifying centrosome protein abundance in human KE37 cells (Andersen et al., 2003; Bauer et al., 2016; Jakobsen et al., 2011). The distinct protein datasets produced following different mass spectrometry approaches highlights the need to identify a mass spectrometry approach that addresses the type of data relevant for the

study, whether protein identification, relative abundance or absolute quantification.

4.1.3 Cell lines for cilia and centrosome studies

To address the concerns that cell models that are incapable of making cilia and are not relevant to healthy conditions are being studied, I wanted to develop an approach to study centrosome proteins in alternative cell lines. Additionally, it was important to identify a cell line that could be used to study the TALPID3 protein interacting network. Human RPE1 cells and human Jurkat cells were included alongside chicken Primordial Germ Cells (PGCs). The human RPE1 cell line is an immortalised, ciliated cell line that is commonly used for studying the centrosome and cilia (Spalluto et al., 2013). RPE1 cells have been well characterised in the centrosome and cilia field through protein localisation and gene editing studies (Bauer et al., 2016; Jakobsen et al., 2011; Kobayashi et al., 2014; Prosser & Morrison, 2015), therefore can act as a good benchmark for the Jurkat cells and chicken PGCs.

Jurkat cells, a human T-lymphocyte cell line, have not previously been used to carry out proteomic studies in the centrosome. Like KE37 cells, they are classed as T cells and both lines are derived from acute lymphoblastic leukaemia cells, making them the malignant version of their healthy T cell counterparts (Burger et al., 1999). Despite some differences in receptor expression between Jurkat cells and KE37 cells (Burger et al., 1999), Jurkat cells were included in this study because they have similar origins and

characteristics to KE37 cells (Orkin & Zon, 2008; Rothenberg, 2007). Chicken PGCs are a primary cell line that can easily be derived and cultured (Lavoir et al., 2006; Macdonald et al., 2010), meaning they can be derived from the *talpid*^{3} flock. As a pluripotent cell line, PGCs are suitable for addressing concerns about completing studies in a cell line that are more likely to mimic healthy physiological conditions (Park & Han, 2000). Moreover the chicken is a good model for studying human cranio-facial ciliopathies as shown through the *talpid*^{2} and *talpid*^{3} mutant lines (Schock et al., 2016), supporting the need for a chicken cell line that is suitable for studying the centrosome proteome. In conclusion, the study described in this chapter was completed on human Jurkat cells and chicken PGCs, with human RPE1 cells included as a benchmark where relevant.

4.1.4 Aims

To date, proteomic analysis of the centrosome has been carried out in KE37 cells, a non-ciliated, immortalised human cell line (Andersen et al., 2003; Bauer et al., 2016; Jakobsen et al., 2011). In order to investigate the use of centrosome isolation to determine the centrosome proteome in alternative cell lines, the study described in this chapter uses a non-quantitative discovery mass spectrometry approach on cell lines that have not been established in the centrosome and cilia field. The aim of this study was to identify alternative cell lines for centrosome studies and use a discovery mass spectrometry proteomic approach on centrosomes generated from

these cell lines to identify the differences in the centrosome proteome composition. The inclusion of chicken PGCs aimed to provide a cell model that mimicked healthy physiological conditions, while also providing a tool to study TALPID3 in the centrosome that could be applied to *talpid*^{3} flock PGCs.

4.2 Results

4.2.1 Frequency of ciliogenesis in RPE1 cells, Jurkat cells and PGCs.

In order to undertake centrosome proteome studies in cells that are capable of forming primary cilia, I first established if human Jurkat cells and chicken PGCs are capable of forming cilia. I used non-adherent cells because this has been shown to generate higher yields of centrosomes following centrosome isolation (Bornens et al., 1987). Immunofluorescence was used to examine ciliary axoneme marker acetylated tubulin and ciliary membrane marker Arl13B in RPE1 cells, Jurkat cells and PGCs (Figure 4.1 A-F). Following serum starvation, acetylated tubulin and Arl13B marked cilia in all three cell lines, demonstrating that all three cell lines all capable of forming cilia, when given ciliogenesis-inducing conditions in cell culture. Despite demonstrating the capability of ciliogenesis in Jurkat cells and PGCs, ciliogenesis frequency in Jurkat cells was found to be low. Following serum starvation, 79% of RPE1 cells (n = 200) were ciliated and 70% of PGCs (n=90) were ciliated, however, only 8.5% of Jurkat cells (n = 200) were ciliated (Figure 4.1 G). In conclusion, these results suggest that PGCs are a ciliated cell line and that Jurkat cells have a reduced frequency of ciliogenesis.

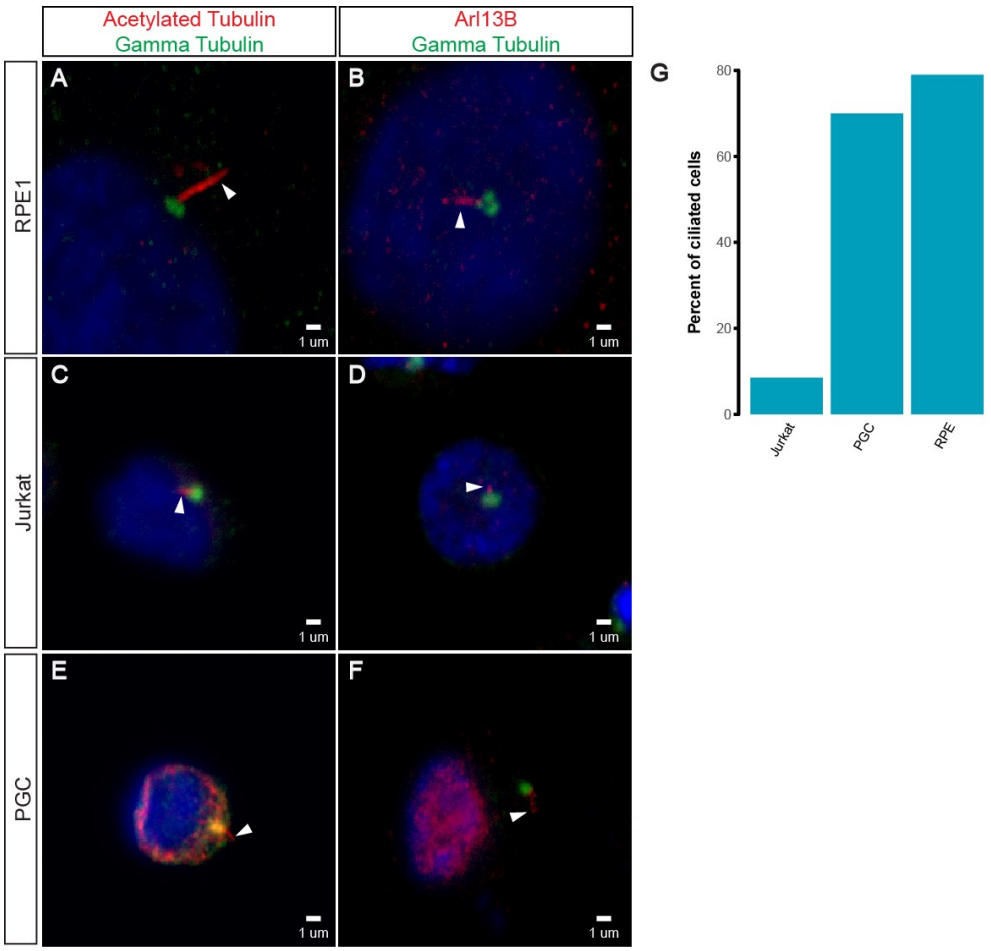

Figure 4.1 Frequency of ciliogenesis in RPE1 cells, Jurkat cells and PGCs. (**A-F**) Immunostaining with Gamma tubulin (green) to mark the centrosome, Acetylated tubulin (red) to mark the ciliary axoneme or Arl13B (red) to mark the ciliary membrane and Dapi (blue) to mark the nucleus. White arrowheads indicate a cilium, showing that RPE1 cells, Jurkat cells and PGCs are capable of forming cilia, with both a ciliary axoneme and ciliary membrane. (**G**) Percent of ciliated cells for each cell line shows, 8.5% of Jurkat cells are ciliated, 70% of PGCs are ciliated and 79% of RPE1 cells are ciliated following serum starvation. All scale bars: 1 µm.

4.2.2 PGCs have centrosome protein localisation patterns that correlate with the ability to form cilia. Jurkat cells have altered centrosome protein localisation patterns associated with reduced ciliogenesis.

In order to understand if reduced frequency of ciliogenesis in Jurkat cells was due to loss of basal body maturation, immunofluorescence was completed for centrosome proteins. Centrosomes modified to basal bodies have key markers such as Cep164, PCM1, CP110 and MACF1. Without these proteins localising to the distal end of the centrioles (Graser et al., 2007; May-Simera et al., 2016; Spektor et al., 2007) or in the Pericentriolar Material (Balczon et al., 1994), ciliogenesis does not occur.

Cep164 is a distal appendage protein that localises specifically to the distal end of the mother centriole (Graser et al., 2007). In RPE1 cells and PGCs, Cep164 localised to only one of the centrioles as expected, however in Jurkat cells Cep164 consistently localised to both mother and daughter centrioles (Figure 4.2 A, E, I). CP110 localises to the distal ends of centrioles and is removed from the mother centriole prior to ciliogenesis (Spektor et al., 2007). In RPE1 cells and PGCs, CP110 localised to the distal end of either one or both of the centrioles as expected (Figure 4.2 B, J). However, Jurkat cells consistently showed excess CP110 staining within both centrioles, as well as around the edges of the centrioles usually marked as pericentriolar material (Figure 4.2 F). PCM1 is a component of the centriolar satellites (Balczon et al., 1994). In all three cell lines, it was localised in a scattered pattern around

the centrioles. There was also co-localisation of PCM1 with gamma tubulin in the centrioles in Jurkat cells, unlike the RPE1 cells and PGCs (Figure 4.2 C, G, K). Microtubule Actin Cross-linking Factor 1 (MACF1) localises to the distal end of the basal body (May-Simera et al., 2016). This expected pattern of MACF1 localisation was seen in RPE1 cells and PGCs, however in the Jurkat cells, MACF1 localised to both centrioles (Figure 4.2 D, H, L).

In order for ciliogenesis to occur, the centriole must migrate to the membrane where the distal appendages play a role in docking. The centriole becomes the modified basal body and distal appendages become transition fibres, following which the IFT (intraflagellar transport) system controls extension of the cilia from the basal body (Avasthi & Marshall, 2012; Dawe et al., 2007). The presence of Cep164 on both centrioles in Jurkat cells suggests that both centrioles contain modifications that are usually only associated with the mother centriole, and therefore the reduction in ciliogenesis could be due to the inability to distinguish between mother and daughter centriole. The accumulation of CP110 and PCM1 around the centrosome in Jurkat cells is similar to abnormal localisation patterns seen in some ciliopathies. For example, a similar localisation pattern presents in RPE1 cells with reduced levels of TALPID3; loss of TALPID3 results in accumulation of Cep290 and PCM1 around the centrosome (Kobayashi et al., 2014). PGCs are ciliated cells that have localisation patterns of Cep164, CP110, PCM1 and MACF1 that correlate with their ability to form cilia. In conclusion, these results suggest that RPE1 cells and PGCs have modification of centrioles that correlate with their ability to form cilia; Jurkat cells

however, have modifications that correlate with their reduced ciliogenesis frequency.

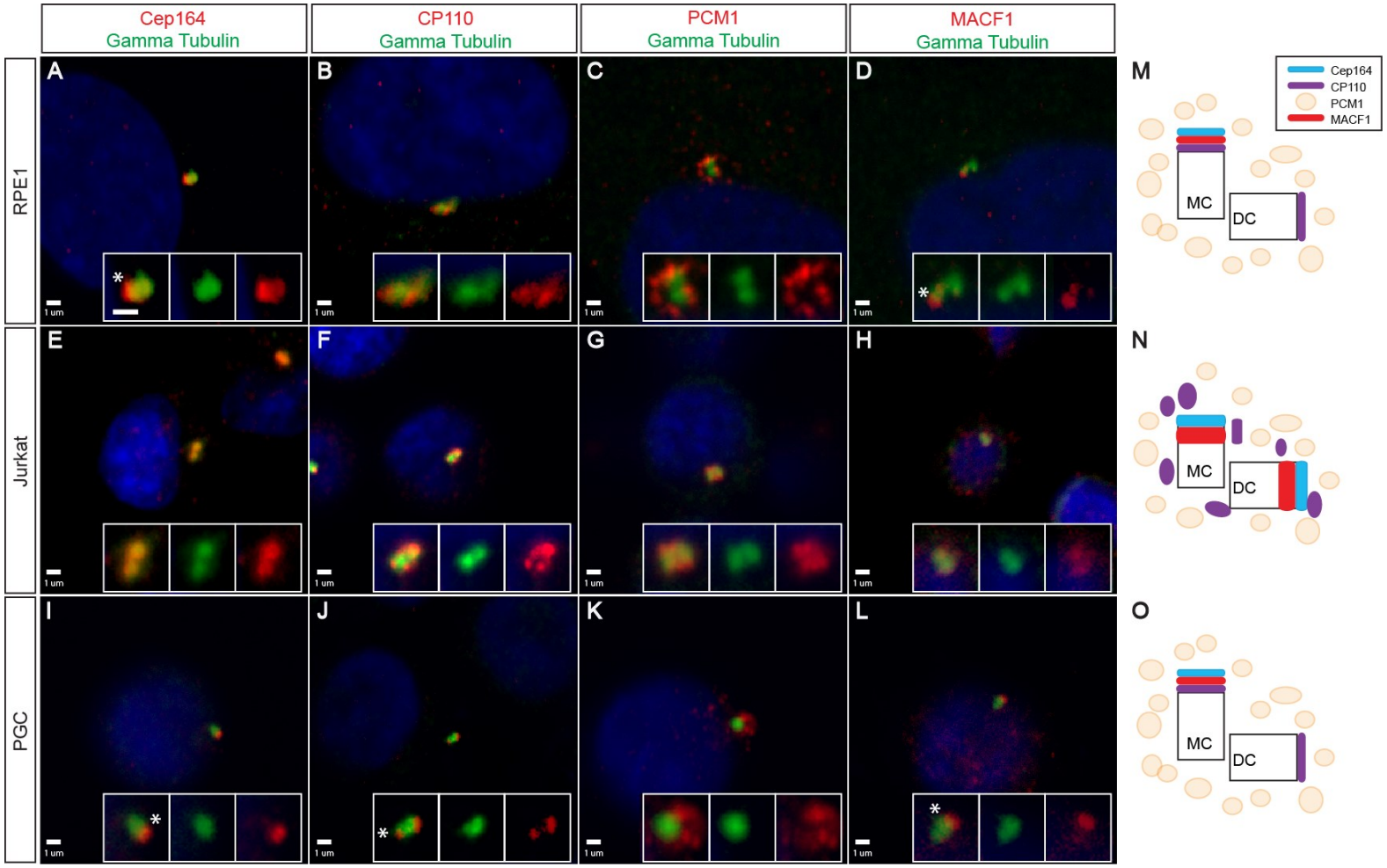
Cep164
Gamma Tubulin
CP110
Gamma Tubulin
PCM1
Gamma Tubulin
MACF1
Gamma Tubulin
RPE1
Jurkat
PGC
A
B
C
D
E
F
G
H
I
J
K
L
M
N
O
Cep164
CP110
PCM1
MACF1
MC
DC
1 um

Figure 4.2 RPE1 cells and PGCs have centrosome protein localisation patterns that correlate with the ability to form cilia. Jurkat cells have altered centrosome protein localisation patterns associated with ciliogenesis. (**A - L**) Immunostaining with antibodies against Gamma Tubulin (green) for the centrioles, Cep164, CP110, PCM1 or MACF1 (red) and Dapi (blue) for the nucleus. A white asterisk marks the mother centriole where protein markers distinguish between mother and daughter centriole. (**M-O**) Schematic to show observed localisation patterns of Cep164 (blue), CP110 (purple), PCM1 (orange) and MACF1 (red) in RPE1 cells, Jurkat cells and PGCs respectively. The observed localisation patterns of Cep164, CP110, PCM1 and MACF1 in Jurkat cells was different to RPE1 cells and PGCs, suggesting that altered centrosome protein localisation in Jurkat cells may be responsible for the reduced frequency of ciliogenesis. All scale bars: 1 µm.

4.2.3 Isolation and validation of centrosome proteins in Jurkat cell samples and PGC samples

In order to complete centrosome studies in alternative cell lines, the protocol used to isolate centrosomes from non-adherent KE37 cells (Andersen et al., 2003; Jakobsen et al., 2011) was applied to the non-adherent human Jurkat cells and chicken PGCs. RPE1 cells were excluded from the proteomic analysis as they are an adherent cell line and thus not suitable for centrosome isolation using this protocol. Centrosomes were isolated from Jurkat cells and PGCs using centrifugation through a discontinuous sucrose gradient (Figure 4.3). By using cell lines that are not typically used for centrosome and cilia studies, I aimed to uncover differences in centrosome protein composition. Having demonstrated that PGCs are a ciliated cell line with centrosome localisation patterns that correlate with their ability to form cilia, I intended to direct centrosome proteome network studies towards conditions that are more physiologically relevant to healthy conditions. Inclusion of PGCs would also provide a means to carry out proteomic studies aimed at uncovering the TALPID3 protein interacting network, because PGCs can be derived from the *talpid*^{3} flock.

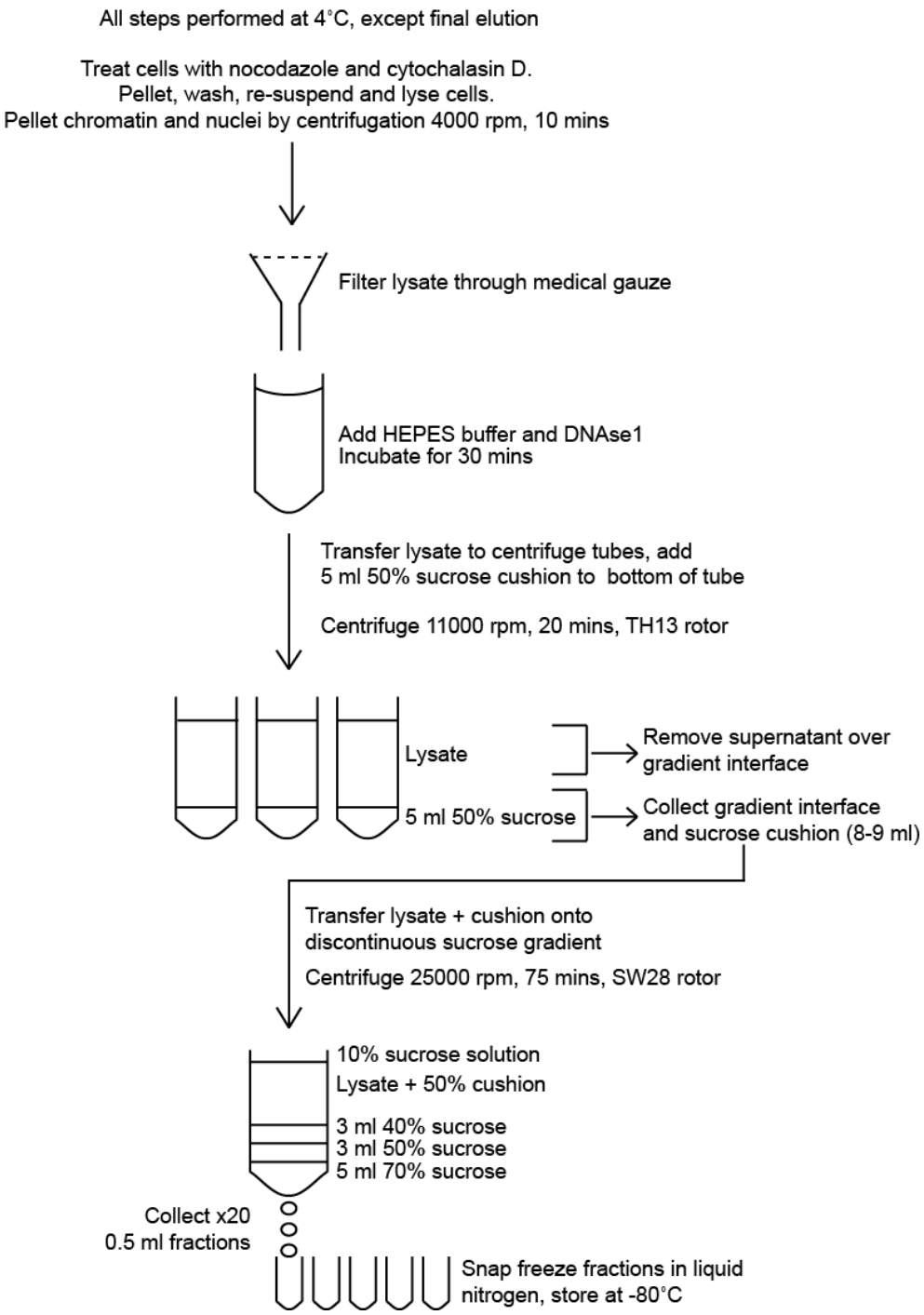

Figure 4.3 Schematic of protocol used to isolate centrosomes from human Jurkat cells and chicken PGCs.

To confirm the presence of protein following the centrosome isolation protocol, the amount of protein was quantified in the Jurkat and PGC protein samples. There was 0.7 – 1.1 µg/µl of protein in the Jurkat centrosome protein samples, whereas the PGC centrosome protein sample only contained 0.53 µg/µl. The reduced amount of protein in the PGC protein sample compared to the Jurkat protein sample suggested that the protocol was not as efficient in PGCs as it was in Jurkat cells.

To confirm enrichment of proteins associated with the centrosome, I undertook a Western Blot for gamma tubulin (Figure 4.4 A), a key component of the pericentriolar material as well as the core of the centrioles (Fuller et al., 1995). Relative quantification of the bands showed a 3.26 fold increase of gamma tubulin in the Jurkat centrosome sample compared to the Jurkat whole cell sample (Figure 4.4 B), suggesting that the centrosome isolation protocol was successful in the Jurkat cells. A loading control was not included in this Western blot and could not be repeated due to the low protein concentration in the sample. A loading control would have confirmed that the protein loading was the same across the gel; without this control it cannot be conclusively stated that the loading was the same across the gel and therefore the quantification may not be exact. Due to the low concentration of protein in the PGC centrosome sample, there was not enough protein to complete a Western Blot. A starting number of approximately 1 x 10^9 cells was needed for isolating centrosomes from Jurkat cells and PGCs. Due to the specific requirements and expenses associated with chicken PGC culture conditions (Whyte et al., 2015), it was

not possible to repeat the centrosome isolation in PGCs to produce more protein.

In order to identify centrosome proteome differences in human Jurkat cells compared to chicken PGCs, discovery shotgun mass spectrometry was undertaken on the Jurkat centrosome protein samples and the PGC centrosome protein sample, despite the low protein content in the PGC centrosome sample. Protein lists generated from mass spectrometry were analysed in the Database for Annotation, Visualisation and Integrated Discovery (DAVID) for associated centrosome function through Gene Onotology (GO) terms associated with the proteins. In the Jurkat centrosome sample, GO term clusters associated with the cytoskeleton, microtubules and actin (Figure 4.4 C), which are families largely associated with the centrosome interactome (Amato et al., 2014). Unlike the Jurkat centrosome sample, GO term clusters associated with the PGC centrosome sample did not show signs of enrichment for families associated with the cytoskeleton, microtubules or actin (Figure 4.4 D). This analysis failed to show enrichment by GO term association for protein families associated with the centrosome interactome (Amato et al., 2014) in the PGC sample. The scores associated with the GO terms identified in the PGC sample were low, suggesting there was no specific enrichment within the samples (Figure 4.4 D). In conclusion, the centrosome isolation protocol yielded a protein sample from the Jurkat cells that suggested enrichment of centrosome proteins by GO term association, but a low yield of protein in the PGCs that lacked evidence of centrosome enrichment by GO term association.

A

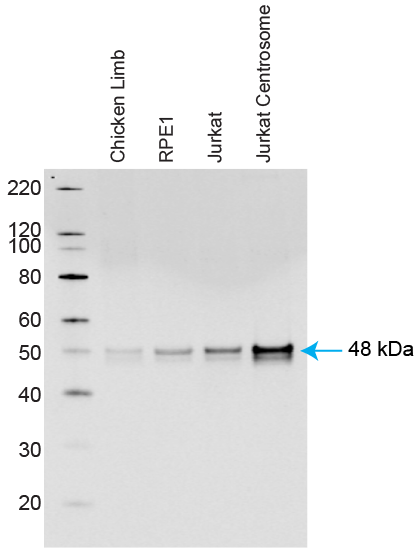

B

Protein Sample	Signal	Area
Chicken limb	4650	666
RPE1	10100	666
Jurkat	19000	666
Jurkat Centrosome	61900	666

C

Cluster	Enrichment Score	GO Terms
1	39.149	Translation, Ribosome, RNA binding
2	33.988	Cytoskeleton, Non-membrane bound organelle
3	15.293	Nucleotide-binding
4	14.403	Mitochondrion
5	14.166	Mitochondrion
6	12.490	Cytoskeleton, Microtubule cytoskeleton
7	10.554	Actin binding, Actin cytoskeleton, Actin filament organisation
8	9.752	Intracellular organelle lumen, Nuclear lumen
9	7.278	Cortical actin cytoskeleton, cell cortex

D

Cluster	Enrichment Score	GO Terms
1	22.670	ATP-binding
2	22.241	Cytosolic large ribosomal subunit, Translation
3	6.730	Nucleotide binding
4	5.686	AAA+ ATPase domain
5	4.447	Proteosome component (PCI) domain
6	4.332	Nuclear proteosome complex
7	4.191	Golgi membrane
8	4.137	ATP-dependent RNA helicase activity

Figure 4.4 Validation of centrosome enrichment in Jurkat cells and GO term analysis in Jurkat and PGC centrosome protein samples. (**A**) Western Blot analysis for gamma tubulin, showing a brighter band in the Jurkat centrosome protein sample compared to the Jurkat whole cell protein sample and controls. Blue arrow marks gamma tubulin band at 48 kDa. (**B**)

Table to show relative quantification of bands in Western Blot. A 3.26 fold increase of band intensity in Jurkat centrosome sample compared to Jurkat whole cell sample supports enrichment for centrosome proteins. (**C**) Top 9 clusters by GO Term, identified in DAVID Functional Cluster Analysis for Jurkat Centrosome Sample suggest proteins belong to families largely associated with the centrosome. (**D**) Top 9 clusters by GO Term, identified in DAVID Functional Cluster Analysis for PGC Centrosome Sample demonstrate lack of enrichment for protein families associated with the centrosome and low enrichment scores.

To determine the relative efficiency of the centrosome isolation protocol completed in the Jurkat cells and the PGCs, proteins from the Jurkat centrosome sample were compared to proteins identified in the KE37 centrosome dataset (Andersen et al., 2003). In addition, proteins from both the Jurkat centrosome sample and the PGC centrosome sample were compared to all currently known centrosome and cilia proteins found in the CCDB protein dataset (1554) (Gupta et al., 2015). There were 88 proteins overlapping across the two datasets when Jurkat centrosome proteins were compared to the KE37 proteomic dataset (Andersen et al., 2003), by accession number (Figure 4.5 A). Comparison of the Jurkat centrosome protein sample and the PGC centrosome protein sample to CCDB showed an overlap of 142 proteins (Figure 4.5 B) (Appendix 2) and 139 proteins (Figure 4.5 C) (Appendix 3) respectively. There were 76 CCDB proteins that were common to both the Jurkat proteins and the PGC proteins (Appendix 4). The 76 overlapping centrosome proteins may be higher abundance proteins in comparison to the other centrosome proteins identified; this conclusion is supported by the lack of any these proteins in the list of low abundance centrosome proteins, which was published while this study was being completed (Bauer et al., 2016).

The overlap of proteins from the Jurkat dataset with the Andersen dataset and CCDB supports enrichment of centrosome proteins. Of the 72 low abundance centrosome proteins (Bauer et al., 2016), only CCDC77, CETN2, NEDD1 and POC5 were identified in the Jurkat centrosome protein sample, suggesting that the centrosome proteins identified are high abundance

centrosome proteins. The non-overlapping protein identifications suggest that there are likely to be more centrosome interactome proteins that have not yet been identified. Based on the GO terms from the DAVID cluster analysis, there is evidence of some mitochondrion contamination, which could also account for some of the non-overlapping proteins.

In conclusion, the Jurkat centrosome sample showed enrichment for centrosome proteins allowing protein candidates to be taken forward for further analysis. The overlap of PGC centrosome proteins with CCDB showed that there was centrosome enrichment in the PGCs, however there were no low abundance proteins (Bauer et al., 2016) identified in the PGC centrosome sample, suggesting that despite centrosome enrichment the protocol was not as efficient in PGCs as in Jurkat cells. The low protein yield and lack of evidence to suggest centrosome enrichment based on the GO term analysis resulted in the decision not to take any PGC proteins forward for further investigation.

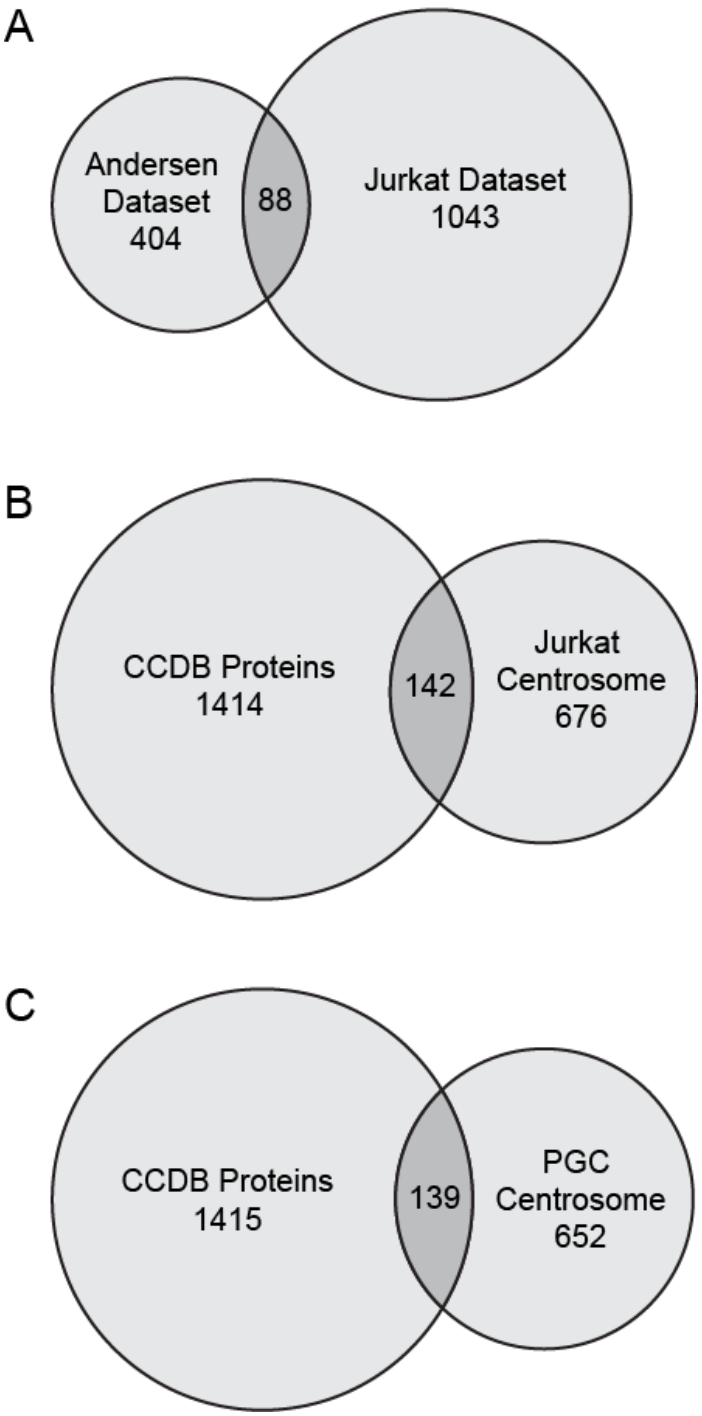

Figure 4.5 Comparison of Jurkat and PGC centrosome protein datasets to known centrosome and cilia proteins. (**A**) Comparison of the Jurkat centrosome sample to the Andersen centrosome dataset by accession number shows an overlap of 88 proteins, suggesting there are centrosome proteins in the Jurkat sample and that this method of centrosome isolation is also applicable to Jurkat cells. (**B**) Comparison of CCDB proteins to the Jurkat centrosome proteins shows an overlap of 142 proteins, confirming that there are centrosome proteins in the Jurkat sample. (**C**) Comparison of CCDB proteins to the PGC centrosome proteins shows an overlap of 139 proteins, showing there are centrosome proteins in the PGC sample.

Both the Jurkat centrosome protein dataset and the PGC centrosome protein dataset were examined for the presence of TALPID3. TALPID3 was not identified in either dataset, leading to the conclusion that centrosome isolation in cell lines is not a feasible way to study the TALPID3 protein interacting network. It has since been suggested that TALPID3 is one of a number of proteins expressed at very low levels in the centrosome and therefore challenging to identify through mass spectrometry (Bauer et al., 2016), which could explain the lack of TALPID3 identification in the Jurkat centrosome or the PGC centrosome dataset. In conclusion, studying the TALPID3 proteome through isolation of centrosomes in PGCs is not possible and identification of an alternative approach to study the TALPID3 proteome is necessary.

4.2.4 Identification of novel centrosome protein candidates from the Jurkat centrosome dataset

Having shown that the Jurkat centrosome sample was enriched for proteins associated with the centrosome, a set of parameters (Table 4.1) was applied to the proteins in order to investigate differences in centrosome protein composition and identify novel centrosome proteins. The parameters were designed to include proteins with characteristics similar to those associated with centrosome and cilia proteins. Microtubules and actin filaments make up the cytoskeleton network, which is responsible for intracellular architecture and cell polarity. The centrosome nucleates and anchors microtubules and can directly promote actin-filament assembly (Farina et

al., 2016). Additionally Rho GTPases play a role in actin cytoskeleton organisation, particularly during cell movement when the centrosome orientates towards the leading edge of the cell (Sit & Manser, 2011; Wittmann & Waterman-Storer, 2001), therefore parameters for taking proteins forward included Rho GTPases, cytoskeletal, actin-related, cell migration or movement and polarity. Centrioles duplicate once during the cell cycle, and their role in forming primary cilia is linked to the cycling of cells (Nigg & Stearns, 2011), therefore association with the cell cycle was included in the parameters to take forward. Coiled-coil domains are a structural feature found in many centrosome proteins (Andersen et al., 2003), therefore presence of one or more coiled-coil domains was also included in the parameters to take forward (Table 4.1).

Proteins with properties or functions that are unlikely to be associated with the centrosome were excluded from further analysis. Proteins that have already been shown to localise to and function in distinct structures, such as ribosomes or mitochondria, are unlikely to overlap with the centrosome and were therefore excluded. ATPase family proteins are classified by a conserved module that promotes ATP hydrolysis and are usually involved in molecular remodelling events. Although the dynein heavy chain proteins, found in cilia, are part of the ATPase family (Snider et al., 2008), these proteins have already been well characterised; therefore, ATPase family proteins were excluded. Heat shock proteins are a ubiquitous family of proteins, produced in response to non-lethal stress such as heat, ethanol, nicotine, surgical stress and viral agents to name a few. These proteins play

a critical role in cellular homeostasis through cell death and disease processes (Whitley et al., 1999), therefore are unlikely to be produced in healthy conditions in the centrosome and were excluded. Apoptosis, or programmed cell death, is controlled by a specific series of signals, therefore production of apoptosis proteins will result in cell death (Papaliagkas et al., 2007) and were not a group of proteins that would be associated with the centrosome in healthy cells. DNA-damage proteins are produced in response to the cell sensing a break in the DNA and interrupt the cell cycle (Polo & Jackson, 2011). Similar to apoptosis-related proteins, the DNA-damage proteins would be expressed in situations where the cell may be unhealthy due to DNA-damage, and were therefore excluded (Table 4.1).

I applied these parameters to Jurkat centrosome protein dataset 1 and Jurkat centrosome protein dataset 2 (datasets described in Chapter 2, section 2.4.2) to produce a list of proteins for further analysis (Appendix 5 and Appendix 6). Following application of parameters to the datasets, proteins that had previously been validated for specific functions or protein networks including but not limited to the centrosome proteome were excluded from further analysis as they were already well characterised. This resulted in the identification of two novel centrosome protein candidates for further analysis, CCDC77 and CCDC127.

Table 4.1 Parameters applied to the Jurkat centrosome protein mass spectrometry dataset to determine which proteins should be carried forward for further analysis.

Carry Forward	Exclude from further analysis
Rho GTPase Association	Mitochondrial
Cytoskeletal	Ribosomal
Actin-related	ATPase family
Cell movement and/or migration	Apoptosis-related
Polarity	DNA damage-related
Cell Cycle	Heat shock proteins
Containing coiled-coil domain(s)	

CCDC77 (POC11 in Chlamydomonas) has previously been identified in a screen for centrosome proteins (Jakobsen et al., 2011) but at the time was not validated or further investigated. In contrast, CCDC127 is a novel protein that has not previously been identified in centrosome or cilia screens. Both CCDC77 and CCDC127 contain coiled-coil domains in their structure, a common feature shared in many centrosome proteins (Andersen et al., 2003; Bauer et al., 2016; Jakobsen et al., 2011).

Examination of the Human Protein Atlas (HPA) and the Allen Mouse Brain Atlas demonstrated localisation patterns of CCDC77 and CCDC127 in tissue sections that contained multi-ciliated cells, such as fallopian tube, brain tissue, lung tissue and the choroid plexus (Barbe et al., 2008; Lein et al., 2007). CCDC77 showed higher levels of expression along the apical edge of

multi-ciliated tissues, consistent with a region containing a higher concentration of centrosomes (Figure 4.6 A). CCDC127 also showed higher expression levels along the apical edge of cells; in addition CCDC127 showed signs of expression in the motile cilia in the fallopian tube (Figure 4.6 B) (Barbe et al., 2008) and in the choroid plexus of the mouse brain (Figure 4.6 C, D) (Lein et al., 2007). CCDC127 also showed high levels of expression along the edge of the cerebellum and the hippocampus in the mouse brain (Figure 4.6 E, F) (Lein et al., 2007). In conclusion, evidence from HPA and the Allen Mouse Brain Atlas, suggests that CCDC77 and CCDC127 are expressed in regions of tissue associated with centrosomes and cilia, therefore supporting a potential role for these proteins in the centrosome.

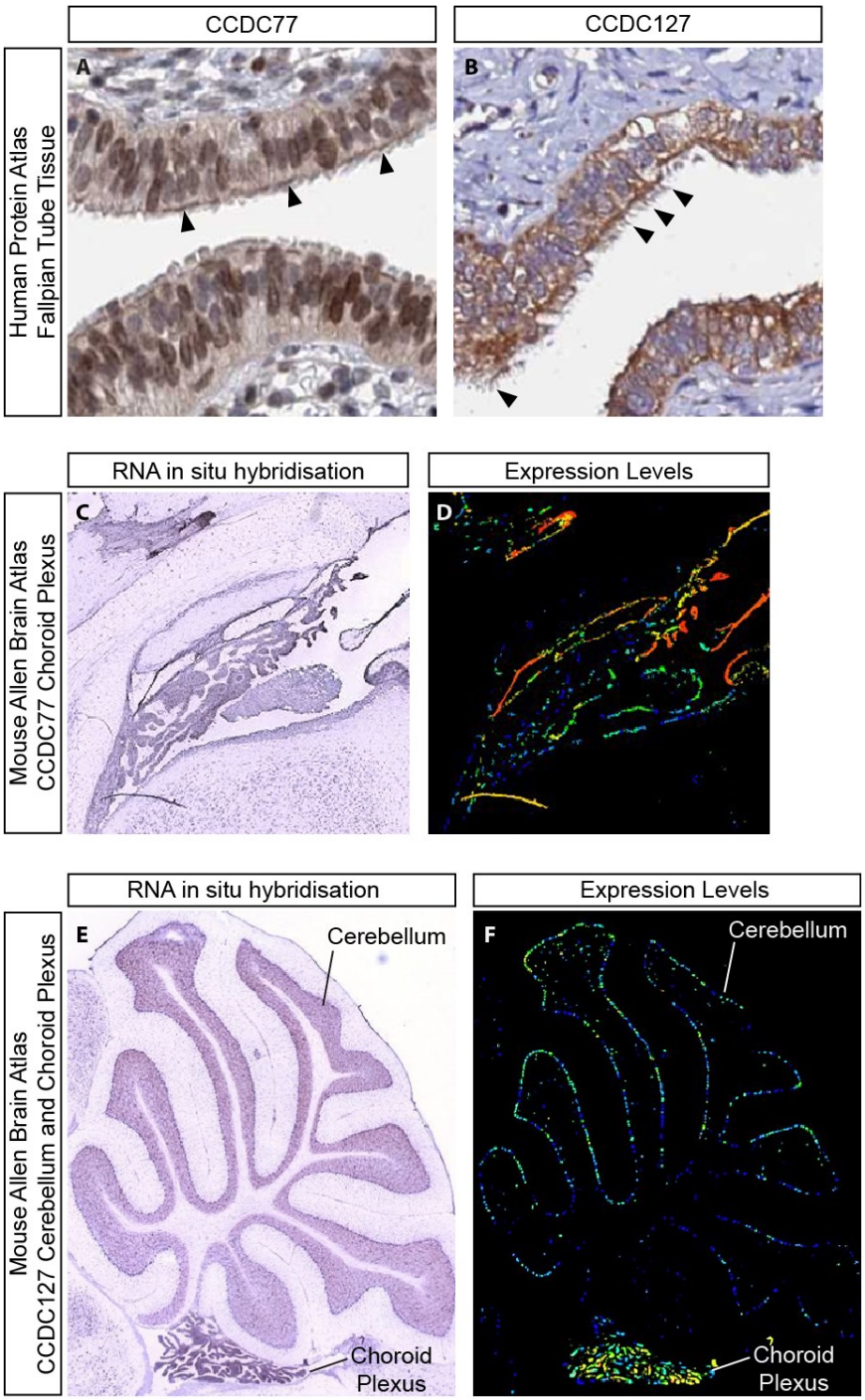

Figure 4.6 Immunohistochemistry from the Human Protein Atlas and RNA *in situ* hybridisation from the Allen Mouse Brain Atlas showing CCDC77 and CCDC127 in regions of tissue containing centrosomes and cilia. (**A**) Immunohistochemistry for an antibody against CCDC77 in the fallopian tube shows localisation to the apical edges of cells where a higher concentration of centrosomes is found, indicated by black arrowheads. (**B**) Immunohistochemistry for an antibody against CCDC127 in the fallopian tube shows localisation to the apical edges of the cells and in the motile cilia lining the fallopian tube, indicated by black arrowheads. (**C**) RNA *in situ*

hybridisation for CCDC77 shows expression in the choroid plexus in the mouse brain. (**D**) The expression levels for CCDC77 show the cells that have the highest probability of gene expression using a heat colour scale (from low/blue to high/red) in the choroid plexus. (**E**) RNA *in situ* hybridisation for CCDC127 shows expression in the choroid plexus and around the edge of the cerebellum in the mouse brain (**F**) The expression levels for CCDC127 show the cells that have the highest probability of gene expression using a heat colour scale (from low/blue to high/red) in the choroid plexus and cerebellum. Images from **A** and **B** are adapted from the Human Protein Atlas (Barbe et al., 2008). Images from **C-F** are adapted from the Allen Mouse Brain Atlas (Lein et al., 2007).

4.2.5 CCDC77 and CCDC127 localise to the centrosome in Jurkat cells and RPE1 cells

To determine if CCDC77 and CCDC127 localise to the centrosome, immunofluorescence was used to examine protein localisation in Jurkat cells and RPE1 cells. In both cell lines, CCDC77 and CCDC127 co-localised with gamma tubulin in the centrosome. In Jurkat cells, CCDC77 localised to the centrosome, showing excess localisation patterns around the centrioles in addition to co-localising with gamma tubulin on both centrioles (Figure 4.7 A). However, in RPE1 cells, CCDC77 predominantly co-localised with gamma tubulin on only one centriole (Figure 4.7 C). In Jurkat cells, CCDC127 co-localised with gamma tubulin across both centrioles as well as additional localisation around the perimeter of the centrioles (Figure 4.7 B). However, in RPE1 cells, CCDC127 predominantly co-localised with a small region of gamma tubulin on one centriole (Figure 4.7 D). These results show that CCDC77 and CCDC127 localise to the centrosome in Jurkat cells and RPE1 cells. The differences in the pattern of localisation seen between the cell lines was expected, consistent with altered centrosome protein localisation patterns seen previously when analysing Cep164, CP110, PCM1 and MACF1 in Jurkat cells.

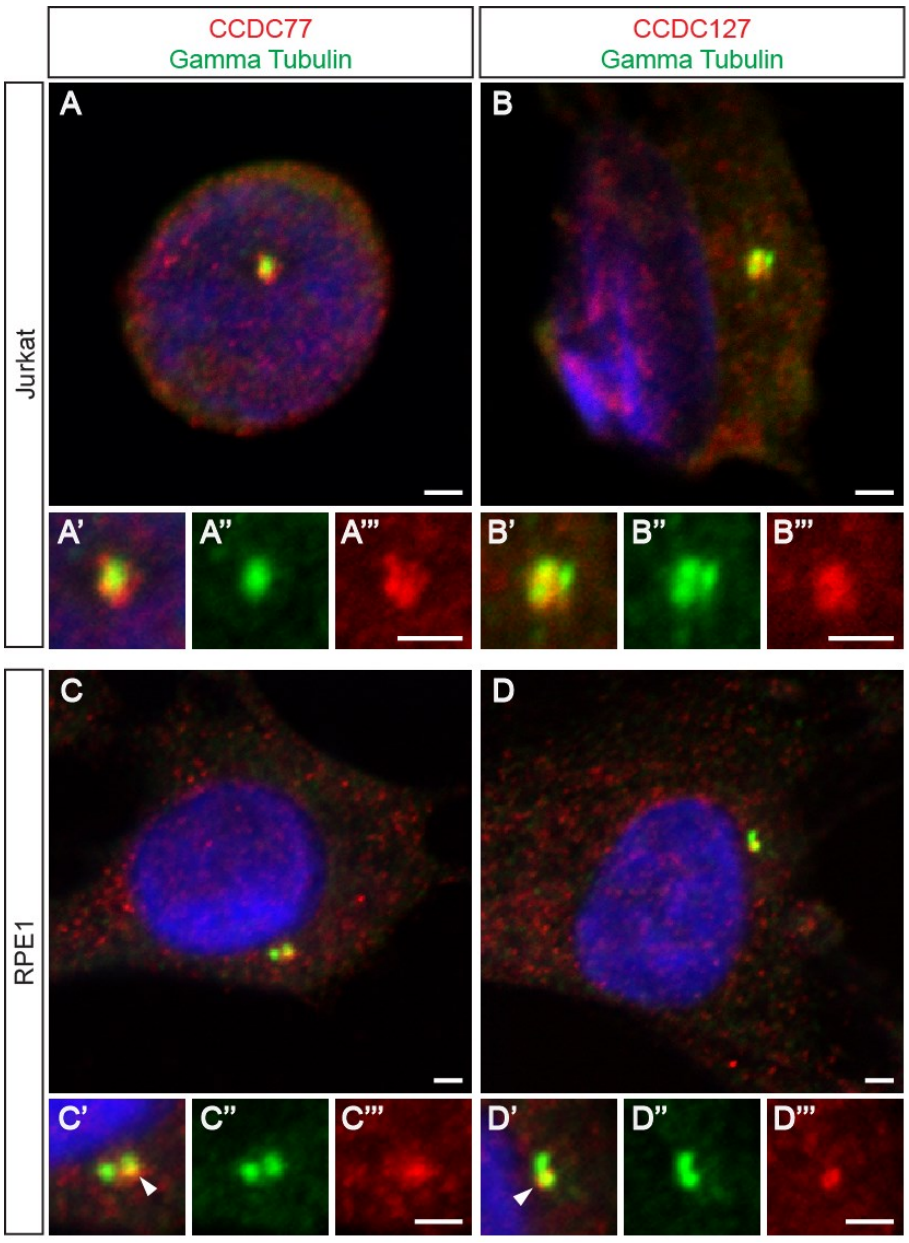

Figure 4.7 CCDC77 and CCDC127 localise to the centrosome in Jurkat cells and RPE1 cells. (**A** and **C**) Immunostaining with gamma tubulin (green), CCDC77 (red) and Dapi (blue) shows co-localisation of CCDC77 and gamma tubulin in the centrosome. White arrowhead marks the centriole where CCDC77 co-localises with gamma tubulin in RPE1 cells. Differences in localisation patterns of CCDC77 between Jurkat cells and RPE1 cells are observed. (**B** and **D**) Immunostaining with gamma tubulin (green), CCDC127 (red) and Dapi (blue) shows co-localisation of CCDC127 and gamma tubulin in the centrosome. White arrowhead marks the centriole where CCDC127 co-localises with gamma tubulin in RPE1 cells. Differences in localisation patterns of CCDC127 between Jurkat cells and RPE1 cells are observed. All scale bars: 2 μm.

To follow up localisation of CCDC77 and CCDC127 at the centrosome, super-resolution imaging was completed in RPE1 cells to identify specific regions of localisation of CCDC77 and CCDC127 in the centrioles. Results from structural illumination microscopy confirmed localisation of CCDC77 to both centrioles, with multiple points of co-localisation with gamma tubulin (Figure 4.8 A-C). Structural illumination microscopy showed localisation of CCDC127 to only one centriole, with two regions of CCDC127 co-localisation with gamma tubulin within the centriole (Figure 4.8 D-F). Western blot analysis using these antibodies was attempted, however the antibodies did not work in western blot (Appendix 7) and therefore could not be confirmed by western blot in the Jurkat centrosome protein samples. In conclusion, localisation studies using confocal imaging and super-resolution imaging produced corresponding results, demonstrating that CCDC77 and CCDC127 both localise to the centrosome.

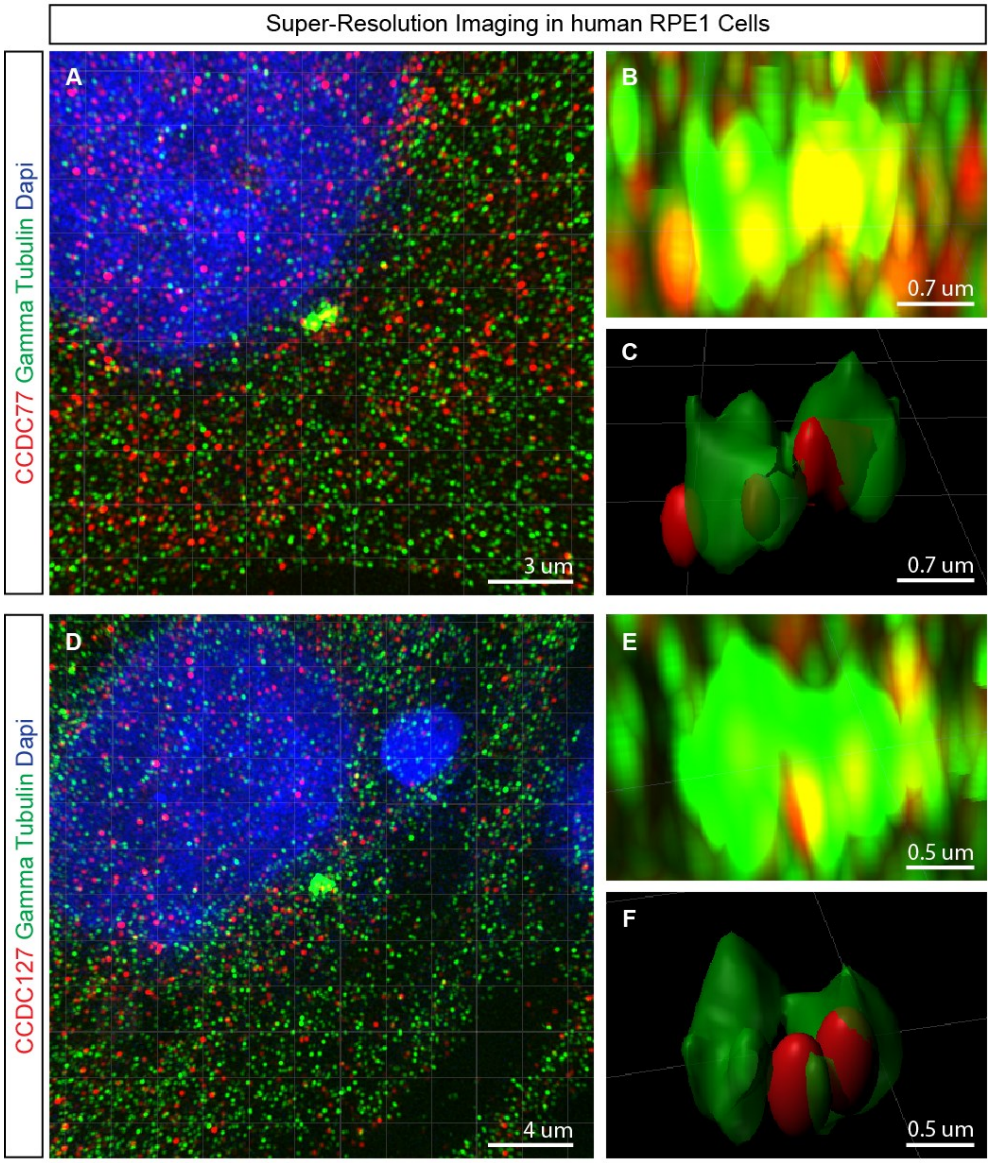

Figure 4.8 Super-resolution imaging of CCDC77 and CCDC127 shows localisation to the centrosome in human RPE1 cells. (**A**) Immunofluorescence for CCDC77 (red), Gamma Tubulin (green) and Dapi (blue) show CCDC77 co-localising with gamma tubulin at the centrioles. (**B**) Single plane reconstruction at a higher magnification shows CCDC77 co-localising at several points in both centrioles. (**C**) 3D modelling in Imaris shows the structural localisation of CCDC77 at the centrioles. (**D**) Immunofluorescence for CCDC127 (red), Gamma Tubulin (green) and Dapi (blue) show CCDC127 co-localising with gamma tubulin in a small region at one of the centrioles. (**E**) Single plane reconstruction at a higher magnification shows CCDC127 localising at two points within one of the centrioles. (**F**) 3D modelling in Imaris shows the structural localisation of CCDC127 in one of the centrioles. All scale bars as annotated on figure.

4.2.6 RNA *in situ* hybridisation of CCDC77, CCDC127 and *TALPID3* shows expression in the developing chick embryo

Having shown that CCDC77 and CCDC127 localise to the centrosome in Jurkat cells and RPE1 cells, RNA *in situ* hybridisation was used to confirm that both genes are expressed in early embryonic development. RNA *in situ* hybridisation for CCDC77, CCDC127 and *TALPID3* was completed in chick embryos at Hamburger Hamilton stage 25-26. *TALPID3* was included in this analysis as a benchmark for expected patterns of expression by a ubiquitously expressed centrosome protein (Davey et al., 2006; Yin et al., 2009).

CCDC77 and CCDC127 showed a ubiquitous expression pattern, when analysed by whole mount *in situ* hybridisation (Figure 4.9 A, B). This pattern of expression is similar to the ubiquitous expression seen in whole mount *in situ* hybridisation for *TALPID3* (Figure 4.9 C). In conclusion, these results support expression of CCDC77 and CCDC127 in early development and suggest that both genes have a ubiquitous expression pattern similar to other centrosome genes such as *TALPID3*.

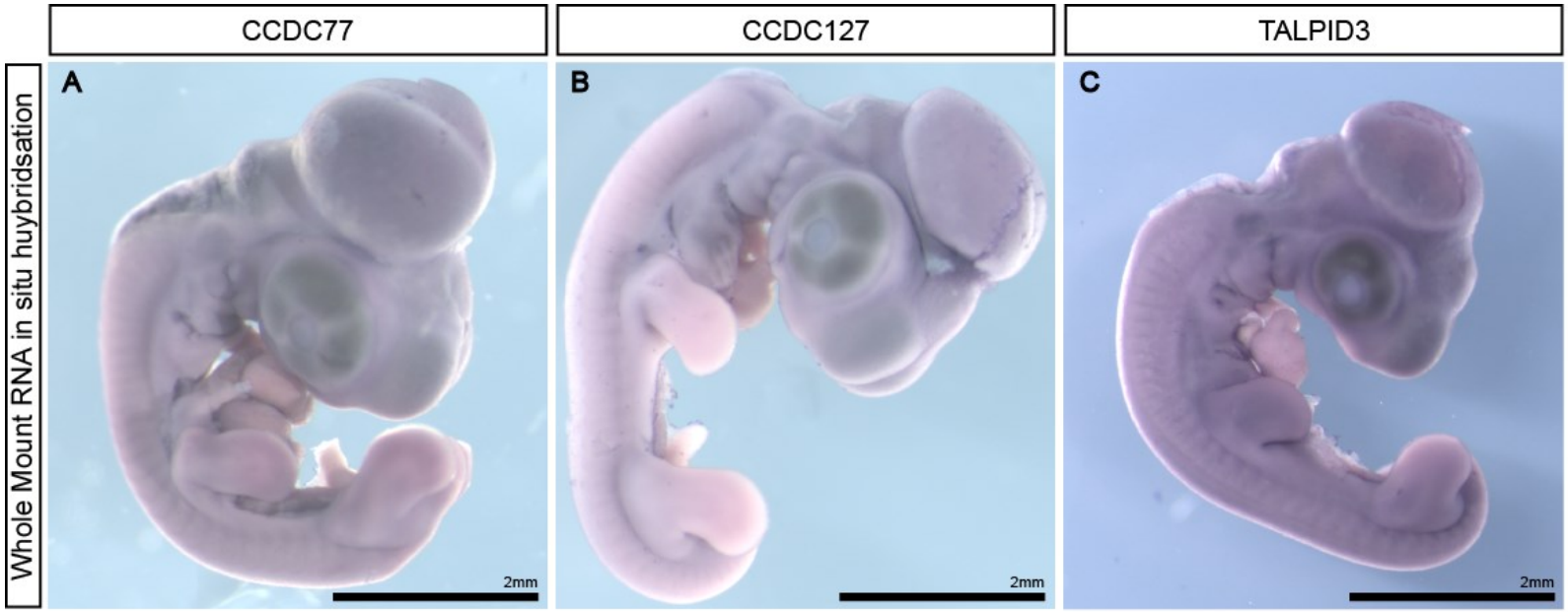

Figure 4.9 Whole mount RNA *in situ* hybridisation of CCDC77, CCDC127 and *TALPID3* shows expression in the developing chick embryo. (**A, B, C**) Whole mount RNA *in situ* hybridisation with probes for CCDC77, CCDC127 and *TALPID3* show ubiquitous expression in Hamburger Hamilton stage 25-26 chick embryos, demonstrating that CCDC77 and CCDC127 have similar ubiquitous expression patterns to centrosomal genes such as *TALPID3*. All scale bars: 2 mm.

Despite an apparent ubiquitous expression pattern by whole mount *in situ* hybridisation, trapping can be difficult to distinguish from specific expression patterns, therefore embryos were sectioned to determine if CCDC77 and CCDC127 have tissue specific expression patterns during development. Sections of the developing head, the choroid plexus (CP) and trunk region at the level of the forelimb (FL) were analysed for expression. The choroid plexus is a multiciliated, secretory organ that develops from the roof plate of the telencephalon, diencephalon and hindbrain (Cohen & Davies, 1937; Dziegielewska et al., 2001). Genes required for multi-ciliogenesis, such as *FOXJ1* (Yu et al., 2008), are expressed in the choroid plexus as well as the telencephalon and diencephalon in the chick (Cruz et al., 2010; Stephen et al., 2013). Evidence of CCDC77 and CCDC127 expression in multiciliated tissues on the Human Protein Atlas and in the choroid plexus on the Allen Mouse Brain Atlas prompted me to look for expression in the choroid plexus tissue in the developing chick to determine if either gene could be specific to early regulation of multi-ciliated organ development.

Sections of Hamburger-Hamilton stage 25-26 embryos which had undergone RNA *in situ* hybridisation for CCDC77 revealed expression in the maxillary and mandibular regions of the first pharyngeal arch (PA1), the second pharyngeal arch (PA2) and extensively in the head mesenchyme (Figure 4.10 A), which contributes to skeletal elements, connective tissue and musculature of the head. CCDC77 RNA expression was also present in the interneurons of the neural tube (NT), the mesenchyme around the neural tube, around the top of the crop and in the forelimb mesenchyme (Figure

4.10 G). The expression seen around the crop is most likely muscle and the forelimb mesenchyme, running ventrally and dorsally is most likely muscle; however, this is not conclusive without a muscle marker, such as MyoD. There was no CCDC77 expression observed in the heart, liver or epithelium.

Tissue sections of Hamburger-Hamilton stage 25-26 embryos which had undergone RNA *in situ* hybridisation for CCDC127 revealed expression in the maxillary and mandibular regions of pharyngeal arch 1 (PA1) and in the head mesenchyme (Figure 4.10 B), which contributes to skeletal elements, connective tissue and musculature of the head. CCDC127 was also expressed in the mesenchyme on both sides of the neural tube (NT), the forelimb (FL) mesenchyme, and at low levels in the endothelia around the dorsal aorta (DA), the right and left anterior cardinal veins (RACV and LACV respectively), and the vessels of the forelimb (Figure 4.10 H). There was no CCDC127 expression observed in the neural tube, dorsal root ganglion, somites, heart or liver.

Tissue sections of Hamburger-Hamilton stage 25-26 embryos which had undergone RNA *in situ* hybridisation for TALPID3 revealed expression in the maxillary and mandibular regions of pharyngeal arch 1 (PA1) and in the head mesenchyme (Figure 4.10 C). TALPID3 was also expressed in the dorsal region of the neural tube (NT), the mesenchyme on both sides of the neural tube, the forelimb mesenchyme and around one side of the gizzard (Figure 4.10 I). There was no TALPID3 expression observed in the heart, liver or blood vessels.

Of note, neither CCDC77 nor CCDC127 showed expression in the developing choroid plexus (CP) (Figure 4.10 D and E), suggesting that neither gene is specific to early regulation of multi-ciliated organ development in the chick. There was no expression of TALPID3 observed in the developing choroid plexus (Figure 4.10 F) as expected (Stephen et al., 2013).

The expression patterns seen following RNA *in situ* hybridisation for CCDC77 and CCDC127 confirm that they are expressed during embryonic development in the chick and show organ specific patterns of expression. The organ specific expression patterns of CCDC77 in the pharyngeal arches, and interneurons of the neural tube suggest that CCDC77 may play a role in early neural development. The extensive expression of both CCDC77 and CCDC127 in the mesenchyme could highlight the role centrosomes play in mesenchymal cell migration at this stage in development. Additionally head mesenchyme, stemming from cranial neural crest and head mesoderm cells populate the branchial arches and give rise to skeletal elements of the skull and face, connective tissue and musculature of the head; ciliopathies are known to result in craniofacial abnormalities and the expression of CCDC77 and CCDC127 in the head mesenchyme could be as a result of the role of cilia in craniofacial development (Brugmann et al., 2010; Brugmann et al., 2010; Xavier et al., 2016).

Ciliopathy mutations are known to have varying levels of tissue penetrance, which suggests that not all centrosome proteins act equally in different tissues or at different stages of development (McIntyre et al., 2013); it is likely that both CCDC77 and CCDC127 follow this trend. Further RNA *in situ*

hybridisation at both earlier and later developmental stages could help to confirm this hypothesis; additionally RNA *in situ* at earlier developmental stages typically results in less trapping and therefore could be used to confirm that the results presented in figures 4.9 and 4.10 are not due to trapping. In conclusion, these results confirm that CCDC77 and CCDC127 are expressed during embryonic development in the chick; additionally the results show similar expression patterns of CCDC77 and CCDC127 to the centrosome protein TALPID3, supporting CCDC77 and CCDC127 as centrosome proteins.

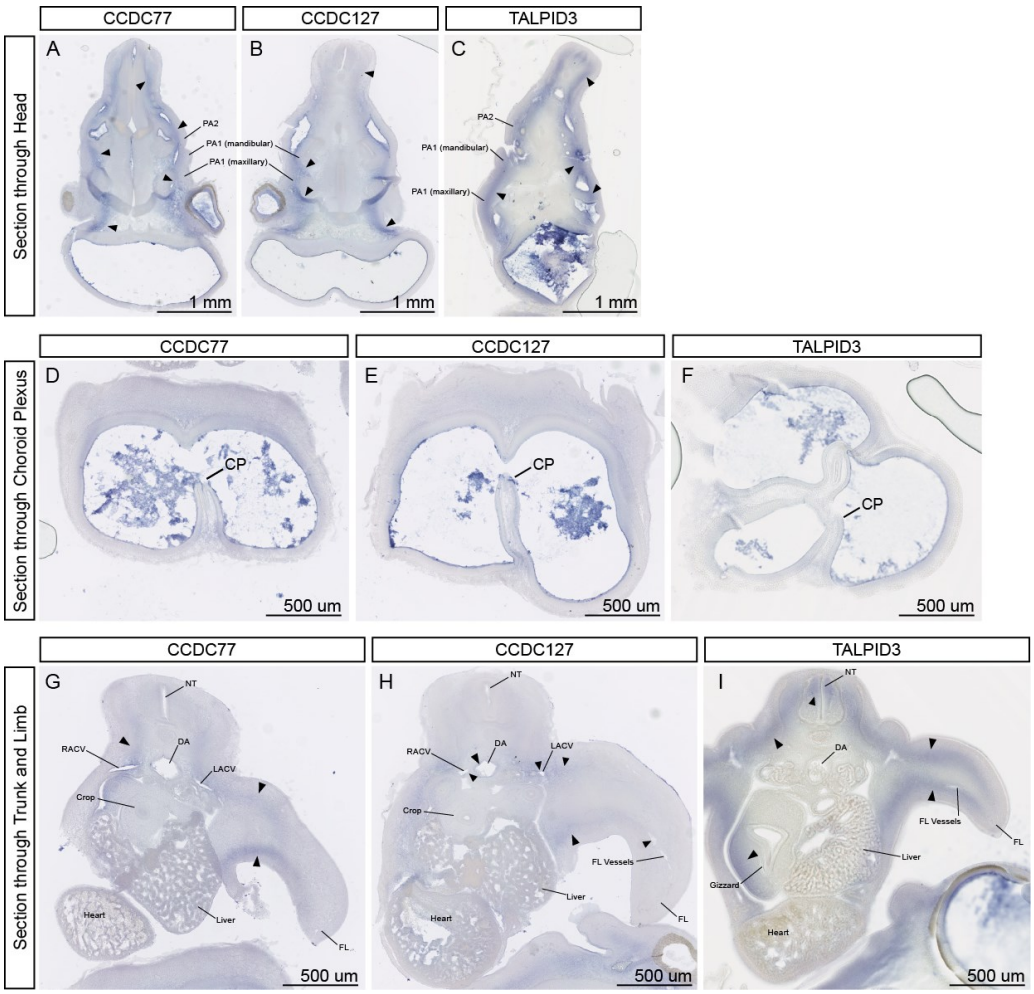

Figure 4.10 RNA *in situ* hybridisation of CCDC77, CCDC127 and *TALPID3* shows expression in specific regions of the developing chick embryo. Sections that had undergone RNA *in situ* hybridisation for CCDC77, CCDC127 and TALPID3 were examined for tissue specific expression patterns. (**A, B, C**) Sections through the head, showing expression of CCDC77, CCDC127 and *TALPID3*, respectively. Expression, marked by black arrowheads, was seen in the head mesenchyme and the pharyngeal arches (PA). (**D, E, F**) Sections through the choroid plexus (CP) show no expression of CCDC77, CCDC127 or *TALPID3* respectively. (**G**) A section through the trunk at the level of the forelimb (FL) shows CCDC77 expression in the interneurons of the NT, the mesenchyme around the NT, around the top of the crop and in the forelimb (FL) mesenchyme. Expression marked by black arrowheads. (**H**) A section through the trunk at the level of the forelimb (FL) shows CCDC127 expression in the mesenchyme on both sides of the NT, the forelimb (FL) mesenchyme, and at low levels in the endothelia around the dorsal aorta (DA), the right and left anterior cardinal veins (RACV and LACV respectively) and the vessels of the forelimb. Expression marked by black arrowheads. (**I**) A section through the trunk at the level of the forelimb (FL) shows *TALPID3* expression in the dorsal region of the neural tube (NT), in the mesenchyme on both sides of the NT, the forelimb (FL) mesenchyme and around one side of the gizzard. Expression marked by black arrowheads. All scale bars as annotated on figure.

4.2.7 Mutations in CCDC127 cause loss of CCDC127 localisation in RPE1 cells

In order to understand the function of CCDC127 in the centrosome, CCDC127 was targeted with CRISPR/Cas9 editing to create functional mutations followed by ciliogenesis assays to determine if CCDC127 plays a role in ciliogenesis. Two independent editing events were identified in RPE1 clonal cell lines, CCDC127 CRISPR Line 1 and CCDC127 CRISPR Line 2. CCDC127 CRISPR Line 1 had four altered nucleotides, CTTA (Figure 4.11 A) compared to GCTG in the unedited cell line (Figure 4.11 C), in the targeted region. CCDC127 CRISPR Line 2 had a deletion of two arginine nucleotides in the targeted region (Figure 4.11 B). These mutations are predicted to result in truncated proteins (Figure 4.11 D).

To determine if the mutations affected localisation of CCDC127 in the centrosome, immunofluorescence was used to analyse localisation. Both CCDC127 CRISPR Line 1 and CCDC127 CRISPR Line 2 showed a loss of punctate localisation of CCDC127 in the centrosome (marked by gamma tubulin) when compared to the unedited RPE1 cells (Figure 4.11 D, E, F). These results suggest that the mutations in CCDC127 CRISPR Line 1 and CCDC127 CRISPR Line 2 affect the production and localisation of the CCDC127 protein.

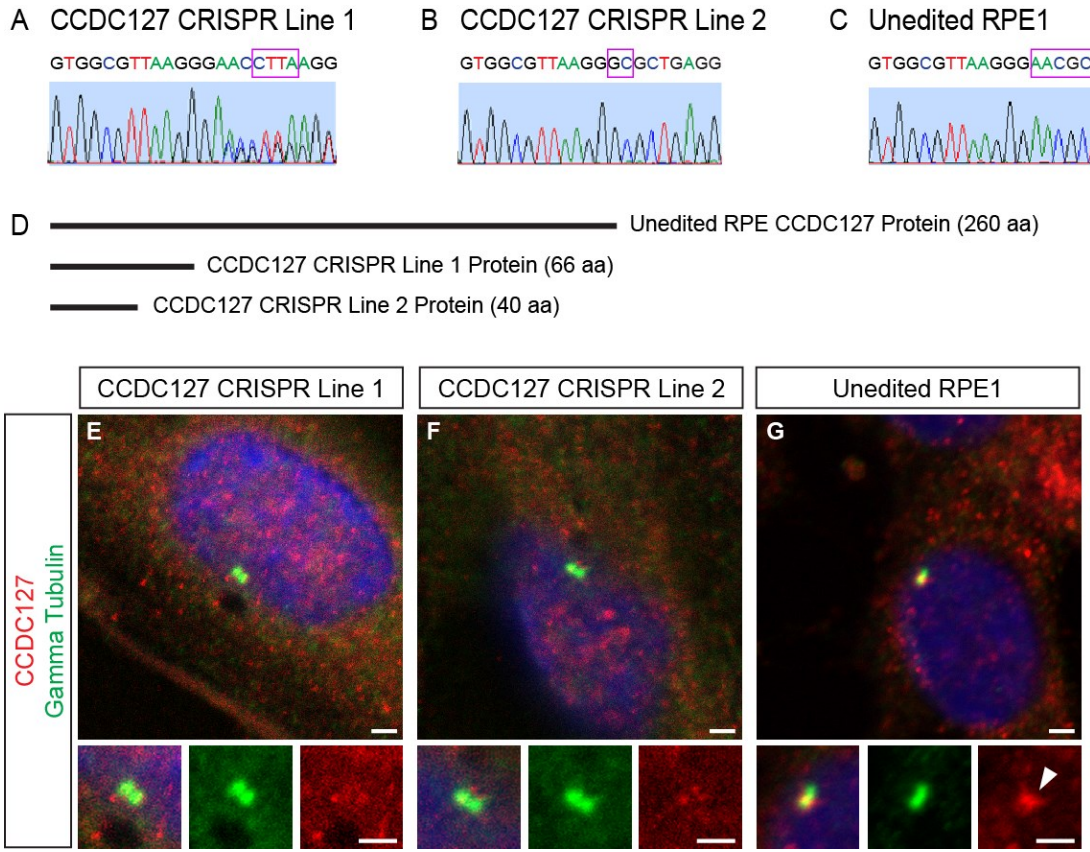

Figure 4.11 Mutations in CCDC127 cause loss of CCDC127 localisation in the centrosome in RPE1 cells. (**A**) Sequence containing a mutation in the targeted region of CCDC127 in CCDC127 CRISPR Line 1. The purple box marks the mutated region containing four altered nucleotides. (**B**) Sequence containing a mutation in the targeted region of CCDC127 in CCDC127 CRISPR Line 2. The purple box marks the mutated region, containing a deletion of two arginine nucleotides. (**C**) Sequence of the targeted region of CCDC127 in unedited RPE1 cells. The purple box marks the unedited region containing correct wildtype sequence that has been altered in the edited cell lines. (**D**) Schematic of the CCDC127 protein in unedited RPE1 cells and the truncated CCDC127 protein in CCDC127 CRISPR Line 1 and CCDC127 CRISPR Line 2. (**E-G**) Immunostaining with gamma tubulin (green), CCDC127 (red) and

Dapi (blue) shows a loss of CCDC127 in the centrosome in CCDC127 CRISPR Line 1 and CCDC127 CRISPR Line 2. CCDC127 localisation in the centrosome marked with a white arrowhead in unedited RPE1 cells. All scale bars: 2 µm.

4.2.8 Mutations in CCDC127 cause loss of ciliogenesis and altered centrosome protein localisation in RPE1 cells

To determine if the mutations in CCDC127 CRISPR Line 1 and CCDC127 CRISPR Line 2 affects ciliogenesis, edited RPE1 cells were examined using immunofluorescence. Both CCDC127 CRISPR Line 1 and CCDC127 CRISPR Line 2 showed a significant reduction in ciliogenesis compared to the unedited RPE1 cells (Figure 4.12 A, B, C, D). Only 28% of cells were ciliated in CCDC127 CRISPR Line 1 (*p=0.048) and 19% of cells were ciliated in CCDC127 CRISPR Line 2 (**p=0.001) compared to 69% of cells being ciliated in the unedited RPE1 cells (Figure 4.12 D). To determine if the mutations in CCDC127 affected the ciliary membrane, Arl13b was examined. Despite the reduced number of ciliated cells, both edited cell lines showed similar localisation patterns of Arl13b in cilia to that seen in the unedited RPE1 cells (Figure 4.12 E, F, G). In conclusion, the mutations in CCDC127 cause a significant reduction of ciliogenesis in CCDC127 CRISPR Lines 1 and CCDC12 CRISPR Line 2; however, the mutations do not appear to affect the localisation of Arl13b in the ciliary membrane.

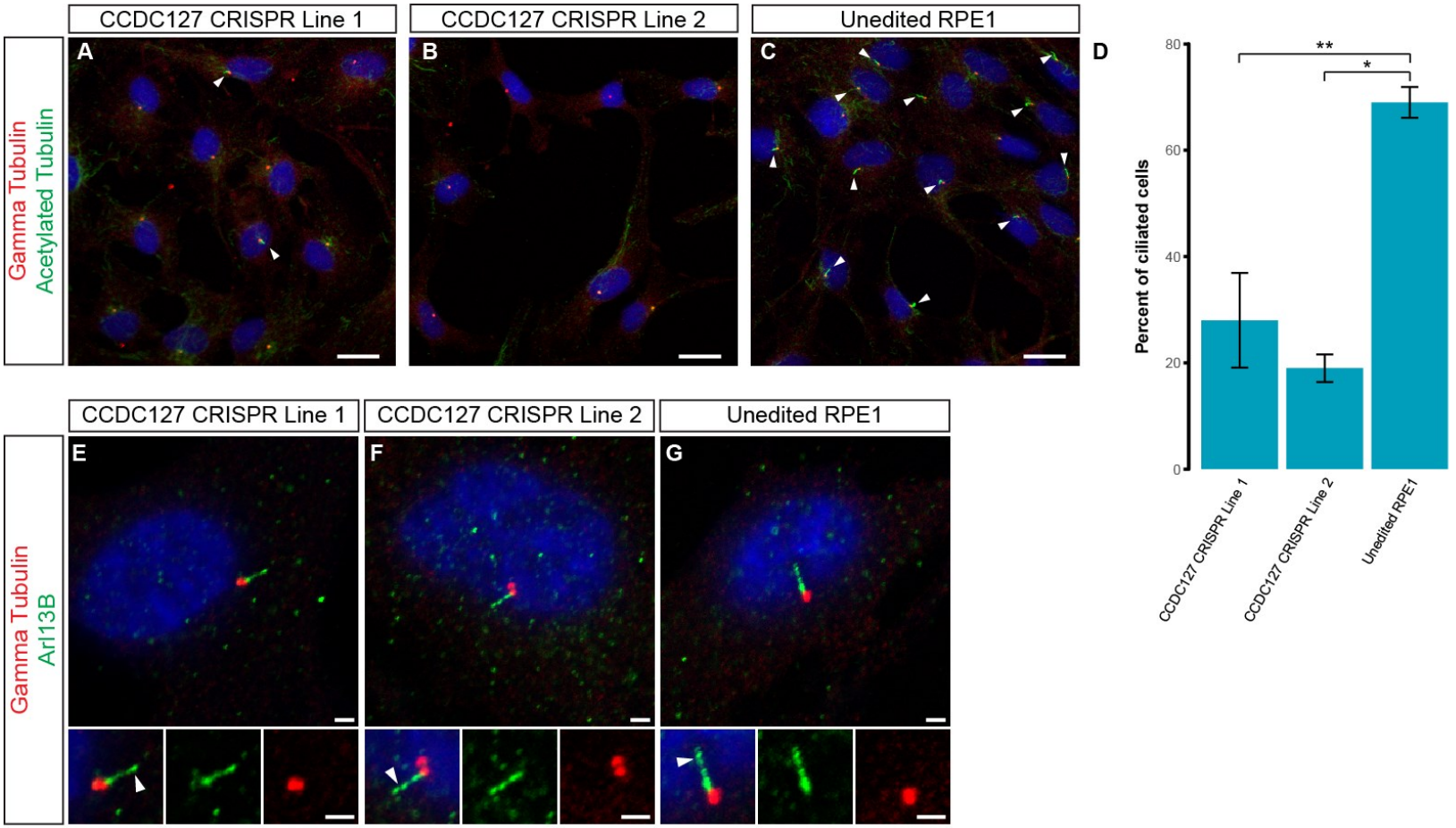

Figure 4.12 Mutations in CCDC127 cause loss of ciliogenesis in RPE1 cells. Immunostaining for gamma tubulin (red), acetylated tubulin (green) and Dapi (blue), with white arrowheads indicating cilia. (**A**) Image of CCDC127 CRISPR Line 1 with cilia marked by a white arrowhead. (**B**) Image of CCDC127 CRISPR Line 2 shows no ciliated cells. (**C**) Unedited RPE1 cells are ciliated, with all cilia identified by a white arrowhead. (**D**) Bar chart represents percent of ciliated cells in each cell line. CCDC127 CRISPR Line 1 and CCDC127 CRISPR Line 2 showed a significant reduction in ciliogenesis (*p = 0.048 and **p = 0.001 respectively) Unpaired two-tailed Student's t-test was used, with standard error bars included. *p<0.05, **p<0.01. (**E-G**) Immunostaining for gamma

tubulin (red), Arl13b (green) to mark the ciliary membrane and Dapi (blue). Cilia are identified with white arrowheads in all cell lines showing that the ciliary membrane is able to form with expected patterns of Arl13b localisation, despite the mutations in CCDC127. Scale bars in **A-C**: 20 µm. Scale bars in **E-G**: 2 µm.

In order to determine if the reduction of ciliogenesis in CCDC127 CRISPR Line 1 and CCDC127 CRISPR Line 2 was due to a loss of basal body maturation, localisation of Cep164, CP110 and PCM1 was examined. CCDC127 CRISPR Line 1 showed localisation patterns of both Cep164 and CP110 (Figure 4.13 A, B) that were consistent with unedited RPE1 cells (Figure 4.13 G, H). Although PCM1 localised around the centrosome as expected, it consistently showed a more widespread distribution around the centrioles in CCDC127 CRISPR Line 1 (Figure 4.13 C) when compared to unedited RPE1 cells (Figure 4.13 I). In CCDC127 CRISPR Line 2, Cep164 localisation (Figure 4.13 D) was consistent with unedited RPE1 cells (Figure 4.13 G), however CP110 showed co-localisation with gamma tubulin on both centrioles (Figure 4.13 E), not just at the distal end as was seen in unedited RPE1 cells (Figure 4.13 H). PCM1 in CCDC127 CRISPR Line 2 looked similar to PCM1 in CCDC127 CRISPR Line 1, with localisation around the centrioles as well as a more widespread pattern of PCM1 around the centriole in the pericentriolar material (Figure 4.13 F) compared to unedited RPE1 cells. In conclusion, these results show that Cep164 localisation in CCDC127 CRISPR Line 1 and CCDC127 CRISPR Line 2 is like that of the unedited RPE1 cells suggesting that the distal appendages are modified as expected during basal body maturation. CP110 and PCM1 however, have altered localisation patterns in the edited cell lines suggesting that the mutations in CCDC127 may have an effect on centrosome proteins involved in ciliogenesis.

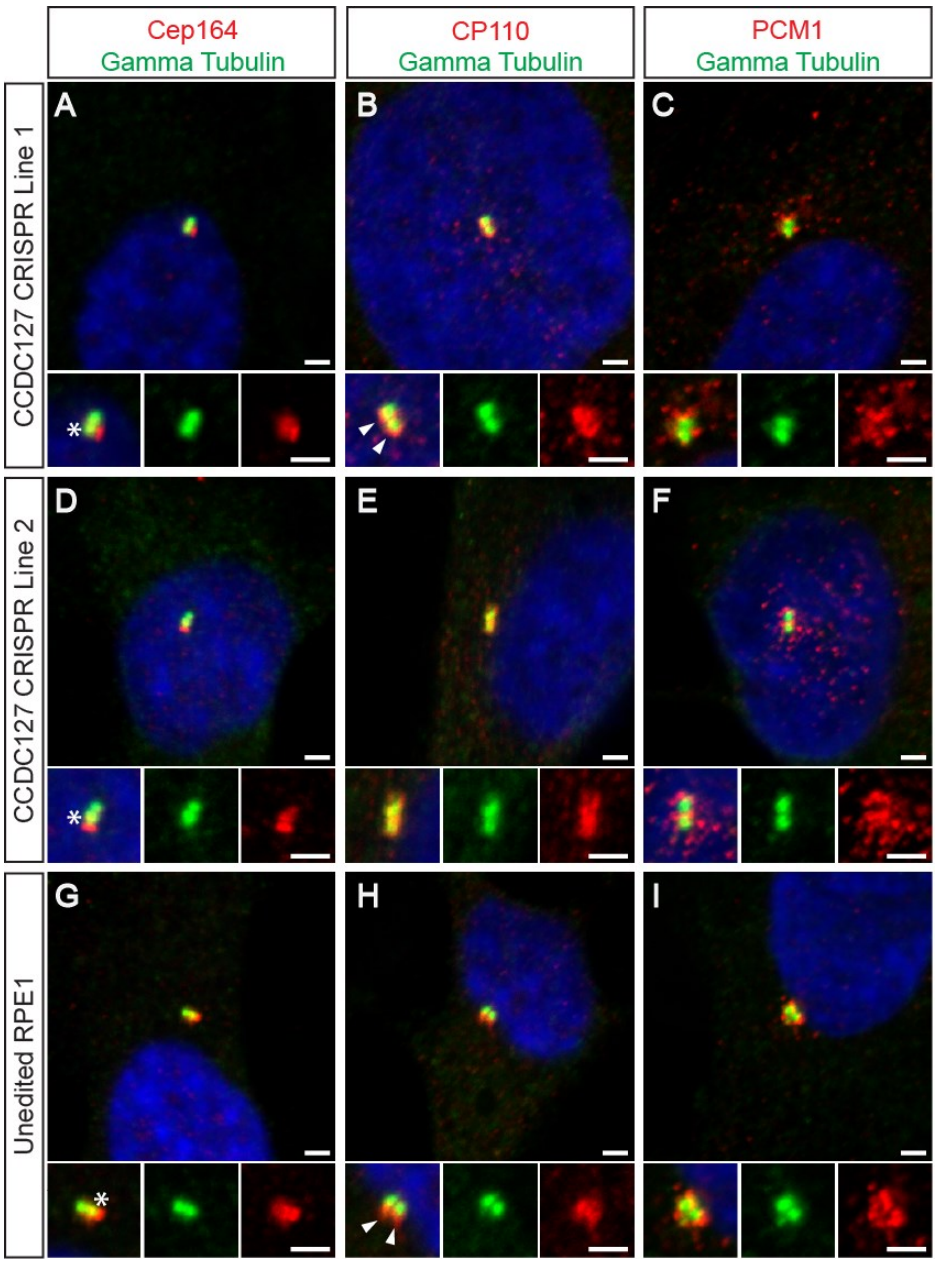

Figure 4.13 Mutations in CCDC127 cause changes to localisation patterns of CP110 and PCM1. (**A, D, G**) Immunostaining with Cep164 (red), gamma tubulin (green) and Dapi (blue) in CCDC127 CRISPR Line 1, CCDC127 CRISPR Line 2 and unedited RPE1 cells respectively shows Cep164 at the distal end of the mother centriole. Mother centrioles indicated with white asterisk. (**B, E, H**) Immunostaining with CP110 (red), gamma tubulin (green) and Dapi (blue) in CCDC127 CRISPR Line 1, CCDC127 CRISPR Line 2 and unedited RPE1 cells respectively. White arrowheads indicate CP110 at the distal end of each centriole in CCDC127 CRISPR Line 1 and unedited RPE1 cells. CCDC127 CRISPR Line 2 shows co-localisation of CP110 with gamma tubulin across both centrioles. (**C, F, I**) Immunostaining with PCM1 (red), gamma tubulin (green) and Dapi (blue) in CCDC127 CRISPR Line 1, CCDC127 CRISPR Line 2 and unedited RPE1 cells respectively shows more widespread distribution of PCM1 around centrioles in CCDC127 CRISPR Line 1 and CCDC127 CRISPR Line 2 in comparison to unedited RPE1 cells. All scale bars: 2 µm.

4.3 Discussion

This study has demonstrated that alternative cell lines to the non-ciliated, immortalised KE37 cells can be used for proteomic studies in the centrosome, and that use of different cell lines can identify novel centrosome proteins such as CCDC127. Although isolation of centrosomes from PGCs combined with mass spectrometry proved an ineffective tool to investigate the TALPID3 protein network, this study has identified chicken PGCs as a ciliated cell line that has modifications of the centriole that correlate with the ability to form cilia. Therefore, chicken PGCs can be used as a potential future model for studying ciliopathies and studying the TALPID3 proteome using a different approach.

Frequency of ciliogenesis is low in Jurkat cells; this is most likely due to a loss of maturation of the mother centriole, supported by the altered localisation patterns of Cep164, CP110, PCM1 and MACF1 in the centrosome. Chicken PGCs however, have modifications of the mother centriole that correlate with their ability to form cilia. The low protein yield and low centrosome enrichment in the PGCs was most likely due to the increased actin cytoskeletal structure preventing efficient isolation of centrosomes, and therefore inefficient protein extraction. However, despite these results, PGCs are a model that can be utilised for studying cilia and centrosomes in the future. Chickens have proven a suitable model for studying ciliopathies (Schock et al., 2016) and their ease of manipulation and potential for genetic modifications (Taylor et al., 2017) makes them an obvious choice for

modelling disease. The awareness that immortalised cell lines may not be the most relevant models for studying disease (Horvath et al., 2016; Masters & Stacey, 2007) has led to the need for new primary cell lines, providing a gap that PGCs can fill in the field of centrosome and cilia research.

By applying a centrosome proteome screen to Jurkat cells in this study, CCDC77 and CCDC127 were identified as novel centrosome proteins. CCDC77 was previously identified in a centrosome proteomic screen (Andersen et al., 2003), however it was not validated and therefore only predicted to localise to the centrosome prior to this study. CCDC127 has not previously been identified in a centrosome or cilia screen, therefore this study is the first to present CCDC127 as a centrosome protein. While this study was ongoing CCDC77 was identified as a low abundance centrosome protein in a quantitative proteomic analysis of the centrosome (Bauer et al., 2016) and was shown to localise to the centrosome in trypanosomes on the TrypTag database through a C-terminal tag with mNeonGreen (Dean et al., 2017). Therefore CCDC77 studies were not taken any further and instead CRISPR/Cas9 gene editing in RPE1 cells was used to examine the role of CCDC127 in the centrosome. Mutations in CCDC127 led to a loss of ciliogenesis and minor alterations in localisation patterns of centrosome proteins. The mutations in CCDC127 resulted in an accumulation of PCM1 in the satellites; this phenotype is similar to changes in other satellite proteins linked to ciliopathy proteins such as OFD1, BBS4, Cep290 and TALPID3 (Kobayashi et al., 2014; Lopes et al., 2011). Changes in CP110 in CCDC127

CRISPR Line 2 however, suggest that the protein interacting network of CCDC127 might be more complicated than just satellite association.

4.3.1 Complex centrosome protein networks are involved in ciliogenesis

A complex set of protein networks within the centrosome must work together in a time-dependent, localisation-specific manner for ciliogenesis to occur. For example, TALPID3 expression is necessary early on to ensure correct orientation and migration of the centriole to the apical surface (Stephen et al., 2013, 2015) as well as maturation of the mother centriole to form distal appendages. Proteins such as Cep164, Cep83 (CCDC41), Cep89 (CCDC123), SCLT1, FBF1 are required for the formation of distal appendages (Tanos et al., 2013), without which docking at the membrane prior to ciliogenesis would not occur; MACF1 is associated with both distal and subdistal appendages (May-Simera et al., 2016). Pericentriolar proteins such as PCM1 and BBS4 localise to the satellites, which are required for transport complex assembly proteins as well as housing proteins that are transported to the centrosome (Bärenz et al., 2011). Meanwhile, proteins such as CP110 and Cep97 work to suppress cilia assembly, and removal of CP110 results in the promotion of ciliogenesis (Spektor et al., 2007). Disruption to any one of these proteins or processes can alter the remaining proteins, due to the tight control and specific order of steps needed to produce a cilium. I have shown that the centrosome proteins Cep164, CP110, PCM1 and MACF1 do not

follow expected protein localisation patterns in Jurkat cells. It is likely that these are not the only centrosome proteins that are altered in Jurkat cells and that these protein changes are disrupting at least one of the processes involved in ciliogenesis such as centriole orientation, distal and subdistal appendage formation or docking to produce the reduced frequency of ciliogenesis observed.

Large-scale proteomic approaches have been successful in further defining protein networks within the centrosome and what roles they play in centrosome and cilia biogenesis (Andersen et al., 2003; Bauer et al., 2016; Gupta et al., 2015; Jakobsen et al., 2011). A study showed that 112 out of 335 polypeptides associated with centriole and cilia regulation generated a phenotype in at least two of the four functional assays in which they were tested (Gupta et al., 2015), demonstrating that genes involved in centriole amplification, ciliogenesis and/or satellite intensity overlap. The study suggested that components of networks that displayed a phenotype were more likely to overlap with other protein networks within the centrosome (Gupta et al., 2015). This complexity of the centrosome and cilia protein networks demonstrates that it is not as simple as individual proteins interacting with only a small subset of proteins within the network to give a well-defined phenotype, but instead much wider overlap of protein networks and their functions.

4.3.2 Centrosomes, ciliogenesis and human health

The centrosome has been linked to many human diseases, from a broad range of ciliopathies to the less understood role abnormal centrosomes play in aneuploidy and cancer (Bettencourt-Dias et al., 2011; Godinho & Pellman, 2014). Mutations in more than 40 genes have been found to associate with human ciliopathy patients; however, more than 1000 polypeptides have been found in the ciliary proteome to date (Waters & Beales, 2011). Given the large number of patients born with ciliopathy-associated phenotypes alongside the large number of cilia-associated proteins not currently linked to a ciliopathy, it is likely that new ciliopathy genes will be identified with future studies. CCDC77 and CCDC127 are both good ciliopathy candidates; in particular, the loss of ciliogenesis in the edited CCDC127 CRISPR cell lines supports CCDC127 as a ciliopathy candidate.

A large deletion in chromosome 12 has been found in a series of patients diagnosed with Autism Spectrum Disorders (ASD); the deletion in the patients includes up to thirteen genes, of which CCDC77 is one. The main diagnosis of these patients is ASD, hypothesised to be due to loss of the gene ERC1; however, the majority of the patients also have additional ciliopathy-like symptoms such as hypotonia, microcephaly and developmental delay (Silva et al., 2014). These phenotypes could be attributed in part to the loss of CCDC77.

A transcriptome-wide analysis study showed that CCDC77 and CCDC127 were among genes that were upregulated in foetuses with homozygous Kif7

mutations (Putoux et al., 2011). Kif7 is a cilia-associated protein that plays a critical role in mammalian Hedgehog signalling, acting downstream of SMO and upstream of the Gli proteins (Cheung et al., 2009; Liem et al., 2009). Kif7 has been associated with ciliopathies, such as Joubert Syndrome, Acrocallosal Sydrome (ACLS) and Bardet-Biedl Syndrome (BBS) (Dafinger et al., 2011; Putoux et al., 2011; Walsh et al., 2013). Fibroblasts derived from individuals with mutations in KIF7 were able to produce cilia with normal components shown by ultrastructural analysis, however the cilia were significantly longer (Putoux et al., 2011). The association of an upregulation of CCDC127 with an increase in cilia length is opposite to the phenotype seen with a reduction or loss of CCDC127, which results in a loss of cilia as shown in the study presented in this chapter. Taken together these phenotypes suggest that CCDC127 could play a role in the regulation of cilia length, similar to the role of KIF7 (Putoux et al., 2011). However, it is more likely that CCDC127 plays a role at the initiation of ciliogenesis, which would explain how a loss of CCDC127 results in a loss of ciliogenesis. Consequently, this would suggest that the upregulation of CCDC127 in the KIF7 mutant is a downstream effect, most likely caused by the loss a of negative feedback cycle that is lost due to the unregulated growth of cilia. Given the predicted role of CCDC127 during initiation of ciliogenesis and the super resolution imaging that shows CCDC127 localising to only one of the centrioles, it is likely that CCDC127 localises to the mother centriole. It most likely localises at the distal end of the mother centriole, with the possibility of localising to the transition zone during ciliogenesis.

The upregulation of CCDC77 and CCDC127 in association with Kif7 mutations highlights the need to better understand the role of these proteins in the centrosome and thus determine their potential as ciliopathy candidate genes. Understanding the implications for human health requires an understanding of the highly complex subcellular protein interactions in the centrosome, alongside identification of novel centrosome proteins and protein interactions to fill the gaps in our understanding of the current known networks.

4.3.3 Conclusions and future studies

In conclusion, I have shown through identification of CCDC127 that there are still centrosome proteins that have not previously been discovered. Methods that use alternative cell lines to study the centrosome proteome should be used to maximise our understanding of the centrosome protein network and to increase our ability to identify new ciliopathy loci. CCDC127 is a novel centrosome protein, that when disrupted causes a loss of ciliogenesis and abnormal localisation patterns of centrosome proteins. The changes observed in localisation patterns of PCM1 and CP110 in the CCDC127 edited RPE1 cell lines suggest that CCDC127 mutations may affect other ciliogenesis proteins.

The study presented in this chapter does not investigate any direct interactions between CCDC127 and other centrosome proteins. To obtain a clearer picture of where CCDC127 fits into the protein interacting network

at the centrosome-cilium interface, future studies could use more targeted proteomic studies. Endogenously tagging CCDC127, followed by a quantitative mass spectrometry approach could be used to determine proteins that directly interact with CCDC127. Combined with super resolution imaging, this would determine what proteins CCDC127 interacts with and the precise subcellular localisation of CCDC127 within the centrosome. This data would provide a more comprehensive understanding of what role CCDC127 plays in the centrosome-cilium interface, thus helping to fill the gap in our knowledge surrounding the centrosome proteome.

Chapter 5. Utilising a quantitative proteomic approach to uncover altered protein pathways in t*alpid*^{3} PGCs compared to wildtype PGCs.

5.1 Introduction

Despite extensive research into TALPID3, there is still very little known about the TALPID3 protein interacting network and which protein networks are involved in producing the mutant phenotype observed. To examine the TALPID3 protein interacting network more comprehensively and determine what protein pathways are altered in *talpid*^{3}, a quantitative proteomic approach was undertaken, comparing *talpid*^{3} chicken primordial germ cells to wildtype chicken primordial germ cells.

5.1.1 Chicken Primordial Germ Cells

In order to carry out a quantitative proteomic study comparing *talpid*^{3} to wildtype, it was important to identify a cell line or tissue that was suitable for studying TALPID3, through protein extraction and mass spectrometry. Primordial germ cells (PGCs) are the precursors of the germ cell lineage and are restricted to formation of the sperm and egg in adult organisms. In avian species, these cells are separated from the somatic cell lineages in the

epiblast of the laid egg (Tsunekawa et al., 2000). Germ cells, through their pluripotent nature, ensure that genetic and epigenetic information is carried forward to the next generation (Park & Han, 2000). They can easily be derived and cultured (Lavoir et al., 2006; Macdonald et al., 2010), meaning that they can be derived from *talpid*^{3} flock embryos for a proteomic comparison between *talpid*^{3} and wildtype conditions. I have already shown that chicken PGCs can be used as a cell model for studying the centrosome and cilia (Chapter 4), therefore supporting the suitability of using PGCs to study the centrosome protein TALPID3.

Studies in human HeLa cells predict that about 10,000 proteins of the 20,000 proteins in the human proteome are expressed in cells (Beck et al., 2011; Nagaraj et al., 2011), demonstrating that cell lines do not express all the proteins in the proteome. This is also true of gene expression in different tissue types in the chicken (Nie et al., 2010) suggesting that proteomic analysis in cells or tissue will not cover the entire proteome. However, extracting protein from cells instead of tissue produces a more homogenous protein set that can be repeated across individual cells lines more accurately (Kaur & Dufour, 2012). *Talpid*^{3} PGCs show characteristics consistent with the *talpid*^{3} mutant such as loss of cilia and slower migration patterns when colonising the gonad (Davey and McGrew labs, unpublished); therefore, despite not expressing the whole proteome the phenotype associated with the *talpid*^{3} PGCs suggests that they will provide a useful model for studying changes in protein expression patterns in *talpid*^{3} compared to wildtype.

In addition, mass spectrometry on protein isolated from chicken PGCs (see Chapter 4) demonstrated that the chicken proteome is complete enough to justify proteomic studies using mass spectrometry on chicken tissue. More than 29,000 proteins are included in the chicken proteome database in Uniprot (The Uniprot Consortium, 2018), which is the database used for protein identification of peptides following mass spectrometry. In conclusion, based on the nature of chicken PGCs, their ease of derivation and the evidence that mass spectrometry is applicable to chicken tissue, PGCs isolated from the *talpid*^{3} flock embryos were used to analyse the protein interacting networks affected in *talpid*^{3}.

5.1.2 TALPID3 protein interactions

Studies to date have shown TALPID3 is involved in several different functions in the centrosome through various protein interactions and more broadly in the whole cell through links to the actin network. A study showed that TALPID3 interacts with CP110 and more weakly interacts with three other proteins in the CP110-containing protein complex, Cep97, Cep290 and Kif24 (Kobayashi et al., 2014). Unlike TALPID3 which promotes ciliogenesis, CP110 localises to the distal end of centrioles and works to suppress ciliogenesis until removed from the mother centriole (Spektor et al., 2007; Tsang et al., 2008). Studies have suggested a model in which TALPID3 and Cep290 played overlapping roles in the appropriate localisation of Rab8a to the ciliary membrane (Kobayashi et al., 2014) and showed that loss of TALPID3 results

in abnormal accumulation of PCM1-positive granules at centrosomes (Kobayashi et al., 2014; Stephen et al., 2015). PCM1 is required for restricting the E3 ligase, Mindbomb1 (Mib1), to the satellites. Loss of PCM1 results in translocation of Mib1 to the centriole, where it interacts with and destabilises TALPID3 resulting in a loss of ciliogenesis (Wang et al., 2016). Another study showed that TALPID3 interacts with Cep120, a centrosome protein that is required for centriole duplication (Mahjoub et al., 2010; Wu et al., 2014); TALPID3 regulates the asymmetric localisation of Cep120 to the daughter centriole (Wu et al., 2014). Additionally TALPID3 has been shown to interact with Microtubule-Actin Cross Linking Factor 1 (MACF1), a ciliogenesis protein that is required in the early stages of ciliogenesis and required for maintenance of basal body positioning in differentiated tissue (May-Simera et al., 2016). In conclusion, these interactions with centrosome proteins involved in various centrosome functions including suppression of cilia assembly, centrosome duplication, restriction of proteins to the satellites and basal body positioning suggest that TALPID3 is essential for distinct roles and protein networks involved in centriole function.

In addition to TALPID3 interactions with centrosome proteins, there is evidence to suggest that Actin and TALPID3 are associated and may depend on one another during basal body orientation, docking and ciliogenesis (May-Simera et al., 2016; Yin et al., 2009). In the developing neural tube of wildtype chick, there is a continuous band of actin at the apex of cells. In contrast, *talpid*^{3} neural tube shows a non-continuous band of actin at the apex of the cells, which can be rescued by electroporation of a full length

TALPID3 construct demonstrating that the *talpid*^{3} mutation is responsible for this defective actin phenotype (Yin et al., 2009). The more recent discovery of the interaction between TALPID3 and MACF1 supports the TALPID3-actin association. In conclusion, the actin phenotype observed in *talpid*^{3} suggests that the role and interacting network of TALPID3 may not be limited to the centrosome, therefore a proteomic study to uncover the wider protein interacting networks affected in *talpid*^{3} is crucial to understanding the role of TALPID3.

5.1.3 Quantitative mass spectrometry approach

In order to determine which proteins are altered in *talpid*^{3} compared to wildtype, a quantitative mass spectrometry approach was completed to compare relative amounts of protein in the two conditions. In order to determine the most appropriate mass spectrometry method to use, accuracy, proteome coverage, sample numbers and whether the method chosen would be applicable to PGCs had to be taken into consideration. To address the question of what proteins are altered in *talpid*^{3} PGCs relative to wildtype PGCs, a labelled mass spectrometry approach was undertaken. Although a label free approach would allow the inclusion of an unlimited number of samples and has a high quantitative proteomic coverage, the accuracy of the process is lower than labelled approaches and the overall protein identification output is lower (Table 5.1) (Bantscheff et al., 2007), therefore a labelled approach was used.

Of the labelled approaches, SILAC was excluded because it did not meet the specific culture conditions necessary for PGCs and only a low number of samples could be included (Bantscheff et al., 2007). PGCs require exact levels of culture medium supplements and any slight changes can disrupt the survival of the cells (Whyte et al., 2015), meaning that metabolic labelling of proteins within cell culture was not viable for PGCs. Therefore, an isobaric labelling approach such as iTRAQ or TMT (Tandem Mass Tag) was considered the most appropriate method of labelling. Both iTRAQ and TMT have similar levels of accuracy, quantitative proteomic coverage, and protein identification output (Table 5.1) (Bantscheff et al., 2007). The difference between iTRAQ and TMT lies within the maximum number of samples that can be included. A TMT approach allowed inclusion of ten samples, meaning that protein from five independent *talpid*^{3} PGC cell lines and protein from five independent wildtype PGC cell lines could be included, therefore a TMT proteomic approach was undertaken.

The main limitation with TMT labelling that had to be considered was the ratio compression (Ow et al., 2011; Savitski et al., 2013). Ratio compression occurs because all peptides are multiplied by a global normalisation factor, to centre the ratio distribution on 1, which corrects for inconsistencies with labelling efficiency and protein digestion efficiency (Karp et al., 2010). This normalisation can lead to smaller changes in protein levels seen in the data than would actually be present in physiological conditions (Karp et al., 2010; Ow et al., 2011; Savitski et al., 2013). Despite this potential limitation, I hypothesised that the changes that occur as a result of the *talpid*^{3} mutation,

such as altered Hedgehog pathway signalling and polarity defects, are significant enough that altered protein levels would still be detected despite ratio compression.

Table 5.1 Characteristics of quantitative mass spectrometry methods taken into consideration for analysing the *talpid*^{3} proteome compared to the wildtype proteome.

	Accuracy of the process	Quantitative Proteomic Coverage	Protein Identification Output	Maximum Number of Samples
Label Free	+	+ + +	+ +	Unlimited
SILAC Metabolic Labelling	+ + +	+ +	+ + +	3
iTRAQ Isobaric Labelling	+ +	+ +	+ + +	8
TMT Isobaric Labelling	+ +	+ +	+ + +	10

5.1.4 Aims

To date, studies on proteins that interact with TALPID3 have focused on individual proteins within the centrosome (Kobayashi et al., 2014; May-Simera et al., 2016; L. Wang et al., 2016; Wu et al., 2014) and have not attempted protein pathway analysis to understand the broader picture of the TALPID3 protein interacting network. In order to determine which

proteins are changed in the *talpid*^{3} mutant relative to the wildtype chick and how this translates to protein pathway changes in *talpid*^{3}, a quantitative proteomic approach was undertaken. The aim of this study was to use a labelled TMT mass spectrometry approach on protein isolated from *talpid*^{3} PGCs and wildtype PGCs, to identify proteins that are altered in *talpid*^{3}. Additionally, protein pathway analysis on the quantitative dataset aimed to uncover protein pathways that are altered in *talpid*^{3} thus providing an insight into some of the protein networks in which TALPID3 is involved.

5.2 Results

5.2.1 Protein isolation from *talpid*^{3} flock PGCs for TMT mass spectrometry

Having determined that a TMT quantitative mass spectrometry approach in PGCs was the most appropriate method of studying the changes in protein levels in *talpid*^{3}, PGC cell lines were derived from *talpid*^{3} flock embryos. A previous attempt to isolate centrosomes from PGCs, for studying the TALPID3 protein network proved unsuccessful (see Chapter 4); therefore, protein extracted from whole cell lysate was used for this study. Instead of focusing on TALPID3 in the centrosome, protein was extracted from *talpid*^{3} PGCs and compared to protein extracted from wildtype PGCs to look for differences in the proteomes. PGCs were isolated from the *talpid*^{3} mutants in the flock and also their wildtype counterparts to ensure the most direct comparison. Different breeds contain differences in protein expression levels (Zanetti et al., 2011) so for the most relevant quantitative protein comparison, wildtype from the *talpid*^{3} flock was used.

Protein extracted from five independent *talpid*^{3} PGC cell lines and five independent wildtype PGC cell lines was used for the proteomic analysis. Including a larger sample size of five samples per condition increases the confidence and precision of the experimental analysis (Karp et al., 2005). In conclusion, five independent *talpid*^{3} protein samples and five independent wildtype protein samples from the *talpid*^{3} flock were included in the quantitative proteomic analysis.

5.2.2 Validation of the quantitative *talpid*^{3} flock PGC mass spectrometry dataset

Following TMT mass spectrometry analysis on *talpid*^{3} and wildtype PGC protein samples, 7052 proteins were identified in all ten protein samples (five wildtype and five *talpid*^{3}). All proteins lacking quantitative values were excluded from further analysis. All proteins lacking at least one unique identifying peptide were excluded from further analysis. Ensuring identification with at least one unique peptide, allows increased confidence in the protein identification within the dataset (Zhao & Lin, 2010). This left 6606 proteins to carry forward for analysis. To validate the quantitative TMT mass spectrometry dataset, western blot analysis was used to confirm that proteins identified during mass spectrometry were in the protein samples and to confirm that the values associated with the proteins matched the quantitative values produced during mass spectrometry. Many proteins that were identified in the dataset did not have antibodies raised against the protein that were specific for the chicken protein and worked in western blot (Appendix 7); however, gamma tubulin, E-cadherin, Testin and gamma actin were identified in all ten PGC protein samples following mass spectrometry and were identified as suitable for western blot validation. Western blot analysis produced a band at 48 kDa for gamma tubulin in all protein samples (Figure 5.1 A), a band at 100 kDa for E-cadherin in all protein samples (Figure 5.1 A), a band at 48 kDa for Testin in all protein samples (Figure 5.1 B) and a band at 41 kDa for gamma actin in all protein samples (Figure 5.1 B). These

results demonstrate that the proteins identified by mass spectrometry are components of the protein samples, thus validating the dataset.

Western blot analysis for E-cadherin was used to validate the reporter intensity values produced in the TMT mass spectrometry dataset. E-cadherin had varying reporter signal intensities across the ten samples, with Wt1, Wt4, Wt5, Ta4 and Ta5 having higher reporter intensities than Wt2, Wt3, Ta1, Ta2 and Ta3 (Figure 5.1 C). The western blot band signal values (Figure 5.1 C), although not exactly the same, followed the same trend, therefore confirming the reporter intensity values found in the TMT dataset for the PGC protein samples. In conclusion, the results of the western blots validate the proteins identified in *talpid*^{3} and wildtype PGCs using mass spectrometry and additionally validates the quantitative values associated with those proteins.

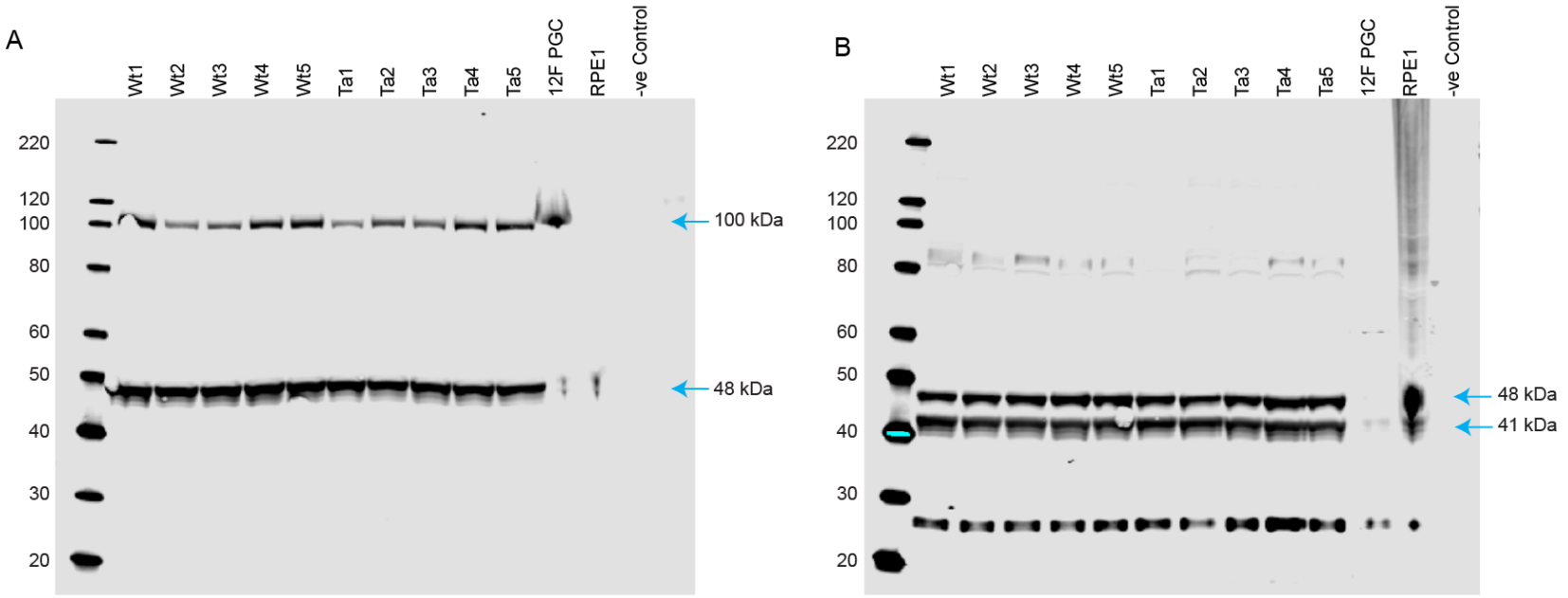

C

	Wt1	Wt2	Wt3	Wt4	Wt5	Ta1	Ta2	Ta3	Ta4	Ta5
E-cadherin Reporter Intensity	105140	89770	76409	11000	97121	62701	92667	81829	137840	106120
E-cadherin Western Blot Band Signal	57200	29300	34100	55200	60100	23600	40500	36500	54900	63700

Figure 5.1 Validation of quantitative *talpid*^{3} flock PGC mass spectrometry dataset through Western Blot. (**A**) Western blot for gamma tubulin shows a band at 48 kDa in all ten protein samples sent for mass spectrometry. Western blot for E-cadherin shows a band at 100 kDa in all ten protein samples sent for mass spectrometry. (**B**) Western blot for Testin shows a band at 48 kDa in all ten protein samples sent for mass spectrometry. Western blot for gamma actin shows a band at 41 kDa in all ten protein samples sent for mass spectrometry. Together the results from both western blots validate the dataset by confirming

that the proteins identified during mass spectrometry are in the protein samples. (**C**) Table containing mass spectrometry reporter intensity values for E-cadherin for each protein sample sent for mass spectrometry and western blot band values for E-cadherin for each protein sample, quantified in Image Studio Lite. Although these values do not match exactly the trend in the report intensities matches the trend of the western blot band signal, with higher values for Wt1, Wt4, Wt5, Ta4 and Ta5 and lower values for Wt2, Wt3, Ta1, Ta2 and Ta3. These results confirm that the quantitative data provided in the mass spectrometry dataset matches the amounts of protein in each sample.

5.2.3 Dataset of proteins for Ingenuity Pathway Analysis Software

Having validated the mass spectrometry dataset, I carried out analysis in Ingenuity Pathway Analysis software (IPA) to uncover altered protein pathways in *talpid*^{3}. Before completing pathway analysis, the mass spectrometry dataset was filtered to include only proteins identified by two or more unique peptides. This filter ensures that the dataset is robust by guaranteeing the proteins in the dataset, annotated by peptide identification, are correct (Zhao & Lin, 2010). IPA identifies networks by gene name; therefore, any proteins in the dataset that were not identifiable by gene name were also excluded. This allowed a dataset containing 5192 proteins with the relevant fold change values (*talpid*^{3}/wildtype) to be imported into IPA.

Within IPA, a fold change minimum limit of 1.2 was applied to the dataset of 5192 proteins, prior to completing the pathway analysis. This limit ensured that only proteins that had a minimum change of 20% in the *talpid*^{3} PGCs when compared to the wildtype PGCs were included in the analysis; therefore, 163 proteins (Appendix 8) were included in pathway analysis in IPA (Figure 5.2). Included in the dataset of proteins are GLI2 and NRP2 (Neuropilin2) (Figure 5.2). These proteins have previously been shown to be altered in *talpid*^{3} (Bangs et al., 2011; Ben et al., 2011; Davey et al., 2007; Davey et al., 2006; Li et al., 2017) and therefore support the quantitative mass spectrometry data for proteins altered in *talpid*^{3}.

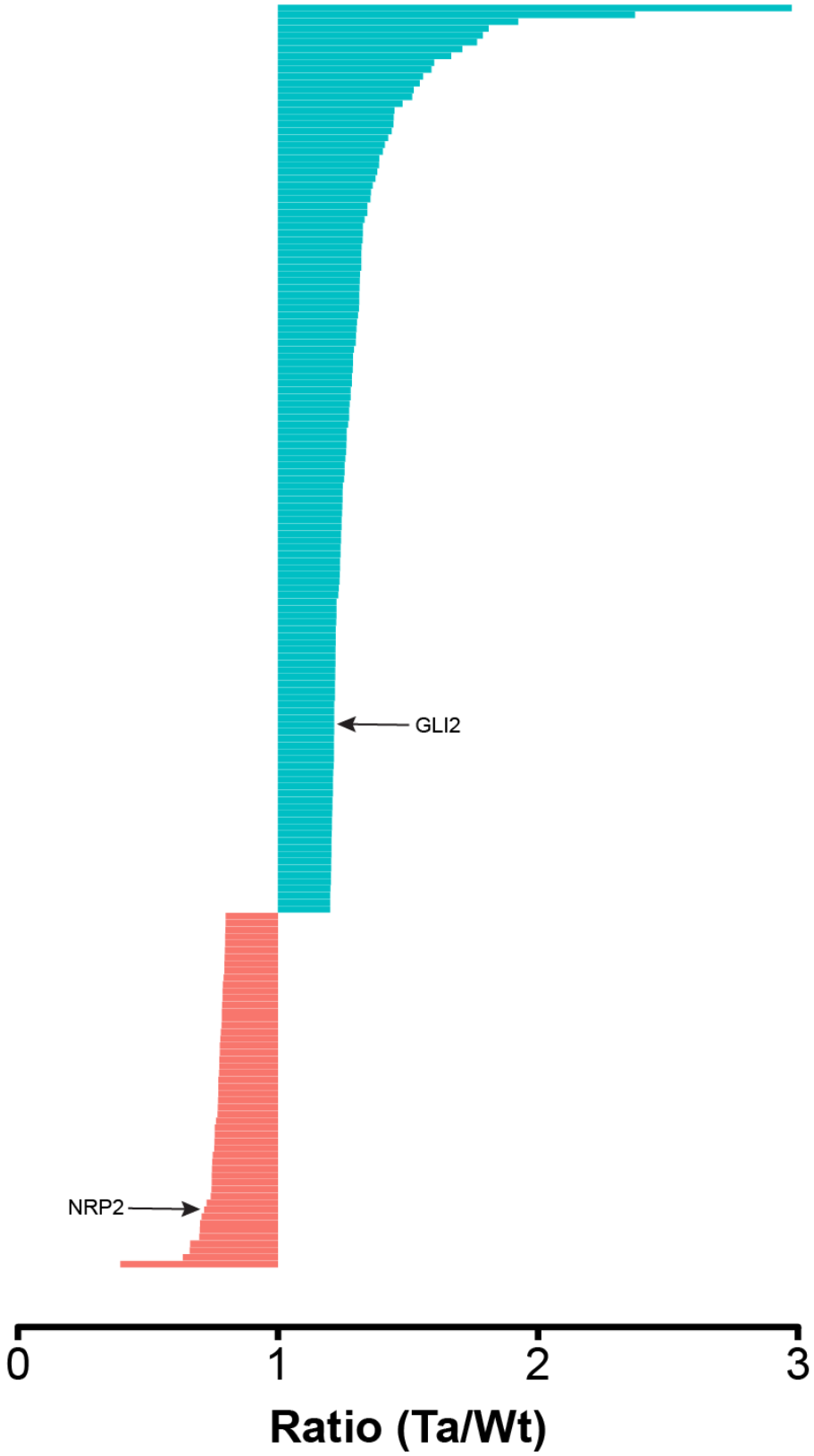

Figure 5.2 Proteins identified with two or more unique peptides that have a minimum fold change of 1.2 in *talpid*^{3} compared to wildtype. The fold change represents the average *talpid*^{3} protein reporter intensities over the

average wildtype protein reporter intensities. Black arrows mark GLI2, which is upregulated in *talpid*^{3} compared to wildtype PGCs and NRP2, which is downregulated in *talpid*^{3} compared to wildtype PGCs. The proteins and fold change values plotted on this graph are listed by gene name in Appendix 8.

5.2.4 Protein pathway analysis in *talpid*^{3} PGCs

Having validated the mass spectrometry dataset and identified a list of 163 proteins to include, pathway analysis was completed in IPA. By looking at the overall protein networks that are changed in *talpid*^{3} PGCs, the aim was to understand what networks TALPID3 is involved in, instead of protein-specific interactions of TALPID3. IPA produced a set of canonical signalling pathways that are predicted to be altered in *talpid*^{3} PGCs compared to wildtype PGCs (Figure 5.3).

Of the canonical signalling pathways that were identified, two groups of pathways taken from the top 15 hits were focused on for further analysis. The groups included the pathways linked to cholesterol biosynthesis and pathways associated with Rho and Actin (Table 5.2). The proteins identified in the cholesterol biosynthesis pathways did not amount specifically to upregulation or downregulation of the pathway, but instead were annotated with no activity pattern available. However, the pathways associated with Actin and Rho were consistently downregulated with the Actin Cytoskeleton Signalling Pathway having the lowest z-score, which meant it was more highly downregulated than the RhoA Signalling pathway or the Regulation of Actin-based Motility by Rho pathway.

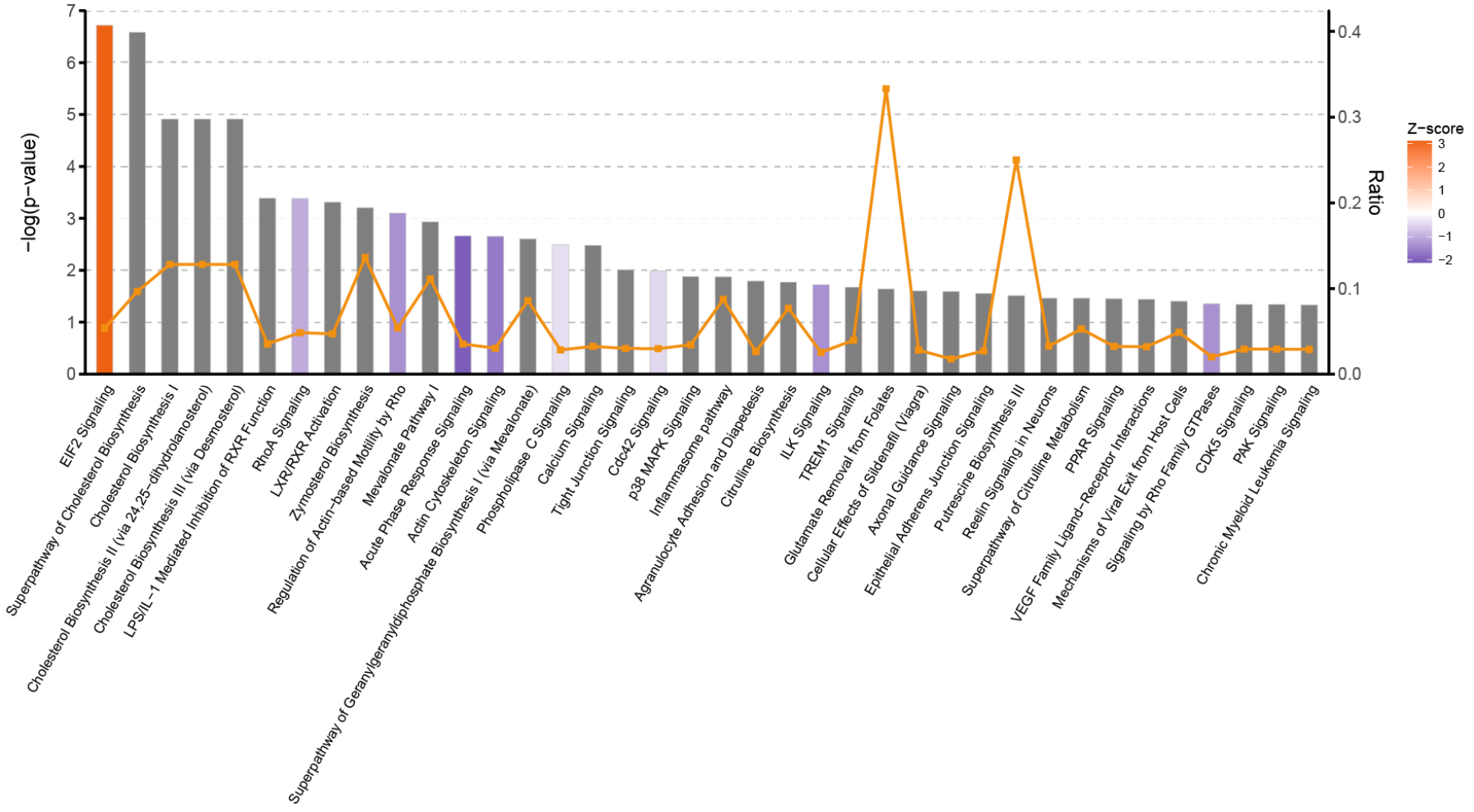
−log(p−value)
Ratio
Z−score
3
2
1
0
−1
−2
0
1
2
3
4
5
6
7
0.0
0.1
0.2
0.3
0.4
EIF2 Signaling
Superpathway of Cholesterol Biosynthesis
Cholesterol Biosynthesis I
Cholesterol Biosynthesis II (via 24,25−dihydrolanosterol)
Cholesterol Biosynthesis III (via Desmosterol)
LPS/IL−1 Mediated Inhibition of RXR Function
RhoA Signaling
LXR/RXR Activation
Zymosterol Biosynthesis
Regulation of Actin−based Motility by Rho
Mevalonate Pathway I
Acute Phase Response Signaling
Actin Cytoskeleton Signaling
Superpathway of Geranylgeranyldiphosphate Biosynthesis I (via Mevalonate)
Phospholipase C Signaling
Calcium Signaling
Tight Junction Signaling
Cdc42 Signaling
p38 MAPK Signaling
Inflammasome pathway
Agranulocyte Adhesion and Diapedesis
Citrulline Biosynthesis
ILK Signaling
TREM1 Signaling
Glutamate Removal from Folates
Cellular Effects of Sildenafil (Viagra)
Axonal Guidance Signaling
Epithelial Adherens Junction Signaling
Putrescine Biosynthesis III
Reelin Signaling in Neurons
Superpathway of Citrulline Metabolism
PPAR Signaling
VEGF Family Ligand−Receptor Interactions
Mechanisms of Viral Exit from Host Cells
Signaling by Rho Family GTPases
CDK5 Signaling
PAK Signaling
Chronic Myeloid Leukemia Signaling

Figure 5.3 Canonical pathways identified in Ingenuity Pathway Analysis software (IPA) that are altered in *talpid*^{3} PGCs compared to wildtype PGCs. The canonical pathways identified are based on the 163 proteins that have a fold change minimum of 1.2 when comparing *talpid*^{3} protein levels to wildtype protein levels. Orange refers to a positive z-score that correlates with upregulation of a pathway. Purple represents a negative z-score that correlates with downregulation of a pathway. Grey represents a pathway that contains changed components that do not correlate specifically with either upregulation or downregulation, instead an overall change. The –log (p-value) annotates the most significant changes in pathways.

Table 5.2 Canonical pathways, identified in the top 15 pathways in IPA that are associated with cholesterol biosynthesis or Rho and Actin signalling. Negative z-scores represent down regulation of a pathway. Where a z-score is annotated as unchanged, there was no activity pattern available on IPA.

Canonical Pathway	P-value (-log)	Z-score
Superpathway of Cholesterol Biosynthesis	6.58	Unchanged
Cholesterol Biosynthesis I	4.91	Unchanged
Cholesterol Biosynthesis II (via 24,25-dihydrolanosterol)	4.91	Unchanged
Cholesterol Biosynthesis III (via Desmosterol)	4.91	Unchanged
RhoA Signalling	3.38	-1
Regulation of Actin-based motility by Rho	3.1	-1.342
Actin Cytoskeleton Signalling	2.65	-1.633

5.2.5 Cholesterol Biosynthesis pathways are altered in *talpid*^{3} PGCs

Cholesterol biosynthesis pathways made up four of the top 15 hits of the canonical pathways changed in *talpid*^{3} PGCs compared to wildtype PGCs. This result was not completely unexpected as changes in morphology, structure or adhesion of cells is often associated with changes in cholesterol biosynthesis (Pace & Esfahani, 1987; Sun et al., 2007). Cholesterol is a principal component of cell membranes, with all subcellular membranes

containing cholesterol (Pace & Esfahani, 1987); cilia membranes have been shown to be rich in cholesterol (Chailley & Boisvieux-Ulrich, 1985; Cuevas et al., 1985). Additionally, cholesterol has been shown to be an efficient regulator of biophysical properties of the membrane, with decreased cholesterol resulting in actin cytoskeleton disorganisation (Sun et al., 2007). With the characteristics of *talpid*^{3} PGCs including loss of ciliogenesis and slower migration to colonise the gonads (Davey and McGrew labs, unpublished) as well as an overall *talpid*^{3} actin phenotype that could affect the cytoskeleton (Yin et al., 2009), a change in biosynthesis of cholesterol would be expected.

The cholesterol pathways identified all share a common region and then branch after lanosterol production (Figure 5.4). Following branching after lanosterol production, the pathways differ only slightly and within each of the different branches, the same protein changes are seen, including sterol 14-demethylase, methylsterol monooxygenase, 3beta-hydroxy-4alpha-methylcholestencarboxylate 3-dehydrogenase (decarboxylating) and D24-sterol reductase. The Superpathway of Cholesterol Biosynthesis contains three additional altered proteins at the top of the pathway (Figure 5.4), which are not part of the other identified cholesterol biosynthesis pathways. Despite making up four of the top 15 altered pathways, the cholesterol biosynthesis pathways were identified due to the same protein changes in each pathway and the overlap meant that it was the same region of each pathway that was changing. In conclusion, further analysis into the cholesterol biosynthesis pathways was not completed, as evidence from the

literature suggested this result is expected with changes in cell conditions such as those seen in *talpid*^{3} PGCs compared to wildtype PGCs.

Superpathway of Cholesterol Biosynthesis

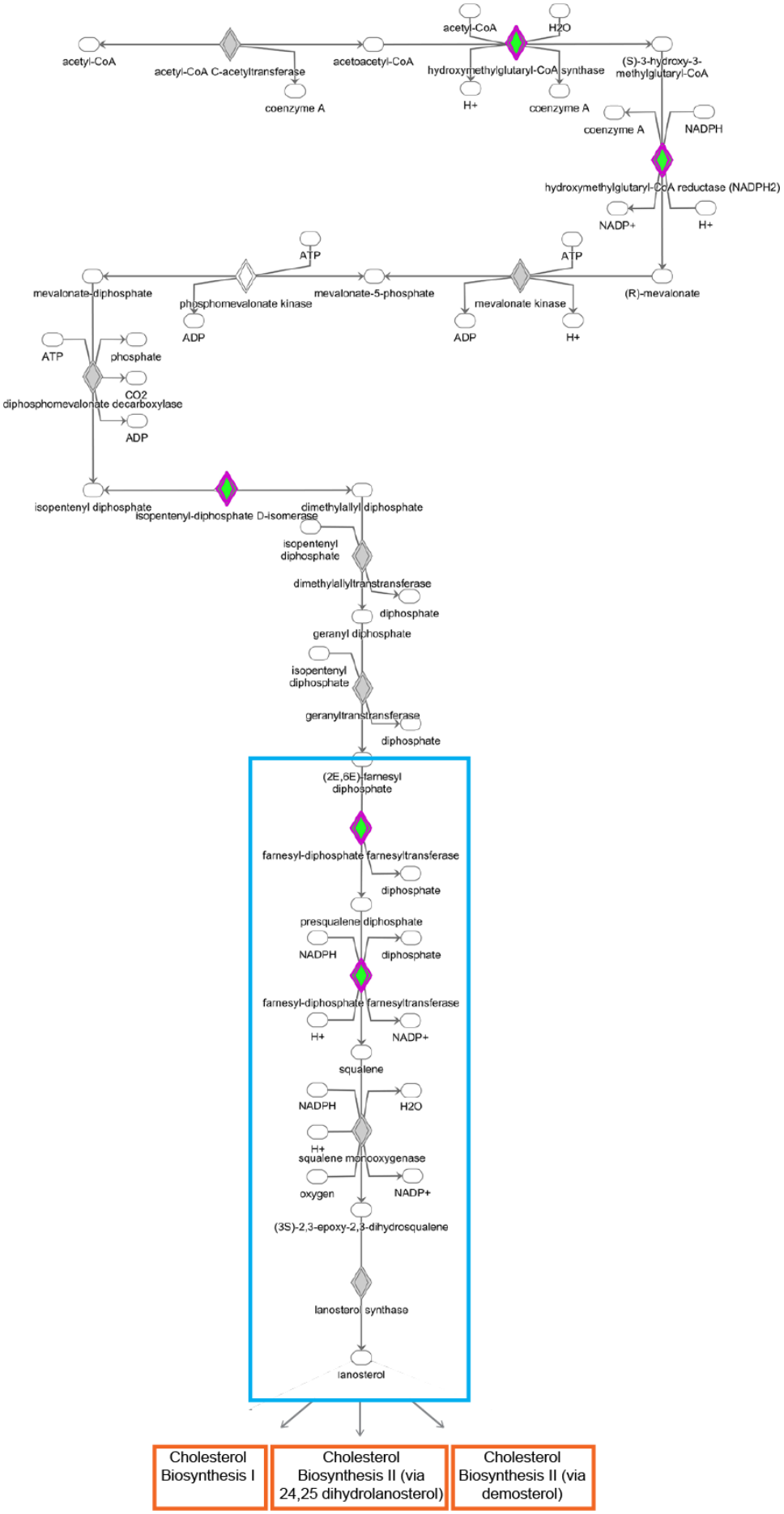

Figure 5.4 Superpathway of Cholesterol Biosynthesis identified in IPA as altered in *talpid*^{3} PGCs compared to wildtype PGCs. Nodes that are shaded green indicate proteins that are downregulated. Nodes that are shaded grey indicate a protein that is contained in the dataset but that does not contain a change over the minimum 1.2 fold change limit. Nodes with no shading (white) indicate a protein that is integral to the network but not included in the dataset. Of the four cholesterol biosynthesis pathways identified in IPA, they all share the same region marked by the blue box. The superpathway contains the first region of the pathway shown in this figure. The other three pathways, marked with orange boxes, branch after lanosterol.

5.2.6 Rho and Actin signalling pathways that control actin cytoskeleton dynamics are downregulated in *talpid*^{3} PGCs

Actin and Rho pathways that are involved in actin signalling and cytoskeleton organisation were identified as downregulated in *talpid*^{3} in three of the top 15 canonical pathways in IPA. In order to further explore the role of TALPID3 in actin cytoskeleton signalling, these pathways were carried forward for further investigation. The downregulation predicted in IPA correlates with the actin phenotype previously described in *talpid*^{3} (Yin et al., 2009). *Talpid*^{3} has been shown to have a punctate, non-continuous band of F-actin at the apex of cells in the neural tube, along with other characteristics such as increased actin at the ruffled membrane of cells (Yin et al., 2009). In order to determine if the change in actin cytoskeleton previously described and predicted by IPA could be observed, immunofluorescence was carried out on sections of *talpid*^{3} chick embryos and compared to sections of wildtype chick embryos, focussing on components of the RhoA Signalling pathway (Figure 5.5). The two remaining pathways, Regulation of Actin-based Motility by Rho pathway and the Actin Cytoskeleton Signalling pathway (Appendix 9), were not a focus of this investigation. The RhoA Signalling pathway is a less complex pathway to investigate than Actin Cytoskeleton Signalling; and unlike Regulation of Actin-based motility by Rho, it has a focus on F-actin instead of G-actin, hence the decision to take the RhoA Signalling pathway forward for further investigation.

To examine proteins that are involved in actin cytoskeleton signalling, Alexafluor-conjugated phalloidin was used to visualise the previously

reported *talpid*^{3} F-actin phenotype; in addition, profilin, cofilin, twinfilin and RhoC were included. Profilin, cofilin and twinfilin were identified in the mass spectrometry dataset but were not included in the final pathway analysis, as they did not make the cut-off fold change of 1.2. Profilin and Cofilin are both involved in the RhoA Signalling pathway (Figure 5.5); profilin has a direct interaction with F-actin and thus controls actin polymerisation (Figure 5.5), similarly cofilin has a direct role in actin polymerisation and actin nucleation (Figure 5.5). Due to the control of actin polymerisation, *talpid*^{3} embryos were examined for evidence of altered localisation of profilin and cofilin. Twinfilin was identified in the mass spectrometry dataset and is similar to cofilin both in domains and through functioning to prevent actin filament assembly (Goode et al., 1998; Palmgren et al., 2002). The Rho proteins, including RhoC, promote reorganisation of the actin cytoskeleton and regulate cell shape, motility and attachment (Wheeler & Ridley, 2004). In addition, RhoC is required for initiation of centrosome duplication (Kanai et al., 2011). RhoC was only identified by one unique peptide so was not included in the pathway analysis, however the fold change between *talpid*^{3} and wildtype was 0.75 demonstrating a downregulation of RhoC in *talpid*^{3}. In conclusion, profilin and cofilin were included due to their role in the RhoA Signalling pathway identified in IPA and Twinfilin was included due to the role it plays in actin organisation. RhoC was included because despite being identified by only one unique peptide, proteomic analysis showed that it was downregulated in *talpid*^{3}, and it plays a role in actin organisation and centrosome duplication.

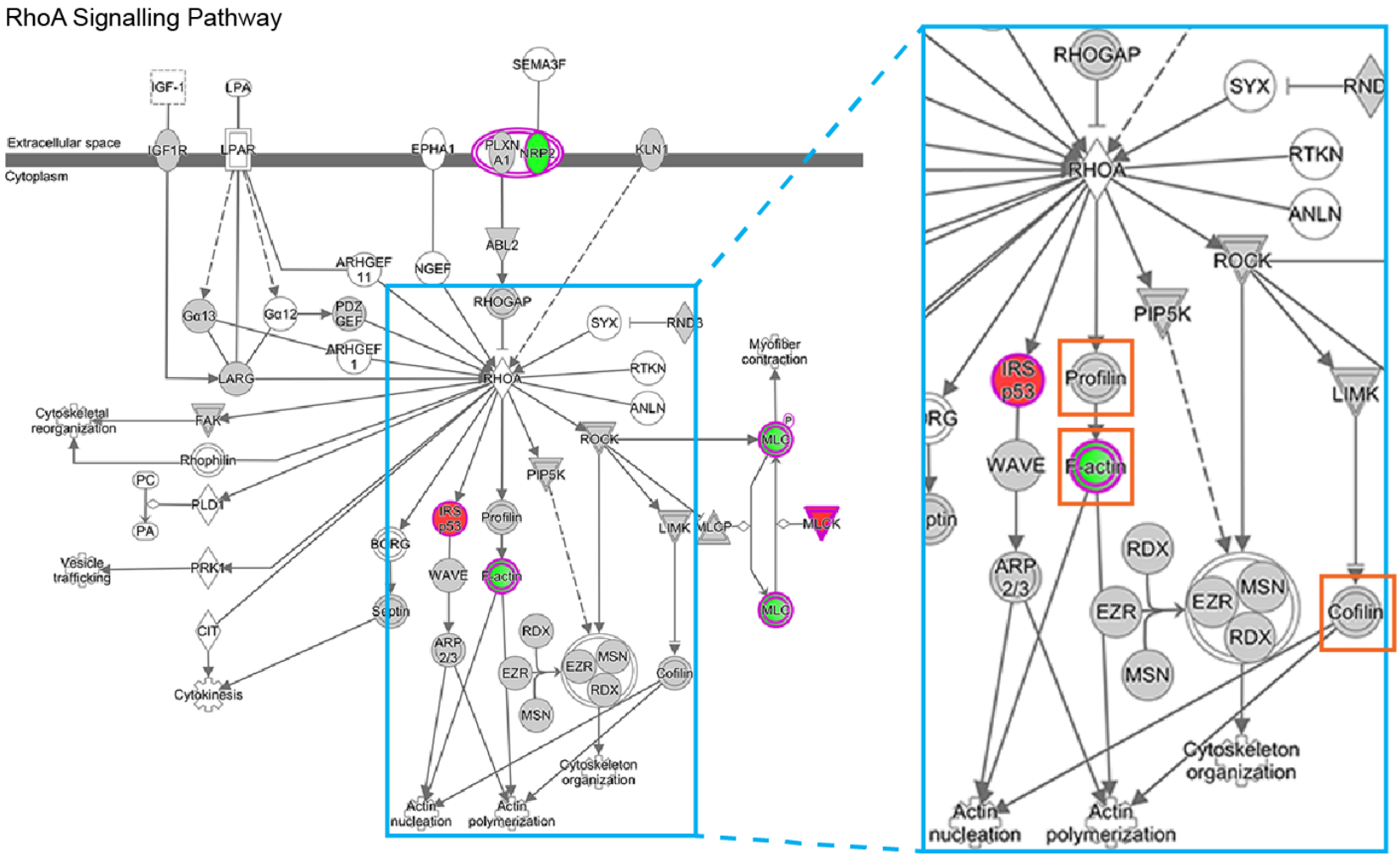

Figure 5.5 RhoA Signalling Pathway identified in IPA as downregulated in *talpid*^{3} PGCs compared to wildtype PGCs. Nodes that are shaded red indicate proteins that are upregulated. Nodes that are shaded green indicate proteins that are

downregulated. Nodes that are shaded grey indicate a protein contained in the dataset that does not contain a change over the minimum 1.2 fold change limit. Nodes with no shading (white) indicate a protein that is integral to the network but not included in the dataset. The blue box surrounds a region of the pathway that was targeted for further studies in this chapter, containing Profilin, F-actin and Cofilin, identified by orange boxes.

5.2.7 Localisation patterns of proteins involved in the regulation of Actin are altered in *talpid*^{3}

To investigate the pathway analysis results produced in IPA, immunofluorescence was carried out using phalloidin to stain the filamentous-actin (F-actin) in *talpid*^{3} embryo sections and wildtype embryo sections. F-actin is shown to be downregulated in the RhoA Signalling pathway (Figure 5.5) and the Actin Cytoskeleton Signalling pathway (Appendix 9), which is consistent with changes in actin localisation patterns previously reported (Yin et al., 2009). Phalloidin staining showed that F-actin filaments were disorganised in the *talpid*^{3} embryos in comparison to the wildtype. Specifically F-actin in the myotome was disorganised when compared to the myotome in wildtype embryos (Figure 5.6 A-D). The wildtype myotome had a regular or ordered pattern of filaments that extended ventrally, unlike *talpid*^{3} myotome, which had a more rounded and clumped pattern of filaments that did not extend as ventrally as the wildtype myotome. Additionally *talpid*^{3} appeared to have greater expression of F-actin in the floor plate, which could be due to disorganisation of filaments around the neural tube (Figure 5.6 A-D). F-actin patterns at the apical edge of the neural tube were consistent with previous reports, demonstrating that F-actin fails to form a continuous band at the apical edge of the neural tube in *talpid*^{3} embryos, unlike wildtype embryos (Figure 5.6 E, F). Quantitative analysis of fluorescent imaging is highly complex, with many factors such as background signal or noise, biological sample variation and photobleaching, contributing to inaccuracy and imprecision (Waters, 2009; Wolf et al., 2007), therefore the fluorescent signal

was not quantified, following immunofluorescence analysis in this study. In conclusion, the data from the quantitative mass spectrometry shows that actin regulatory pathways are down regulated in *talpid*^{3} PGCs, which is consistent with reports of loss of continuous F-actin at the apical edge of the neural tube in *talpid*^{3} embryos and the disorganisation of actin filaments.

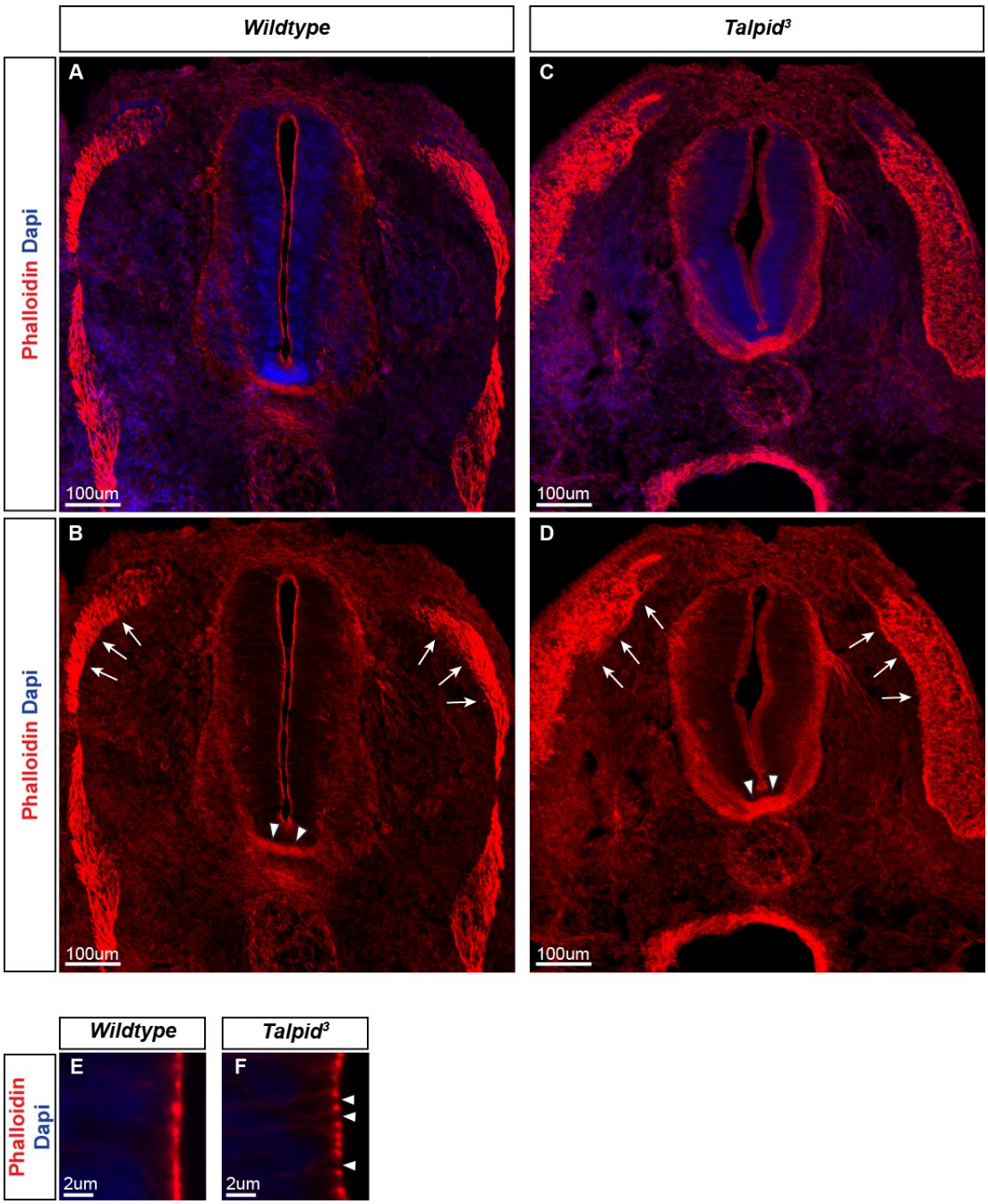

Figure 5.6 Actin is disorganised in *talpid*^{3} embryos compared to wildtype embryos. (**A-D**) Immunostaining for phalloidin (red) to mark the filamentous actin (F-actin) demonstrates actin disorganisation in *talpid*^{3} compared to wildtype. White arrows mark the myotome, where actin is highly disorganised in *talpid*^{3}, unlike wildtype, which has organised actin fibres. White arrowheads indicate the floor plate where there appears to be more F-actin in *talpid*^{3} than wildtype, most likely due to disorganisation of actin fibres. (**E, F**) Immunostaining with phalloidin at the apical edge of the neural tube shows disruption of the F-actin in *talpid*^{3} as marked by white arrowheads, unlike wildtype, which has a continuous band of F-actin at the apical edge of cells. All scale bars as annotated on figure.

Having confirmed that actin organisation is disrupted in *talpid*^{3}, localisation patterns of proteins that regulate assembly and disassembly of actin were examined to determine if they are altered in *talpid*^{3}. I examined localisation patterns in two regions of polarised tissue that require actin during formation, the apical edge of the lumen of the dorsal aorta and the apical edge of the neural tube. Endothelial cells that form the lumen of the dorsal aorta are polarised and F-actin is required to form the apical pole of vascular lumen development (Strilic et al., 2009). Formation of the neural tube requires controlled changes in cell shape and polarised organisation of microtubules along the apicobasal axis, with actin playing a role at the apical side (Suzuki et al., 2012). Additionally I examined the localisation patterns in non-polarised mesenchyme tissue (Ekblom, 1989), where differences in localisation of actin regulators would not be expected, due to the lack of polarisation and lack of organisation of the cells.

Profilin is a small actin-binding protein that is involved in actin polymerisation (Carlsson et al., 1977; Krishnan & Moens, 2009). Although a quantitative change in profilin was not detected in the *talpid*^{3} PGC proteomic dataset, it is a component of the RhoA signalling pathway and acts directly on F-actin (Figure 5.5). I hypothesised that localisation patterns of Profilin might be altered in *talpid*^{3} compared to wildtype. Localisation patterns of profilin did not change between *talpid*^{3} and wildtype in the lumen of the dorsal aorta (Figure 5.7 A-D), the mesenchyme (Figure 5.7 E-H) or the neural tube (Figure 5.7 I-L). Profilin showed specific patterns of enhanced localisation in the nucleus, seen clearly in the lumen of the dorsal aorta (Figure 5.7 A-D), which

did not differ between wildtype and *talpid*^{3}. In conclusion, localisation of profilin is not altered in *talpid*^{3}.

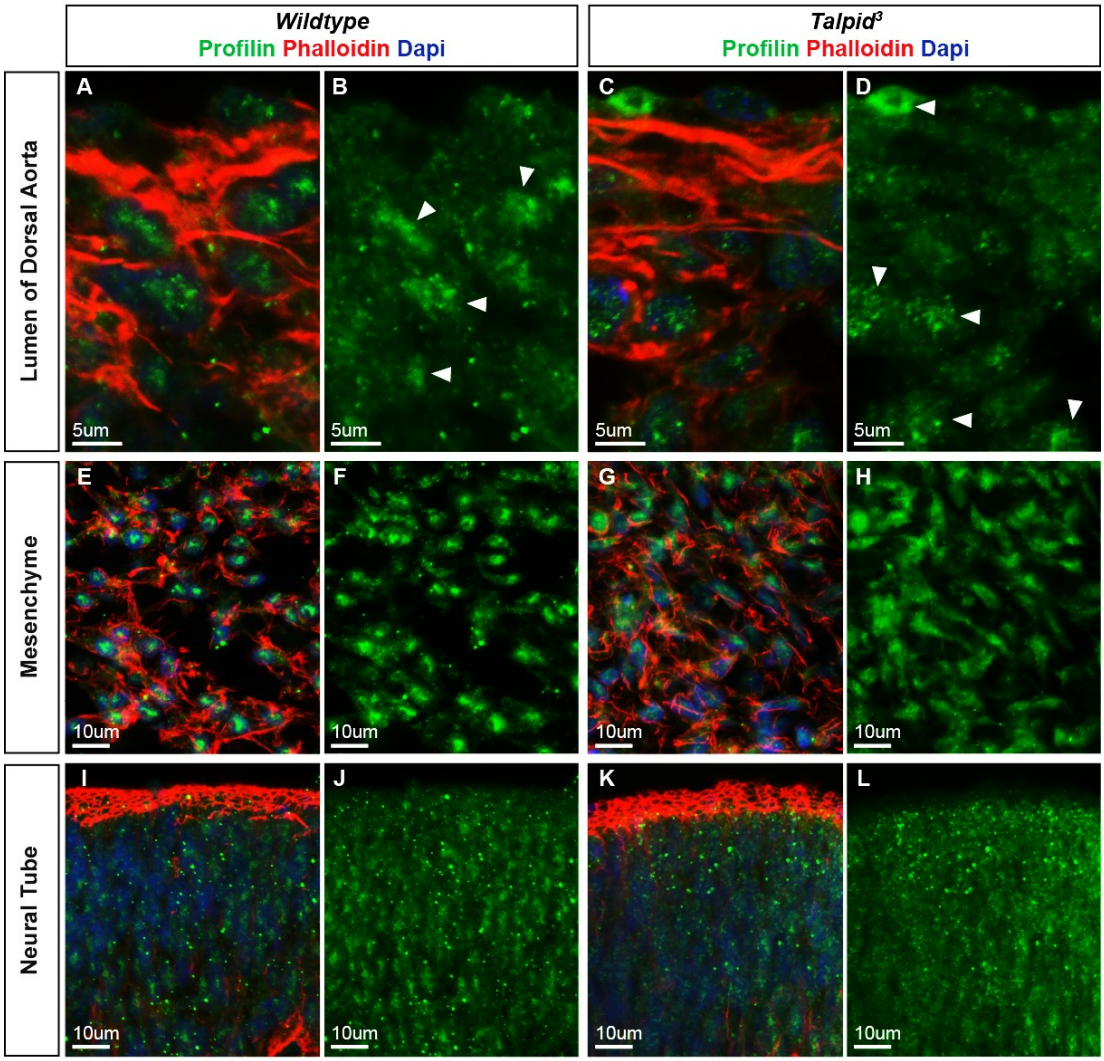

Figure 5.7 Profilin localisation does not change in *talpid*^{3} during development. (**A-D**) Immunostaining for Profilin (green), Phalloidin (red) and Dapi (blue) in the lumen of the dorsal aorta showed that localisation patterns of Profilin remain unchanged in *talpid*^{3}. White arrowheads mark regions in the nucleus that appear to have higher levels of expression of Profilin. (**E-H**) Immunostaining for Profilin, Phalloidin and Dapi in regions of non-polarised mesenchyme show that Profilin localisation remains unchanged in *talpid*^{3} when compared to wildtype. (**I-L**) Immunostaining for Profilin, Phalloidin and Dapi at the apical edge of the neural tube shows that Profilin localisation remains unchanged in t*alpid*^{3} compared to wildtype. All scale bars as annotated on figure.

Cofilin, another protein that regulates actin, induces depolymerisation of actin filaments (Nishida et al., 1984). This promotes actin filament disassembly by severing and consequently promotes actin polymerisation by generating free actin monomers, generating rapid actin filament turnover (Bamburg et al., 1999; Lappalainen & Drubin, 1997; Ohashi, 2015). Similar to profilin, a quantitative change was not detected in cofilin in the *talpid*^{3} PGC proteomic dataset; however, it was shown to be involved in the RhoA Signalling pathway thus due to its role in actin polymerisation there might be a change in localisation patterns in *talpid*^{3} compared to wildtype. Immunostaining for cofilin in the lumen of the dorsal aorta showed regions of increased localisation at the apex of the cells in both wildtype and *talpid*^{3}; this increased localisation was more pronounced in *talpid*^{3}, with localisation patterns resembling a more rounded shaped compared to wildtype (Figure 5.8 A-D). However, localisation patterns of cofilin were not altered in *talpid*^{3} in the mesenchyme (Figure 5.8 E-H) or at the apical edge of the neural tube (Figure 5.8 I-L). In conclusion, cofilin localisation appears more abundant and has a more rounded localisation pattern in the lumen of the dorsal aorta in *talpid*^{3}, but is unchanged in the mesenchyme and apical edge of the neural tube.

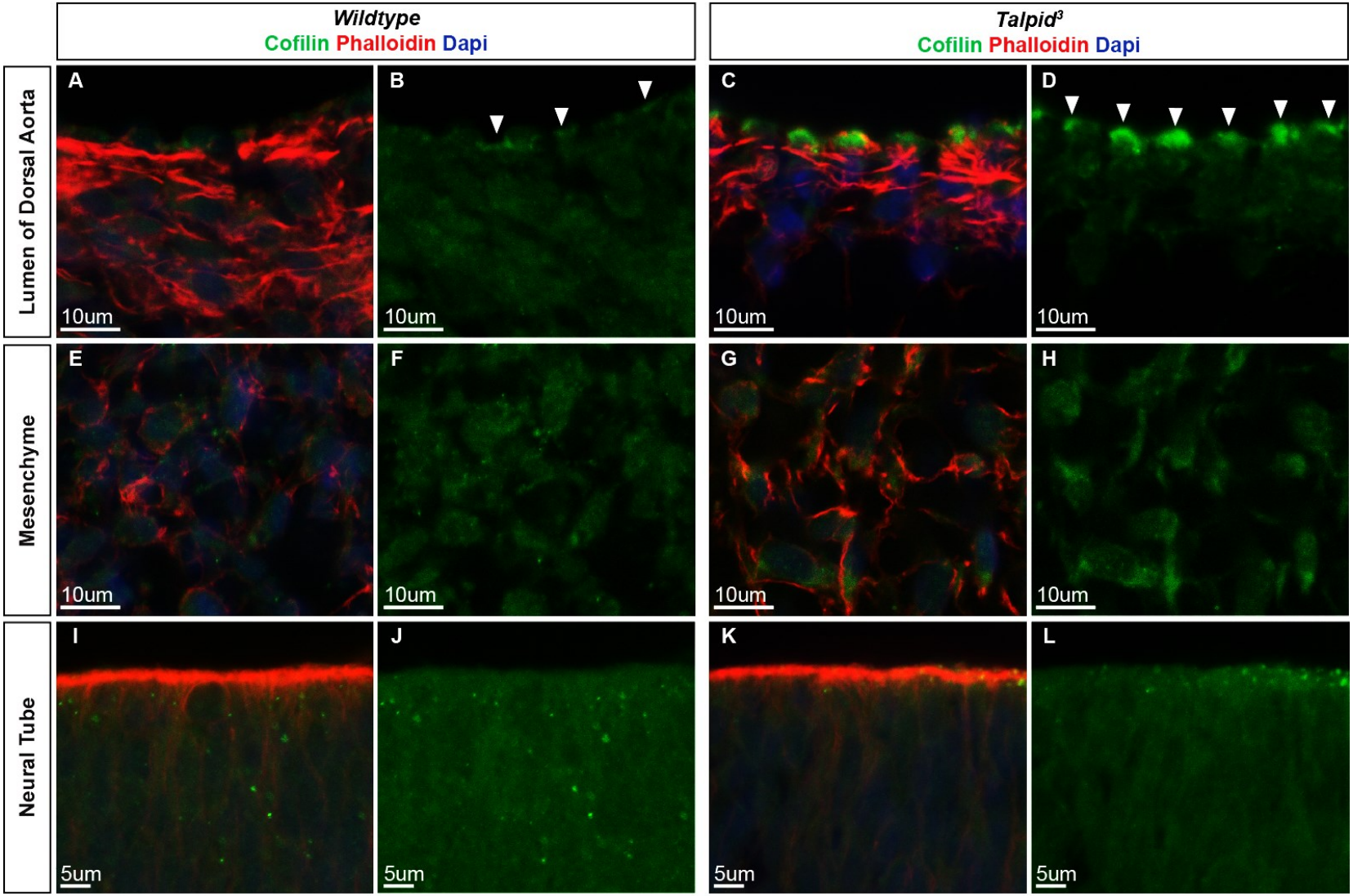
Wildtype
Cofilin Phalloidin Dapi
Talpid3
Cofilin Phalloidin Dapi
Lumen of Dorsal Aorta
Mesenchyme
Neural Tube
A
B
C
D
E
F
G
H
I
J
K
L
10um
10um
10um
10um
10um
10um
10um
10um
5um
5um
5um
5um

Figure 5.8 Cofilin localisation is altered in the lumen of the dorsal aorta but remains unchanged in the mesenchyme and neural tube of *talpid*^{3}. (**A-D**) Immunostaining for Cofilin (green), Phalloidin (red) and Dapi (blue) in the lumen of the dorsal aorta in wildtype and *talpid*^{3}. White arrowheads mark regions of more abundant Cofilin localisation at the apex of cells in *talpid*^{3} and wildtype. The cofilin localisation at the apex of *talpid*^{3} cells has a rounder localisation pattern when compared to wildtype. (**E-H**) Immunostaining for Cofilin, Phalloidin and Dapi in regions of non-polarised mesenchyme show that Cofilin localisation remains unchanged in *talpid*^{3} when compared to wildtype. (**I-L**) Immunostaining for Cofilin, Phalloidin and Dapi at the apical edge of the neural tube shows that Cofilin localisation remains unchanged in t*alpid*^{3} compared to wildtype. All scale bars as annotated on figure.

Twinfilin is an actin monomer binding protein that inhibits nucleotide exchange on actin monomers and prevents assembly of the monomers into filaments. Loss of twinfilin results in uncontrolled polymerisation of actin filaments (Goode et al., 1998; Palmgren et al., 2002). Twinfilin was not included in the pathway analysis or identified in any of the canonical pathways identified, however due to its role in preventing filament assembly, I hypothesised that localisation might be altered in *talpid*^{3} compared to wildtype. Twinfilin localises more abundantly to the apex of the cells in the lumen of the dorsal aorta of wildtype embryos (Figure 5.9 A, B); in *talpid*^{3} there appeared to be less twinfilin localisation at the apex of the cell. Where localisation was detected in *talpid*^{3}, it appeared more disorganised than in wildtype (Figure 5.9 C, D). There was no change in localisation pattern of twinfilin observed in the non-polarised mesenchyme tissue in *talpid*^{3} compared to wildtype (Figure 5.9 E-H). The apical edge of the neural tube in *talpid*^{3} showed higher abundance of twinfilin than the apical edge of the neural tube in wildtype (Figure 5.9 I-L). In conclusion, polarised tissue in *talpid*^{3} shows altered localisation patterns of twinfilin when compared to wildtype, however the non-polarised mesenchyme remains unchanged.

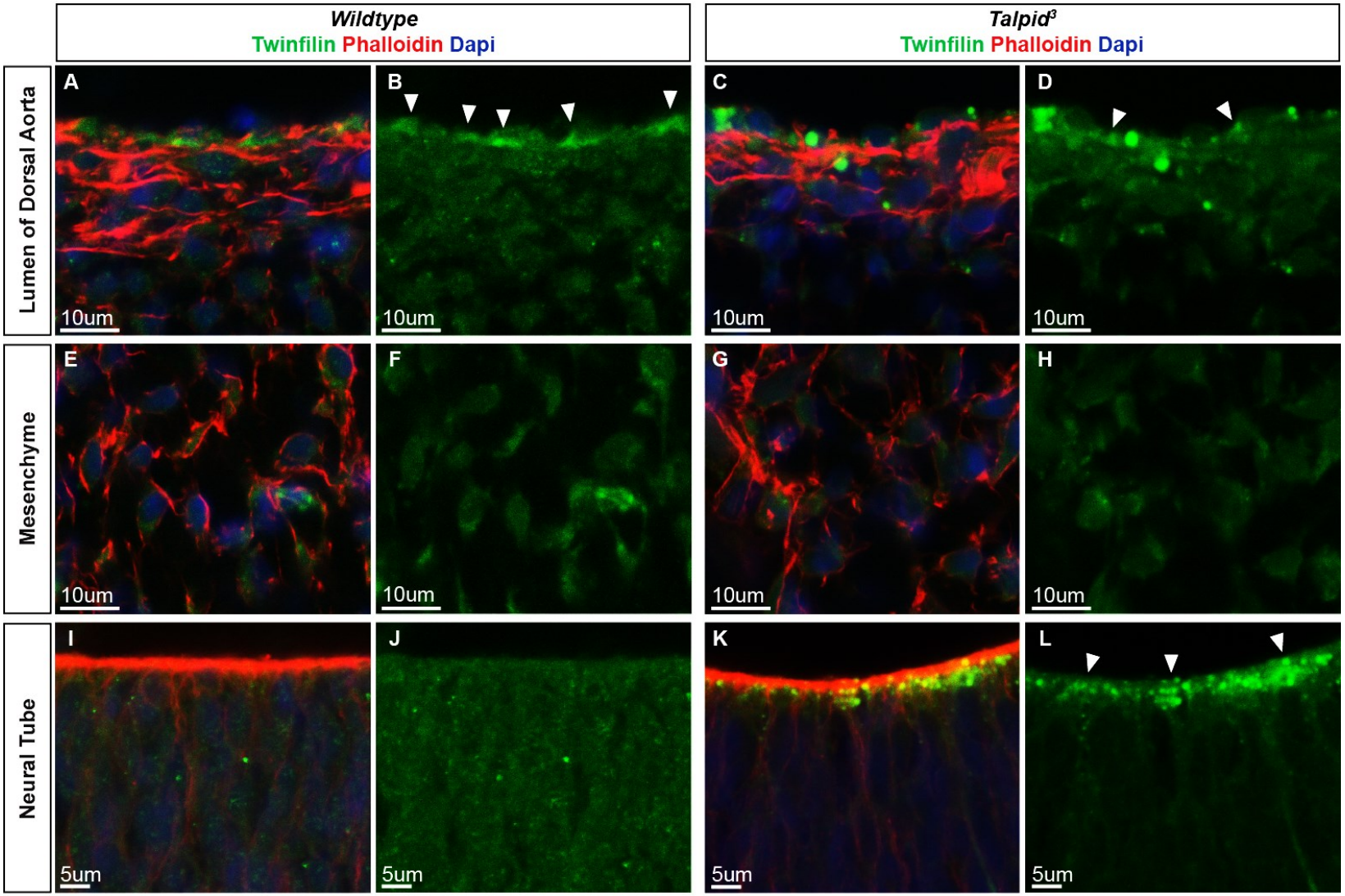
Wildtype
Twinfilin Phalloidin Dapi
Talpid3
Twinfilin Phalloidin Dapi
Lumen of Dorsal Aorta
Mesenchyme
Neural Tube
A
B
C
D
E
F
G
H
I
J
K
L
10um
10um
10um
10um
10um
10um
10um
10um
5um
5um
5um
5um

Figure 5.9 Twinfilin localisation patterns are altered in polarised tissue in *talpid*^{3}. (**A-D**) Immunostaining for Twinfilin (green), Phalloidin (red) and Dapi (blue) in the lumen of the dorsal aorta of wildtype and *talpid*^{3}. White arrowheads indicate localisation of Twinfilin at the apex of cells, with wildtype showing abundant and organised localisation patterns of twinfilin. T*alpid*^{3} showed lower abundance of twinfilin, with less cells showing twinfilin localisation at the apex of cells. (**E-H**) Immunostaining for Twinfilin, Phalloidin and Dapi in regions of non-polarised mesenchyme show that Twinfilin localisation remains unchanged in *talpid*^{3} when compared to wildtype. (**I-L**) Immunostaining for Twinfilin, Phalloidin and Dapi at the apical edge of the neural tube shows more abundant localisation of twinfilin, marked by white arrowheads in *talpid*^{3} compared to wildtype. All scale bars as annotated on figure.

The Rho proteins consist of three isoforms, A, B and C, that belong to the Rho GTPase family, a distinct family within the superfamily of Ras-related small GTPases (Jaffe & Hall, 2005). The Rho proteins promote reorganisation of the actin cytoskeleton and regulate cell shape, motility and attachment (Wheeler & Ridley, 2004). Despite similar functions, the Rho proteins have distinct roles, with RhoC playing a role in initial stages of digit chondrogenesis and stress fibre generation (Hakem et al., 2005; Montero et al., 2007). The final component of actin regulation that was tested by immunofluorescence in *talpid*^{3} was RhoC. Although only identified by one unique peptide in the proteomic dataset, RhoC was shown to be downregulated in *talpid*^{3} PGCs; therefore, *talpid*^{3} was examined for changes in localisation patterns of RhoC. Localisation of RhoC was examined at the apex of cells in the lumen of the dorsal aorta (Figure 5.10 A-D) and at the apex of the neural tube (Figure 5.10 I-L); however RhoC remained unchanged in *talpid*^{3} when compared to wildtype. Similarly, localisation of RhoC in non-polarised mesenchyme tissue remains unchanged in *talpid*^{3} (Figure 5.10 E-H). In conclusion, RhoC localisation patterns are not altered in *talpid*^{3}.

Taken together, the results of profilin, cofilin, twinfilin and RhoC suggest that some regulators of actin are altered in *talpid*^{3}. Twinfilin and cofilin are involved in depolymerisation of actin filaments and prevention of actin filament assembly respectively, and appear to be altered in polarised tissue in *talpid*^{3}, therefore could be contributing to the actin phenotype seen. Profilin and RhoC however, are responsible for the opposite regulation of

actin through actin polymerisation and re-organisation respectively, and localisation remains unchanged in *talpid*^{3}.

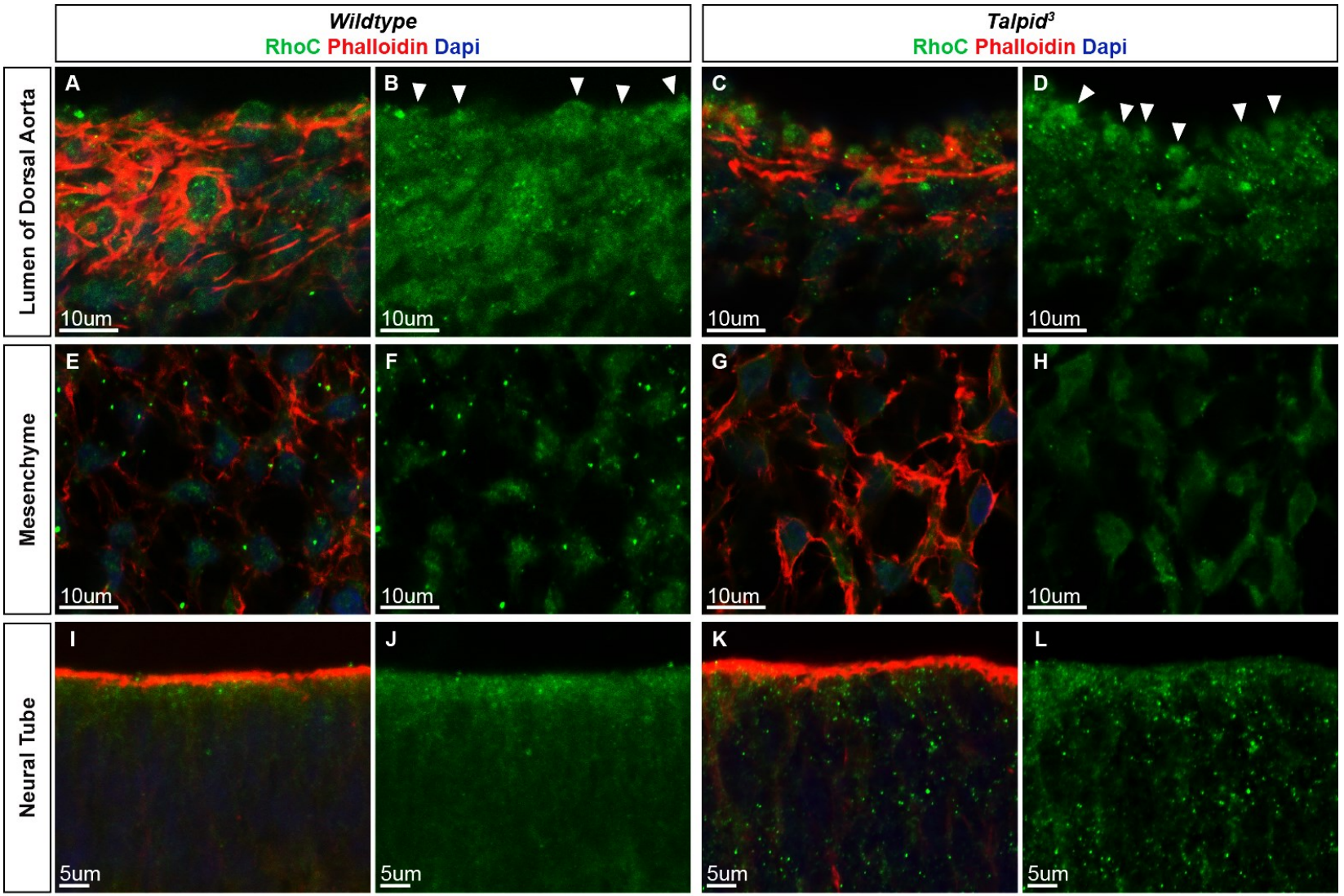

Figure 5.10 RhoC localisation patterns remain unchanged in *talpid*^{3}. (**A-D**) Immunostaining for RhoC (green), Phalloidin (red) and Dapi (blue) in the lumen of the dorsal aorta showed that localisation patterns of RhoC remain unchanged in *talpid*^{3}. White

arrowheads mark the apex of cells in wildtype and *talpid*^{3} respectively. (**E-H**) Immunostaining for RhoC, Phalloidin and Dapi in regions of non-polarised mesenchyme show that RhoC localisation remains unchanged in *talpid*^{3} when compared to wildtype. (**I-L**) Immunostaining for RhoC, Phalloidin and Dapi at the apical edge of the neural tube shows that RhoC localisation remains unchanged in t*alpid*^{3} compared to wildtype. All scale bars as annotated on figure.

5.3 Discussion

This study has shown that labelled quantitative mass spectrometry in chicken PGCs, derived from the *talpid*^{3} flock, is a viable way to study protein pathways that are altered in *talpid*^{3}. Completion of pathway analysis in *talpid*^{3} for the first time, has presented cholesterol biosynthesis pathways as being altered and actin and Rho signalling pathways as being down regulated in *talpid*^{3}. This study has shown that proteins involved in actin regulatory pathways are altered in *talpid*^{3}, leading to an overall down regulation of the RhoA Signalling pathway, the Regulation of Actin-based Motility by Rho pathway and the Actin Cytoskeleton Signalling pathway. These results are supported by changes in localisation patterns of F-actin in *talpid*^{3}. Additionally regulators of F-actin such as twinfilin and cofilin show altered localisation patterns in *talpid*^{3} in polarised tissue. However, no changes were observed in localisation patterns of profilin and RhoC, suggesting that different regulators of actin are altered in *talpid*^{3} to produce the phenotype observed.

During early embryonic development in the chick, a new pair of somites are formed every 90 minutes from the presomitic mesoderm. Sonic hedgehog signalling from the notochord precedes somite formation and contributes to regulating the pace of somitogenesis. The maturation of somites is dependent on a balance of Wnt signalling, Hedgehog and Noggin signalling and also signalling between the bone morphogenic proteins (BMPs) (Resende et al., 2010). Ventral somatic cells go on to form the mesenchymal

sclerotome and the dorsal somatic cells form epithelial dermomyotome. Precursors of the trunk skeletal muscle migrate underneath the dermomyotome to form the myotome (Andrade et al., 2007). This myotome is marked by F-actin which is a key component of muscle. The F-actin filaments in the myotome of *talpid*^{3} appear dysregulated, this could in part be due to a loss of Hedgehog signalling much earlier in development. The lack of cilia in *talpid*^{3} mutants means that cells cannot respond to Sonic hedgehog, therefore the initiation and regulation of somite formation in *talpid*^{3} is disrupted. The disruption in Hedgehog signalling has been shown to cause displacement of cells between myotome and dermomyotome, which results in an expression of MyoD in the dermomyotome in *talpid*^{3}, instead of being limited to expression in the myotome as seen in wildtype (Davey et al., 2006). This dorsal expansion or shift of MyoD expression can be mimicked by overexpression of Sonic Hedgehog in wildtype somites, thus suggesting this is a gain of function phenotype (Davey et al., 2006). Similar to what is seen in the intermediate neural tube of *talpid*^{3} mutants with expansion of thePax7 expression domain, this gain of function phenotype is likely due to a loss of Gli repressor. The role of Hedgehog signalling in determining boundaries between myotome and dermomyotome suggests that TALPID3 plays an indirect role on the dysregulation of actin in the *talpid*^{3} mutant. It is the loss of cilia in the *talpid*^{3} mutant cells that leads to an inability for cells to respond to Sonic Hedgehog, thus actin dysregulation in the myotome as shown in Figure 5.6 is likely to be a secondary effect of the loss of Hedgehog signalling.

During early development of the neural tube, progenitor cells at the apical surface of the neural tube undergo symmetric division to produce two daughter cells that continue as progenitor cells. During later stages of neural tube development, progenitors at the apical edge of the neural tube undergo asymmetric division to produce one cell that continues as a progenitor at the apical surface and one that will become a neuron (Wilcock et al., 2007). The apical edge of the neural tube is characterised by cadherin-based adherens junctions with acto-myosin cable and proteins linked to tight junctions. Progenitors attach at this apical surface, meaning following asymmetric division the newly produced neurons must detach and move out of the proliferative progenitor zone and undergo neuronal differentiation; the detachment from the apical surface by differentiated neurons is known as delamination (Singh & Solecki, 2015; Wilcock et al., 2007). Detachment of the neuron occurs by apical abscission, which is triggered by constriction of the acto-myosin cable at the apical surface of the neural tube (Das & Storey, 2014). The disruption of continuous actin seen at the apical edge of the neural tube in *talpid*^{3} could have negative implications on neurogenesis based on the acto-myosin cable's role in apical abscission of newly formed neurons. The disruption of actin could lead to a failure of progenitor cells to attach at the apical surface leading to a loss of the progenitor pool at the apical edge of the neural tube. The final number of neurons in the brain is determined by the time at which progenitors start dividing and the number of divisions that occur (Homem et al., 2016). If the progenitor pool is depleted than this could lead to a loss of neurons and thus neuronal defects.

If the disruption of actin at the apical edge of the *talpid*^{3} neural tube does negatively affect neurogenesis, this could help to understand the neural defects seen in the *talpid*^{3} chicken mutant, as well as the human patients with mutations in *KIAA0586*.

Taken together, the results of twinfilin, cofilin, profilin and RhoC suggest that only some regulators of actin are altered in *talpid*^{3}. Twinfilin and cofilin are involved in depolymerisation of actin filaments and prevention of actin filament assembly respectively, and appear to be altered in polarised tissue in *talpid*^{3}. Profilin and RhoC however, are responsible for the opposite regulation of actin through actin polymerisation and re-organisation respectively, and localisation remains unchanged in *talpid*^{3}. The downregulation of pathways associated with actin that was identified in IPA, could be caused by changes in proteins that act as negative regulators of actin as shown by twinfilin and cofilin. Proteins that promote actin assembly, such as Profilin and RhoC, might not be involved in the downregulation of pathways associated with actin, as identified in IPA. Alternatively, the changes in localisation patterns of these proteins could be as a result of the altered actin organisation in *talpid*^{3}, instead of causing the altered actin organisation.

For cell motility to occur, a single polarised lamellipodia must form to direct cell migration (Krause & Gautreau, 2014). Cofilin defines the site of actin polymerisation to form a protrusion, and maintenance of active non-phosphorylated ADF/Cofilin is necessary to maintain a polarised lamellipodia during cell migration, thus cofilin acts as a component of the 'steering wheel'

of the cell during migration (Dawe et al., 2003; Ghosh et al., 2004). Changes in cofilin localisation in polarised tissue in *talpid*^{3} were not consistent; changes were observed in the lumen of the dorsal aorta, but not in the lumen of the neural tube. This could reflect on different dynamics of cell movements between the two regions of polarised tissue. Additionally, *talpid*^{3} has been shown to have disrupted polarity (Stephen et al., 2015). *Talpid*^{3} embryos lose characteristic rostral-caudal polarisation of skin, examined through feather bud studies; *talpid*^{3} also loses polarity of stereocilia bundles in the hair cells of the inner ear, known as basilar papilla in the chicken (Stephen et al., 2015). The abnormal polarity findings in *talpid*^{3} suggest that through its role in centriole migration and orientation, KIAA0586 (TALPID3) affects cell and tissue polarity (Stephen et al., 2015). The results of the study discussed in this chapter highlight a close link between components of actin regulation and TALPID3, suggesting that the abnormal cell and tissue polarity seen in *talpid*^{3} is most likely linked to the downregulation of actin signalling pathways.

An actin phenotype in *talpid*^{3} has previously been reported (Yin et al., 2009); *talpid*^{3} was shown to have a discontinuous band of F-actin at the apical edge of the developing neural tube. In addition, *talpid*^{3} mutant limb cells were shown to have fewer stress fibres (and fewer focal adhesions) in comparison to the wildtype limb cells (Yin et al., 2009). RhoA is responsible for formation of stress fibres, and the analysis in this study has suggested a down regulation of the RhoA Signalling pathway in *talpid*$^{3.}$ It is possible that this down regulation could account for the loss of stress fibres seen in *talpid*^{3}

mutant cells. Stress fibres are important as the major contractile force in animal cells (Tojkander et al., 2012). The loss of stress fibres in cultured *talpid*^{3} cells (Yin et al., 2009) could be contributing to the disorganisation during development due to cells decreased ability to migrate. Although stress fibres were not examined in *talpid*^{3} PGCs, the reduction of stress fibres could be causing the slower migration of PGCs when colonising the gonad in *talpid*^{3} (Davey and McGrew labs, unpublished). RhoA is also important in actin regulation for ciliogenesis; RhoA is required for the formation of a characteristic apical actin web in ciliated cells. This actin web is necessary for basal body docking and formation of the ciliary axoneme (Pan et al., 2007), again suggesting that the down regulation of the RhoA Signalling pathway and the down regulation of the Regulation of Actin-based Motility by Rho is crucial to causing the phenotype seen in *talpid*^{3}. RhoC was identified as downregulated in the *talpid*^{3} PGC dataset; however, localisation studies did not show a change in patterns of RhoC in *talpid*^{3} when compared to wildtype. This result was unexpected due to the role of RhoC in generation of actin stress fibres (Hakem et al., 2005; Montero et al., 2007). However, the Rho proteins have distinct roles during development with RhoC playing a key role in digit morphogenesis during limb development (Montero et al., 2007); it is possible that altered localisation of RhoC might be seen in *talpid*^{3} at different stages or in different tissue. It is also possible that despite lower levels of RhoC, the localisation pattern does not change; however, without using quantitative fluorescent imaging it is not possible to draw that conclusion from the immunofluorescence data presented in this study.

Recent evidence shows that TALPID3 interacts with MACF1 (May-Simera et al., 2016); this interaction supports a role for TALPID3 associating with actin. MACF1, also known as ACF1 (actin cross-linking factor 7), is important for the coordination of microtubules and actin filaments in many cellular processes (Escobar-Aguirre et al., 2017; Karakesisoglou et al., 2000). It plays a critical role in ciliogenesis, with loss of MACF1 in the retina resulting in a failure of basal bodies to migrate apically and dock with the cell membrane, thus resulting in a loss of ciliogenesis (May-Simera et al., 2016). The conditional MACF1 knockout in the retina, produces a phenotype that is similar to that seen in *talpid*^{3} (Stephen et al., 2015; Yin et al., 2009). In both the conditional MACF1 knockout and *talpid*^{3} mutants, there is a loss of association of the basal body with ciliary vesicles. However, MACF1 mutant mouse embryonic fibroblasts, unlike *talpid*^{3} mutant cells, show an accumulation of actin stress fibres (May-Simera et al., 2016 Yin et al., 2009). This difference in actin stress fibre phenotypes between the conditional MACF1 knockout and *talpid*^{3} mutant, suggests that TALPID3 interacts with additional actin regulatory proteins to produce the actin phenotype observed. Previous investigation into microtubules in *talpid*^{3} showed that there was no obvious differences in microtubule organisation in *talpid*^{3} chicken embryonic fibroblasts when compared to wildtype chicken embryonic fibroblasts. There was however a delay in microtubule regrowth in the *talpid*^{3} chicken embryonic fibroblasts following nocodazol treatment, a reagent used to depolymerise microtubules (Yin et al., 2009). Although TALPID3 does not appear to directly affect microtubule organisation, its

interaction with MACF1 could play a role in this delay of microtubule re-growth.

TALPID3 plays a role in and is necessary for several different functions within the centrosome. It is well established that loss of TALPID3 results in failure of centrosomes to orientate, migrate and dock therefore resulting in a loss of ciliogenesis (Stephen et al., 2013, 2015; Yin et al., 2009). The actin cytoskeleton at the apical region of the cell plays a role in orientation of the basal body prior to docking and ciliogenesis and enrichment of apical actin is thought to be required for ciliogenesis (Pan et al., 2007; Park et al., 2006). Cytoplasmic stress fibres appear to interfere with basal body migration while cortical actin can stabilise and organise basal body orientation and positioning (Avasthi & Marshall, 2012). Although *talpid*^{3} shows a loss of actin stress fibres, the combination of actin-related phenotypes found in *talpid*^{3} along with the role actin plays in centrosome orientation and ciliogenesis is likely to be linked. This study has shown through pathway analysis that the mutation in *TALPID3* is disrupting actin regulation and it is possible that the disruption of actin is playing a role in the misorientation of basal bodies and the polarity defects seen in t*alpid*^{3}.

5.3.1 Conclusions and future studies

In conclusion, the study presented in this chapter has shown that quantitative proteomic analysis in chicken PGCs can be used to identify and investigate altered protein interacting pathways in *talpid*^{3}. Following

validation of the proteomic dataset, pathway analysis showed that the mutation in *TALPID3* affects the cholesterol biosynthesis pathway and pathways involved in actin cytoskeleton organisation. Pathways controlling actin organisation are down regulated in *talpid*^{3}, and the actin regulatory proteins cofilin and twinfilin have altered localisation patterns in *talpid*^{3}.

It is still unknown how TALPID3 controls down regulation of actin regulatory protein pathways, whether through a direct interaction with actin or whether it interacts with a protein upstream of actin. To identify additional proteins that are linked to the regulation of actin that could interact with TALPID3 directly or indirectly, the remaining proteins in the *talpid*^{3} PGC quantitative proteomic dataset that have links to actin (Figure 5.11) could be examined. Immunofluorescence to look at localisation patterns could be analysed to determine whether the proteins are altered in *talpid*^{3} in polarised and non-polarised tissue. If changes in localisation were observed, electroporation of constructs containing the proteins of interest, into the neural tube of *talpid*^{3}, could be used to determine whether these proteins were able to rescue actin phenotypes seen in *talpid*^{3}. If overexpression of a particular protein was able to rescue the phenotype caused by the mutation in *TALPID3*, it would confirm that the protein acted downstream of TALPID3 in the pathway or mechanism that produces the actin phenotype in *talpid*^{3}. Alternatively, an approach aimed at identifying direct TALPID3 protein interactors could be undertaken; a co-immunoprecipitation assay followed by mass spectrometry could be used to identify proteins that directly

interact with TALPID3. The dataset produced by this method could then be examined for proteins involved in the regulation of actin.

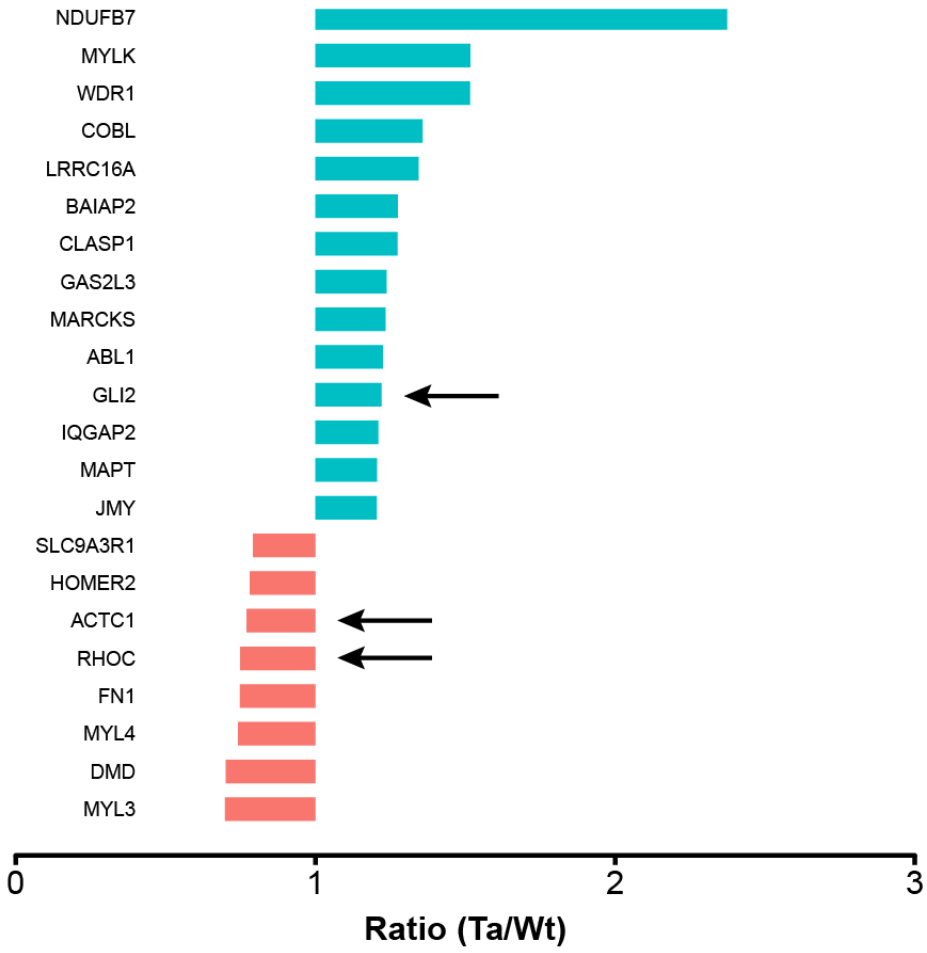

Figure 5.11 Proteins identified in the TMT dataset, linked to actin signalling, that are upregulated or downregulated with a fold change minimum of 1.2 in *talpid*^{3} PGCs compared to wildtype PGC. Black arrows identify three proteins that have been investigated in relation to *talpid*^{3}. RhoC and Actin were both investigated and presented in this study. Gli2 was investigated and presented in a previous study.

Future studies could use the data produced by IPA to explore different avenues, such as potential upstream regulators and molecular activators or inhibitors. IPA predicts upstream targets of the altered pathways identified and provides suggestions of drugs or molecules that can activate or inhibit the altered pathways. To demonstrate that the pathways identified in IPA are altered in *talpid*^{3}, an upstream target of a pathway such as the RhoA Signalling pathway could be knocked out of wildtype PGCs and the resulting PGCs could be examined for phenotypes similar to *talpid*^{3} PGCs. Furthermore, drug or molecular activators identified in IPA could be tested on developing *talpid*^{3} embryos, which could be examined for signs of rescue of the phenotype being targeted. Further investigation into the protein pathways that are altered in *talpid*^{3} would increase our understanding of the phenotype and produce alternative avenues to explore and to uncover the TALPID3 protein interacting network.

Chapter 6. General Discussion

Collectively, the results presented in this thesis provide the first evidence to support the *talpid*^{3} chicken mutant as a tool to model human *KIAA0586* ciliopathy patient mutations to understand C-terminal functional protein domains. The results identify CCDC77 and CCDC127 as novel centrosome proteins and demonstrate that loss of CCDC127 results in a significant decrease in ciliogenesis. Finally, the results demonstrate that chicken PGCs are a suitable model for studying the centrosome and present the first study aimed at analysing the *talpid*^{3} proteome through quantitative mass spectrometry of the mutant proteome compared to a wildtype proteome, finding a downregulation of pathways regulating the actin cytoskeleton.

During the course of this thesis, I have explored many different tools to understand TALPID3; however despite these attempts, the dynamic localisation of TALPID3 in space and time and the protein networks it interacts with remain unknown. TALPID3 is a low abundance protein that localises to a tiny organelle, it contains a predicted intrinsically disordered domain that has made structural modelling unsuccessful and localisation studies have not been extended to live cell imaging to determine the dynamic localisation of the endogenous TALPID3 protein due to a lack of viable tools. Attempts to overcome these challenges have provided insights into proteomic approaches that can be used to study TALPID3 despite its low abundance within the centrosome, however these attempts still have not

answered the fundamental questions of what proteins TALPID3 interacts with and what processes these interactions control.

By combining what is currently known about the role of TALPID3 in the centrosome with the data presented in this thesis, I have identified two distinct roles for TALPID3 (Figure 6.1). The first role is a result of the relationship between TALPID3 and ciliogenesis. As previously shown, TALPID3 interacts with a group of centrosome proteins, to control processes such as centrosome orientation, migration and consequently ciliogenesis (Kobayashi et al., 2014; Wang et al., 2016; Wu et al., 2014); through interactions with Cep120 and C2CD3, TALPID3 has been shown to play a role in the maturation of the mother centriole and asymmetric localisation of proteins to the daughter centriole (Wang et al., 2018; Wu et al., 2014). As a result of the role of TALPID3 in ciliogenesis, the loss of TALPID3 causes a loss of the Hedgehog signal transduction pathway leading to phenotypes such as the loss of neural tube patterning during development, the loss of patterning during limb development and polydactyly and the lung abnormalities found in *talpid*^{3}. The loss of ciliogenesis plays a role in loss of polarity in *talpid*^{3}, contributing to phenotypes such as polycystic kidneys, skin defects and inner ear defects. The second role for TALPID3 is in the regulation of the actin cytoskeleton, suggesting that loss of TALPID3 results in downregulation of protein pathways that regulate the actin cytoskeleton. Although specific TALPID3 protein interactions that control the regulation of actin have not yet been identified, evidence from the discontinuous band of F-actin at the apical edge of the neural tube suggests that this dysregulation of actin, when

TALPID3 is lost, could lead to changes in neural progenitor proliferation and migration events. In turn this could cause a loss of neural progenitor pools leading to the neural defects seen when TALPID3 is lost.

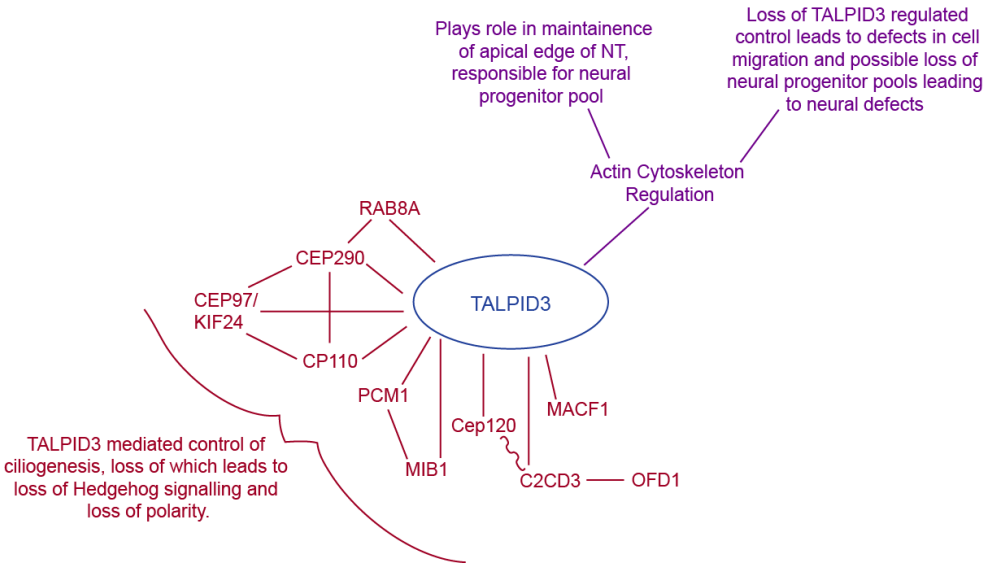

Figure 6.1 Two distinct roles for TALPID3 during development. Lines represent direct links between proteins and processes. The group of proteins in red represent the protein interactions between TALPID3 and other centrosome proteins. These interactions are predicted to contribute to the role of TALPID3 in ciliogenesis. Loss of TALPID3 and consequently loss of the interactions between TALPID3 and the centrosome proteins in red, leads to a loss of cilia and therefore a loss of the Hedgehog signal transduction pathway and loss of polarity. TALPID3 also plays a role in the regulation of the actin cytoskeleton, shown in purple. Although direct protein interactions have not been identified for this role, evidence suggests that this role is important for neural progenitors at the apical edge of the developing neural tube (NT).

The quantitative proteomics analysis presented in chapter 5 of this thesis, provides an extensive dataset regarding changes in protein expression levels in *talpid*^{3} compared to wildtype. However, the results and analysis presented in chapter 5 only focus on a small portion of this data. Moving away from the IPA data and the potential future studies that could be completed using the IPA analysis discussed in chapter 5, two proteins of interest were identified. Neuropilin1 (NRP1) and Neuropilin2 (NRP2) were both identified as altered in *talpid*^{3} compared to wildtype. The neuropilins (NRPs) are single transmembrane receptors that are well conserved in vertebrates. NRPs bind to Semaphorin 3 (SEMA 3) proteins and vascular endothelial growth factors (VEGF) and are known for their crucial role in neurogenesis and cardiovascular development (Schellenburg et al., 2017; Takashima et al., 2002). Knockout of NRP1 in mice leads to early embryonic death with a wide range of cardiovascular defects. A knockout of NRP2, although not embryonic lethal, results in abnormal guidance of nerves and fewer small vessels and capillaries (Schellenburg et al., 2017; Takashima et al., 2002). The quantitative data showed that NRP1 was upregulated in *talpid*^{3} compared to wildtype, but that NRP2 was downregulated in *talpid*^{3} compared to wildtype. Although NRP1 and NRP2A have been studied in relation to the abnormalities in the limb vasculature (Davey et al., 2007), these proteins have not been examined in *talpid*^{3} in relation to the role they play in guidance of nerves during development. The NRP2 knockout mouse shows defects in axonal projections in the peripheral and central nervous system, demonstrating the role of NRP2 in axon guidance; the

downregulation of NRP2 could contribute to the neural defects seen in *talpid*^{3} and human KIAA0586 patients, therefore worth following up in future studies.

It is likely that TALPID3 is involved in multiple distinct protein networks to control specific functions rather than forming one 'TALPID3 protein network;' if this hypothesis is correct then it will be necessary to identify specific TALPID3-interacting proteins in order to identify these smaller networks of proteins. One of the shortcomings of the method used to study the *talpid*^{3} proteome in chapter 5, is that pathway analysis is designed to predict an overall change to a large network of proteins based on the upregulation and downregulation of individual proteins within that network, which most likely explains the lack of small centrosome protein networks identified as being changed in *talpid*^{3}. Despite providing valuable insight into the regulation of actin protein networks that TALPID3 is involved in, this study highlights the need for a way to carry out targeted proteomic studies on TALPID3. Given that TALPID3 is a low abundance protein within the centrosome, it is likely that some of the proteins it interacts with are also low abundance proteins within the centrosome, supporting the need for a targeted TALPID3 proteomic approach.

One such targeted approach that has shown recent success in uncovering protein – protein interactions is the proximity-dependent biotinylation technique, BioID (Roux et al., 2012). Briefly, this approach relies on BirA* being fused to a protein of interest, or a bait protein, which is introduced into a cell where it biotinylates proteins within close proximity. Biotinylated

proteins can be identified following cell lysis, protein extraction, streptavidin pulldown and mass spectrometry (Kim et al., 2016; Roux et al., 2012). This would provide a more targeted method of identifying TALPID3 interacting proteins that could overcome the shortcomings of previous attempts. A modification of the BioID approach relies on splitting BirA* into two fragments that can be fused to two different bait proteins that are known to interact, therefore preventing biotinylated labelling of nearby proteins prior to the interaction of the two bait proteins (Schopp et al., 2017). This modification allows identification of additional proteins that are associated with a pair of interacting proteins and could be used to identify the multiple small protein networks that are predicted to involve TALPID3. Using the split-BioID approach, TALPID3 could be fused to one of the BirA* fragments in combination with another protein of interest. For example TALPID3 and PCM1 could be fused to the two BirA* fragments in an attempt to identify the network of proteins involved in the satellite phenotype that TALPID3 controls. Additionally TALPID3 and Cep120 could be fused to the two BirA* fragments with the aim of identifying other proteins in that network, which could provide some answers as to what process the TALPID3-Cep120 interaction controls. Alternatively TALPID3 and MACF1 could be fused to the two BirA* fragments to determine whether this interaction is likely to be controlling centrosome and cilia processes or whether it is likely to be involved in the ability of TALPID3 to regulate the actin cytoskeleton. By identifying additional proteins that are associated with individual TALPID3-protein interactions and determining whether these proteins are the same

or different, some understanding could be gained as to whether these individual protein interactions overlap to form one network or whether TALPID3 is part of lots of smaller protein networks as predicted. In addition, the identification of these networks could provide insight into the processes controlled by TALPID3.

The study presented in chapter 3, demonstrated that human *KIAA0586* can be modelled in the *talpid*^{3} mutant with the aim of identifying functional domains through modelling the ciliopathy patient mutations. However, this assay is limited to analysis of Hedgehog-dependent expression in the neural tube and the availability of *talpid*^{3} embryos. An alternative approach for modelling an allelic series of human *KIAA0586* mutations would be to use gene editing to introduce the mutations from an allelic series into *TALPID3* in chicken PGCs. Four lines of PGCs could be generated through gene editing, each modelling a different mutation, which could then be mixed together and introduced (approximately equal numbers of cells from each edited cell line) into a sterile surrogate host (McGrew lab, unpublished). The offspring generated would contain a range of mutations in TALPID3, including homozygous and compound heterozygous mutations, that could be analysed for severity of different phenotypes. The abnormal phenotypes associated with limb, vasculature, liver, kidney and skeletal development in the *talpid*^{3} mutant have been well characterised (Davey et al., 2007; Davey et al., 2006; Stephen et al., 2013, 2015; Stephen et al., 2014); this means that the time point during development, at which the embryos containing *TALPID3* mutations should be examined for signs of specific abnormal

phenotypes, is already known. Evidence from human *KIAA0586* ciliopathy patients suggests that some cilia are still formed (Alby et al., 2015; Malicdan et al., 2015); by using PGCs to model an allelic series of the human patients, the frequency of cilia in different tissue types in the chicken could also be analysed, which could provide insight into the different levels of tissue penetrance of the mutation, based on which tissues and cell types were still capable of forming cilia. The severity of the phenotype and reduction of cilia associated with each of the mutations, would allow conclusions to be drawn about the human mutations, but even more importantly would provide insight into and identification of additional functional domains at the C-terminal of TALPID3.

Appendices

Appendix 1

The full alignment of the TALPID3/KIAA0586 protein is shown below. The first sequence, *Nematostella vectensis* (Starlet sea anemone), is conserved, containing both the coiled-coil domain and an intrinsically disordered domain. The second sequence, *Saccoglossus kowalevskii* (Acorn worm), is not conserved. It contains a coiled-coil domain in a similar region, but does not appear to share sequence similarity and does not contain an intrinsically disordered domain. The bottom four sequences are *Danio rerio* (zebrafish), *Gallus gallus* (chicken), *Homo sapiens* (human) and *Mus musculus* (mouse) respectively and all contain the conserved coiled-coil domain and the intrinsically disordered domain. The conserved coiled-coil domain is marked in blue and the predicted intrinsically disordered domain is marked in red.

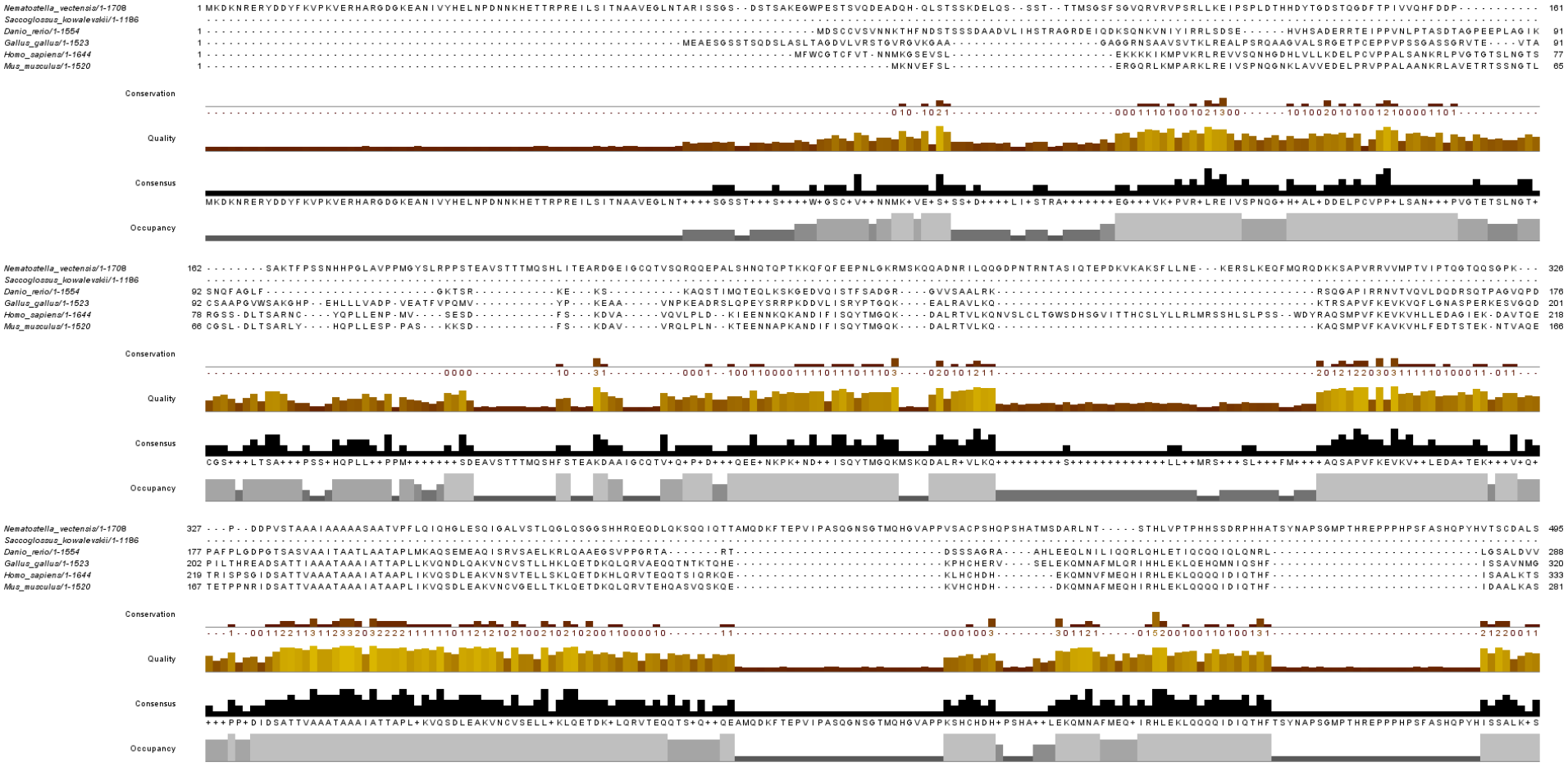
Nematostella_vectensis/1-1708
Saccoglossus_kowalevskii/1-1186
Danio_rerio/1-1554
Gallus_gallus/1-1523
Homo_sapiens/1-1644
Mus_musculus/1-1520
Conservation
Quality
Consensus
Occupancy

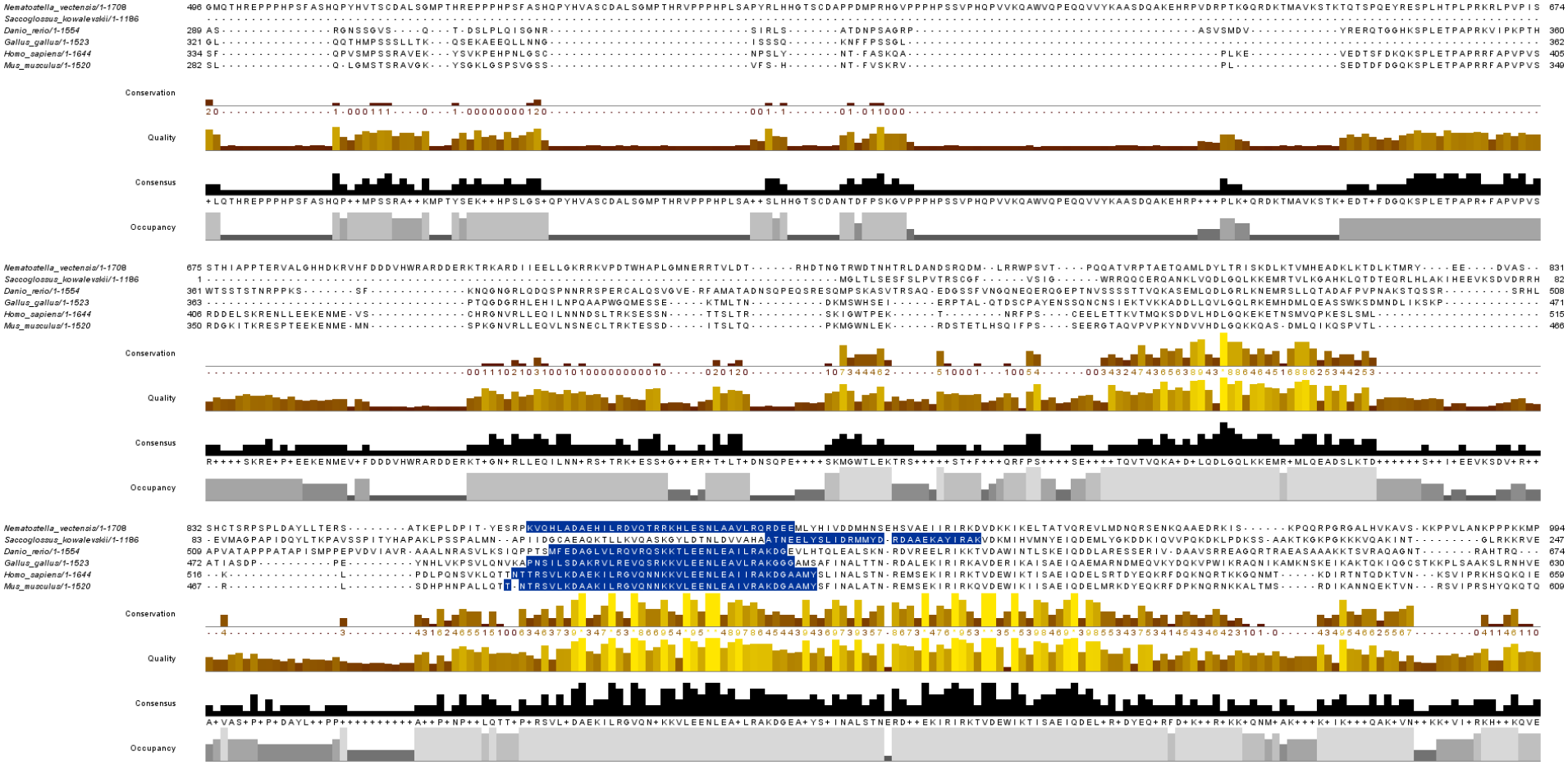
Nematostella_vectensis/1-1708
Saccoglossus_kowalevskii/1-1186
Danio_rerio/1-1554
Gallus_gallus/1-1523
Homo_sapiens/1-1644
Mus_musculus/1-1520
Conservation
Quality
Consensus
Occupancy

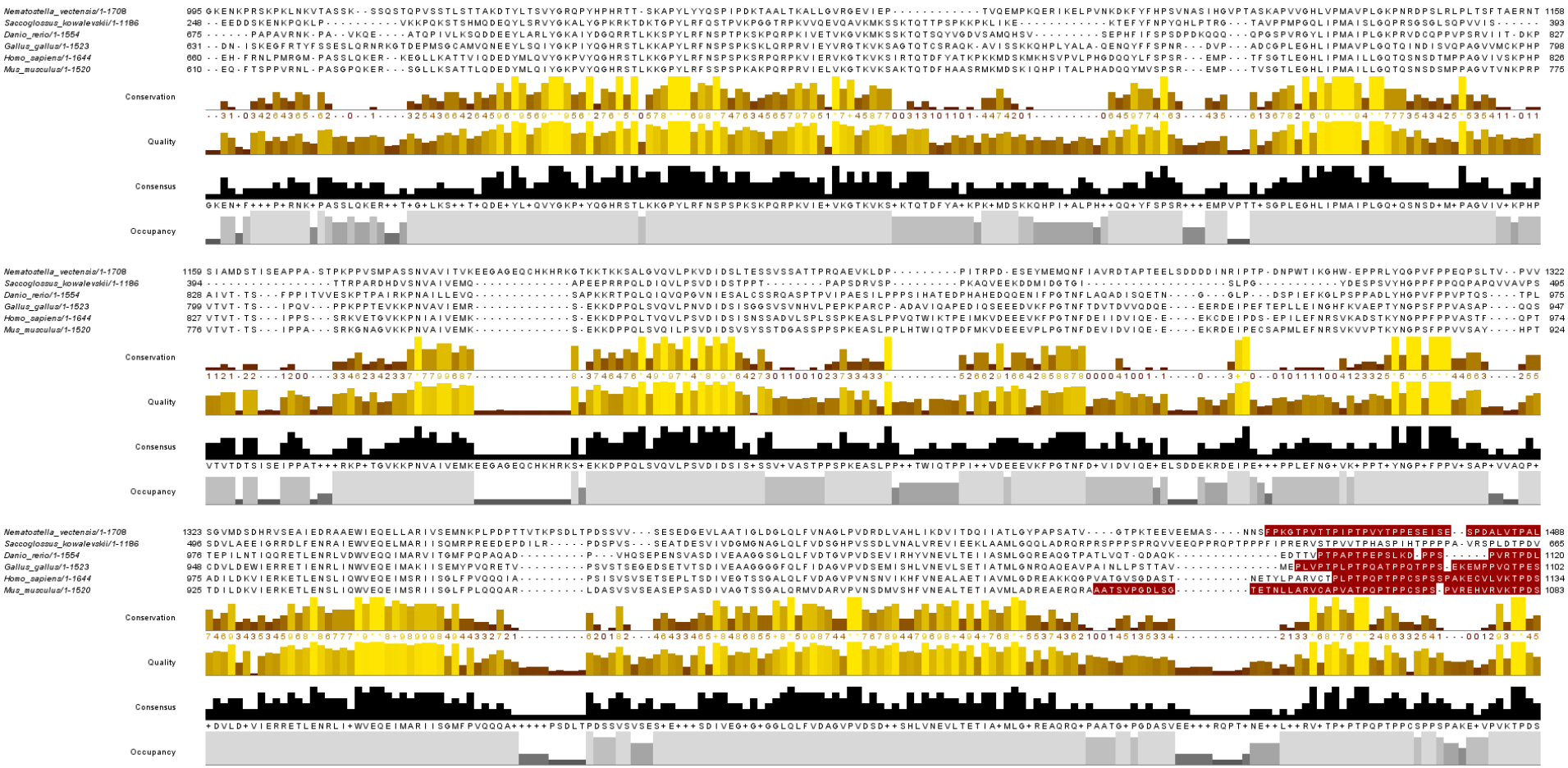
Nematostella_vectensis/1-1708
Saccoglossus_kowalevskii/1-1186
Danio_rerio/1-1554
Gallus_gallus/1-1523
Homo_sapiens/1-1644
Mus_musculus/1-1520
Conservation
Quality
Consensus
Occupancy

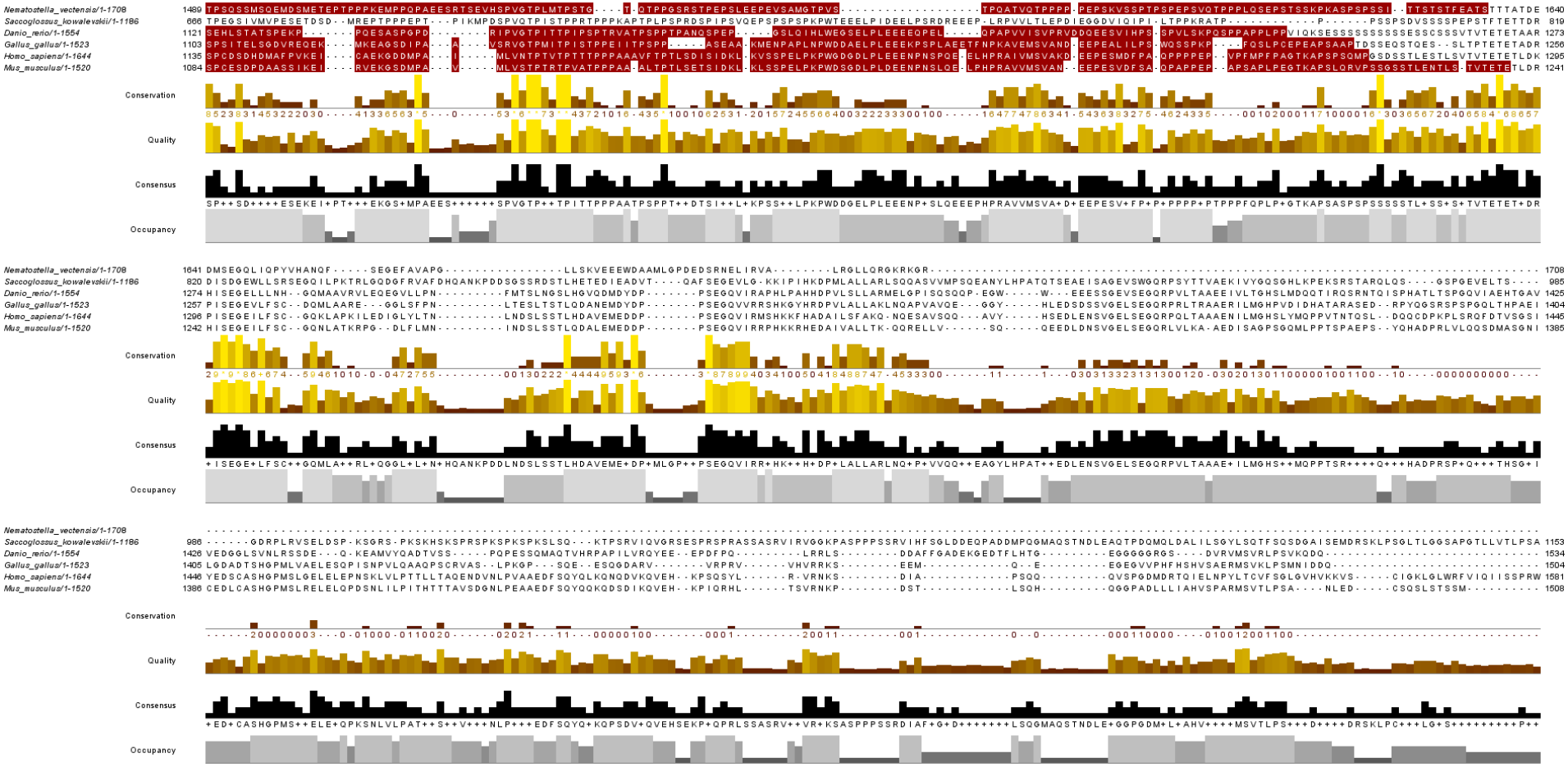
Nematostella_vectensis/1-1708
Saccoglossus_kowalevskii/1-1186
Danio_rerio/1-1554
Gallus_gallus/1-1523
Homo_sapiens/1-1644
Mus_musculus/1-1520
Conservation
Quality
Consensus
Occupancy

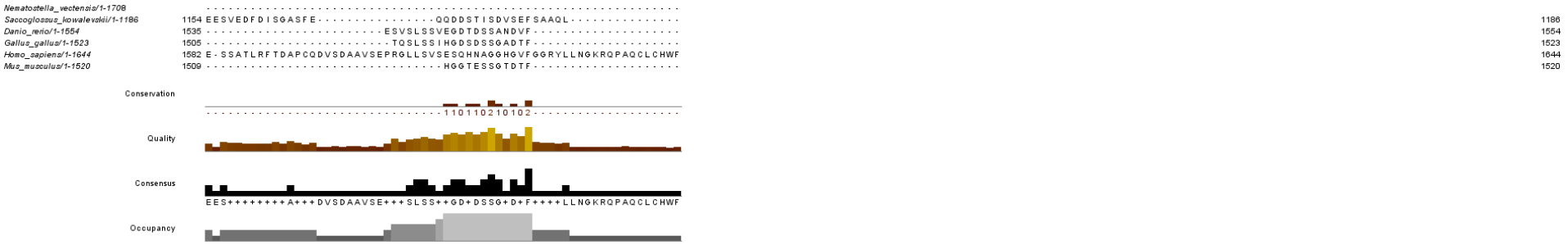
Nematostella_vectensis/1-1708
Saccoglossus_kowalevskii/1-1186 1154 E E S V E D F D I S G A S F E - - - - - - - - - - - - - - - - Q Q D D S T I S D V S E F S A A Q L - - - - - - - - - - - - - - - - 1186
Danio_rerio/1-1554 1535 - E S V S L S S V E G D T D S S A N D V F - 1554
Gallus_gallus/1-1523 1505 - T Q S L S S I H G D S D S S G A D T F - 1523
Homo_sapiens/1-1644 1582 E - S S A T L R F T D A P C Q D V S D A A V S E P R G L L S V S E S Q H N A G G H G V F G G R Y L L N G K R Q P A Q C L C H W F 1644
Mus_musculus/1-1520 1509 - H G G T E S S G T D T F - 1520
Conservation
1 1 0 1 1 1 0 2 1 0 1 0 2
Quality
Consensus
E E S + + + + + + + + A + + + D V S D A A V S E + + + S L S S + + G D + D S S G + D + F + + + + L L N G K R Q P A Q C L C H W F
Occupancy

Appendix 2

The following list of proteins contains 142 proteins that are found in both the Jurkat centrosome dataset and the CCDB dataset.

ACTR1A
AFG3L2
AKAP9
APEX1
ATP5A1
ATXN10
CAD
CAMK2G
CCDC77
CCT2
CCT3
CCT5
CCT8
CDK1
CDK5RAP3
CENPF
CEP128
CEP131
CEP135
CEP250
CEP290
CEP55
CEP57
CEP63
CETN2
CKAP5
CLIP1
CLPX
CNOT1
CNTRL
CROCC
CSE1L
CSNK2A1
CSNK2A2
CTBP1
DARS
DCTN1
DCTN2
DCXR
DIAPH1
DYNC1H1
DYNC1LI1
DYNLRB1
DYNLT1
EEF1B2
EEF2
EIF2S1
FGFR1OP
FLII
FLNA
FLOT1
GNB2L1
GOLGA3
GSTP1
HADHA
HAUS6
HOOK3
HSD17B4
HSP90AA1
HSPA5
HSPA8
HSPD1
IMMT
IPO5
KARS
KIF14
KIF23
LCK
LCP1
LONP1
LRRC59
MACF1
MAP4
METAP1
NCAPG
NDUFS1
NEDD1
NPM1

NUP107
NUP214
NUP93
PCNT
PDHB
PHB
POC5
PPP1CC
PPP2CA
PRC1
PRDX3
PRKAR2A
PSMA6
PSMC1
PSMC2
PSMD1
PSMD2
PSMD3
RACGAP1
RAN
RARS
RFC4
RPL10A
RPL12
RPL27
RPL35
RPS13
RPS14
RPS19
RPS27A
RPS7
RPS9
RUVBL1
RUVBL2
SARS
SCCPDH
SEC22B
SEPT2
SEPT6
SEPT7
SLC25A3
SNRNP200
SPTAN1
STAT3
STIP1
TCP1
TDRKH
TLN1
TMX2
TNPO1
TOP2A
TUBB4B
TUBG1
TUBGCP3
TXLNA
UBA1
UBC
UQCRC2
USP14
VDAC3
WDR1
YWHAB
YWHAE
YWHAQ

Appendix 3

The following list of proteins contains 139 proteins that are found in both the PGC centrosome dataset and the CCDB dataset.

ACAT1
ACTR1A
AFG3L2
ANK3
AP1M1
ASNS
ASPH
ATP5A1
CAPZB
CCDC102A
CCT2
CCT3
CCT5
CCT8
CDK1
CEP131
CEP170
CEP55
CEP57
CHD4
CHEK1
CLASP1
CNOT1
CSE1L
CSNK2A1
CTNNB1
DARS
DCAF13
DCTN1
DCTN2
DPYSL2
DYNC1H1
EEF1B2
EEF2
EIF2S1
EPB41
ESRP2
ETFA
FLII
GLG1
GSN
HADHA
HAUS2
HOOK3
HSD17B12
HSD17B4
HSP90AA1
HSP90B1
HSPA5
HSPA8
HSPA9
HSPD1
IMMT
KARS
KIF23
KIF2A
KPNA2
LRP2
MACF1
MAD1L1
MAP2K2
MAPRE1
MASTL
MCM3
MLEC
MYO5A
MYO6
NDUFS1
NEK9
NPM1
NUP107
NUP85
NUP93
NUP98
P4HB
PAFAH1B1
PARP1
PDCD6IP

PDHB
PHB
PLK1
PPP1CB
PPP4R1
PRC1
PSMC1
PSMC2
PSMD1
PSMD2
PSMD3
PXDN
RAB11A
RAB18
RACGAP1
RAN
RANBP1
RANGAP1
RARS
RFC4
RPL10A
RPL12
RPL27
RPL35
RPS13
RPS14
RPS19
RPS27A
RPS7
RUVBL1
SCCPDH
SEC22B
SEPT6
SEPT7
SF3B3
SLC9A3R1
SMC3
SNRNP200
SPTAN1
STAT3
STK24
STK3
STXBP1
TCP1
TDRKH
TF
TNPO1
TOP2A
TRAPPC10
TUBA1C
TUBG1
TUBGCP3
TXNL1
UGP2
UQCRC2
USP14
VCL
VPS35
XPO7
YWHAE
YWHAQ

Appendix 4

The following list of proteins contains 76 proteins that are found in the Jurkat centrosome dataset, the PGC centrosome dataset, and the CCDB dataset.

ACTR1A
AFG3L2
ATP5A1
CCT2
CCT3
CCT5
CCT8
CDK1
CEP131
CEP55
CEP57
CNOT1
CSE1L
CSNK2A1
DARS
DCTN1
DCTN2
DYNC1H1
EEF1B2
EEF2
EIF2S1
FLII
HADHA
HOOK3
HSD17B4
HSP90AA1
HSPA5
HSPA8
HSPD1
IMMT
KARS
KIF23
MACF1
NDUFS1
NPM1
NUP107
NUP93
PDHB
PHB
PRC1
PSMC1
PSMC2
PSMD1
PSMD2
PSMD3
RACGAP1
RAN
RARS
RFC4
RPL10A
RPL12
RPL27
RPL35
RPS13
RPS14
RPS19
RPS27A
RPS7
RUVBL1
SCCPDH
SEC22B
SEPT6
SEPT7
SNRNP200
SPTAN1
STAT3
TCP1
TDRKH
TNPO1
TOP2A
TUBG1
TUBGCP3
UQCRC2
USP14
YWHAE
YWHAQ

Appendix 5

The following list of proteins contains 52 proteins from a combined Jurkat centrosome sample 1 and Jurkat centrosome sample 2 dataset that were identified as fitting the criteria for taking proteins forward for further analysis (specified in Table 4.1).

ARPC2
ARPC4
CAPRIN1
CCDC127
CEP250
CEP55
CETN2
CFL1
CIT
DCTN1
DIAPH1
DNAJB1
DNM2
DOCK2
DRG1
DYNC1H1
EIF3A
EIF6
ELMO1
EZR
FLII
FLNA
FLNB
INF2
IQGAP1
KIF14
KIF20A
KIF23
KIF4A
LRPPRC
MACF1
MSN
NEDD1
PRC1
RAC1
RCC2
SPTBN1
SPTBN2
TLN1
TUBB5
TUBGCP3
VIM
WDR1

Appendix 6

The following list of proteins contains 29 proteins from Jurkat centrosome sample 2 alone that were identified as fitting the criteria for taking proteins forward for further analysis (specified in Table 4.1).

ACTR1A
AKAP9
ARPC5
CCDC77
CCT5
CDC2
CDK6
CEP128
CEP131
CEP135
CEP290
CEP57
CEP63
CNTRL
CROCC
DYNLRB1
EMD
FMNL1
HAUS5
OXSR1
PCNT
PFN1
PLEC1
RMDN3
SDCBP
SHCBP1
SNTB2
SEPT1
SEPT2

Appendix 7

Western Blots display antibodies that were tested on protein extracted from human RPE1 cells and chicken PGCs. The expected size of each band is annotated with a red arrow to mark where the band was expected. Antibodies are often non-specific for chicken proteins, therefore it was important to test all the antibodies in control protein samples before carrying out Western Blots on protein samples sent for mass spectrometry to validate the dataset. Included are the test western blots for antibodies against CCDC77 and CCCDC127, which also did not work and therefore could not be used for validation in the Jurkat centrosome protein samples.

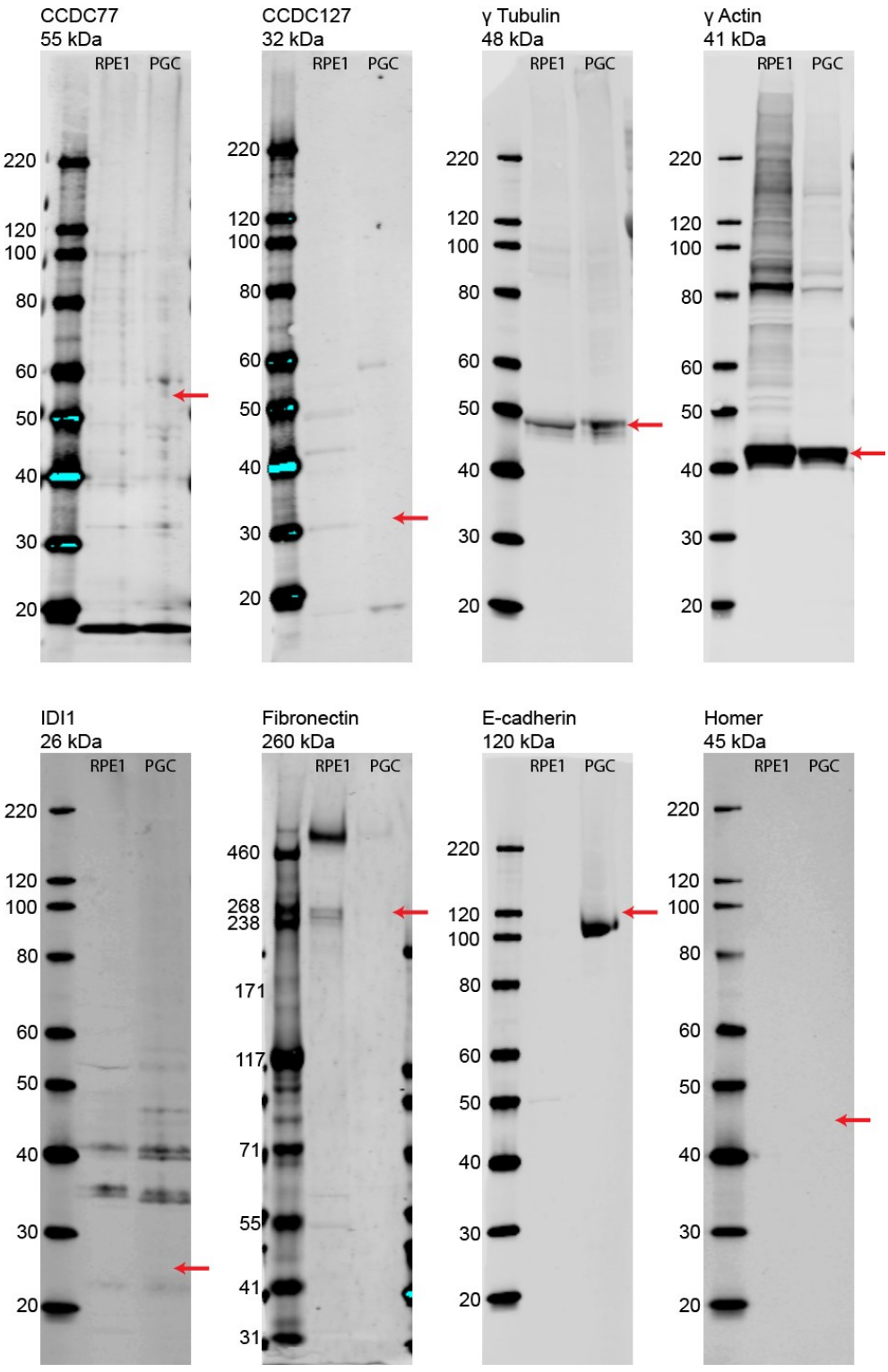
CCDC77
55 kDa
RPE1 PGC
220
120
100
80
60
50
40
30
20
CCDC127
32 kDa
RPE1 PGC
220
120
100
80
60
50
40
30
20
γ Tubulin
48 kDa
RPE1 PGC
220
120
100
80
60
50
40
30
20
γ Actin
41 kDa
RPE1 PGC
220
120
100
80
60
50
40
30
20
IDI1
26 kDa
RPE1 PGC
220
120
100
80
60
50
40
30
20
Fibronectin
260 kDa
RPE1 PGC
460
268
238
171
117
71
55
41
31
E-cadherin
120 kDa
RPE1 PGC
220
120
100
80
60
50
40
30
20
Homer
45 kDa
RPE1 PGC
220
120
100
80
60
50
40
30
20

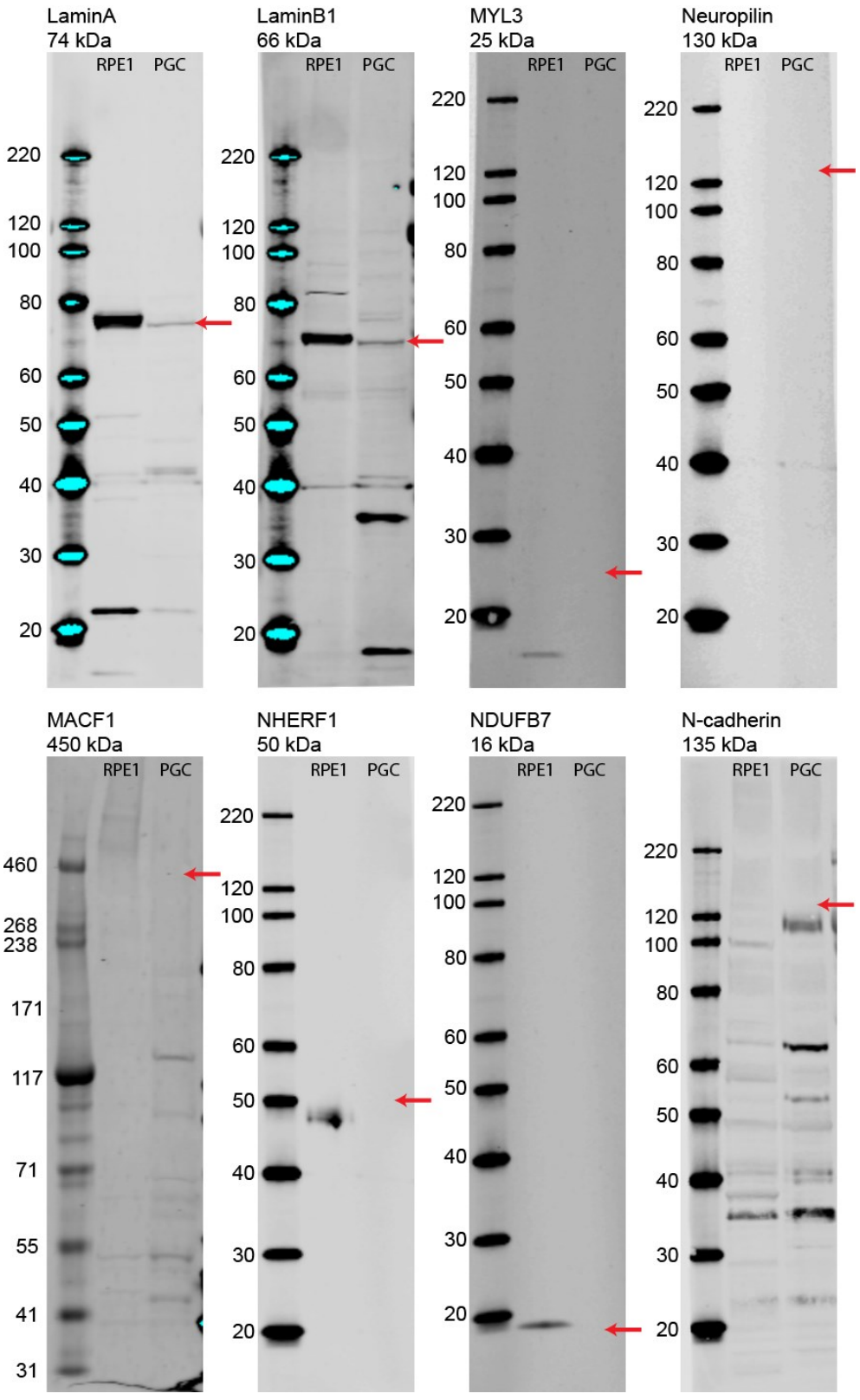
LaminA
74 kDa
RPE1 PGC
220
120
100
80
60
50
40
30
20
LaminB1
66 kDa
RPE1 PGC
220
120
100
80
60
50
40
30
20
MYL3
25 kDa
RPE1 PGC
220
120
100
80
60
50
40
30
20
Neuropilin
130 kDa
RPE1 PGC
220
120
100
80
60
50
40
30
20
MACF1
450 kDa
RPE1 PGC
460
268
238
171
117
71
55
41
31
NHERF1
50 kDa
RPE1 PGC
220
120
100
80
60
50
40
30
20
NDUFB7
16 kDa
RPE1 PGC
220
120
100
80
60
50
40
30
20
N-cadherin
135 kDa
RPE1 PGC
220
120
100
80
60
50
40
30
20

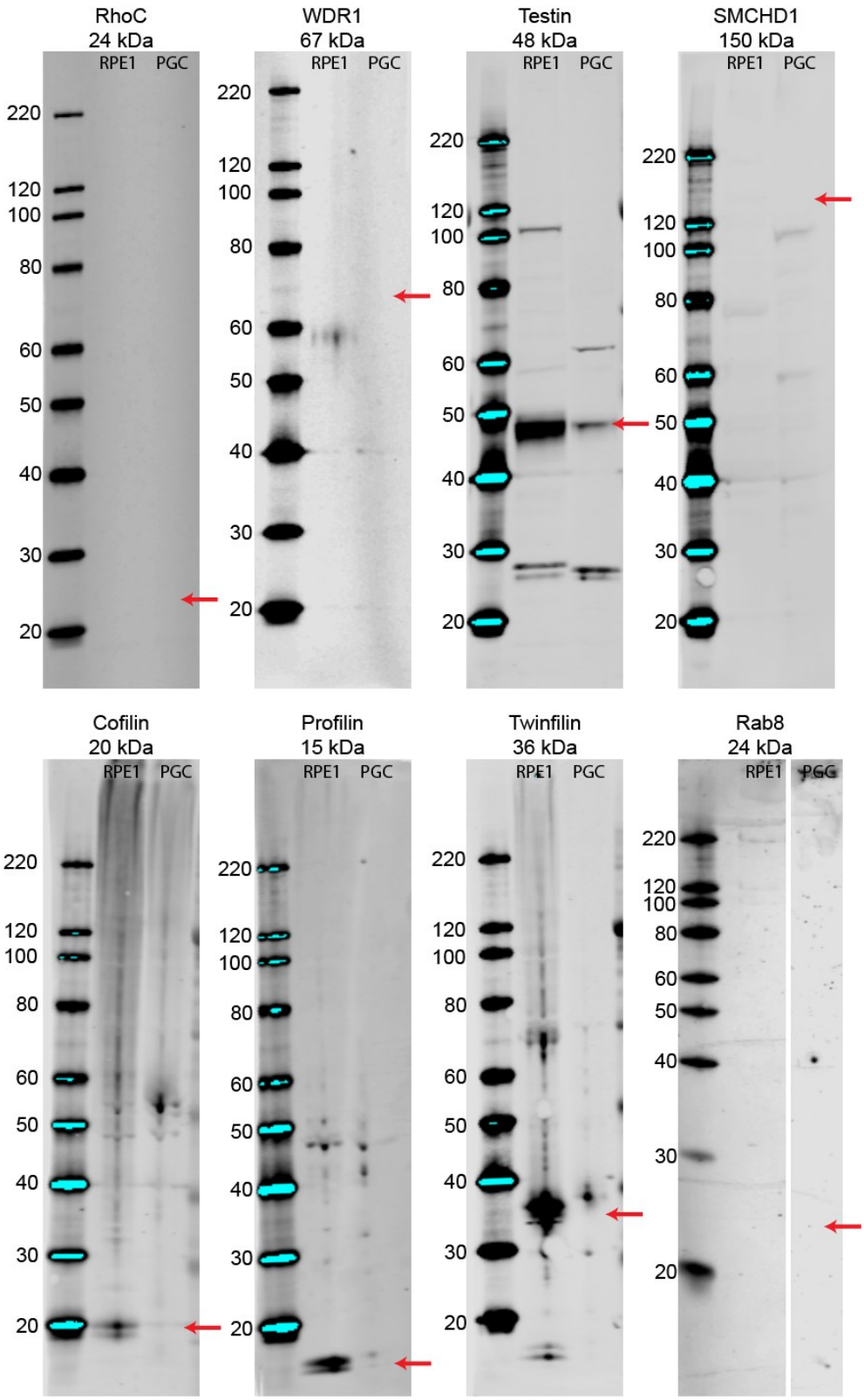
RhoC
24 kDa
RPE1 PGC
220
120
100
80
60
50
40
30
20
WDR1
67 kDa
RPE1 PGC
220
120
100
80
60
50
40
30
20
Testin
48 kDa
RPE1 PGC
220
120
100
80
60
50
40
30
20
SMCHD1
150 kDa
RPE1 PGC
220
120
100
80
60
50
40
30
20
Cofilin
20 kDa
RPE1 PGC
220
120
100
80
60
50
40
30
20
Profilin
15 kDa
RPE1 PGC
220
120
100
80
60
50
40
30
20
Twinfilin
36 kDa
RPE1 PGC
220
120
100
80
60
50
40
30
20
Rab8
24 kDa
RPE1 PGG
220
120
100
80
60
50
40
30
20

Appendix 8

The following list is comprised of the proteins (identified by gene name) that were filtered for two or more unique peptides and a minimum fold change of 1.2 when *talpid*^{3} PGC protein reporter intensities were compared to wildtype PGC protein reporter intensities, from the TMT mass spectrometry dataset. The left column represents the gene name and the right column in light blue contains the fold change value. This list of proteins was used for the pathway analysis in IPA. The genes and their respective fold change values are plotted on the graph seen in Figure 4.2.

Gene Name	Ratio Ta/WT Reporter Intensity
ATP5A1W	0.39384908
IDI1	0.6350744
SLC22A5	0.6605697
MYL3	0.6983478
NLN	0.6999261
DMD	0.7012115
RBP5	0.706802
IL18	0.7166216
NRP2	0.7260198
MYL4	0.7419387
PM20D2	0.7445304
HMGCS1	0.7462363
HDHD1	0.7467302
FN1	0.7476846
DHCR24	0.7497696
SLC1A4	0.7562514
BFIV21	0.7573186
CHURC1	0.7577402
FAM114A1	0.7625899
ATP2B4	0.7685991
FABP3	0.7691596
ACTC1	0.7703391
MYD88	0.7711465
GNS	0.7712704
FDFT1	0.7713011
VPS45	0.7737246
MSMO1	0.7748104
LCN15	0.7753657
C12ORF10	0.7769788
LOC107056092	0.7790017
HOMER2	0.7810424
CYP51A1	0.7840815
COX17	0.7850283
NSDHL	0.7850763
TBC1D13	0.7873287
C1H21ORF33	0.7875785
DBI	0.7919774
TMED8	0.7944101
CST7	0.7945917
SFR1	0.7957101
SCD	0.7961454
ODC1	0.7975218
GYG1	0.7976631
NANP	0.798287
NUDT15	0.7989097

NGFR	0.7989975
IER3IP1	1.2004905
BHMT	1.200646
SPON1	1.201618
DDX55	1.2034727
RPL6	1.204394
JMY	1.2048205
ALDH7A1	1.2048913
RAD51AP1	1.2057043
MAPT	1.2057123
SIVA1	1.2064545
CCDC137	1.2082928
RPL36	1.209075
IQGAP2	1.2095534
HSDL2	1.211142
LYN	1.2111608
HPD	1.2112409
FAM129A	1.2124925
CZH9ORF64	1.21417
CA2	1.2147537
RPS6KA5	1.214774
SH3GL3	1.215033
GKAP1	1.2152678
TOPORS	1.2156651
TOMM20	1.2160541
LOC107053190	1.2162851
FAM168A	1.2165885
ADHFE1	1.2186999
GLI2	1.2201559
FBL12	1.2201816
NUDCD2	1.22079
MBLAC2	1.2208966
HEP21	1.2214954
LOC418927	1.2215015
CHCHD3	1.2216814
RFC1	1.2235309
VDAC2	1.22469
RPL13	1.2247828
ABL1	1.2253438
GTF3C1	1.2321855
MARCKS	1.2340439
GAS2L3	1.2370282
XRCC4	1.2379149
OXCT1	1.238223
MRPL2	1.2382549
BASP1	1.2402087
SPTY2D1	1.2405934
LGMN	1.2419602
NUDT12	1.2442229
ACAA2	1.2467456
DPY19L3	1.2472309
RSL24D1	1.2478658
SCAMP1	1.249364
ACOX2	1.2538378
CAST	1.256124
AKR1D1	1.2565352
TBC1D25	1.2589256
FAM169A	1.2615137
CHD1	1.2633286
SH3RF1	1.2636599
SLC25A38	1.2637555
BLNK	1.2701259
MAP1B	1.2730872
CLASP1	1.2738066
BAIAP2	1.2752104
CNTNAP5	1.27979
RNF170	1.2839498
TCOF1	1.2844006
HMGI-C	1.2872596
RPL32	1.2879233
PSIP1	1.2880934
DCX	1.2917459
RPL22L1	1.2990648
XPA	1.2998035
SEC62	1.3014484
CKS2	1.304022
COA5	1.3073867
SERINC5	1.311221
RBMS1	1.3125473
PLIN2	1.3134457
CCDC59	1.3140463
RPL37	1.3151929
BDP1L	1.3197878
DACH1	1.3203337
BRIX1	1.3208305
RPL15	1.3251791
RPL36A	1.3263415
NRP1	1.3264355
SLC34A2	1.3334416
HTRA1	1.3436504
LRRC16A	1.3439138
RPL35	1.3557617
COBL	1.3573376
HMGN2	1.3645721

MTIF3	1.3752333
STK10	1.3821385
SNRPG	1.3887482
H3-IX	1.3895835
NID1	1.4030951
ACYP2	1.4108687
PPAP2A	1.4231924
C18ORF32	1.4371299
CHD2	1.4440066
PRODH	1.4449592
PCP4	1.4475571
NQO1	1.4790721
MYLK	1.5165135
BBOX1	1.521765
NPL	1.5580281
HMGN3	1.5896685
ACOT9	1.6007308
SMC1B	1.6657416
EIF2AK1	1.7084085
LOC415664	1.7654149
LYRM2	1.7872963
RPS29	1.8102749
GLRX2	1.9237383
NDUFB7	2.3734373

Appendix 9

The following pathways were generated in Ingenuity Pathway Analysis from the list of proteins found in Appendix 8. The pathways represent two of the three pathways identified in the top 15 canonical signalling pathways that involve Actin and Rho; the third pathway is found in Chapter 4. Nodes that are shaded red indicate proteins that are upregulated. Nodes that are shaded green indicate proteins that are downregulated. Nodes that are shaded grey indicate a protein contained in the dataset that does not contain a change over the minimum 1.2 fold change limit. Nodes with no shading (i.e. white) indicate a protein that is integral to the network but not included in the dataset.

Regulation of Actin-based Motility by Rho Pathway

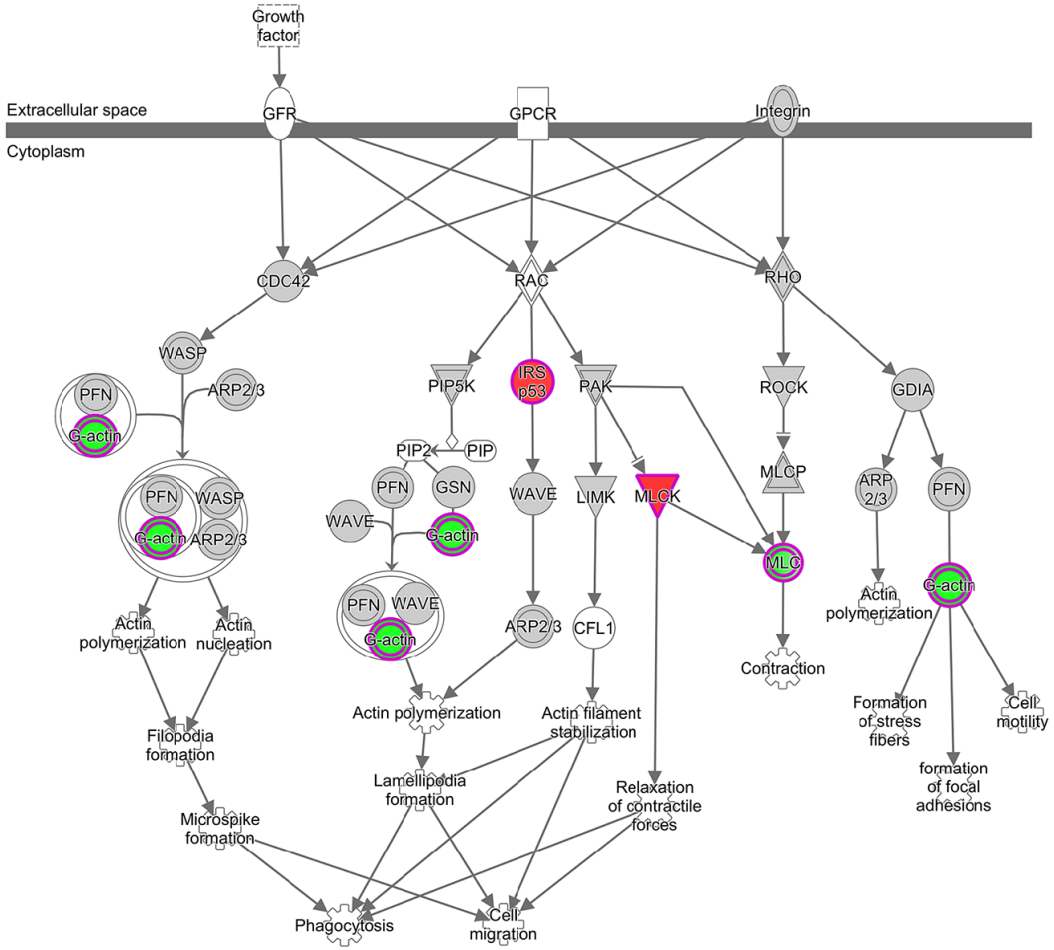

Actin Cytoskeleton Signalling Pathway

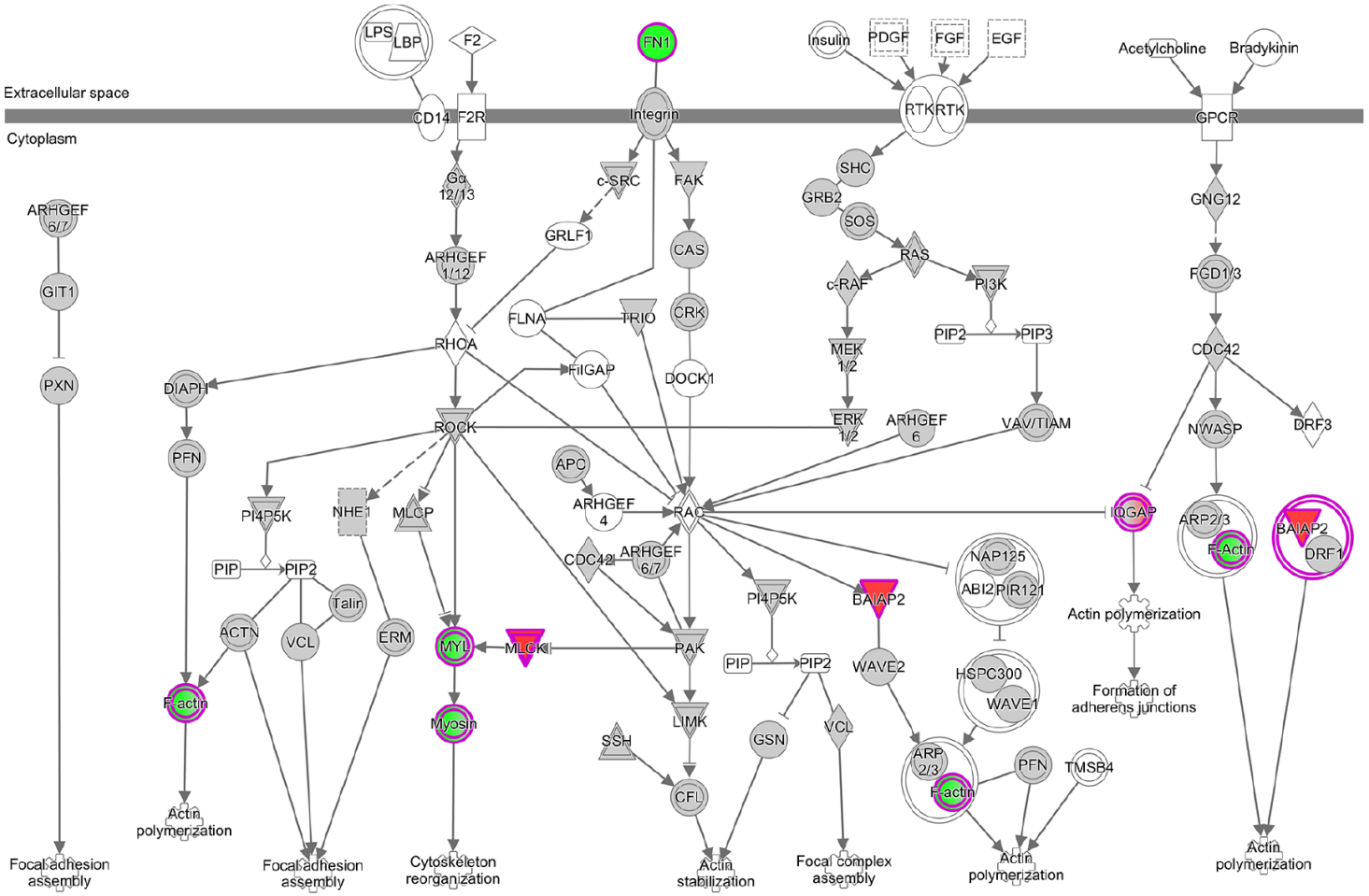

Bibliography

Abal, M., Piel, M., Bouckson-Castaing, V., Mogensen, M., Sibarita, J. B., & Bornens, M. (2002). Microtubule release from the centrosome in migrating cells. *Journal of Cell Biology*, *159*(5), 731–737. https://doi.org/10.1083/jcb.200207076

Abdelhamed, Z. a, Wheway, G., Szymanska, K., Natarajan, S., Toomes, C., Inglehearn, C., & Johnson, C. A. (2013). Variable expressivity of ciliopathy neurological phenotypes that encompass Meckel-Gruber syndrome and Joubert syndrome is caused by complex de-regulated ciliogenesis, Shh and Wnt signalling defects. *Human Molecular Genetics*, *22*(7), 1358–72. https://doi.org/10.1093/hmg/dds546

Akawi, N., McRae, J., Ansari, M., Balasubramanian, M., Blyth, M., Brady, A. F., … Hurles, M. E. (2015). Discovery of four recessive developmental disorders using probabilistic genotype and phenotype matching among 4,125 families. *Nature Genetics*, *47*(11), 1363–1369. https://doi.org/10.1038/ng.3410

Alby, C., Piquand, K., Huber, C., Megarbané, A., Ichkou, A., Legendre, M., … Thomas, S. (2015). Mutations in KIAA0586 Cause Lethal Ciliopathies Ranging from a Hydrolethalus Phenotype to Short-Rib Polydactyly Syndrome. *American Journal of Human Genetics*, *97*(2), 311–8. https://doi.org/10.1016/j.ajhg.2015.06.003

Alcantara, D., & O'Driscoll, M. (2014). Congenital Microcephaly. *American Journal of Medical Genetics*, *166*(2).

Alman, B. A. (2015). The role of hedgehog signalling in skeletal health and disease. *Nature Reviews Rheumatology*, *11*, 552–560. https://doi.org/10.1038/nrrheum.2015.84

Alves-Cruzeiro, J. M. da C., Nogales-Cadenas, R., & Pascual-Montano, A. D. (2013). CentrosomeDB : a new generation of the centrosomal proteins database for Human and Drosophila melanogaster, *42*(November 2013), 430–436. https://doi.org/10.1093/nar/gkt1126

Amato, R., Morleo, M., Giaquinto, L., Bernardo, D., & Franco, B. (2014). A network-based approach to dissect the cilia / centrosome complex interactome, 1–12.

Anand, M., & Khanna, H. (2012). Ciliary Transition Zone (TZ) Proteins RPGR and CEP290: Role in Photoreceptor Cilia and Degenerative Diseases. *Expert Opinion Therapeutic Targets*, *16*(6), 541–551. https://doi.org/10.1002/9780471729259.mc01f01s24.Identification

Andersen, J. S., Wilkinson, C. J., Mayor, T., Mortensen, P., Nigg, E. A., & Mann, M. (2003). Proteomic characterization of the human centrosome by protein correlation profiling. *Nature*, *426*(6966), 570–574. https://doi.org/10.1038/nature02163.1.

Andrade, R. P., Palmeirim, I., & Bajanca, F. (2007). Molecular Clocks Underlying Vertebrate Embryo Segmentation : A 10-Year-Old hairy -Go-Round. *Birth Defects Research. Part C, Embryo Today : Reviews*, *81*(Part C), 65–83. https://doi.org/10.1002/bdrc.20094

Arensdorf, A. M., Marada, S., & Ogden, S. K. (2016). Smoothened Regulation: A Tale of Two Signals. *Trends in Pharmacological Science*, *37*(1), 62–72. https://doi.org/10.1016/j.tips.2015.09.001.Smoothened

Argos, P. (1990). An Investigation of Oligopeptides Linking Domains in Protein Tertiary Structures and Possible Candidates for General Gene Fusion. *Journal of Molecular Biology*, *211*, 943–958.

Arnaiz, O., Malinowska, A., Klotz, C., Sperling, L., Dadlez, M., Koll, F., & Cohen, J. (2009). Cildb : a knowledgebase for centrosomes and cilia. *Database*, *2009*, 1–14. https://doi.org/10.1093/database/bap022

Aubusson-Fleury, A., Lemullois, M., de Loubresse, N. G., Laligne, C., Cohen, J., Rosnet, O., … Koll, F. (2012). The conserved centrosomal protein FOR20 is required for assembly of

the transition zone and basal body docking at the cell surface. *Journal of Cell Science*, *125*(18), 4395–4404. https://doi.org/10.1242/jcs.108639

Avasthi, P., & Marshall, W. F. (2012). Stages of ciliogenesis and regulation of ciliary length. *Differentiation; Research in Biological Diversity*, *83*(2), S30-42. https://doi.org/10.1016/j.diff.2011.11.015

Bachmann-Gagescu, R., Dempsey, J., Phelps, I. G., O'Roak, B. J., Knutzen, D. M., Rue, T. C., … Doherty, D. (2015). Joubert Syndrome: A model for untangling recessive disorders with extreme genetic heterogeneity. *Journal of Medical Genetics*, *52*(8), 514–522. https://doi.org/10.1016/j.contraception.2015.12.017.Women

Bachmann-Gagescu, R., Phelps, I. G., Dempsey, J. C., Sharma, V. a, Ishak, G. E., Boyle, E. a, … Doherty, D. (2015). KIAA0586 is Mutated in Joubert Syndrome. *Human Mutation*, *36*(9), 831–5. https://doi.org/10.1002/humu.22821

Balczon, R., Bao, L., & Zimmer, W. E. (1994). PCM-1, A 228-kD Centrosome Autoantigen with a Distinct Cell Cycle Distribution. *Journal of Cell Biology*, *124*(5), 783–793.

Bale, A. E. (2002). Hedgehog Signaling and Human Disease. *Annual Review of Genomics and Human Genetics*, *3*, 47–65. https://doi.org/10.1146/annurev.genom.3.022502.103031

Bamburg, J. R., McGough, A., & Ono, S. (1999). Putting a new twist on actin: ADF / cofilins modulate actin dynamics. *Trends in Cell Biology*, *9*(1), 364–370.

Bangs, F., & Anderson, m K. V. (2017). Primary Cilia and Mammalian Hedgehog Signaling. *Cold Spring Harbor Perspectives in Biology*, *9*(5), 1–30. https://doi.org/10.1016/S2214-109X(16)30265-0.Cost-effectiveness

Bangs, F., Antonio, N., Thongnuek, P., Welten, M., Davey, M. G., Briscoe, J., & Tickle, C. (2011). Generation of mice with functional inactivation of talpid3, a gene first identified in chicken. *Development (Cambridge, England)*, *138*(15), 3261–72. https://doi.org/10.1242/dev.063602

Bantscheff, M., Schirle, M., Sweetman, G., Rick, J., & Kuster, B. (2007). Quantitative mass spectrometry in proteomics : a critical review. *Analytical and Bioanalytical Chemistry*, *389*, 1017–1031. https://doi.org/10.1007/s00216-007-1486-6

Barbe, L., Lundberg, E., Oksvold, P., Stenius, A., Lewin, E., Björling, E., … Andersson-Svahn, H. (2008). Toward a confocal subcellular atlas of the human proteome. *Molecular & Cellular Proteomics : MCP*, *7*(3), 499–508. https://doi.org/10.1074/mcp.M700325-MCP200

Bärenz, F., Mayilo, D., & Gruss, O. J. (2011). Centriolar satellites: Busy orbits around the centrosome. *European Journal of Cell Biology*, *90*(12), 983–989. https://doi.org/10.1016/j.ejcb.2011.07.007

Bauer, M., Cubizolles, F., Schmidt, A., & Nigg, E. a. (2016). Quantitative analysis of human centrosome architecture by targeted proteomics and fluorescence imaging. *Embo*, *35*(19), 1–15. https://doi.org/10.15252/embj

Baujat, G., Huber, C., El Hokayem, J., Caumes, R., Do Ngoc Thanh, C., David, A., … Cormier-Daire, V. (2013). Asphyxiating thoracic dysplasia: clinical and molecular review of 39 families. *Journal of Medical Genetics*, *50*(2), 91–8. https://doi.org/10.1136/jmedgenet-2012-101282

Beck, M., Schmidt, A., Malmstroem, J., Claassen, M., Ori, A., Szymborska, A., … Aebersold, R. (2011). The quantitative proteome of a human cell line. *Molecular Systems Biology*, *7*(549), 1–8. https://doi.org/10.1038/msb.2011.82

Ben, J., Elworthy, S., Ng, A. S. M., van Eeden, F., Ingham, P. W., & Eeden, F. (2011). Targeted mutation of the talpid3 gene in zebrafish reveals its conserved requirement for ciliogenesis and Hedgehog signalling across the vertebrates. *Development (Cambridge, England)*, *138*(22), 4969–78. https://doi.org/10.1242/dev.070862

Bettencourt-Dias, M., Hildebrandt, F., Pellman, D., Woods, G., & Godinho, S. a. (2011). Centrosomes and cilia in human disease. *Trends in Genetics : TIG*, *27*(8), 307–15. https://doi.org/10.1016/j.tig.2011.05.004

Blackburn, K., Bustamante, X., Yin, W., Goshe, M. B., & Ostrowski, L. E. (2017). Quantitative Proteomic Analysis of Human Airway Cilia Identifies Previously Uncharacterised Proteins of High Abundance. *Journal of Proteome Research*, *16*(4), 1579–1592. https://doi.org/10.1021/acs.jproteome.6b00972.Quantitative

Bornens, M., Paintrand, M., Berges, J., Marty, M. C., & Karsenti, E. (1987). Structural and chemical characterization of isolated centrosomes. *Cell Motility and the Cytoskeleton*, *8*(3), 238–249. https://doi.org/10.1002/cm.970080305

Briscoe, J., & Ericson, J. (1999). The specification of neuronal identity by graded sonic hedgehog signalling. *Cell and Developmental Biology*, *10*, 353–362.

Brooks, E. R., & Wallingford, J. B. (2014). Multiciliated Cells. *Current Biology*, *24*(19), R973–R982. https://doi.org/10.1016/j.cub.2014.08.047

Brugmann, S. A., Allen, N. C., James, A. W., Mekonnen, Z., Madan, E., & Helms, J. A. (2010). A primary cilia-dependent etiology for midline facial disorders. *Human Molecular Genetics*, *19*(8), 1577–92. https://doi.org/10.1093/hmg/ddq030

Brugmann, S. A., Cordero, D. R., & Helms, J. A. (2010). Craniofacial ciliopathies: a new classification for craniofacial disorders. *American Journal Of Medical Genetics*, *152A*(12), 2995–3006. https://doi.org/10.1002/ajmg.a.33727.Craniofacial

Burger, R., Hansen-Hagge, T. E., Drexler, H. G., & Gramatzki, M. (1999). Heterogeneity of T-acute lymphoblastic leukemia (T-ALL) cell lines: Suggestion for classification by immunophenotype and T-cell receptor studies. *Leukemia Research*, *23*, 19–27.

Campbell, E. P., Quigley, I. K., & Kintner, C. (2016). Foxn4 promotes gene expression required for the formation of multiple motile cilia Foxn4 promotes gene expression required for the formation of multiple motile cilia. *Development*, *143*, 4654–4664. https://doi.org/10.1242/dev.149567

Carlsson, L., Nystrom, L.-E., Sundkvist, I., Markey, F., & Lindberg, U. (1977). Actin Polymerizability is Influenced by Profilin , a Low Molecular Weight Protein in Non-muscle Cells. *Journal of Molecular Biology*, *115*, 465–483.

Chailley, B., & Boisvieux-Ulrich, E. (1985). Detection of Plasma Membrane Cholesterol during Microvillogenesis and Ciliogenesis in Quail Oviduct. *The Journal of Histochemistry and Cytochemistry : Official Journal of the Histochemistry Society*, *33*(1), 1–10.

Chavali, P. L., Putz, M., & Gergely, F. (2014). Small organelle , big responsibility : the role of centrosomes in development and disease. *Philosophical Transactions of the Royal Society*, *369*, 1–12.

Chen, X., Zaro, J., & Shen, W.-C. (2013). Fusion Protein Linkers: Property, Design and Functionality. *Advanced Drug Delivery Review*, *65*(10), 1357–1369. https://doi.org/10.1016/j.addr.2012.09.039.Fusion

Chen, Y., & Struhl, G. (1998). In vivo evidence that Patched and Smoothened constitute distinct binding and transducing components of a Hedgehog receptor complex. *Development*, *125*, 4943–4948.

Cheung, H. O.-L., Zhang, X., Ribeiro, A., Mo, R., Makino, S., Puviindran, V., … Hui, C.-C. (2009). The kinesin protein Kif7 is a critical regulator of Gli transcription factors in mammalian hedgehog signaling. *Science Signaling*, *2*(76), ra29. https://doi.org/10.1126/scisignal.2000405

Chhin, B., Negre, D., Merrot, O., Pham, J., Tourneur, Y., Ressnikoff, D., … Bouvagnet, P. (2009). Ciliary beating recovery in deficient human airway epithelial cells after lentivirus ex vivo gene therapy. *PLoS Genetics*, *5*(3), 1–7. https://doi.org/10.1371/journal.pgen.1000422

Choksi, S. P., Babu, D., Lau, D., Yu, X., & Roy, S. (2014). Systematic discovery of novel ciliary genes through functional genomics in the zebrafish. *Development*, *141*, 3410–3419. https://doi.org/10.1242/dev.108209

Chung, M., Kwon, T., Tu, F., Brooks, E. R., Gupta, R., Meyer, M., … Wallingford, J. B. (2014). Coordinated genomic control of ciliogenesis and cell movement by RFX2. *eLife*, 1–23. https://doi.org/10.7554/eLife.01439

Cohen, H., & Davies, S. (1937). The Development of the cerebrospinal fluid spaces and choroid plexuses in the chick. *Journal of Anatomy*, *72*, 25–53.

Comartin, D., Gupta, G. D., Fussner, E., Coyaud, É., Hasegan, M., Archinti, M., … Pelletier, L. (2013a). CEP120 and SPICE1 cooperate with CPAP in centriole elongation. *Current Biology*, *23*(14), 1360–1366. https://doi.org/10.1016/j.cub.2013.06.002

Comartin, D., Gupta, G. D., Fussner, E., Coyaud, É., Hasegan, M., Archinti, M., … Pelletier, L. (2013b). CEP120 and SPICE1 cooperate with CPAP in centriole elongation. *Current Biology : CB*, *23*(14), 1360–6. https://doi.org/10.1016/j.cub.2013.06.002

Corbit, K. C., Aanstad, P., Singla, V., Norman, A. R., Stainier, D. Y. R., & Reiter, J. F. (2005). Vertebrate Smoothened functions at the primary cilium. *Nature*, *437*(7061), 1018–21. https://doi.org/10.1038/nature04117

Cortés, C. R., McInerney-Leo, A. M., Vogel, I., Rondón Galeano, M. C., Leo, P. J., Harris, J. E., … Wicking, C. (2016). Mutations in human C2CD3 cause skeletal dysplasia and provide new insights into phenotypic and cellular consequences of altered C2CD3 function. *Scientific Reports*, *6*(April), 1–10. https://doi.org/10.1038/srep24083

Craige, B., Tsao, C. C., Diener, D. R., Hou, Y., Lechtreck, K. F., Rosenbaum, J. L., & Witman, G. B. (2010). CEP290 tethers flagellar transition zone microtubules to the membrane and regulates flagellar protein content. *Journal of Cell Biology*, *190*(5), 927–940. https://doi.org/10.1083/jcb.201006105

Cruz, C., Ribes, V., Kutejova, E., Cayuso, J., Lawson, V., Norris, D., … Briscoe, J. (2010). Foxj1 regulates floor plate cilia architecture and modifies the response of cells to sonic hedgehog signalling. *Development (Cambridge, England)*, *137*(24), 4271–82. https://doi.org/10.1242/dev.051714

Cuevas, P., Angel, J., & Diaz, G. (1985). Absence of filipin-sterol complexes from the ciliary necklace of ependymal cells. *Anatomy and Embryology*, *1*(I 985), 97–99.

Czarnecki, P. G., & Shah, J. V. (2012). The ciliary transition zone: from morphology and molecules to medicine. *Trends in Cell Biology*, *22*(4), 201–10. https://doi.org/10.1016/j.tcb.2012.02.001

D.A. Ede, & Kelly, W. A. (1964). Developmental abnormalities in the trunk and limbs of the talpid3 mutant of the fowl. *Journal of Embryology and Experimental Morphology*, *12*(Part 2), 339–356.

Dafinger, C., Liebau, M. C., Elsayed, S. M., Hellenbroich, Y., Boltshauser, E., Korenke, G. C., & Fabretti, F. (2011). Mutations in KIF7 link Joubert syndrome with Sonic Hedgehog signaling and microtubule dynamics, *121*(7), 3–8. https://doi.org/10.1172/JCI43639.2662

Dale, R. M., Sisson, B. E., & Topczewski, J. (2009). The emerging role of Wnt/PCP signaling in organ formation. *Zebrafish*, *6*(1), 9–14. https://doi.org/10.1089/zeb.2008.0563

Dam, T. J. P. Van, Wheway, G., Slaats, G. G., Group, S. S., Huynen, M. A., & Giles, R. H. (2013). The SYSCILIA gold standard (SCGSv1) of known ciliary components and its applications within a systems biology consortium. *Cilia*, *2*(1), 1. https://doi.org/10.1186/2046-2530-2-7

Das, R. M., & Storey, K. G. (2014). Apical abscission, a novel cell biological mechanism regulating neurogenesis. *Neurogenesis*, *e29555*. https://doi.org/10.4161/neur.29555

Davey, M. G., James, J., Paton, I. R., Burt, D. W., & Tickle, C. (2007). Analysis of talpid3 and

wild-type chicken embryos reveals roles for Hedgehog signalling in development of the limb bud vasculature. *Developmental Biology*, *301*(1), 155–65. https://doi.org/10.1016/j.ydbio.2006.08.017

Davey, M. G., Mcteir, L., Barrie, M. A., Freem, L. J., & Stephen, L. A. (2014). Loss of cilia causes embryonic lung hypoplasia , liver fibrosis , and cholestasis in the talpid 3 ciliopathy mutant. *Organogenesis*, *10*(2), 177–185.

Davey, M. G., Paton, I. R., Yin, Y., Schmidt, M., Bangs, F. K., Morrice, D. R., … Burt, D. W. (2006). The chicken talpid3 gene encodes a novel protein essential for Hedgehog signaling. *Genes & Development*, *20*(10), 1365–77. https://doi.org/10.1101/gad.369106

Davey, M. G., Towers, M., Vargesson, N., & Tickle, C. (2018). The chick limb: Embryology, genetics and teratology. *International Journal of Developmental Biology*, *62*(1–3), 85–95. https://doi.org/10.1387/ijdb.170315CT

Dawe, H. R., Farr, H., & Gull, K. (2007). Centriole/basal body morphogenesis and migration during ciliogenesis in animal cells. *Journal of Cell Science*, *120*(Pt 1), 7–15. https://doi.org/10.1242/jcs.03305

Dawe, H. R., Minamide, L. S., Bamburg, J. R., & Cramer, L. P. (2003). ADF / Cofilin Controls Cell Polarity during Fibroblast Migration. *Current Biology*, *13*, 252–257.

Dean, S., Sunter, J. D., & Wheeler, R. J. (2017). TrypTag . org : A Trypanosome Protein Localisation Resource. *Trends in Parasitology*, *33*(2), 80–82. https://doi.org/10.1016/j.pt.2016.10.009

Doxsey, S. J., Stein, P., Evans, L., Calarco, P. D., & Kirschner, M. (1994). Pericentrin, a highly conserved centrosome protein involved in microtubule organization. *Cell*, *76*(4), 639–650. https://doi.org/10.1016/0092-8674(94)90504-5

Doxsey, S., McCollum, D., & Theurkauf, W. (2005). Centrosomes in cellular regulation. *Annual Review of Cell and Developmental Biology*, *21*, 411–34. https://doi.org/10.1146/annurev.cellbio.21.122303.120418

Doxsey, S., Zimmerman, W., & Mikule, K. (2005). Centrosome control of the cell cycle. *Trends in Cell Biology*, *15*(6), 303–311. https://doi.org/10.1016/j.tcb.2005.04.008

Dunker, A. K., Brown, C. J., Lawson, J. D., Iakoucheva, L. M., & Obradovic, Z. (2002). Current Topics Intrinsic Disorder and Protein Function. *Proteins*, *41*(21).

Dziegielewska, K. M., Ek, J., & Habgood, M. D. (2001). Development of the Choroid Plexus, *20*(June 2000), 5–20.

Ede, D. A., & Kelly, W. A. (1964). Developmental abnormalities in the head region of the talpid3 mutant of the fowl. *Journal of Embryology and Experimental Morphology*, *12*(Part 1), 161–182.

Eguether, T., Cordelieres, F. P., & Pazour, G. J. (2018). Intraflagellar transport is deeply integrated in hedgehog signaling. *Molecular Biology of the Cell*, *29*(10), 1178–1189. https://doi.org/10.1091/mbc.E17-10-0600

Eguether, T., San Agustin, J. T., Keady, B. T., Jonassen, J. A., Liang, Y., Francis, R., … Pazour, G. J. (2014). IFT27 Links the BBSome to IFT for Maintenance of the Ciliary Signaling Compartment. *Developmental Cell*, *31*(3), 279–290. https://doi.org/10.1016/j.dci.2009.07.003.Characterization

Ehlen, H. W. a, Buelens, L. a, & Vortkamp, A. (2006). Hedgehog signaling in skeletal development. *Birth Defects Research*, *78*, 267–279. https://doi.org/10.1002/bdrc.20076

Ekblom, P. (1989). Developmentally regulated conversion of mesenchyme to epithelium. *The FASEB Journal*, *3*, 2141–2150.

El Zein, L., Ait-lounis, A., Morlé, L., Thomas, J., Chhin, B., Spassky, N., … Durand, B. (2009). RFX3 governs growth and beating efficiency of motile cilia in mouse and controls the

expression of genes involved in human ciliopathies. *Journal of Cell Science*, *122*, 3180–3189. https://doi.org/10.1242/jcs.048348

Escobar-Aguirre, M., Zhang, H., Jamieson-Lucy, A., & Mullins, M. C. (2017). Microtubule-actin crosslinking factor 1 (Macf1) domain function in Balbiani body dissociation and nuclear positioning. *PLoS Genetics*, *1*, 1–29.

Fan, S., Hurd, T. W., Liu, C., Straight, S. W., Weimbs, T., Hurd, E. A., … Margolis, B. (2004). Polarity Proteins Control Ciliogenesis via Kinesin Motor Interactions. *Current Biology*, *14*, 1451–1461. https://doi.org/10.1016/j

Farina, F., Gaillard, J., Guérin, C., Couté, Y., Sillibourne, J., Blanchoin, L., & Théry, M. (2016). The centrosome is an actin-organizing centre. *Nature Cell Biology*, *18*(1), 65–75. https://doi.org/10.1038/ncb3285

Fetter, J., Samsonov, A., Zenser, N., Zhang, F., Zhang, H., & Malkov, D. (2015). Endogenous Gene Tagging with Fluorescent Proteins. *Methods in Molecular Biology*, *1239*.

Finetti, F., Paccani, S. R., Riparbelli, M. G., Giacomello, E., Perinetti, G., Pazour, G. J., … Baldari, C. T. (2009). Intraflagellar transport is required for polarized recycling of the TCR/CD3 complex to the immune synapse. *Nature Cell Biology*, *11*(11), 1332–1339. https://doi.org/10.1038/ncb1977.Intraflagellar

Fleming, L. R., Doherty, D. A., Parisi, M. A., Glass, I. A., Bryant, J., Fischer, R., … Gunay-Aygun, M. (2017). Prospective Evaluation of Kidney Disease in Joubert Syndrome. *Clinical Journal of the American Society of Nephrology*, *12*(12), 1962–1973.

Fu, J., Hagan, I. M., & Glover, D. M. (2015). The Centrosome and Its Duplication Cycle. *Cold Spring Harbor Perspectives in Biology*, *7*, 1–36.

Fuller, S. D., Gowen, B. E., Reinsch, S., Sawyer, A., Buendiat, B., Wepf, R., & Karsentit, E. (1995). The core of the mammalian centriole contains γ-tubulin. *Current Biology*, *5*(12), 1384–1393.

Gabriel, E., Ramani, A., Karow, U., Gottardo, M., Natarajan, K., Gooi, L. M., … Gopalakrishnan, J. (2017). Recent Zika Virus Isolates Induce Premature Differentiation of Neural Progenitors in Human Brain Organoids. *Cell Stem Cell*, *20*(3), 397–406. https://doi.org/10.1016/j.stem.2016.12.005

Gabriel, E., Wason, A., Ramani, A., Gooi, L. M., Keller, P., Pozniakovsky, A., … Gopalakrishnan, J. (2016). CPAP promotes timely cilium disassembly to maintain neural progenitor pool. *The EMBO Journal*, *35*(8), 803–819. https://doi.org/10.15252/embj.201593679

Galati, D. F., Sullivan, K. D., Pham, A. T., Espinosa, J. M., & Pearson, C. G. (2018). Trisomy 21 Represses Cilia Formation and Function. *Developmental Cell*, *46*, 641–650. https://doi.org/10.1016/j.devcel.2018.07.008

Gerdes, J. M., Liu, Y., Zaghloul, N. A., Leitch, C. C., Lawson, S. S., Kato, M., … Katsanis, N. (2007). Disruption of the basal body compromises proteasomal function and perturbs intracellular Wnt response. *Nature Genetics*, *39*(11), 1350–1360. https://doi.org/10.1038/ng.2007.12

Ghosh, M., Song, X., Mouneimne, G., Sidani, M., Lawrence, D. S., & Condeelis, J. S. (2004). Cofilin Promotes Actin Polymerization and Defines the Direction of Cell Motility. *Science*, *304*, 743–747.

Gibbons, I. R., & Grimstone, A. V. (1960). On flagellar structure in certain flagellates. *J Biophys Biochem Cytol*, *7*(4), 697–716. https://doi.org/10.1083/jcb.7.4.697

Gibson, T. J., Seiler, M., & Veitia, R. A. (2013). The transience of transient overexpression. *Nature Publishing Group*, *10*(8), 715–721. https://doi.org/10.1038/nmeth.2534

Gleeson, J. G., Keeler, L. C., Parisi, M. a, Marsh, S. E., Chance, P. F., Glass, I. a, … Dobyns, W. B. (2004). Molar tooth sign of the midbrain-hindbrain junction: occurrence in multiple distinct syndromes. *American Journal of Medical Genetics. Part A*, *125A*, 125–134.

https://doi.org/10.1002/ajmg.a.20437

Godinho, S. A., & Pellman, D. (2014). Causes and consequences of centrosome abnormalities in cancer.

Goetz, S. C., Ocbina, P. J. R., & Anderson, K. V. (2009). The Primary Cilium as a Hedgehog Signal Transduction Machine. *Methods Cell Biology*, *94*, 199–222. https://doi.org/10.1016/S0091-679X(08)94010-3.The

Goode, B. L., Drubin, D. G., & Lappalainen, P. (1998). Regulation of the Cortical Actin Cytoskeleton in Budding Yeast by Twinfilin, a Ubiquitous Actin Monomer-sequestering Protein. *Journal of Cell Biology*, *142*(3), 723–733.

Goodrich, L. V, Johnson, R. L., Milenkovic, L., McMahon, J. a, & Scott, M. P. (1996). Conservation of the hedgehog/patched signaling pathway from flies to mice: induction of a mouse patched gene by Hedgehog. *Genes & Development*, *10*(3), 301–312. https://doi.org/10.1101/gad.10.3.301

Gould, R. O. Y. R., & Borisy, G. G. (1977). The pericentrioalr material in chinese hamster ovar cells nucleates microtubule formation. *Journal of Cell Biology*, *73*, 601–615.

Graser, S., Stierhof, Y., Lavoie, S. B., Gassner, O. S., Lamla, S., Clech, M. Le, & Nigg, E. A. (2007). Cep164, a novel centriole appendage protein required for primary cilium formation, *179*(2), 321–330. https://doi.org/10.1083/jcb.200707181

Gray, R. S., Abitua, P. B., Wlodarczyk, B. J., Szabo-Rogers, H. L., Blanchard, O., Lee, I., … Finnell, R. H. (2009). The planar cell polarity effector Fuz is essential for targeted membrane trafficking, ciliogenesis and mouse embryonic development. *Nature Cell Biology*, *11*(10), 1225–32. https://doi.org/10.1038/ncb1966

Gudi, R., Zou, C., Li, J., & Gao, Q. (2011). Centrobin-tubulin interaction is required for centriole elongation and stability. *Journal of Cell Biology*, *193*(4), 711–725. https://doi.org/10.1083/jcb.201006135

Guernsey, D. L., Jiang, H., Hussin, J., Arnold, M., Bouyakdan, K., Perry, S., … Samuels, M. E. (2010). Mutations in centrosomal protein CEP152 in primary microcephaly families linked to MCPH4. *American Journal of Human Genetics*, *87*(1), 40–51. https://doi.org/10.1016/j.ajhg.2010.06.003

Guichard, P., Hachet, V., Majubu, N., Neves, A., Demurtas, D., Olieric, N., … Steinmetz, M. O. (2013). Native Architecture of the Centriole Proximal Region Reveals Features Underlying Its 9-Fold Radial Symmetry, 1620–1628. https://doi.org/10.1016/j.cub.2013.06.061

Gupta, G. D., Coyaud, É., Goncalves, C., Mojarad, B. A., Liu, Y., Wu, Q., … Pelletier, L. (2015). A dynamic protein interaction landscape of the human centrosome-cilium interface, *25*(3), 1–30. https://doi.org/10.1016/j.pmr.2014.05.001.Functional

Habedanck, R., Stierhof, Y. D., Wilkinson, C. J., & Nigg, E. A. (2005). The Polo kinase Plk4 functions in centriole duplication. *Nature Cell Biology*, *7*(11), 1140–1146. https://doi.org/10.1038/ncb1320

Habermann, K., & Lange, B. M. H. (2012). New insights into subcomplex assembly and modifications of centrosomal proteins, (108), 1–10.

Hakem, A., Sanchez-sweatman, O., You-ten, A., Duncan, G., Wakeham, A., Khokha, R., & Mak, T. W. (2005). RhoC is dispensable for embryogenesis and tumor initiation but essential for metastasis. *Genes and Development*, *19*, 1974–1979. https://doi.org/10.1101/gad.1310805.1974

Happé, H., Heer, E. De, & Peters, D. J. M. (2011). Polycystic kidney disease: The complexity of planar cell polarity and signaling during tissue regeneration and cyst formation. *Biochemica et Biophysica Acta*, *1812*(10), 1249–1255. https://doi.org/10.1016/j.bbadis.2011.05.005

Haycraft, C. J., Banizs, B., Aydin-Son, Y., Zhang, Q., Michaud, E. J., & Yoder, B. K. (2005). Gli2

and Gli3 localize to cilia and require the intraflagellar transport protein polaris for processing and function. *PLoS Genetics*, *1*(4), e53. https://doi.org/10.1371/journal.pgen.0010053

Hildebrandt, F., Benzing, T., & Katsanis, N. (2011). Ciliopathies. *The New England Journal of Medicine*, *364*(16), 1533–1543.

Hirono, M. (2014). Cartwheel assembly. *Philosophical Transactions of the Royal Society of London. Series B, Biological Sciences*, *369*(1650), 20130458-. https://doi.org/10.1098/rstb.2013.0458

Hirose, Y., Itoh, T., & Miyajima, A. (2009). Hedgehog signal activation coordinates proliferation and differentiation of fetal liver progenitor cells. *Experimental Cell Research*, *315*(15), 2648–57. https://doi.org/10.1016/j.yexcr.2009.06.018

Ho, N. C., Francomano, C. a, & van Allen, M. (2000). Jeune asphyxiating thoracic dystrophy and short-rib polydactyly type III (Verma-Naumoff) are variants of the same disorder. *American Journal of Medical Genetics*, *90*(4), 310–4. Retrieved from http://www.ncbi.nlm.nih.gov/pubmed/10710229

Homem, C. C. F., Repic, M., & Knoblich, J. A. (2016). Proliferation control in neural stem and progenitor cells. *Nature Reviews Neuroscience*, *16*(11), 647–659. https://doi.org/10.1038/nrn4021.Proliferation

Hori, A., & Toda, T. (2017). Regulation of centriolar satellite integrity and its physiology. *Cellular and Molecular Life Sciences*, *74*, 213–229. https://doi.org/10.1007/s00018-016-2315-x

Horvath, P., Aulner, N., Bickle, M., Davies, A. M., Nery, E. Del, Ebner, D., … Carragher, N. O. (2016). Screening out irrelevant cell-based models of disease. *Nature Publishing Group*, *15*(11), 751–769. https://doi.org/10.1038/nrd.2016.175

Huang, L., & Lipschutz, J. H. (2014). Cilia and Polycystic Kidney Disease, Kith and Kin. *Birth Defects Research. Part C, Embryo Today*, *102*(2), 174–185. https://doi.org/10.1002/bdrc.21066.Cilia

Huang, P., & Schier, A. F. (2009). Dampened Hedgehog signaling but normal Wnt signaling in zebrafish without cilia. *Development*, *136*, 3089–3098. https://doi.org/10.1242/dev.041343

Huangfu, D., Liu, A., Rakeman, A. S., & Murcia, N. S. (2003). Hedgehog signalling in the mouse requires intraflagellar transport proteins. *Nature*, *426*(November), 83–87. https://doi.org/10.1038/nature02080.1.

Huber, C., & Cormier-Daire, V. (2012). Ciliary disorder of the skeleton. *American Journal of Medical Genetics*, *160C*(3).

Inaba, K., & Mizuno, K. (2016). Sperm dysfunction and ciliopathy. *Reproductive Medicine and Biology*, *15*(2), 77–94. https://doi.org/10.1007/s12522-015-0225-5

Ishikawa, H., Kubo, A., Tsukita, S., & Tsukita, S. (2005). Odf2-deficient mother centrioles lack distal/subdistal appendages and the ability to generate primary cilia. *Nature Cell Biology*, *7*(5), 517–24. https://doi.org/10.1038/ncb1251

Ishikawa, H., & Marshall, W. F. (2011). Ciliogenesis: building the cell's antenna. *Nature Reviews. Molecular Cell Biology*, *12*(4), 222–34. https://doi.org/10.1038/nrm3085

Jaffe, A. B., & Hall, A. (2005). Rho GTPases : Biochemistry and Biology. *Annual Review of Cell and Developmental Biology*, *21*, 247–269. https://doi.org/10.1146/annurev.cellbio.21.020604.150721

Jakobsen, L., Vanselow, K., Skogs, M., Toyoda, Y., Lundberg, E., Poser, I., … Andersen, J. S. (2011). Novel asymmetrically localizing components of human centrosomes identified by complementary proteomics methods. *The EMBO Journal*, *30*(8), 1520–35. https://doi.org/10.1038/emboj.2011.63

Jin, H., White, S. R., Shida, T., Schulz, S., Aguiar, M., Gygi, S. P., … Nachury, M. V. (2010). The

conserved Bardet-Biedl Syndrome proteins assemle a coat that traffics membrane proteins to cilia. *Cell*, *141*(7), 1208–1219. https://doi.org/10.1016/j.cell.2010.05.015.The

Jones, C., Roper, V. C., Foucher, I., Qian, D., Banizs, B., Petit, C., … Chen, P. (2008). Ciliary proteins link basal body polarization to planar cell polarity regulation. *Nature Genetics*, *40*(1), 69–77. https://doi.org/10.1038/ng.2007.54

Joshi, H. C., Palacios, M. J., McNamara, L., & Cleveland, D. W. (1992). Gamma tublin is a centrosomal protein required for cell cycle-dependent microtubule nucleation. *Letters to Nature*, *356*, 80–83.

Jurczyk, A., Gromley, A., Redick, S., San Agustin, J., Witman, G., Pazour, G. J., … Doxsey, S. (2004). Pericentrin forms a complex with intraflagellar transport proteins and polycystin-2 and is required for primary cilia assembly. *Journal of Cell Biology*, *166*(5), 637–643. https://doi.org/10.1083/jcb.200405023

Kanai, M., Crowe, M. S., Zheng, Y., Woude, G. F. Vande, & Fukasawa, K. (2011). RhoA and RhoC Are Both Required for the ROCK II-Dependent Promotion of Centrosome Duplication. *Oncogene*, *29*(45), 6040–6050. https://doi.org/10.1038/onc.2010.328.RhoA

Kang, K., Bae, J., Han, K., Kim, E. S., Kim, T., & Yi, J. M. (2016). A Genome-Wide Methylation Approach Identifies a New Hypermethylated Gene Panel in Ulcerative Colitis. *International Journal of Molecular Sciences*, *17*, 1–12. https://doi.org/10.3390/ijms17081291

Karakesisoglou, I., Yang, Y., & Fuchs, E. (2000). An Epidermal Plakin that Integrates Actin and Microtubule Networks at Cellular Junctions. *The Journal of Cell Biology*, *149*(1), 195–208.

Karp, N. A., Huber, W., Sadowski, P. G., Charles, P. D., Hester, S. V, & Lilley, K. S. (2010). Addressing Accuracy and Precision Issues in iTRAQ Quantitation. *Molecular & Cellular Proteomics*, 1885–1897. https://doi.org/10.1074/mcp.M900628-MCP200

Karp, N. A., Spencer, M., Lindsay, H., Dell, K. O., & Lilley, K. S. (2005). Impact of Replicate Types on Proteomic Expression Analysis. *Journal of Proteome Research*, *4*, 1867–1871. https://doi.org/10.1021/pr050084g

Kaur, G., & Dufour, J. M. (2012). Cell lines valuable tools or useless artifacts, *2*(1), 1–5.

Keeling, J., Tsiokas, L., & Maskey, D. (2016). Cellular Mechanisms of Ciliary Length Control. *Cells*, *5*(1).

Kim, D. I., Jensen, S. C., Berendra, K. C., Roux, K. H., Motamedchaboki, K., & Roux, K. J. (2016). An improved smaller biotin ligase for BioID proximity labeling. *Molecular Biology of the Cell*, *27*(8), 1188–1196. https://doi.org/10.1091/mbc.E15-12-0844

Kitagawa, D., Kohlmaier, G., Keller, D., Strnad, P., Balestra, F. R., Fluckiger, I., & Gonczy, P. (2011). Spindle positioning in human cells relies on proper centriole formation and on the microcephaly proteins CPAP and STIL. *Journal of Cell Science*, *124*(22), 3884–3893. https://doi.org/10.1242/jcs.089888

Knowles, M. R., Daniels, L. A., Davis, S. D., Zariwala, M. A., & Leigh, M. W. (2013). Primary Ciliary Dyskinesia. Recent Advances in Diagnostics, Genetics and Characterization of Clinical Disease. *American Journal of Critcal Care Medicine*, *188*(8), 913–922.

Kobayashi, T., & Dynlacht, B. D. (2011). Regulating the transition from centriole to basal body. *The Journal of Cell Biology*, *193*(3), 435–44. https://doi.org/10.1083/jcb.201101005

Kobayashi, T., Kim, S., Lin, Y. C., Inoue, T., & Dynlacht, B. D. (2014). The CP110-interacting proteins talpid3 and cep290 play overlapping and distinct roles in cilia assembly. *Journal of Cell Biology*, *204*(2), 215–229. https://doi.org/10.1083/jcb.201304153

Komiya, Y., & Habas, R. (2008). Wnt signal transduction pathways. *Organogenesis*, *4*(2), 68–

75.

Krause, M., & Gautreau, A. (2014). Steering cell migration : lamellipodium dynamics and the regulation of directional persistence. *Nature Publishing Group*, *15*(9), 577–590. https://doi.org/10.1038/nrm3861

Krishnan, K., & Moens, P. D. J. (2009). Structure and functions of profilins. *Biophysical Reviews*, *2*, 71–81. https://doi.org/10.1007/s12551-009-0010-y

Lancaster, M. A., Renner, M., Martin, C. A., Wenzel, D., Bicknell, L. S., Hurles, M. E., … Knoblich, J. A. (2013). Cerebral organoids model human brain development and microcephaly. *Nature*, *501*, 373–379. https://doi.org/10.1038/nature12517

Lapébie, P., Borchiellini, C., & Houliston, E. (2011). Dissecting the PCP pathway: One or more pathways?: Does a separate Wnt-Fz-Rho pathway drive morphogenesis? *BioEssays*, *33*, 759–768. https://doi.org/10.1002/bies.201100023

Lappalainen, P., & Drubin, D. G. (1997). Cofilin promotes rapid actin filament turnover in vivo Cofilin promotes rapid actin filament turnover in vivo. *Letters to Nature*, *389*(September), 1–6.

Larkins, C. E., Gonzalez, G. D., East, M. P., Kahn, R. A., & Brennwald, P. (2011). Arl13b regulates ciliogenesis and the dynamic localization of Shh signaling proteins. https://doi.org/10.1091/mbc.E10-12-0994

Lavoir, M. Van De, Diamond, J. H., Leighton, P. A., Mather-love, C., Heyer, B. S., Bradshaw, R., … Etches, R. J. (2006). Germline transmission of genetically modified primordial germ cells, *441*(June), 766–769. https://doi.org/10.1038/nature04831

Lechtreck, K. F. (2015). IFT-Cargo Interactions and Protein Transport in Cilia. *Trends in Biochemical Sciences*, *40*(12), 765–778. https://doi.org/10.1016/j.tibs.2015.09.003

Lein, E. S., Hawrylycz, M. J., Ao, N., Ayres, M., Bensinger, A., Bernard, A., … Jones, A. R. (2007). Genome-wide atlas of gene expression in the adult mouse brain, *445*(January). https://doi.org/10.1038/nature05453

Li, J., Wang, C., Wu, C., Cao, T., Xu, G., & Meng, Q. (2017). PKA-mediated Gli2 and Gli3 phosphorylation is inhibited by Hedgehog signaling in cilia and reduced in Talpid3 mutant. *Developmental Biology*, *429*(1), 147–157. https://doi.org/10.1016/j.ydbio.2017.06.035

Li, S., Fernandez, J., Marshall, W. F., & Agard, D. A. (2012). Three-dimensional structure of basal body triplet revealed by electron cryo-tomography. *The EMBO Journal*, *31*(3), 552–562. https://doi.org/10.1038/emboj.2011.460

Li, X., Liu, B., Ji, C. N., Kang, Y., & Mao, Y. (2006). Cloning and Expression of ARMC3 _ v2 , a Novel Splicing Variant of Human ARMC3 Gene *. *Russian Journal of Genetics*, *42*(7), 824–828. https://doi.org/10.1134/S1022795406070209

Liem, K. F., He, M., Jymmiel, P., Ocbina, R., & Anderson, K. V. (2009). Mouse Kif7 / Costal2 is a cilia-associated protein that regulates Sonic hedgehog signaling, *106*(32), 13377–13382.

Lin, Y.-N., Wu, C.-T., Lin, Y.-C., Hsu, W.-B., Tang, C.-J. C., Chang, C.-W., & Tang, T. K. (2013). CEP120 interacts with CPAP and positively regulates centriole elongation. *The Journal of Cell Biology*, *202*(2), 211–9. https://doi.org/10.1083/jcb.201212060

Lippincott-Schwartz, J., & Patterson, G. H. (2003). Development and Use of Fluorescent Protein Markers in Living Cells. *Science*, *300*(5616), 87–91.

Liu, A., Wang, B., & Niswander, L. a. (2005). Mouse intraflagellar transport proteins regulate both the activator and repressor functions of Gli transcription factors. *Development (Cambridge, England)*, *132*(13), 3103–11. https://doi.org/10.1242/dev.01894

Lizio, M., Harshbarger, J., Shimoji, H., Severin, J., Kasukawa, T., Sahin, S., … Kawaji, H. (2015). Gateways to the FANTOM5 promoter level mammalian expression atlas. *Genome Biology*, *16*(22), 1–14. https://doi.org/10.1186/s13059-014-0560-6

Lopes, C. A. M., Prosser, S. L., Romio, L., Hirst, R. A., Callaghan, C. O., Woolf, A. S., & Fry, A. M. (2011). Centriolar satellites are assembly points for proteins implicated in human ciliopathies , including oral-facial- digital syndrome 1, *1*, 600–612. https://doi.org/10.1242/jcs.077156

Macdonald, J., Glover, J. D., Taylor, L., Sang, H. M., & McGrew, M. J. (2010). Characterisation and germline transmission of cultured avian primordial germ cells. *PloS One*, *5*(11), e15518. https://doi.org/10.1371/journal.pone.0015518

Madden, S. F., Clarke, C., Stordal, B., Carey, M. S., Broaddus, R., Gallagher, W. M., … Hennessy, B. T. (2014). OvMark : a user-friendly system for the identification of prognostic biomarkers in publically available ovarian cancer gene expression datasets. *Molecular Cancer*, *13*(241), 1–11.

Mahjoub, M. R., Xie, Z., & Stearns, T. (2010). Cep120 is asymmetrically localized to the daughter centriole and is essential for centriole assembly, *191*(2), 331–346. https://doi.org/10.1083/jcb.201003009

Malicdan, M. C. V, Vilboux, T., Stephen, J., Maglic, D., Mian, L., Konzman, D., … Gunay-Aygun, M. (2015). Mutations in human homologue of chicken talpid3 gene (KIAA0586) cause a hybrid ciliopathy with overlapping features of Jeune and Joubert syndromes. *Journal of Medical Genetics*, *52*(12), 830–9. https://doi.org/10.1136/jmedgenet-2015-103316

Malvezzi, J. V. M., Magalhaes, I. H., Costa, S. S., Otto, P. A., Rosenberg, C., Bertola, D. R., … Krepischi, A. C. V. (2018). KIF11 microdeletion is associated with microcephaly , chorioretinopathy and intellectual disability. *Human Genome Variation*, *5*, 1–3. https://doi.org/10.1038/hgv.2018.10

Maria, B. L., Boltshauser, E., Palmer, S. C., & Tran, T. X. (1999). Clinical features and revised diagnostic criteria in Joubert syndrome. *Journal of Child Neurology*, *14*(9), 581–583. https://doi.org/10.1177/088307389901400906

Marigo, V., Scott, M. P., Johnson, R. L., Goodrich, L. V, & Tabin, C. J. (1996). Conservation in hedgehog signaling : induction of a chicken patched homolog by Sonic hedgehog in the developing limb, *1233*, 1225–1233.

Marthiens, V., Rujano, M. A., Pennetier, C., Tessier, S., Paul-Gilloteaux, P., & Basto, R. (2013). Centrosome amplification causes microcephaly. *Nature Cell Biology*, *15*(7), 731–740. https://doi.org/10.1038/ncb2746

Masters, J. R., & Stacey, G. N. (2007). Changing medium and passaging cell lines, *2*(9), 2276–2284. https://doi.org/10.1038/nprot.2007.319

Masyuk, A. I., Masyuk, T. V, Splinter, P. L., Huang, B. Q., Stroope, A. J., & LaRusso, N. F. (2006). Cholangiocyte cilia detect changes in luminal fluid flow and transmit them into intracellular Ca2+ and cAMP signaling. *Gastroenterology*, *131*(3), 911–20. https://doi.org/10.1053/j.gastro.2006.07.003

May-Simera, H. L., Gumerson, J. D., Gao, C., Campos, M., Stephanie, M., Beyer, T., … Li, T. (2016). Loss of MACF1 abolishes ciliogenesis and disrupts apicobasal polarity establishment in the retina, *17*(5), 1399–1413. https://doi.org/10.1016/j.celrep.2016.09.089.Loss

May-Simera, H. L., & Kelley, M. W. (2012). Cilia, Wnt signaling, and the cytoskeleton. *Cilia*, *1*(1), 1–16. https://doi.org/10.1186/2046-2530-1-7

May, S. R., Ashique, A. M., Karlen, M., Wang, B., Shen, Y., Zarbalis, K., … Peterson, A. S. (2005). Loss of the retrograde motor for IFT disrupts localization of Smo to cilia and prevents the expression of both activator and repressor functions of Gli. *Developmental Biology*, *287*(2), 378–89. https://doi.org/10.1016/j.ydbio.2005.08.050

Mcgorum, B. C., Pirie, R. S., Eaton, S. L., Keen, J. A., Cumyn, E. M., Arnott, D. M., … Wishart, T. M. (2015). Proteomic Profiling of Cranial (Superior) Cervical Ganglia Reveals Beta-Amyloid and Ubiquitin Proteasome System Perturbations in an Equine Multiple System Neuropathy * □. *Molecular and Cellular Proteomics*, 3072–3086.

https://doi.org/10.1074/mcp.M115.054635

Mcintyre, J. C., Davis, E. E., Joiner, A., Williams, C. L., Tsai, I., Jenkins, P. M., … Martens, J. R. (2012). Gene therapy rescues cilia defects and restores olfactory function in a mammalian ciliopathy model. *Nature Me*, *18*(9), 1423–1428. https://doi.org/10.1038/nm.2860.Gene

McIntyre, J. C., Williams, C. L., & Martens, J. R. (2013). Smelling the Roses and Seeing the Light: Gene Therapy for Ciliopathies. *Trends Biotechnology*, *31*(6), 355–363. https://doi.org/10.1021/nl061786n.Core-Shell

Mitchison, H. M., & Valente, E. M. (2017). Motile and non-motile cilia in human pathology: from function to phenotypes. *The Journal of Pathology*, *241*, 294–309.

Mitchison, T., & Kirschner, M. (1984). Microtubule assembly nucleated by isolated centrosomes. *Nature*, *312*, 232–237.

Mohammed, M. B. H. (1986). Vascular system in the developing wing bud of normal and talpid mutant chick embryos. *Cell Differenitation*, *19*, 133–137.

Mönnich, M., Borgeskov, L., Breslin, L., Jakobsen, L., Rogowski, M., Doganli, C., … Pedersen, L. B. (2018). CEP128 Localizes to the Subdistal Appendages of the Mother Centriole and Regulates TGF-β/BMP Signaling at the Primary Cilium. *Cell Reports*, *22*(10), 2601–2614. https://doi.org/10.1016/j.celrep.2018.02.043

Montero, J. A., Zuzarte-luis, V., Garcia-martinez, V., & Hurle, J. M. (2007). Role of RhoC in digit morphogenesis during limb development, *303*, 325–335. https://doi.org/10.1016/j.ydbio.2006.11.019

Nachury, M. V, Loktev, A. V, Zhang, Q., Westlake, C. J., Peränen, J., Merdes, A., … Jackson, P. K. (2007). A core complex of BBS proteins cooperates with the GTPase Rab8 to promote ciliary membrane biogenesis. *Cell*, *129*(6), 1201–13. Retrieved from http://www.ncbi.nlm.nih.gov/pubmed/17574030

Nagai, T., Ibata, K., Park, E. S., Kubota, M., Mikoshiba, K., & Miyawaki, A. (2001). A variant of yellow fluorescent protein with fast and efficient maturation for cell-biological applications. *Nature Biotechnology*, *20*, 87–90.

Nagaraj, N., Wisniewski, J. R., Geiger, T., Cox, J., Kircher, M., Kelso, J., … Mann, M. (2011). Deep proteome and transcriptome mapping of a human cancer cell line, *60*(548), 1–8. https://doi.org/10.1038/msb.2011.81

Naharros, I. O., Cristi, F. B., Zang, J., Gesemann, M., Ingham, P. W., Neuhauss, S. C. F., & Bachmann-gagescu, R. (2018). The ciliopathy protein TALPID3 / KIAA0586 acts upstream of Rab8 activation in zebrafish photoreceptor outer segment formation and maintenance, (January), 1–13. https://doi.org/10.1038/s41598-018-20489-9

Nakayama, K., & Katoh, Y. (2018). Ciliary protein trafficking mediated by IFT and BBSome complexes with the aid of kinesin-2 and dynein-2 motors. *Journal of Biochemistry*, *163*(3), 155–164. https://doi.org/10.1093/jb/mvx087

Nie, H., Crooijmans, R. P. M. A., Lammers, A., Schothorst, E. M. Van, Keijer, J., Neerincx, P. B. T., … Groenen, M. A. M. (2010). Gene Expression in Chicken Reveals Correlation with Structural Genomic Features and Conserved Patterns of Transcription in the Terrestrial Vertebrates, *5*(8), 1–7. https://doi.org/10.1371/journal.pone.0011990

Nigg, E. a., & Stearns, T. (2011). The centrosome cycle: Centriole biogenesis, duplication and inherent asymmetries. *Nature Cell Biology*, *13*(10), 1154–1160. https://doi.org/10.1038/ncb2345

Nishida, E., Maekawa, S., & Sakai, H. (1984). Cofilin, a Protein in Porcine Brain That Binds to Actin Filaments and Inhibits Their Interactions with Myosin and Tropomyosin. *Biochemistry*, 5307–5313. https://doi.org/10.1021/bi00317a032

Nogales-Cadenas, R., Abascal, F., Diez-Perez, J., Carazo, J. M., & Pascual-Montano, A. (2009). CentrosomeDB : a human centrosomal proteins database, *37*(October 2008), 175–

180. https://doi.org/10.1093/nar/gkn815

Novarino, G., Akizu, N., & Gleeson, J. G. (2011). Modeling Human Disease in Humans : the Ciliopathies, *147*(1), 70–79. https://doi.org/10.1016/j.cell.2011.09.014.Modeling

Novorol, C., Burkhardt, J., Wood, K. J., Iqbal, A., Roque, C., Coutts, N., … Harris, W. A. (2013). Microcephaly models in the developing zebrafish retinal neuroepithelium point to an underlying defect in metaphase progression. *Open Biology*, *3*, 1–16.

Ocbina, P. J. R., Tuson, M., & Anderson, K. V. (2009). Primary Cilia Are Not Required for Normal Canonical Wnt Signaling in the Mouse Embryo. *PloS One*, *4*(8), 1–8. https://doi.org/10.1371/journal.pone.0006839

Ochoa, B., Syn, W.-K., Delgado, I., Karaca, G. F., Jung, Y., Wang, J., … Diehl, A. M. (2010). Hedgehog signaling is critical for normal liver regeneration after partial hepatectomy in mice. *Hepatology (Baltimore, Md.)*, *51*(5), 1712–23. https://doi.org/10.1002/hep.23525

Oh, E. C., & Katsanis, N. (2013). Context-Dependent Regulation of Wnt Signaling through the Primary Cilium. *Journal of the American Society of Nephrology*, *24*, 10–18. https://doi.org/10.1681/ASN.2012050526

Ohashi, K. (2015). Roles of cofilin in development and its mechanisms of regulation, 275–290. https://doi.org/10.1111/dgd.12213

Oishi, I., Kawakami, Y., Raya, Á., Callol-Massot, C., & Belmonte, J. C. I. (2006). Regulation of primary cilia formation and left-right patterning in zebrafish by a noncanonical Wnt signaling mediator, duboraya. *Nature Genetics*, *38*(11), 1316–1322. https://doi.org/10.1038/ng1892

Orkin, S. H., & Zon, L. I. (2008). Review Hematopoiesis : An Evolving Paradigm for Stem Cell Biology, 631–644. https://doi.org/10.1016/j.cell.2008.01.025

Ostrowski, L. E. (2002). A Proteomic Analysis of Human Cilia: Identification of Novel Components. *Molecular & Cellular Proteomics*, *1*(6), 451–465. https://doi.org/10.1074/mcp.M200037-MCP200

Otto, E. A., Schermer, B., Obara, T., Toole, J. F. O., Hiller, K. S., Mueller, A. M., … Hildebrandt, F. (2003). Mutations in INVS encoding inversin cause nephronophthisis type 2, linking renal cystic disease to the function of primary cilia and left-right axis determination. *Nature Genetics*, *34*(4), 413–420. https://doi.org/10.1038/ng1217.Mutations

Ow, S. Y., Salim, M., Noirel, J., Evans, C., & Wright, P. C. (2011). Minimising iTRAQ ratio compression through understanding LC-MS elution dependence and high-resolution HILIC fractionation, (ii), 2341–2346. https://doi.org/10.1002/pmic.201000752

Pace, D. M. D. E., & Esfahani, M. (1987). The Effects of Cholesterol Depletion on Cellular Morphology. *The Anatomical Record*, *143*, 135–143.

Palmer, E., & Freeman, T. (2004). Investigation into the use of C- and N-terminal GFP fusion proteins for subcellular localization studies using reverse transfection microarrays. *Comparative and Functional Genomics*, *5*, 342–353. https://doi.org/10.1002/cfg.405

Palmgren, S., Vartiainen, M., & Lappalainen, P. (2002). Twinfilin, a molecular mailman for actin monomers. *Journal of Cell Science*.

Pan, J., You, Y., Huang, T., & Brody, S. L. (2007). RhoA-mediated apical actin enrichment is required for ciliogenesis and promoted by Foxj1. *Journal of Cell Science*, *120*(Pt 11), 1868–76. https://doi.org/10.1242/jcs.005306

Papakrivopoulou, E., Dean, C. H., Copp, A. J., & Long, D. A. (2014). Planar cell polarity and the kidney. *Nephrology Dialysis Transplantatino*, *29*(7), 1320–1326. https://doi.org/10.1093/ndt/gft484

Papaliagkas, V., Anogianaki, A., Anogianakis, G., & Ilonidis, G. (2007). The proteins and the mechanisms of apoptosis : A mini-review of the fundamentals. *Hippokratia*, *11*(3), 108–113.

Parisi, M. A. (2009). Clinical and molecular features of Joubert syndrome and related disorders, (4), 326–340. https://doi.org/10.1002/ajmg.c.30229.Clinical

Parisi, M. A., Doherty, D., Eckert, M. L., Shaw, D. W. W., Ozyurek, H., Aysun, S., … Glass, I. A. (2006). AHI1 mutations cause both retinal dystrophy and renal cystic disease in Joubert syndrome. *Journal of Medical Genetics*, *43*(4), 334–339. https://doi.org/10.1136/jmg.2005.036608

Parisi, M. a, Doherty, D., Chance, P. F., & Glass, I. a. (2007). Joubert syndrome (and related disorders) (OMIM 213300). *European Journal of Human Genetics : EJHG*, *15*(5), 511–21. https://doi.org/10.1038/sj.ejhg.5201648

Park, T. J., Haigo, S. L., & Wallingford, J. B. (2006). Ciliogenesis defects in embryos lacking inturned or fuzzy function are associated with failure of planar cell polarity and Hedgehog signaling. *Nature Genetics*, *38*(3), 303–11. https://doi.org/10.1038/ng1753

Park, T. J., Mitchell, B. J., Abitua, P. B., Kintner, C., & Wallingford, J. B. (2008). Dishevelled controls apical docking and planar polarization of basal bodies in ciliated epithelial cells. *Nature Genetics*, *40*(7), 871–9. https://doi.org/10.1038/ng.104

Park, T. S., & Han, J. Y. (2000). Derivation and Characterization of Pluripotent Embryonic Germ Cells in Chicken, *482*(October 1999).

Patir, A., Fraser, A.M., Barnette, M.W., McTeir, L., Rainger, J., Davey, M.G., Freeman, T.C. (2019). The Human Motile Cilia Associated Transcriptional Signature. In prepratation.

Pauli, S., Altmüller, J., Schröder, S., Ohlenbusch, A., Dreha-Kulaczewski, S., Bergmann, C., … Brockmann, K. (2018). Homozygosity for the c.428delG variant in KIAA0586 in a healthy individual: implications for molecular testing in patients with Joubert syndrome. *Journal of Medical Genetics*, jmedgenet-2018-105470. https://doi.org/10.1136/jmedgenet-2018-105470

Pausch, H., Venhoranta, H., Wurmser, C., Hakala, K., Iso-touru, T., Sironen, A., … Andersson, M. (2016). A frameshift mutation in ARMC3 is associated with a tail stump sperm defect in Swedish Red (Bos taurus) cattle. *BMC Genetics*, *17*(49), 1–9. https://doi.org/10.1186/s12863-016-0356-7

Pedersen, L. B., Mogensen, J. B., & Christensen, S. T. (2016). Endocytic Control of Cellular Signaling at the Primary Cilium. *Trends in Biochemical Sciences*, *41*(9), 784–797. https://doi.org/10.1016/j.tibs.2016.06.002

Pedersen, L. B., Veland, I. R., Schrøder, J. M., & Christensen, S. T. (2008). Assembly of primary cilia. *Developmental Dynamics*, *237*(8), 1993–2006. https://doi.org/10.1002/dvdy.21521

Pitaval, A., Senger, F., Letort, G., Gidrol, X., Guyon, L., Sillibourne, J., & Théry, M. (2017). Microtubule stabilization drives 3D centrosome migration to initiate primary ciliogenesis. *Journal of Cell Biology*, *216*(11), 3713–3728. https://doi.org/10.1083/jcb.201610039

Polo, S. E., & Jackson, S. P. (2011). Dynamics of DNA damage response proteins at DNA breaks: a focus on protein modifications. *Genes and Development*, *25*, 409–433. https://doi.org/10.1101/gad.2021311.critical

Praveen, K., Davis, E. E., & Katsanis, N. (2015). Unique among ciliopathies: primary ciliary dyskinesia, a motile cilia disorder. *F1000Prime Reports*, *7*(36).

Prosser, S. L., & Morrison, C. G. (2015). Centrin2 regulates CP110 removal in primary cilium formation, *208*(6), 693–701. https://doi.org/10.1083/jcb.201411070

Putoux, A., Thomas, S., Coene, K. L. M., Davis, E. E., Alanay, Y., Ogur, G., … Gonzales, M. (2011). KIF7 mutations cause fetal hydrolethalus and acrocallosal syndromes. *Nature Publishing Group*, *43*(6), 601–606. https://doi.org/10.1038/ng.826

R Core Team. (2013). R: A language and environment for statistical computing. R Foundation for Statistical Computing, Vienna, Austria.

Ralston, K. S., Kabututu, Z. P., Melehani, J. H., Oberholzer, M., & Hill, K. L. (2009). The Trypanosoma brucei Flagellum: Moving Parasites in New Directions. *Annual Review of Microbiology*, *63*. https://doi.org/10.1146/annurev.micro.091208.073353.The

Ran, F. A., Hsu, P. D., Lin, C., Gootenberg, J. S., Konermann, S., Trevino, A. E., … Zhang, F. (2013). Resource Double Nicking by RNA-Guided CRISPR Cas9 for Enhanced Genome Editing Specificity. *CELL*, *154*(6), 1380–1389. https://doi.org/10.1016/j.cell.2013.08.021

Rauch, A., Thiel, C. T., Schindler, D., Wick, U., Crow, Y. J., Ekici, A. B., … Reis, A. (2008). Mutations in the Pericentrin (PCNT) Gene Cause Primordial Dwarfism. *Science*, *319*, 816–819.

Reisinger, E., Zimmermann, U., Knipper, M., Ludwig, J., Klocker, N., Fakler, B., & Oliver, D. (2005). Cod106, a novel synaptic protein expressed in sensory hair cells of the inner ear and in CNS neurons. *Molecular and Cellular Neuroscience*, *28*, 106–117.

Reiter, J. F., & Leroux, M. R. (2017). Genes and molecular pathways underpinning ciliopathies. *Nature Reviews Molecular Cell Biology*, *18*(9), 533–547. https://doi.org/10.1038/nrm.2017.60

Resende, T. P., Ferreira, M., Teillet, M., Tavares, T. A., Andrade, R. P., & Palmeirim, I. (2010). Sonic hedgehog in temporal control of somite formation. *PNAS*, *107*(29), 12907–12912. https://doi.org/10.1073/pnas.1000979107

Roberts, B., Casillas, C., Alfaro, A. C., Ja, C., & Roelink, H. (2016). Patched1 and Patched2 inhibit Smoothened non-cell autonomously. *eLife*, 1–19. https://doi.org/10.7554/eLife.17634

Roepman, R., Ueffing, M., Kremer, H., Huynen, M. A., Gibson, T. J., Katsanis, N., … Omran, H. (2012). SYSCILIA , " A systems biology approach to dissect cilia function and its disruption in human genetic disease ." *Cilia*, *1*(Suppl 1), P41. https://doi.org/10.1186/2046-2530-1-S1-P41

Romani, M., Micalizzi, A., & Valente, E. M. (2013). Joubert syndrome: congenital cerebellar ataxia with the "molar tooth." *The Lancet. Neurology*, *12*(9), 984–905. https://doi.org/10.1016/S1474-4422(13)70136-4.Joubert

Roosing, S., Hofree, M., Kim, S., Scott, E., Copeland, B., Romani, M., … Gleeson, J. G. (2015). Functional genome-wide siRNA screen identifies KIAA0586 as mutated in Joubert syndrome. *eLife*, *4*, e06602. https://doi.org/10.7554/eLife.06602

Ross, A. J., May-Simera, H., Eichers, E. R., Kai, M., Hill, J., Jagger, D. J., … Beales, P. L. (2005). Disruption of Bardet-Biedl syndrome ciliary proteins perturbs planar cell polarity in vertebrates. *Nature Genetics*, *37*(10), 1135–40. https://doi.org/10.1038/ng1644

Rothenberg, E. V. (2007). Reviews Negotiation of the T Lineage Fate Decision by Transcription-Factor Interplay and Microenvironmental Signals. https://doi.org/10.1016/j.immuni.2007.06.005

Roux, K. J., Kim, D. I., Raida, M., & Burke, B. (2012). A promiscuous biotin ligase fusion protein identifies proximal and interacting proteins in mammalian cells. *Journal of Cell Biology*, *196*(6), 801–810. https://doi.org/10.1083/jcb.201112098

Satir, P., Heuser, T., & Sale, W. S. (2014). A structural basis for how motile cilia beat. *BioScience*, *64*(12), 1073–1083. https://doi.org/10.1093/biosci/biu180

Savitski, M. M., Mathieson, T., Zinn, N., Sweetman, G., Doce, C., Becher, I., … Bantsche, M. (2013). Measuring and Managing Ratio Compression for Accurate iTRAQ/ TMT Quantification. https://doi.org/10.1021/pr400098r

Schatten, H. (2008). The mammalian centrosome and its functional significance. *Histochemistry and Cell Biology*, *129*(6), 667–686. https://doi.org/10.1007/s00418-008-0427-6

Schellenburg, S., Schulz, A., Poitz, D. M., & Muders, M. H. (2017). Role of neuropilin-2 in the

immune system. *Molecular Immunology*, *90*(August), 239–244. https://doi.org/10.1016/j.molimm.2017.08.010

Schmidt, K. N., Kuhns, S., Neuner, A., Hub, B., Zentgraf, H., & Pereira, G. (2012). Cep164 mediates vesicular docking to the mother centriole during early steps of ciliogenesis. *Journal of Cell Biology*, *199*(7), 1083–1101. https://doi.org/10.1083/jcb.201202126

Schmidt, T. I., Kleylein-Sohn, J., Westendorf, J., Le Clech, M., Lavoie, S. B., Stierhof, Y.-D., & Nigg, E. a. (2009). Control of centriole length by CPAP and CP110. *Current Biology : CB*, *19*(12), 1005–11. https://doi.org/10.1016/j.cub.2009.05.016

Schock, E. N., Chang, C., Youngworth, I. A., Davey, M. G., Delany, M. E., & Brugmann, S. A. (2016). Utilizing the chicken as an animal model for human craniofacial ciliopathies. *Developmental Biology*, *415*(2), 326–337. https://doi.org/10.1016/j.ydbio.2015.10.024

Schopp, I. M., Amaya Ramirez, C. C., Debeljak, J., Kreibich, E., Skribbe, M., Wild, K., & Béthune, J. (2017). Split-BioID a conditional proteomics approach to monitor the composition of spatiotemporally defined protein complexes. *Nature Communications*, *8*. https://doi.org/10.1038/ncomms15690

Silva, I. M. W., Rosenfeld, J., Antoniuk, S. A., Raskin, S., & Sotomaior, V. S. (2014). A 1 . 5 Mb terminal deletion of 12p associated with autism spectrum disorder. *Gene*, *542*(1), 83–86. https://doi.org/10.1016/j.gene.2014.02.058

Simons, D., Boye, S. L., Hauswirth, W. W., & Wu, S. M. (2011). Gene therapy prevents photoreceptor death and preserves retinal function in a Bardet-Biedl syndrome mouse model. *Proceedings of the National Academy of Sciences of the United States of America*, *108*(15), 6276–6281. https://doi.org/10.1073/pnas.1019222108/-/DCSupplemental.www.pnas.org/cgi/doi/10.1073/pnas.1019222108

Simons, M., Gloy, J., Ganner, A., Bullerkotte, A., Bashkurov, M., Kronig, C., … Walz, G. (2005). Inversin, the gene product mutated in nephronophthisis type II, functions as a molecular switch between Wnt signaling pathways. *Nature Genetics*, *37*(5), 537–543. https://doi.org/10.1038/ng1552.Inversin

Singh, S., & Solecki, D. J. (2015). Polarity transitions during neurogenesis and germinal zone exit in the developing central nervous system. *Frontiers in Cellular Neuroscience*, *9*(62), 1–8. https://doi.org/10.3389/fncel.2015.00062

Sit, S., & Manser, E. (2011). Rho GTPases and their role in organizing the actin cytoskeleton. https://doi.org/10.1242/jcs.064964

Sloboda, R. D. (2002). A healthy understanding of intraflagellar transport. *Cell Motility and the Cytoskeleton*, *52*, 1–8. https://doi.org/10.1002/cm.10035

Snider, J., Thibault, G., & Houry, W. A. (2008). The AAA+ superfamily of functionaly diverse proteins, *9*, 1–8. https://doi.org/10.1186/gb-2008-9-4-216

Sormanni, P., Aprile, F. A., & Vendruscolo, M. (2015). Rational design of antibodies targeting specific epitopes within intrinsically disordered proteins. *PNAS*, *112*(32), 9902–9907. https://doi.org/10.1073/pnas.1422401112

Sorokin, S. (1962). Centrioles and the formation of rudimentary cilia by fibroblasts and smooth muscle cells. *The Journal of Cell Biology*, *15*(10), 363–377. https://doi.org/10.1083/jcb.15.2.363

Sorokin, S. P. (1968). Reconstructions of centriole formation and ciliogenesis in mammalian lungs. *Journal of Cell Science*, *3*, 207–230. https://doi.org/10.1242/jcs.00282

Spalluto, C., Wilson, D. I., & Hearn, T. (2013). Evidence for reciliation of RPE1 cells in late G1 phase , and ciliary localisation of cyclin. *Elsevier*, *3*, 334–340. https://doi.org/10.1016/j.fob.2013.08.002

Spassky, N., Han, Y. G., Aguilar, A., Strehl, L., Besse, L., Laclef, C., … Alvarez-Buylla, A. (2008). Primary cilia are required for cerebellar development and Shh-dependent expansion

of progenitor pool. *Developmental Biology*, *317*, 246–259. https://doi.org/10.1016/j.ydbio.2008.02.026

Spektor, A., Tsang, W. Y., Khoo, D., & Dynlacht, B. D. (2007). Cep97 and CP110 Suppress a Cilia Assembly Program. *Cell*, *130*(4), 678–690. https://doi.org/10.1016/j.cell.2007.06.027

Stephen, L. A., Davis, G. M., McTeir, K. E., James, J., McTeir, L., Kierans, M., … Davey, M. G. (2013). Failure of centrosome migration causes a loss of motile cilia in talpid(3) mutants. *Developmental Dynamics : An Official Publication of the American Association of Anatomists*, *242*(8), 923–31. https://doi.org/10.1002/dvdy.23980

Stephen, L. A., Tawamie, H., Davis, G. M., Tebbe, L., Nürnberg, P., Nürnberg, G., … Bolz, H. J. (2015). TALPID3 controls centrosome and cell polarity and the human ortholog KIAA0586 is mutated in Joubert syndrome (JBTS23). *eLife*, *4*(September2015), 1–22. https://doi.org/10.7554/eLife.08077

Stephen, L. a, Johnson, E. J., Davis, G. M., McTeir, L., Pinkham, J., Jaberi, N., & Davey, M. G. (2014). The chicken left right organizer has nonmotile cilia which are lost in a stage-dependent manner in the talpid(3) ciliopathy. *Genesis (New York, N.Y. : 2000)*, *52*(6), 600–13. https://doi.org/10.1002/dvg.22775

Strazzabosco, M., & Somlo, S. (2011). Polycystic liver diseases: congenital disorders of cholangiocyte signaling. *Gastroenterology*, *140*(7), 1855–1859. https://doi.org/10.1053/j.gastro.2011.04.030.POLYCYSTIC

Strilic, B., Kucera, T., Eglinger, J., Hughes, M. R., McNagny, K. M., Tsukita, S., … Lammert, E. (2009). The Molecular Basis of Vascular Lumen Formation in the Developing Mouse Aorta. *Developmental Cell*, *17*(4), 505–515. https://doi.org/10.1016/j.devcel.2009.08.011

Sun, M., Northup, N., Marga, F., Huber, T., Byfield, F. J., Levitan, I., & Forgacs, G. (2007). The effect of cellular cholesterol on membrane- cytoskeleton adhesion. *Journal of Cell Science*. https://doi.org/10.1242/jcs.001370

Suzuki, M., Morita, H., & Ueno, N. (2012). Molecular mechanisms of cell shape changes that contribute to vertebrate neural tube closure. *Development, Growth & Differentiation*, *54*, 266–276. https://doi.org/10.1111/j.1440-169X.2012.01346.x

Tabler, J. M., Barrell, W. B., Szabo-Rogers, H. L., Healy, C., Yeung, Y., Perdiguero, E. G., … Liu, K. J. (2013). Fuz Mutant Mice Reveal Shared Mechanisms between Ciliopathies and FGF-Related Syndromes. *Developmental Cell*, *25*(6), 623–635. https://doi.org/10.1016/j.devcel.2013.05.021

Takashima, S., Kitakaze, M., Asakura, M., Asanuma, H., Sanada, S., Tashiro, F., … Hori, M. (2002). Targeting of both mouse neuropilin-1 and neuropilin-2 genes severely impairs developmental yolk sac and embryonic angiogenesis. *Developmental Biology*, *99*(6), 6–11.

Tang, C. C., Fu, R., Wu, K., Hsu, W., & Tang, T. K. (2009). CPAP is a cell-cycle regulated protein that controls centriole length. *Nature Publishing Group*, *11*, 825–831. https://doi.org/10.1038/ncb1889

Tang, C. J. C., Lin, S. Y., Hsu, W. Bin, Lin, Y. N., Wu, C. T., Lin, Y. C., … Tang, T. K. (2011). The human microcephaly protein STIL interacts with CPAP and is required for procentriole formation. *EMBO Journal*, *30*(23), 4790–4804. https://doi.org/10.1038/emboj.2011.378

Tanos, B. E., Yang, H.-J., Soni, R., Wang, W.-J., Macaluso, F. P., Asara, J. M., & Tsou, M.-F. B. (2013). Centriole distal appendages promote membrane docking, leading to cilia initiation. *Genes & Development*, *27*(2), 163–8. https://doi.org/10.1101/gad.207043.112

Tateishi, K., Yamazaki, Y., Nishida, T., Watanabe, S., Kunimoto, K., Ishikawa, H., & Tsukita, S. (2013). Two appendages homologous between basal bodies and centrioles are

formed using distinct, *203*(3), 417–425. https://doi.org/10.1083/jcb.201303071

Taylor, L., Carlson, D. F., Nandi, S., Sherman, A., Fahrenkrug, S. C., & McGrew, M. J. (2017). Efficient TALEN-mediated gene targeting of chicken primordial germ cells. *Development*, *144*(5), 928–934.

The Uniprot Consortium. (2018). UniProt : the universal protein knowledgebase. *Nucleic Acids Research*, *45*(D1), 158–169. https://doi.org/10.1093/nar/gkw1099

Thomas, S., Legendre, M., Saunier, S., Bessières, B., Alby, C., Bonnière, M., … Attié-Bitach, T. (2012). TCTN3 mutations cause Mohr-Majewski syndrome. *American Journal of Human Genetics*, *91*(2), 372–378. https://doi.org/10.1016/j.ajhg.2012.06.017

Thornton, G. K., & Woods, C. G. (2009). Primary microcephaly : do all roads lead to Rome ? *Trends in Genetics*, *25*(11), 501–510. https://doi.org/10.1016/j.tig.2009.09.011

Tojkander, S., Gateva, G., & Lappalainen, P. (2012). Actin stress fibers – assembly , dynamics and biological roles. *The Journal of Cell Science*, *125*, 1855–1864. https://doi.org/10.1242/jcs.098087

Tollenaere, M. A. X., Mailand, N., & Bekker-Jensen, S. (2015). Centriolar satellites: Key mediators of centrosome functions. *Cellular and Molecular Life Sciences*, *72*(1), 11–23. https://doi.org/10.1007/s00018-014-1711-3

Tsang, W. Y., Bossard, C., Khanna, H., Peranen, J., Swaroop, A., Malhotra, V., & Dynlacht, B. D. (2008). CP110 Suppresses Primary Cilia Formation through its Interaction with CEP290, a Protein Deficient in Human Ciliary Disease, *15*(2), 187–197. https://doi.org/10.1016/j.devcel.2008.07.004.CP110

Tsunekawa, N., Naito, M., Sakai, Y., Nishida, T., & Noce, T. (2000). Isolation of chicken vasa homolog gene and tracing the origin of primordial germ cells, *2750*, 2741–2750.

Vilboux, T., Doherty, D. A., Glass, I. A., Parisi, M. A., Phelps, I. G., Cullinane, A. R., … Gunay-Aygun, M. (2017). Molecular genetic findings and clinical correlations in 100 patients with Joubert syndrome and related disorders prospectively evaluated at a single center. *Genetics in Medicine*, *19*(8), 875–882. https://doi.org/10.1038/gim.2016.204

Walsh, D. M., Shalev, S. a, Simpson, M. a, Morgan, N. V, Gelman-Kohan, Z., Chemke, J., … Maher, E. R. (2013). Acrocallosal syndrome: identification of a novel KIF7 mutation and evidence for oligogenic inheritance. *European Journal of Medical Genetics*, *56*(1), 39–42. https://doi.org/10.1016/j.ejmg.2012.10.004

Wang, G., Jiang, Q., & Zhang, C. (2014). The role of mitotic kinases in coupling the centrosome cycle with the assembly of the mitotic spindle. *Journal of Cell Science*, *127*, 4111–4122. https://doi.org/10.1242/jcs.151753

Wang, L., Failler, M., Fu, W., & Dynlacht, B. D. (2018). A distal centriolar protein network controls organelle maturation and asymmetry. *Nature Communications*, *9*(1). https://doi.org/10.1038/s41467-018-06286-y

Wang, L., Lee, K., Malonis, R., Sanchez, I., & Dynlacht, B. D. (2016). Tethering of an E3 ligase by PCM1 regulates the abundance of centrosomal KIAA0586/Talpid3 and promotes ciliogenesis. *eLife*, *5*(MAY2016), 1–18. https://doi.org/10.7554/eLife.12950

Ware, S. M., Aygun, M. G.-, & Hildebrandt, F. (2011). Spectrum of clinical diseases caused by disorders of primary cilia. *Proceedings of the American Thoracic Society*, *8*(5), 444–50. https://doi.org/10.1513/pats.201103-025SD

Waterhouse, A. M., Procter, J. B., Martin, D. M. A., Clamp, M., & Barton, G. J. (2009). Jalview Version 2 - a multiple sequence alignment editor and analysis workbench. *Bioinformatics*, *25*(9), 1189–1191.

Waters, A. M., Asfahani, R., Carroll, P., Bicknell, L., Lescai, F., Bright, A., … Beales, P. L. (2015). The kinetochore protein , CENPF , is mutated in human ciliopathy and microcephaly phenotypes. *Journal of Medical Genetics*, 1–10. https://doi.org/10.1136/jmedgenet-2014-102691

Waters, A. M., & Beales, P. L. (2011). Ciliopathies: an expanding disease spectrum. *Pediatric Nephrology (Berlin, Germany)*, *26*(7), 1039–56. https://doi.org/10.1007/s00467-010-1731-7

Waters, J. C. (2009). Accuracy and precision in quantitative fluorescence microscopy. *The Journal of Cell Biology*, *185*(7), 1135–1148. https://doi.org/10.1083/jcb.200903097

Wei, Q., Zhang, Y., Li, Y., Zhang, Q., Ling, K., & Hu, J. (2012). The BBSome controls IFT assembly and turnaround in cilia. *Nature Cell Biology*, *14*(9), 950–957. https://doi.org/10.1038/ncb2560.The

Wheeler, A. P., & Ridley, A. J. (2004). Why three Rho proteins ? RhoA , RhoB , RhoC , and cell motility. *Experimental Cell Research*, *301*, 43–49. https://doi.org/10.1016/j.yexcr.2004.08.012

Wheway, G., Nazlamova, L., & Hancock, J. T. (2018). Signaling through the Primary Cilium. *Frontiers in Cell and Developmental Biology*, *6*, 1–13.

Whitley, D., Goldberg, S. P., Jordan, W. D., & Johnston, K. W. (1999). Heat shock proteins : A review of the molecular chaperones. *JOurnal of Vascular Surgery*, *29*(4), 748–751.

Whyte, J., Glover, J. D., Woodcock, M., Brzeszczynska, J., Taylor, L., Sherman, A., … Mcgrew, M. J. (2015). FGF, Insulin, and SMAD Signaling Cooperate for Avian Primordial Germ Cell Self-Renewal. *Stem Cell Reports*, *5*(6), 1171–1182. https://doi.org/10.1016/j.stemcr.2015.10.008

Wijgerde, M., Mcmahon, J. A., Rule, M., & Mcmahon, A. P. (2002). A direct requirement for Hedgehog signaling for normal specification of all ventral progenitor domains in the presumptive mammalian spinal cord. *Genes and Development*, *16*, 2849–2864. https://doi.org/10.1101/gad.1025702.produced

Wilcock, A. C., Swedlow, J. R., & Storey, K. G. (2007). Mitotic spindle orientation distinguishes stem cell and terminal modes of neuron production in the early spinal cord. *Development*, *134*, 1943–1954. https://doi.org/10.1242/dev.002519

Williams, C. L., Mcintyre, J. C., Norris, S. R., Jenkins, P. M., Zhang, L., Pei, Q., … Martens, J. R. (2014). Direct evidence for BBSome-associated intraflagellar transport reveals distinct properties of native mammalian cilia. *Nature Communications*, *5*, 1–13. https://doi.org/10.1038/ncomms6813

Winey, M., & O'Toole, E. (2014). Centriole structure. *Philosophical Transactions of the Royal Society of London. Series B, Biological Sciences*, *369*(1650), 20130457-. https://doi.org/10.1098/rstb.2013.0457

Wisniewski, J. R., Zougman, A., Nagaraj, N., & Mann, M. (2009). Universal sample preparation method for proteome analysis. *Nature Methods*, *6*(5), 359–362. https://doi.org/10.1038/NMETH.1322

Wittmann, T., & Waterman-Storer, C. M. (2001). Cell motility : can Rho GTPases and microtubules point the way ? *Journal of Cell Science*, *114*, 3795–3803.

Wolf, D. E., Samarasekera, C., & Swedlow, J. R. (2007). Quantitative Analysis of Digital Microscope Images. *Methods in Cell Biology*, *81*, 365–396. https://doi.org/10.1016/S0091-679X(06)81017-4

Wu, C., Yang, M., Li, J., Wang, C., Cao, T., Tao, K., & Wang, B. (2014). Talpid3-binding centrosomal protein Cep120 is required for centriole duplication and proliferation of cerebellar granule neuron progenitors. *PloS One*, *9*(9), e107943. https://doi.org/10.1371/journal.pone.0107943

Xavier, G. M., Seppala, M., Barrell, W., Birjandi, A. A., Geoghegan, F., & Cobourne, M. T. (2016). Hedgehog receptor function during craniofacial development. *Developmental Biology*, *415*(2), 198–215. https://doi.org/10.1016/j.ydbio.2016.02.009

Yadav, S. P., Sharma, N. K., Liu, C., Dong, L., Li, T., Swaroop, A., … Liu, a. (2016). Centrosomal protein CP110 controls maturation of the mother centriole during cilia biogenesis.

Development (Cambridge, England), *143*(9), 1491–501. https://doi.org/10.1242/dev.130120

Yang, J., Andre, P., Ye, L., & Yang, Y.-Z. (2015). The Hedgehog signalling pathway in bone formation. *International Journal of Oral Science*, *7*, 73–79. https://doi.org/10.1038/ijos.2015.14

Yin, Y., Bangs, F., Paton, I. R., Prescott, A., James, J., Davey, M. G., … Tickle, C. (2009). The Talpid3 gene (KIAA0586) encodes a centrosomal protein that is essential for primary cilia formation. *Development (Cambridge, England)*, *136*(4), 655–64. https://doi.org/10.1242/dev.028464

Yu, X., Ng, C. P., Habacher, H., & Roy, S. (2008). Foxj1 transcription factors are master regulators of the motile ciliogenic program. *Nature Genetics*, *40*(12), 1445–53. https://doi.org/10.1038/ng.263

Yukitake, H., Furusawa, M., Taira, T., Iguchi-Ariga, S. M., & Ariga, H. (2002). AMAP-1, a novel testis-specific AMY-1-binding protein, is differentially expressed during the course of spermatogenesis. *Biochemica et Biophysica Acta*, 126–132.

Zanetti, E., Molette, C., Chambon, C., Pinguet, J., Remignon, H., & Cassandro, M. (2011). Using 2-DE for the differentiation of local chicken breeds. *Proteomics*, *11*, 2613–2619. https://doi.org/10.1002/pmic.201000639

Zhao, Y., & Lin, Y. (2010). Whole-Cell Protein Identification Using the Concept of Unique Peptides. *Genetics Proteomics Bioinformatics*, *8*(1), 33–41. https://doi.org/10.1016/S1672-0229(10)60004-6